The apparent sedimentation coefficient, s*, and its distribution function, g(s*), within -∞ < s* < ∞

Background regarding simulations

The data presented here were generated by simulations (Moody, 2012). The method of simulation is an implementation of an integral, finite-element solution to the relevant continuity equation (Moody, 2011a, 2011b). The method is built on that which Claverie, Dreux and Cohen (1975) described in their solution to the Lamm equation, but differs in several respects. To correctly implement their concentration dependence, the transport coefficients are defined as spatially-independent parameters. To correctly evaluate the concentration-dependent transport coefficients at the time to be evaluated, the concentrations are calculated iteratively. By such an evaluation of the concentration-dependent transport coefficients at both the time already evaluated and the time being evaluated, the accuracy of each new set of concentrations is maximised. Computational artefacts are reduced by first calculating all concentrations in one order, then recalculating all concentrations in the opposite order, and averaging the results. For the cylindrical coordinate system of analytical ultracentrifugation, simpler results of integration are obtained by using one-half the square of the radial position, rather than the radial position, as the spatial parameter of the continuity equation (Moody, 2011a). For the rectangular coordinate system of membrane-confined electrophoresis, the time-and-distance-dependent continuity equation yields results of integration that are simpler than those obtained from the Lamm equation, which is the time-and-radial-position-dependent continuity equation that pertains to analytical ultracentrifugation (Moody, 2011b). Additionally, a simple coupled-flow equation has been implemented.

g(s) analysis of data obtained by analytical ultracentrifugation*

The data collected during analytical ultracentrifugation (AUC) include the values of a dependent variable related to the total mass concentration, c, of all solutes, and the corresponding independent variables of time, t, and radial position, r. Data regarding rotor speed, temperature and other parameters that are likely to affect $\left(\frac{\partial c}{\partial r}\right)_t$ and $\left(\frac{\partial c}{\partial t}\right)_r$ are also recorded. The proportionality between an experimentally measured signal and a specific solute concentration may vary from one solute to another. For example, it is often the case that some solutes, such as buffer salts, are completely undetectable, or nearly so.

Regardless of how the signal relates to c, the analysis of AUC data can be viewed as an attempt to describe a system without reference to most of the experimental parameters. Such a description is nearly achieved by g(s*) analysis, which is to say, the analysis of AUC data in terms of the apparent sedimentation coefficient, s*, and its distribution function, g(s*). In essence, g(s*) analysis is a transformation of AUC data that minimises all effects that depend on r, t or rotor speed. As in practically all methods of analysis of AUC data, reference to temperature and solvent remains unavoidable. Reference to concentration is not really avoidable, either, but the results of g(s*) analysis can be normalised with respect to total signal. Such normalisation can be useful when comparing the results of g(s*) analysis obtained from systems that vary with respect to c.

Before delving into the details of g(s*) analysis, it is worth noting a time-dependent effect that results from the system having the geometry of a cylindrical sector. Due to this geometry, over time, the concentration of a negatively-buoyant solute decreases in the region between its zone of depletion and the pellet that accumulates toward the base of the system, while the concentration

of a positively-buoyant solute increases in the region between its zone of depletion and the supernatant that accumulates toward the meniscus of the system. Collectively, these geometrically rooted phenomena are referred to as the radial dilution/concentration effect.

Each value of s* is a combined transformation of a value of r, a value of t, the rotor speed, and a reference position. By definition, s* is equal to the sedimentation coefficient of a thermodynamically ideal solute that, in the limit of zero diffusion, would exhibit a hyper-sharp boundary in its concentration at a specific radial position and a specific time. There are two possible orientations of that hyper-sharp boundary, one of which would arise from a positively-buoyant solute for which s* is less than zero, the other of which would arise from a negatively-buoyant solute for which s* is greater than zero. Thus, each value of s* describes the behaviour of a step function that can represent a hypothetical solute concentration in an all-or-none fashion.

Henceforth, a hypothetical solute is defined as an imaginary, thermodynamically ideal, non-diffusing solute characterised by an s* value and a constant of concentration. Of the two oppositely signed s* values that correspond to a transition in a hypothetical solute concentration at radial position r and time t, the one having $s^* < 0$ corresponds to the transition for which the hypothetical solute concentration at time t is zero at all radial positions greater than r, and the one having $s^* > 0$ corresponds to the transition for which the hypothetical solute concentration at time t is zero at all radial positions less than r.

A hypothetical solute can be said to exhibit a zone of depletion where its concentration is zero, and a plateau region within which its concentration is greater than zero and independent of radial position. The concentration of a hypothetical solute in its plateau region is, by virtue of

being independent of radial position, called its plateau concentration. The plateau concentration of a hypothetical solute is equal to a value that, due to the radial dilution/concentration effect, depends on time. One time-independent exception is a hypothetical solute for which $s^* = 0$. A seemingly trivial time-independent exception is a hypothetical solute for which the concentration is zero above and below what would otherwise be its transition.

The data transformation obtained by g(s*) analysis takes the radial dilution/concentration effect into account, albeit imperfectly. To within some approximation, however, g(s*) analysis reveals the relationship between s* values and the initial concentrations of the corresponding, hypothetical solutes. With the possible exceptions of the extreme time points, the number of s* values is infinite at any given time. Thus, within a g(s*) distribution, for any given hypothetical solute characterised by a randomly chosen s* value, the apparent initial concentration is most likely zero, or of a magnitude attributable to noise.

Given a function to convert between r and s* at any given time (Equation 27), the independent variables of AUC data can be transformed from t and r to t and s*. It is then possible to plot c versus s* at time t, but in doing so, the value of c at any single radial position at that time will map to the two values of s* that are calculated for that radial position and time. Likewise, following such a transformation, it is straightforward to obtain the derivative, $\left(\frac{\partial c}{\partial s^*}\right)_t$, which is single-valued when viewed as a function of s*, but is double-valued when viewed as a function of r.

At any given time, where $\left|\left(\frac{\partial c}{\partial r}\right)_t\right|$ is greater than zero at some value of r, $\left|\left(\frac{\partial c}{\partial s^*}\right)_t\right|$ will be greater than zero at the two values of s* calculated from that value of r, but the sign of $\left(\frac{\partial c}{\partial s^*}\right)_t$ will match

the sign of just one of those s* values. The s* value where the signs of $\left(\frac{\partial c}{\partial s^*}\right)_t$ and s* match will be the s* value that matches the orientation of $\left(\frac{\partial c}{\partial r}\right)_t$ at the corresponding r value. Each $\left(\frac{\partial c}{\partial s^*}\right)_t$ that matches the sign of s* is deemed essential with respect to calculating g(s*). Each $\left(\frac{\partial c}{\partial s^*}\right)_t$ that is opposite in sign to s* is deemed redundant, and a value of zero is used in its place when calculating g(s*). At any given time, half of the nonzero $\left(\frac{\partial c}{\partial s^*}\right)_t$ values will be deemed essential, and half will be deemed redundant.

Nullifying the redundant nonzero values of $\left(\frac{\partial c}{\partial s^*}\right)_t$, and modifying the remaining values in an effort to reverse the effects of radial dilution/concentration, yields g(s*). The integral of |g(s*)| with respect to s* yields the cumulative distribution function, G(s*), which equates to a substantially time-normalised, but not entirely time-independent, measure of the concentration of all solutes for which the apparent sedimentation coefficient is less than or equal to s*, but greater than or equal to the minimum possible value (Equation 35) of s* at some specific time.

Previous derivations (Bridgeman, 1942; Stafford, 1992, 1994, 2000) of g(s*) encompassed values of $s^* \geq 0$. In the derivation described here, g(s*) is extended to include values of $s^* < 0$. As will be shown, when applied to data spanning a short time frame, and in the absence of fitting for time-independent noise, the ls-g(s*) function (Schuck & Rossmanith, 2000) obtained by least squares boundary modeling is nearly identical to |g(s*)|.

An overview of the remaining contents

Following a general description and derivation of g(s*) and related functions (Equations 1 to 38; Figure 1), nearly noise-free data from simulations are subjected to g(s*) analysis. In the first set of examples, a concentration-independent system is used to show each step of g(s*) analysis (Equations 39 to 45; Figures 2 to 22), and to illustrate some complications that can occur with relatively simple systems (Figures 23 to 31). To show the effects of concentration dependence on g(s*) results, a more complicated system is used in a subsequent set of examples of g(s*) analysis (Figures 32 to 39). A set of equations describing c as a collection of step functions is then presented, and g(s*) is described in terms of derivatives of those step functions (Equations 46 to 87). Next, the effects of radially-independent (RI) and time-independent (TI) noise on $\left(\frac{\partial c}{\partial s^*}\right)_t$, determined from finite-difference forms of spatial (Equation 3) or temporal (Equation 6) derivatives, are explored in some detail (Equations 88 to 99; Table 1; Figures 40 to 50). Lastly, the analogue of g(s*) that pertains to membrane-confined electrophoresis is described mathematically (Equations 100 to 170).

Basic derivations of g(s)*

Bridgeman's (1942) derivation of g(s*) starts with the total differential of c with respect to r and t,

$$dc = \left(\frac{\partial c}{\partial r}\right)_t dr + \left(\frac{\partial c}{\partial t}\right)_r dt\,.$$

(1)

At constant t, this equation reduces to

$$dc_t = \left(\frac{\partial c}{\partial r}\right)_t dr.$$

(2)

Thus, where c is defined as a function of r and t, the partial derivative of c with respect to s* at constant t, obtained through division by an infinitesimally small change in s* at constant t, is

$$\left(\frac{\partial c}{\partial s^*}\right)_t = \left(\frac{\partial c}{\partial r}\right)_t \left(\frac{\partial r}{\partial s^*}\right)_t.$$

(3)

The functional form of s* can be derived from the equations of continuity and mass flow that apply to AUC. Detailed descriptions of these equations can be found in many places, including the reference relied upon here (Moody, 2011a). As will also be shown (Equation 27), s* can be described entirely in terms of r, t and the angular velocity, ω. (The relationship between rotor speed and ω is given by Equation 11.) From s* described in those terms, $\left(\frac{\partial r}{\partial s^*}\right)_t$ is derived.

Equation 3 shows that $\left(\frac{\partial c}{\partial s^*}\right)_t$ can only be nonzero where $\left(\frac{\partial c}{\partial r}\right)_t$ is nonzero. The orientation of $\left(\frac{\partial c}{\partial r}\right)_t$ is given by its sign. Where $\left(\frac{\partial c}{\partial r}\right)_t > 0$, its orientation is that of a negatively-buoyant solute. Where $\left(\frac{\partial c}{\partial r}\right)_t < 0$, its orientation is that of a positively-buoyant solute.

As previously noted, for a given radial position r at time t, there are two oppositely signed values of s* that, if respectively equal to the sedimentation coefficients of two oppositely directed, thermodynamically ideal solutes with vanishingly small diffusion coefficients, would lead to the expectation of two oppositely oriented, hyper-sharp transitions in concentration at that position at that time. The thermodynamically ideal solute for which the signs of s* and $\left(\frac{\partial c}{\partial r}\right)_t$ are the same, if given a diffusion coefficient of the appropriate value greater than zero, would exhibit a spatial

derivative of its concentration that is equal to $\left(\frac{\partial c}{\partial r}\right)_t$ at position r and time t, so that the s* value of this solute reflects both the location and orientation of $\left(\frac{\partial c}{\partial r}\right)_t$. In contrast, the thermodynamically ideal solute for which the signs of s* and $\left(\frac{\partial c}{\partial r}\right)_t$ are opposite, if given any diffusion coefficient greater than zero, would exhibit a spatial derivative of its concentration that is opposite in sign to that of $\left(\frac{\partial c}{\partial r}\right)_t$ at position r and time t, so that the s* value of this solute reflects the location but not the orientation of $\left(\frac{\partial c}{\partial r}\right)_t$.

As has been stated, and as will be shown in some detail, all nonzero values of g(s*) are calculated from nonzero values of $\left(\frac{\partial c}{\partial s^*}\right)_t$, but not all nonzero values of $\left(\frac{\partial c}{\partial s^*}\right)_t$ are included in the calculation of g(s*). Those nonzero values of $\left(\frac{\partial c}{\partial s^*}\right)_t$ that do contribute to g(s*) are deemed essential, while those that do not are deemed redundant. Essential nonzero values of $\left(\frac{\partial c}{\partial s^*}\right)_t$ will be found where s* reflects both the location and the sign of $\left(\frac{\partial c}{\partial r}\right)_t$. Redundant nonzero values of $\left(\frac{\partial c}{\partial s^*}\right)_t$ will be found where s* reflects the location but not the sign of $\left(\frac{\partial c}{\partial r}\right)_t$.

As will be shown (Equation 28), the signs of $\left(\frac{\partial c}{\partial r}\right)_t$ and $\left(\frac{\partial c}{\partial s^*}\right)_t$ must be the same, or $\left(\frac{\partial c}{\partial r}\right)_t$ and $\left(\frac{\partial c}{\partial s^*}\right)_t$ must both equal zero. Thus, if the signs of s* and $\left(\frac{\partial c}{\partial s^*}\right)_t$ are the same, $\left(\frac{\partial c}{\partial s^*}\right)_t$ is essential. In contrast, if the signs of s* and $\left(\frac{\partial c}{\partial s^*}\right)_t$ are opposite, $\left(\frac{\partial c}{\partial s^*}\right)_t$ is redundant. (Even if the signs of s* and $\left(\frac{\partial c}{\partial s^*}\right)_t$ are the same, $\left(\frac{\partial c}{\partial s^*}\right)_t$ might be deemed redundant if, by its magnitude, its value is attributable to noise.)

Before moving on to the calculation of g(s*), the time-derivative approach (Stafford, 1992, 1994, 2000) for determining g(s*) will be described up to the point at which $\left(\frac{\partial c}{\partial s^*}\right)_t$ is obtained. From $\left(\frac{\partial c}{\partial s^*}\right)_t$ on, the calculation of g(s*) is the same, regardless of which approach is used to obtain $\left(\frac{\partial c}{\partial s^*}\right)_t$.

Stafford's (1992, 1994, 2000) derivation of g(s*) starts with the total differential of c with respect to s* and t,

$$dc = \left(\frac{\partial c}{\partial s^*}\right)_t ds^* + \left(\frac{\partial c}{\partial t}\right)_{s^*} dt \,,$$

(4)

from which, through division by an infinitesimally small change in t at constant r, the partial derivative of c with respect to t at constant r,

$$\left(\frac{\partial c}{\partial t}\right)_r = \left(\frac{\partial c}{\partial s^*}\right)_t \left(\frac{\partial s^*}{\partial t}\right)_r + \left(\frac{\partial c}{\partial t}\right)_{s^*},$$

(5)

is obtained. Solving Equation 5 for $\left(\frac{\partial c}{\partial s^*}\right)_t$ yields

$$\left(\frac{\partial c}{\partial s^*}\right)_t = \left[\left(\frac{\partial c}{\partial t}\right)_r - \left(\frac{\partial c}{\partial t}\right)_{s^*}\right]\left(\frac{\partial t}{\partial s^*}\right)_r.$$

(6)

Equation 6 can be applied using finite differences in c, t and s*. In the limit as the finite time-difference approaches zero, Equation 6 and Equation 3 yield identical results.

In yet another approach to obtain $\left(\frac{\partial c}{\partial s^*}\right)_t$, the variables on which c depends can first be

transformed from t and r to t and s*, following which, c can be differentiated with respect to s* at constant t. The result of this latter approach is identical to that obtained by Equation 3. Regardless of how it is obtained, $\left(\frac{\partial c}{\partial s^*}\right)_t$ is used identically for the remainder of this section, in which the time dependence of $\left(\frac{\partial c}{\partial s^*}\right)_t$ is minimised until all that remains is g(s*).

There are four time-dependent effects exhibited by $\left(\frac{\partial c}{\partial s^*}\right)_t$. The first of those addressed here is the time dependence of the positions (in terms of s*) and magnitudes of redundant nonzero values of $\left(\frac{\partial c}{\partial s^*}\right)_t$. This is the one time dependence that can be unambiguously eliminated, which is accomplished simply by subtracting the redundant nonzero values from $\left(\frac{\partial c}{\partial s^*}\right)_t$. Doing so leaves the nonredundant derivative of c with respect to s* at constant t,

$$q(s^*, t) = \left(\frac{\partial c}{\partial s^*}\right)_t - e(s^*, t) \,,$$

(7)

where e(s*,t) is equal $\left(\frac{\partial c}{\partial s^*}\right)_t$ wherever and whenever $\left(\frac{\partial c}{\partial s^*}\right)_t$ is redundant, but is equal to zero at all other s* and t. A test to determine which values of $\left(\frac{\partial c}{\partial s^*}\right)_t$ are redundant is described later (Equation 29).

The radial dilution/concentration effect is another time-dependent effect exhibited by $\left(\frac{\partial c}{\partial s^*}\right)_t$, and is the second such effect addressed here. This is one of the three time-dependent effects that remain present in q(s*,t). With respect to all hypothetical solutes, the radial dilution/concentration effect can be eliminated. Doing so leaves g(s*), which can thus be described as the plateau-corrected form of q(s*,t), given that the dilution/concentration effect

manifests itself as the time-dependence of plateau concentrations.

The most basic but least practical equation describing g(s*) in terms of q(s*,t) is

$$g(s^*) = q(s^*, t)\left(\frac{c_{0,s^*}}{c_{p,s^*}}\right),$$

(8)

where, for a hypothetical solute with a time-independent sedimentation coefficient of s*, c_{0,s^*} is the initial concentration throughout the system, and c_{p,s^*} is the plateau concentration at time t. Thus, multiplication of q(s*,t) by $\frac{c_{0,s^*}}{c_{p,s^*}}$ yields a product, g(s*,t), that is normalised for the effects of radial dilution or radial concentration that the plateau of the hypothetical solute would have accumulated by time t. As $\frac{c_{0,s^*}}{c_{p,s^*}}$ is always positive, the signs of g(s*) and q(s*,t) are the same, so that g(s*) differs from q(s*,t) solely with respect to magnitude. As will be shown (Equations 31 and 32), $\frac{c_{0,s^*}}{c_{p,s^*}}$ can be described entirely in terms of t, s* and ω.

The results of normalisation for the radial dilution/concentration may depend on the time, t, at which Equation 8 is applied to real systems, or simulated systems that model concentration-dependent transport. Real solutes tend to exhibit concentration-dependent, and thus time-dependent, sedimentation coefficients, and the real radial dilution/concentration effect depends, in part, on the sedimentation coefficients of real solutes. Consequently, the contribution of the radial dilution/concentration effect to the time-dependence of q(s*,t) is minimised in, but may not be entirely eliminated from, g(s*).

In the limit of zero diffusion, the boundary between the solute-depleted and plateau regions of a

real solute concentration would become hyper-sharp. Such a hyper-sharp transition would produce a sharp spike, upward or downward, in g(s*), and in a concentration-independent system, the position (s*) and magnitude (|g(s*)|) of such a spike would be time-independent. Where the diffusion coefficient of such a solute is nonzero, each such spike in g(s*) broadens into a peak or valley, the central position of which is time-independent in a concentration-independent system, but the height and breadth of which varies with time, even as the area of the peak or valley remains stable. This phenomenon, which is discussed next, is one of the two time-dependent effects that are not minimised in g(s*). The other is concentration-dependent transport, which is discussed shortly.

Nonzero diffusion coefficients cause the third time-dependent effect exhibited by $\left(\frac{\partial c}{\partial s^*}\right)_t$, and is one of the three time-dependent effects exhibited by q(s*,t). The effect is due to the fact that the range of s* (Equation 27; Figure 1) narrows in proportion to $\frac{1}{t}$, while the range of r encompassed by a diffusing boundary region broadens in proportion to $\frac{1}{\sqrt{t}}$ in the simplest, concentration-independent case (van Holde, 1985). (In terms of c as a function of r and t, a boundary region can be defined as any region within r where $\left|\left(\frac{\partial c}{\partial r}\right)_t\right| \neq 0$ at time t.) As a consequence of this effect, in an ideal system, g(s*) peaks grow higher with time, g(s*) valleys grow deeper with time, and in terms of g(s*) versus s*, the breadth of those peaks and valleys narrows with time, while the area of each peak or valley remains constant. In the limit of zero diffusion, g(s*) peaks and valleys are infinitesimally narrow at all times, and in the absence of concentration-dependent transport, their positions are time-independent.

In q(s*,t), the radial dilution/concentration effect, in combination with nonzero diffusion

coefficients, causes the area of each q(s*,t) peak to decrease with time, and causes the area of each q(s*,t) valley to increase with time. Although the magnitude of q(s*,t) is more time-dependent than that of g(s*), the peak and valley positions of the two functions are identical, as are the signs of their nonzero values. The essential nonzero values of $\left(\frac{\partial c}{\partial s^*}\right)_t$ are identical to q(s*,t) with respect to sign, magnitude and position. The essential and redundant nonzero values of $\left(\frac{\partial c}{\partial s^*}\right)_t$ differ with respect to position only. Compared to the essential nonzero values, the redundant nonzero values of $\left(\frac{\partial c}{\partial s^*}\right)_t$ are dislocated to highly time-dependent s* values of opposite sign.

Concentration-dependent transport causes the fourth time-dependent effect exhibited by $\left(\frac{\partial c}{\partial s^*}\right)_t$, and is the second of the two time-dependent effects that are not minimised in g(s*). In the simplest case, compared to a concentration-independent system, concentration-dependent transport simply adds a time-dependence to the weight-average positions of the peaks and valleys of q(s*,t) and g(s*). Concentration-dependent transport may also skew the shape of a peak or valley, and a chemical reaction can render the area of a g(s*) peak or valley time-dependent. Where concentration-dependent transport results in Johnston-Ogston effects, the number, position and magnitude of peaks and valleys in g(s*) can differ from that which would be seen otherwise. As with the previous effect, g(s*) and q(s*,t) differ only in magnitude, q(s*,t) is identical to the essential nonzero values of $\left(\frac{\partial c}{\partial s^*}\right)_t$, and redundant nonzero values of $\left(\frac{\partial c}{\partial s^*}\right)_t$ are located at highly time-dependent s* values at which $s^*\left(\frac{\partial c}{\partial s^*}\right)_t < 0$ (Equation 29).

Undetectable solutes, which do not contribute to the signal by which c (or some quantity related

to c) can be measured, will not directly contribute to $\left(\frac{\partial c}{\partial s^*}\right)_t$ anywhere at any time. No matter what its initial concentration, a solute that does not directly contribute to $\left(\frac{\partial c}{\partial s^*}\right)_t$ will not directly contribute to g(s*). Due to the concentration-dependence of real systems, however, a solute that does not directly contribute to g(s*) is likely to affect the results observed for all the detectable solutes. As such, indirect evidence for the presence of undetectable solutes may be observed in the form of an otherwise inexplicable time-dependence in g(s*).

The third and fourth time-dependent effects, which stem from nonzero diffusion coefficients and concentration-dependent transport, respectively, are fully present in g(s*). Given that, for any realistic system, g(s*) is expected to exhibit such time-dependent effects, it might be argued that g(s*) should be written as g(s*,t). Such a change in notation would be useful, in fact, when the focus is on time-dependent characteristics of that function. For now, however, the customary notation is retained. After all the explanatory equations are described, illustrative examples of the above time-dependent effects, and a comparison of |g(s*)| with ls-g(s*), will be shown and discussed. Later still, the equations describing c as a collection of step functions, to which g(s*) truly applies, will be presented.

Equations of continuity and mass flow

The Lamm equation, which is the continuity equation for centrifugation in a system with the geometry of a cylindrical sector, can be written as

$$\left(\frac{\partial c}{\partial t}\right)_r = -\frac{1}{r}\left(\frac{\partial rI}{\partial r}\right)_t,$$

(9)

where I is the total mass flow of all solutes.

In terms of D and s, the gradient-average diffusion and weight-average sedimentation coefficients, respectively, for all solute components,

$$I = rs\omega^2 c - D\left(\frac{\partial c}{\partial r}\right)_t ,$$

(10)

where ω is the angular velocity of the centrifuge rotor in the reference frame of the centrifuge. The angular velocity is given by

$$\omega = 2\pi\left(\frac{RPM}{60\ \frac{s}{min}}\right),$$

(11)

where RPM is the rotor speed in rotations per minute. As the angular velocity varies while the rotor accelerates, it is convenient to define ω as the time-independent angular velocity of the rotor after acceleration, and to define the centrifugation time as

$$t = \frac{1}{\omega}\int_{\tau_0}^{\tau_{clock}} \omega_\tau d\tau$$

(12)

(Stafford, 2000), where τ is the time in the reference frame of the system, τ_0 is equal to τ when the rotor acceleration starts, τ_{clock} is equal to a specific value of $\tau > \tau_0$, and ω_τ is the time-dependent angular velocity of the rotor. As $\omega_\tau = 0$ at τ_0, $t = 0$ at τ_0. (Henceforth, t_0 is used to denote $t = 0$.) Once rotor acceleration has stopped, ω_τ is equal to ω, and remains equal to ω for an extended time.

The continuity equation in the limit as $\left(\frac{\partial c}{\partial r}\right)_t$ *approaches zero*

In regions of the system where $\left(\frac{\partial c}{\partial r}\right)_t = 0$, which condition can only persist if $\left(\frac{\partial s}{\partial r}\right)_t = 0$ wherever $\left(\frac{\partial c}{\partial r}\right)_t = 0$, Equations 9 and 10 lead to

$$\lim_{\left(\frac{\partial c}{\partial r}\right)_t \to 0} \left(\frac{\partial c}{\partial t}\right)_r = \frac{dc}{dt} = -2s\omega^2 c.$$

(13)

To describe this condition in detail, let the lowest and highest radial positions of a region where Equation 13 holds be denoted as r_{min} and r_{max}, respectively, where, in general, r_{min} and r_{max} are time-dependent. Within a time-dependent region where Equation 13 holds, which is to say, within $r_{min} \leq r \leq r_{max}$, $c = c_p$, where c_p is the time-dependent plateau concentration. The plateau concentration is the total concentration of all solutes within $r_{min} \leq r \leq r_{max}$, and its time dependence stems from the radial dilution/concentration effect. At any given time, $\left(\frac{\partial c_p}{\partial r}\right)_t = 0$. For the systems considered here, at t_0, at all r, $c = c_0$, where c_0 is the initial total concentration of all solutes. Thus, $c_p = c_0$ at t_0, at which time, $r_{min} = r_m$ and $r_{max} = r_b$, where r_m is the radial position of the meniscus, and r_b is the radial position of the base of the system. (All r lie within r_m and r_b.)

Within any region where Equation 13 holds, the equation can be solved by separation of variables and integration. Assuming that any apparent dependence of s on t is really a dependence of s on c, such a solution takes the form of

$$\int_{c_0}^{c_p} \frac{dc}{sc} = -2\omega^2 \int_{t_0}^{t_p} dt\,,$$

(14)

where the right-hand side evaluates to $-2\omega^2 t_p$, and t_p is the time at which $c = c_p$ within $r_{min} \leq r \leq r_{max}$. The left-hand side cannot be evaluated without knowing the function that describes the dependence of s on c. In what follows, however, a realistic description of s is not needed, as what is sought is a function that quantifies the distribution of the solute components with respect to an independent variable, s*.

At a given time and radial position, there are as many concentration-dependent sedimentation coefficients as there are solute species, and s is equal to their weight average. Instead of describing the system in terms of this finite number of concentration-dependent sedimentation coefficients that underlie s at a given time and radial position, the system is described in terms of an infinite number of apparent sedimentation coefficients, each of which is concentration-independent. Each apparent sedimentation coefficient, s*, satisfies an equation,

$$\int_{c_{0,s^*}}^{c_{p,s^*}} \frac{dc_{s^*}}{c_{s^*}} = -2s^*\omega^2 \int_{t_0}^{t_p} dt \,,$$

(15)

in which c_{s^*} is the concentration of a hypothetical solute characterised by s* in the limit as D*, the diffusion coefficient of that solute, approaches zero. There is an infinite number of such integrals. At t_0, within $r_m \leq r \leq r_b$, c_{s^*} would equal c_{0,s^*}. More generally, at t_p, within $r_{min} \leq r \leq r_{max}$, c_{s^*} would equal c_{p,s^*}.

The right-hand side of Equation 15 evaluates to $-2s^*\omega^2 t_p$, and the left-hand side evaluates to $ln\left(\frac{c_{p,s^*}}{c_{0,s^*}}\right)$. Solving for c_{p,s^*} yields

$$c_{p,s^*} = c_{0,s^*} e^{-2s^*\omega^2 t_p} \,.$$

(16)

The exponential term is equal to the extent of radial dilution (if $s^* > 0$) or radial concentration (if $s^* < 0$) that would be observed from t_0 to t_p in the plateau region of a purely hypothetical solute characterised by a concentration-independent sedimentation coefficient of s* and an initial ($t = t_0$) concentration of c_{0,s^*}. Solving Equation 16 for $\frac{c_{0,s^*}}{c_{p,s^*}}$ yields an expression of the normalisation factor (for the effects of radial dilution or concentration) of Equation 8 in terms of ω, t_p and s*.

Solving Equation 16 for s* yields, for $t_p > t_0$,

$$s^* = \frac{1}{2\omega^2 t_p} ln\left(\frac{c_{0,s^*}}{c_{p,s^*}}\right).$$

(17)

At time $t_p > t_0$ and angular velocity ω, and for a given c_{0,s^*}, Equation 17 expresses s* as a function of c_{p,s^*}, such that $s^* < 0$ for $c_{0,s^*} < c_{p,s^*}$, $s^* = 0$ for $c_{0,s^*} = c_{p,s^*}$, and $s^* > 0$ for $c_{0,s^*} > c_{p,s^*}$. At t_0, s* is undefined.

Solving Equation 17 for t_p and taking the partial derivative with respect to s* at constant $\frac{c_{0,s^*}}{c_{p,s^*}}$ yields

$$\left(\frac{\partial t_p}{\partial s^*}\right)_{\frac{c_{0,s^*}}{c_{p,s^*}}} = \frac{-1}{2\omega^2 {s^*}^2} ln\left(\frac{c_{0,s^*}}{c_{p,s^*}}\right) = -\frac{t_p}{s^*},$$

(18)

which, if equal to $\left(\frac{\partial t}{\partial s^*}\right)_r$, is one of the terms needed to make use of Equation 6. A more general expression for $\left(\frac{\partial t}{\partial s^*}\right)_r$ will be derived shortly (Equation 30).

The equation of mass flow in the limit as $\left(\frac{\partial c}{\partial r}\right)_t$ *approaches zero*

An equation is sought that describes s* in terms of r and t, which are the independent variables of Equations 9 and 10. To that end, the same limit that was applied to Equation 9 is now applied to Equation 10.

In the limit as $\left(\frac{\partial c}{\partial r}\right)_t$ approaches 0, Equation 10 reduces to

$$\lim_{\left(\frac{\partial c}{\partial r}\right)_t \to 0} I = cs\omega^2 r \, .$$

(19)

The mass flow, I, is equal to cv, where, in the system frame of reference, v is the weight-average velocity of all solute components at t and r. Expressing v as $\frac{dr}{dt}$, and dividing Equation 19 by c, results in

$$\lim_{\left(\frac{\partial c}{\partial r}\right)_t \to 0} v = \frac{dr}{dt} = s\omega^2 r \, .$$

(20)

Wherever $\left(\frac{\partial c}{\partial r}\right)_t = 0$, $\left(\frac{\partial s}{\partial r}\right)_t = 0$, in which case, if the functional form of the t-dependence of s were known, Equation 20 might be solved by separation of variables and integration. Such a solution would take the form of

$$\int_{r_0}^{r_s} \frac{dr}{r} = \omega^2 \int_{t_0}^{t_s} s dt \, ,$$

(21)

where r_0 would be the extreme radial position away from which a hypothetical solute with a sedimentation coefficient of s would travel, and at time t_s, r_s would be the radial position of the

transition in the concentration of that solute in the zero-diffusion limit.

As the relationship between s and t is complicated, Equation 20 is solved using the same approach applied to the similar problem presented by Equation 13. The c-dependent parameter, s, in Equation 20 is replaced with an infinite number of c-independent, and therefore t-independent, s* values, resulting in an infinite number of integrals, each of which applies to a hypothetical solute, and each of which is given by

$$\int_{r_0}^{r_{s^*}} \frac{dr}{r} = s^* \omega^2 \int_{t_0}^{t_{s^*}} dt,$$

(22)

where r_0 is the extreme radial position (r_m for $s^* > 0$, and r_b for $s^* < 0$) away from which a hypothetical solute of sedimentation coefficient s* travels, r_{s^*} is the radial position of the transition in the concentration of that solute in the zero-diffusion limit, and t_{s^*} is the time that corresponds to the location of that transition at r_{s^*}.

For each such hypothetical solute, $r_0 = r_b$ if $s^* < 0$, and $r_0 = r_m$ if $s^* > 0$. At time t_{s^*}, at radial position r_{s^*}, each such solute exhibits a transition in concentration from 0 to c_{p,s^*}, where c_{p,s^*} is the plateau concentration of that solute at t_{s^*}. (The parameter t_p in Equation 15 is thus readily equated to the parameter t_{s^*} in Equation 22, and both will shortly be equated to t.) At any given time, the concentration of such a solute could be described by a step function equal to 0 from r_0 to r_{s^*}, and equal to c_{p,s^*} from r_{s^*} to the extremity at the opposite end of the system from r_0. (The extremity at the opposite end of the system from r_0 is r_m if $r_0 = r_b$, or at r_b if $r_0 = r_m$.)

The right-hand side of Equation 22 evaluates to $s^*\omega^2 t_{s^*}$, and the left-hand of Equation 22

evaluates to $ln\left(\frac{r_{s^*}}{r_0}\right)$. Solving for r_{s^*} yields

$$r_{s^*} = r_0 e^{s^*\omega^2 t_{s^*}} ,$$

(23)

which describes the boundary position (the transition point of the corresponding step function) that would be observed for a purely hypothetical solute characterised by a sedimentation coefficient of s*, in the limit as D* (the solute's diffusion coefficient) approached zero.

If analytic solutions of Equations 14 and 21 existed, they would only apply to a plateau region. In contrast, Equations 16 and 23, which are the analytic solutions of Equations 15 and 22, respectively, can be applied to the entire system. Thus, a description of the whole system is gained at the remarkably low cost of having to cast that description in terms of an infinite set of imaginary, nondiffusing, concentration-independent solutes.

Based on Equations 16 and 23, the relationship between the plateau concentration and the boundary position of a hypothetical solute of sedimentation coefficient s*, in the limit as D* approaches zero, can be described by

$$c_{s^*} = \begin{Bmatrix} 0\ at\ \begin{Bmatrix} r < r_{s^*} = r_m e^{s^*\omega^2 t_{s^*}}\ for\ s^* > 0 \\ r > r_{s^*} = r_b e^{s^*\omega^2 t_{s^*}}\ for\ s^* < 0 \end{Bmatrix} \\ c_{p,s^*}\ at\ \begin{Bmatrix} r \geq r_{s^*} = r_m e^{s^*\omega^2 t_{s^*}}\ for\ s^* \geq 0 \\ r \leq r_{s^*} = r_b e^{s^*\omega^2 t_{s^*}}\ for\ s^* \leq 0 \end{Bmatrix} \end{Bmatrix} .$$

(24)

Equation 24 describes c_{s^*} as a step function with a time-dependent height of c_{p,s^*} (Equation 16), and a time-dependent transition at $r_0 e^{s^*\omega^2 t_{s^*}}$ (Equation 23), where $r_0 = r_m$ for $s^* > 0$, and $r_0 = r_b$

for $s^* < 0$. Over time, for $s^* \neq 0$, the region in which $c_{s^*} = 0$ expands from r_0 to $r_0 e^{s^* \omega^2 t_{s^*}}$. While c_{s^*} depends on r and t, c_{p,s^*} depends on t and c_{0,s^*} (Equation 16). Thus, $\left(\frac{\partial c_{p,s^*}}{\partial r}\right)_t = 0$. As there is an infinite number of s* values, at any given time, there is an infinite number of step functions, each given by Equation 24. The sum of all such step functions at a given time yields c as a function of r at that time.

A real incarnation of a hypothetical solute would accumulate as either a pellet (from r_b to some point back), if negatively buoyant, or a supernatant (from r_m to some point forward), if positively buoyant. Thus, for a real solute, either the pellet or supernatant concentration would exceed the plateau concentration. Each hypothetical solute, however, is only permitted one of two possible concentrations, which are 0 and c_{p,s^*}.

In data obtained from real systems, or realistically simulated systems, including the pellet and supernatant in the regions subjected to g(s*) analysis results in nonzero c_{p,s^*} values being found toward the extrema (Equations 35 and 36) in s* at any given time. Such nonzero c_{p,s^*} values toward the extrema in s* can be misleading, however, as all that can be said of the solutes in a pellet is that their sedimentation coefficients would be greater than or equal to zero if relocated to the radial position just below the pellet, and all that can be said of the solutes in a supernatant is that their sedimentation coefficients would be less than or equal to zero if relocated to the radial position just above the supernatant.

Transforming the independent variables from r and t to s and t*

Solving Equation 23 for s* yields

$$s^* = \frac{1}{\omega^2 t_{s^*}} ln\left(\frac{r_{s^*}}{r_0}\right).$$

(25)

For each time, t, the set of all radial positions, r, is now equated to the set of boundary positions, r_{s^*}, needed to transform the independent variable r to the independent variable s*. Replacing r_{s^*} and t_{s^*} of Equation 23 with r and t, respectively, results in

$$r = r_0 e^{s^* \omega^2 t},$$

(26)

which, solved for s*, yields

$$s^* = \frac{1}{\omega^2 t} ln\left(\frac{r}{r_0}\right) = \begin{Bmatrix} \frac{1}{\omega^2 t} ln\left(\frac{r}{r_b}\right) \leq 0 \\ \frac{1}{\omega^2 t} ln\left(\frac{r}{r_m}\right) \geq 0 \end{Bmatrix}.$$

(27)

At a constant (and nonzero) ω, s* is a function of t, r and r_0, such that $s^* < 0$ for $r_0 > r$, $s^* = 0$ for $r_0 = r$, $s^* > 0$ for $r_0 < r$, and for a given value of $\frac{r}{r_0}$, $|s^*|$ decreases as t increases. As r_m and r_b are the two possible values of r_0, at a given $\omega^2 t > 0$, for each radial position r within $r_m \leq r \leq r_b$, there are two values of s*. For each radial position r within $r_m < r < r_b$, at a given $\omega^2 t > 0$, there is one negative and one positive value of s*. For $r = r_m$, one s* equals zero and the other is less than zero at any $\omega^2 t > 0$. For $r = r_b$, one s* equals zero and the other is greater than zero at any $\omega^2 t > 0$. At a given $\omega^2 t > 0$, the minimum value of s* occurs where $r = r_m$ and $r_0 = r_b$, while the maximum value of s* occurs where $r = r_b$ and $r_0 = r_m$. At t_0, s* is undefined for all r. As can be seen by equating $-\frac{1}{\omega^2 t} ln\left(\frac{r}{r_b}\right)$ to $\frac{1}{\omega^2 t} ln\left(\frac{r}{r_m}\right)$ and solving for r, there is one radial position, $r = (r_m r_b)^{0.5}$, for

which, at any given time, the positive s* equals the absolute value of the negative s*. Figure 1 illustrates the relationship between t, r and s* at 60,000 RPM, $r_m = 6$ cm and $r_b = 7.2$ cm.

As previously discussed, the time-dependent effects of nonzero diffusion coefficients and concentration-dependent transport are fully present in g(s*). To these can be added the trivial time dependence that results from the extrema in s* approaching zero as time approaches infinity (Equation 27; Figure 1).

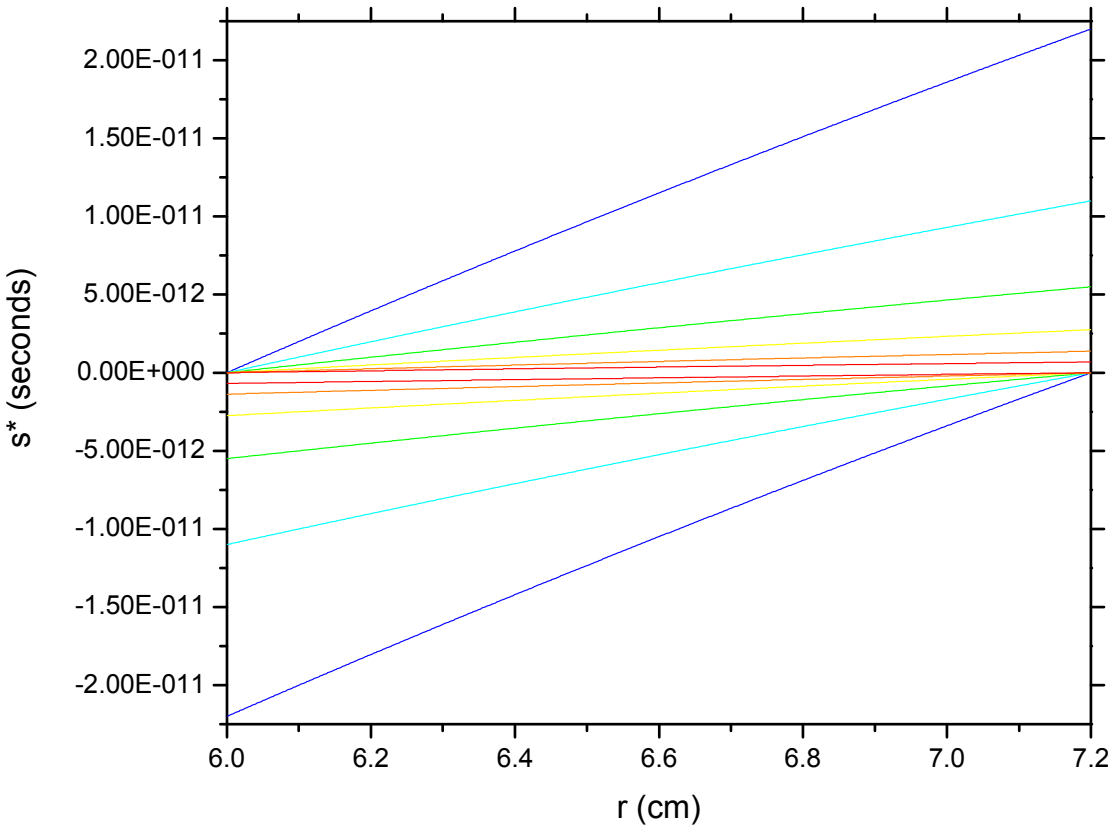

Figure 1. The dependence of s* on radial position at times $t_1 = 210$ s (——), $t_2 = 2t_1$ (——), $t_4 = 4t_1$ (——), $t_8 = 8t_1$ (——), $t_{16} = 16t_1$ (——) and $t_{32} = 32t_1$ (——), for a system in which $r_m = 6$ cm, $r_b = 7.2$ cm, and ω is that calculated (by Equation 11) for 60,000 RPM. (Figure 10 also

illustrates the relationship between t, r and s*, but with the r and s* axes exchanged.) As s* is inversely proportional to t (Equation 27), the range of s* decreases with time, with the extrema approaching $s^* = 0$ symmetrically from above and below as t approaches infinity. Going backwards in time, as t approaches zero, all s* approach either -∞ or ∞. As noted with respect to Equation 27, at any given time, there is one radial position, $r = (r_m r_b)^{0.5}$, for which |s*| is the same, whether $s^* < 0$ or $s^* > 0$. (In the example shown here, $(r_m r_b)^{0.5} = 6.573$ cm.)

Determining q(s,t) from $\left(\frac{\partial c}{\partial s^*}\right)_t$, and expressing g(s*) in terms of q(s*,t), r, t and ω*

Differentiating Equation 26 with respect to s* at constant t yields

$$\left(\frac{\partial r}{\partial s^*}\right)_t = \omega^2 t r_0 e^{s^* \omega^2 t} = r\omega^2 t \,,$$

(28)

which has the dimensions of a velocity. (Compare Equation 28 with Equation 20.) Where r is discontinuous or equal to one of its extrema, however, this derivative is ill defined. (See Figure 10.)

According to Equation 28, $\left(\frac{\partial r}{\partial s^*}\right)_t$ must be greater than zero at all $t > t_0$. Therefore, as Equation 3 states that $\left(\frac{\partial c}{\partial s^*}\right)_t = \left(\frac{\partial c}{\partial r}\right)_t \left(\frac{\partial r}{\partial s^*}\right)_t$, the sign of $\left(\frac{\partial c}{\partial s^*}\right)_t$ must be determined by the sign of $\left(\frac{\partial c}{\partial r}\right)_t$. As discussed with respect to Equation 3, nonzero values of $\left(\frac{\partial c}{\partial s^*}\right)_t$ that contribute to g(s*) are deemed essential, while those that do not are deemed redundant.

Essential nonzero values of $\left(\frac{\partial c}{\partial s^*}\right)_t$ are found where s* reflects both the location (r) and the

orientation (sign) of $\left(\frac{\partial c}{\partial r}\right)_t$. Redundant nonzero values of $\left(\frac{\partial c}{\partial s^*}\right)_t$ are found where s* reflects the location but not the sign of $\left(\frac{\partial c}{\partial r}\right)_t$. This distinction provides the basis for a test parameter,

$$Q_{s^*,t} = s^* \left(\frac{\partial c}{\partial s^*}\right)_t .$$

(29)

If $Q_{s^*,t} > 0$, $\left(\frac{\partial c}{\partial s^*}\right)_t$ is essential and e(s*,t) is equated to zero, but if $Q_{s^*,t} \leq 0$, e(s*,t) is equated to $\left(\frac{\partial c}{\partial s^*}\right)_t$. By definition (Equation 7), q(s*,t) is equal to $\left(\frac{\partial c}{\partial s^*}\right)_t$ minus the redundant values of $\left(\frac{\partial c}{\partial s^*}\right)_t$ collected in e(s*,t). Thus, q(s*,t) is equal to $\left(\frac{\partial c}{\partial s^*}\right)_t$ if $\left(\frac{\partial c}{\partial s^*}\right)_t$ is essential, and zero otherwise.

The relationship between q(s*,t) and $\left[\left(\frac{\partial c}{\partial t}\right)_r - \left(\frac{\partial c}{\partial t}\right)_{s^*}\right]$ of Equation 6 becomes clear once $\left(\frac{\partial t}{\partial s^*}\right)_r$ has been expressed in terms of s* and t. Solving Equation 26 for t and differentiating with respect to s* at constant r yields

$$\left(\frac{\partial t}{\partial s^*}\right)_r = \frac{-1}{(\omega s^*)^2} ln\left(\frac{r}{r_0}\right) = -\frac{t}{s^*},$$

(30)

which, for $t = t_p$, is the same result obtained in Equation 18. As t cannot be less than zero, Equations 18 and 30 show that the signs of $\left(\frac{\partial t}{\partial s^*}\right)_r$ and s* are always opposite. Given this, and given the relationship (Equation 29) between s* and essential nonzero values of $\left(\frac{\partial c}{\partial s^*}\right)_t$, it follows that the sign of any essential nonzero value of $\left(\frac{\partial c}{\partial s^*}\right)_t$ and the sign of $\left(\frac{\partial t}{\partial s^*}\right)_r$ must be opposite at any time after t_0. Thus, in Equation 6, which states that $\left(\frac{\partial c}{\partial s^*}\right)_t = \left[\left(\frac{\partial c}{\partial t}\right)_r - \left(\frac{\partial c}{\partial t}\right)_{s^*}\right]\left(\frac{\partial t}{\partial s^*}\right)_r$, the difference, $\left[\left(\frac{\partial c}{\partial t}\right)_r - \left(\frac{\partial c}{\partial t}\right)_{s^*}\right]$, must be less than zero for all essential nonzero values of $\left(\frac{\partial c}{\partial s^*}\right)_t$, and must be

greater than zero for all redundant nonzero values of $\left(\frac{\partial c}{\partial s^*}\right)_t$.

Equating the right-hand sides of Equations 17 and 25, at $t = t_p = t_{s^*}$, the relationship,

$$\frac{c_{0,s^*}}{c_{p,s^*}} = \left(\frac{r_{s^*}}{r_0}\right)^2,$$

(31)

is obtained. In combination with either Equation 16 or Equation 23, Equation 31 permits Equation 8 to be rewritten in various forms, such as

$$g(s^*) = q(s^*, t)\left(\frac{1}{e^{-2s^*\omega^2 t}}\right) = q(s^*, t)\left(e^{s^*\omega^2 t}\right)^2.$$

(32)

Equation 32 shows that the sign of g(s*) is determined solely by q(s*,t). As noted with respect to Equations 7 and 29, q(s*,t) is equal to $\left(\frac{\partial c}{\partial s^*}\right)_t$ minus the redundant values, so that q(s*,t) is equal to $\left(\frac{\partial c}{\partial s^*}\right)_t$ wherever the signs of s* and $\left(\frac{\partial c}{\partial s^*}\right)_t$ are the same. Thus, where g(s*) is not equal to zero, the signs of s* and g(s*) are the same.

Concentration change across a transition point (r_{s^*}), and concentration within an s range*

A real boundary may encompass multiple species' boundaries, each of which is broadened by diffusion and affected by the concentration of each species present. In g(s*) analysis, such a boundary is modeled as a set of hyper-sharp transitions in concentration, where each transition corresponds to a hypothetical solute characterised by a concentration-independent sedimentation coefficient of s*, an initial concentration of c_{0,s^*}, and a diffusion coefficient that approaches zero.

At a given time, t, the difference in the detectable concentration between two adjacent plateau regions separated by a boundary is Δc_t, where the subscript t indicates a time-dependent quantity. For a boundary located between $r_{s^*_{below}}$ and $r_{s^*_{above}}$,

$$\Delta c_t = \int_{s^*_{below}}^{s^*_{above}} \left(\frac{\partial c}{\partial s^*}\right)_t ds^*,$$

(33)

where s^*_{below} and s^*_{above} are calculated from $r_{s^*_{below}}$ and $r_{s^*_{above}}$, respectively, using Equation 27. In the plateau regions just below s^*_{below} and just above s^*_{above}, $\left(\frac{\partial c}{\partial s^*}\right)_t = 0$. If all s* are less than zero within $s^*_{below} \leq s^* \leq s^*_{above}$, as would be the case for $r_{s^*_{below}} = r_{max}$ of the plateau for which c is higher, Δc_t will be less than zero. If all s* are greater than zero within $s^*_{below} \leq s^* \leq s^*_{above}$, as would be the case for $r_{s^*_{above}} = r_{min}$ of the plateau for which c is higher, Δc_t will be greater than zero. (Respectively, r_{min} and r_{max} are the lowest and highest radial positions of a region where Equation 13 holds.)

The substantially time-normalised, cumulative concentration of detectable solutes that can be characterised by s* within $s^*_{below} \leq s^* \leq s^*_{above}$ is

$$\Delta c = \int_{s^*_{below}}^{s^*_{above}} |g(s^*)| ds^*.$$

(34)

The result cannot be less than zero. If $s^*_{below} \leq s^* \leq s^*_{above}$ encompasses an entire peak or valley of g(s*), Δc should, in the absence of overlapping boundaries of oppositely directed and detectable solutes (Figures 23 to 27), be time-independent for concentration-independent systems, as well as for concentration-dependent systems in which the solute concentrations are

not altered by chemical reactions.

The range of integration in Equation 34 can be extended to the extrema of s*. The extrema in s* are inversely proportional to $\omega^2 t$. At time t and angular velocity ω,

$$s^*_{-x} = \frac{1}{\omega^2 t} ln\left(\frac{r_m}{r_b}\right)$$

(35)

is the minimum value of s*, and

$$s^*_{+x} = \frac{1}{\omega^2 t} ln\left(\frac{r_b}{r_m}\right)$$

(36)

is the maximum value of s*. As noted with respect to Equation 27, each radial position gives rise to two s* values. At $r = r_m$, $s^* = s^*_{-x}$ for $r_0 = r_b$ (Equation 35) and $s^* = 0$ for $r_0 = r_m$. Likewise, at $r = r_b$, $s^* = s^*_{+x}$ for $r_0 = r_m$ (Equation 36) and $s^* = 0$ for $r_0 = r_b$. With the integration limits of Equation 34 set to $s^*_{below} = s^*_{-x}$ and $s^*_{above} = s^*_{+x}$, Δc is equal to the apparent value of c_0, which is to say, the apparent initial concentration of all solutes that contribute to $\left(\frac{\partial c}{\partial s^*}\right)_t$, and thus contribute to g(s*).

The range of integration in Equation 33 can also be extended to the extrema of s*, and with the addition of an offset, can be used to reconstruct c as a function of s* and t. At any given time, t, the concentration at $s^* = s^*_{neg} < 0$ is given by

$$c = c_{-x} + \int_{s^*_{-x}}^{s^*_{neg}} \left(\frac{\partial c}{\partial s^*}\right)_t ds^*,$$

(37a)

and the concentration at $s^* = s^*_{pos} > 0$ is given by

$$c = c_{-x} + \int_{s^*_{-x}}^{0} \left(\frac{\partial c}{\partial s^*}\right)_t ds^* + \int_{0}^{s^*_{pos}} \left(\frac{\partial c}{\partial s^*}\right)_t ds^* = c_{0+} + \int_{0}^{s^*_{pos}} \left(\frac{\partial c}{\partial s^*}\right)_t ds^*,$$

(37b)

where, at time t, c_{-x} is equal to c corresponding to s*in the limit as s^*_{-x} is approached from above, and c_{0+} is equal to c corresponding to s*in the limit as 0 is approached from above. The offsets, c_{-x} and c_{0+}, should be equal.

Experimentally obtained data can be complicated by optical artefacts near r_m and r_b, as well as by inaccuracies wherever the solute concentration is outside the suitable range of the detection system, and over time, unsuitably high solute concentrations are likely to develop toward r_m or r_b. Outside of some well behaved simulations, then, when using Equation 37, the practical range of s* will not extend to either of the theoretical extrema, s^*_{-x} or s^*_{+x}. In general, to accommodate such limitations, the offset of Equation 37a will equal c corresponding to s*in the limit as its lowest practical negative value is approached from above, and the offset of Equation 37b will equal c corresponding to s*in the limit as its lowest practical positive value is approached from above.

The cumulative distribution function,

$$G(s^*) = \int_{s^*_{-x}}^{s^*} |g(\varsigma^*)| d\varsigma^*,$$

(38)

permits Equation 34 to be rewritten as $\Delta c = G(s^*_{above}) - G(s^*_{below})$. The cumulative distribution function is a substantially time-normalised, but not entirely time-independent, measure of the concentration of all solutes for which the apparent sedimentation coefficient is less than or equal

to s*, but greater than or equal to s^*_{-x} at some specific time.

Evaluation of $\left(\frac{\partial c}{\partial s^*}\right)_t$

Although c is a continuous function of either r and t or s* and t, c rarely takes on a convenient functional form. Instead, it is usually necessary to deal with a finite set of discontinuous c versus r or c versus s* values at a finite set of discontinuous time-points. If the data are not too sparse, however, finite differences in c, r, s* and t can yield good approximations of the partial derivatives, $\left(\frac{\partial c}{\partial r}\right)_t$, $\left(\frac{\partial c}{\partial s^*}\right)_t$, $\left(\frac{\partial c}{\partial t}\right)_r$, $\left(\frac{\partial c}{\partial t}\right)_{s^*}$ and $\left(\frac{\partial t}{\partial s^*}\right)_r$, that appear in Equations 3 and 6, but cannot be calculated with an applicable function, such as that (Equation 28) which describes $\left(\frac{\partial r}{\partial s^*}\right)_t$. (Although Equation 30 is a functional description of $\left(\frac{\partial t}{\partial s^*}\right)_r$, that function applies to a specific time. Thus, when using finite differences in time to evaluate the derivatives of Equation 6, the approximation of $\left(\frac{\partial t}{\partial s^*}\right)_r$ described by Equations 42 to 44 is used instead of Equation 30.)

At any given time, $\left(\frac{\partial c}{\partial r}\right)_t$ and $\left(\frac{\partial c}{\partial s^*}\right)_t$ can be approximated as $\frac{\Delta c}{\Delta r}$ and $\frac{\Delta c}{\Delta s^*}$, respectively, using finite differences in c, r and s*. Approximating either derivative from the data at a single time-point eliminates any noise that stems from a radially-independent (RI) offset in the signal related to c, but the approximated derivative of the time-independent (TI) noise in that signal will propagate to either $\frac{\Delta c}{\Delta r}$ or $\frac{\Delta c}{\Delta s^*}$. (Equation 99 describes a TI-noise corrected application of Equation 3.)

Finite differences can also be used to estimate partial derivatives of c with respect to time. Subtracting c versus r data at one time from c versus r data at another time is simple to do,

provided that, as is the case in the examples shown below, the radial positions are the same at all times. Once sets of c versus r data at multiple times have been transformed to c versus s* data at those times, subtracting c versus s* data at one time from c versus s* data at another time requires the interpolation of at least one set of c values with respect to s*.

Evaluation of $\left(\frac{\partial c}{\partial s^*}\right)_t$ *, either directly or from* $\left(\frac{\partial c}{\partial r}\right)_t$

Figure 2 shows AUC simulation results, as c versus r, from a hypothetical system at t = 2916 s. This data set will be used to determine $\left(\frac{\partial c}{\partial s*}\right)_t$ from $\left(\frac{\partial c}{\partial r}\right)_t$ at t = 2916 s. Figure 3 shows the results, plotted as c versus s*, from the same hypothetical system at the same time. This data set will be used to directly determine $\left(\frac{\partial c}{\partial s*}\right)_t$ at t = 2916 s. The hypothetical system is described in Figure 2.

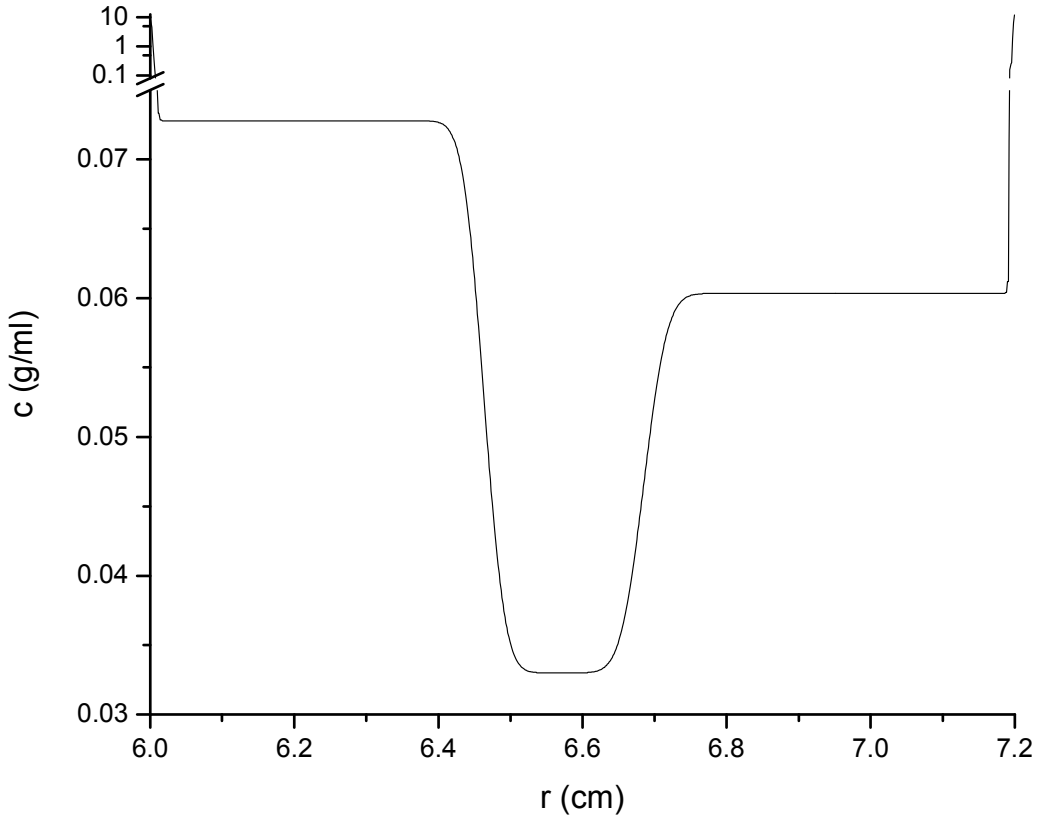

Figure 2. A plot of c versus r at t = 2916 s, with the supernatant (toward $r_m = 6$ cm) and pellet (toward $r_b = 7.2$ cm) regions of c shown on a logarithmic scale above the break. (A few erratic points in the supernatant and pellet regions have been smoothed.) The data are from a simulation of a concentration-independent, three-component system subjected to AUC at 60,000 RPM, and described as follows, where component-specific parameters are subscripted by a numerical identifier (1, 2 or 3): at t_0, at all r, $c_1 = 3.389$E-02 g/ml, $c_3 = 3.211$E-02 g/ml, $c_2 = 3.300$E-02 g/ml; at all t and all r, $s_1 = 9.324$E-13 s, $s_3 = -s_1$, $s_2 = 0$, $D_1 = 9.126$E-08 cm^2/s, $D_3 = D_1$, and $D_2 = 7.243$E-08 cm^2/s. (The unrealistic results in the supernatant and pellet regions are due to the transport coefficients being independent of concentration.) The model system is a simplified version of one described previously (Moody, 2012). The following parameters had no effect on the results, but describe some of the relationships between the components: The

solvent was a model buffer with a density of $\rho_0 = 1.08225$ g/ml; each component was modelled as consisting of spherical solutes for which the anhydrous radius was 0.65 times the hydrated radius; the specific gravities of the solute components were $\rho_1 = 1.11150$ g/ml, $\rho_3 = 1.05300$ g/ml and $\rho_2 = \rho_0$; and the molar masses of the model components were $M_1 = 9{,}462{,}869$ g/mol, $M_3 = 8{,}964{,}823$ g/mol, and $M_2 = M_1 + M_3$. The concentrations and molar masses are such that, at t_0, $c_1/M_1 = c_3/M_3 = 2c_2/M_2$ at all r.

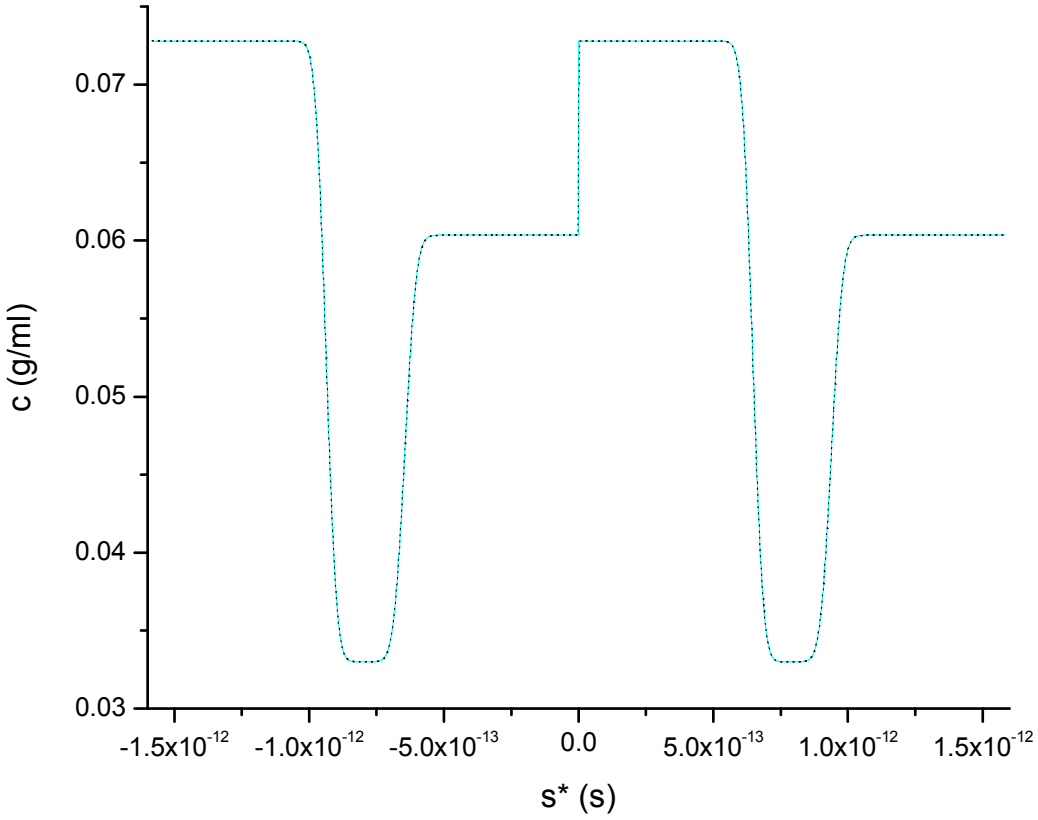

Figure 3. A plot of c versus s* at t = 2916 s (——). The data are the same as those shown in Figure 2, but with the independent variable r transformed to s*. In further contrast to Figure 2, the supernatant (between r = 6.01831 cm and $r_m = 6$ cm in Figure 2) and pellet (between r = 7.18593 cm and $r_b = 7.2$ cm in Figure 2) regions of c have been removed from the data used in this figure, and replaced with the adjacent plateau values of c. The data determined by the

application of Equation 37 (·····) to $\left(\frac{\partial c}{\partial s^*}\right)_t$ (Figure 4), with $c_{-x} = 0.0728$ g/ml, are superimposed on the results obtained by simply plotting c at each value of r (Figure 2) against the two corresponding values of s* calculated (Equation 27) for ω at 60,000 RPM (Equation 11) and t = 2916 s.

$\left(\frac{\partial c}{\partial s^*}\right)_t$ *from the direct differentiation of c versus s* at constant t*

Of the two values of s* obtained for each radial position at any given time, $Q_{s^*,t}$ (Equation 29) will be positive at no more than one. Wherever and whenever $Q_{s^*,t}$ is negative, $\left(\frac{\partial c}{\partial s^*}\right)_t$ is deemed redundant and e(s*,t) is equated to it, so that, upon application of Equation 7, q(s*,t) is either equal to zero or to those values of $\left(\frac{\partial c}{\partial s^*}\right)_t$ deemed essential for determining g(s*). (In the figures that follow, the derivative of c with respect to s* at constant t is denoted as $\left(\frac{\partial c}{\partial s^*}\right)_t$, but estimated as $\frac{\Delta c}{\Delta s^*}$.)

Figure 4 shows $\left(\frac{\partial c}{\partial s^*}\right)_t$ obtained by direct differentiation of c with respect to s* at constant t, where the c versus s* data are those shown in Figure 3. Whenever there is a difference in the concentrations at the extrema in r, a plot of c versus s* will exhibit an equal concentration difference across s* = 0. Thus, direct differentiation of c with respect to s* at constant t produces a sharp upward or downward spike in $\left(\frac{\partial c}{\partial s^*}\right)_t$ about s* = 0. Just such a spike is seen in Figure 4. Figure 4 also shows q(s*,t) obtained by application of Equations 29 and 7.

(In general, the examples presented here proceed from the least complicated to the most complicated, but the more complicated cases are presented. Had the concentrations toward the extrema in s* not been replaced with the adjacent plateau concentrations, for example, Figures 3 and 4 would have looked much like the data at t = 2910 s in Figures 24 and 25.)

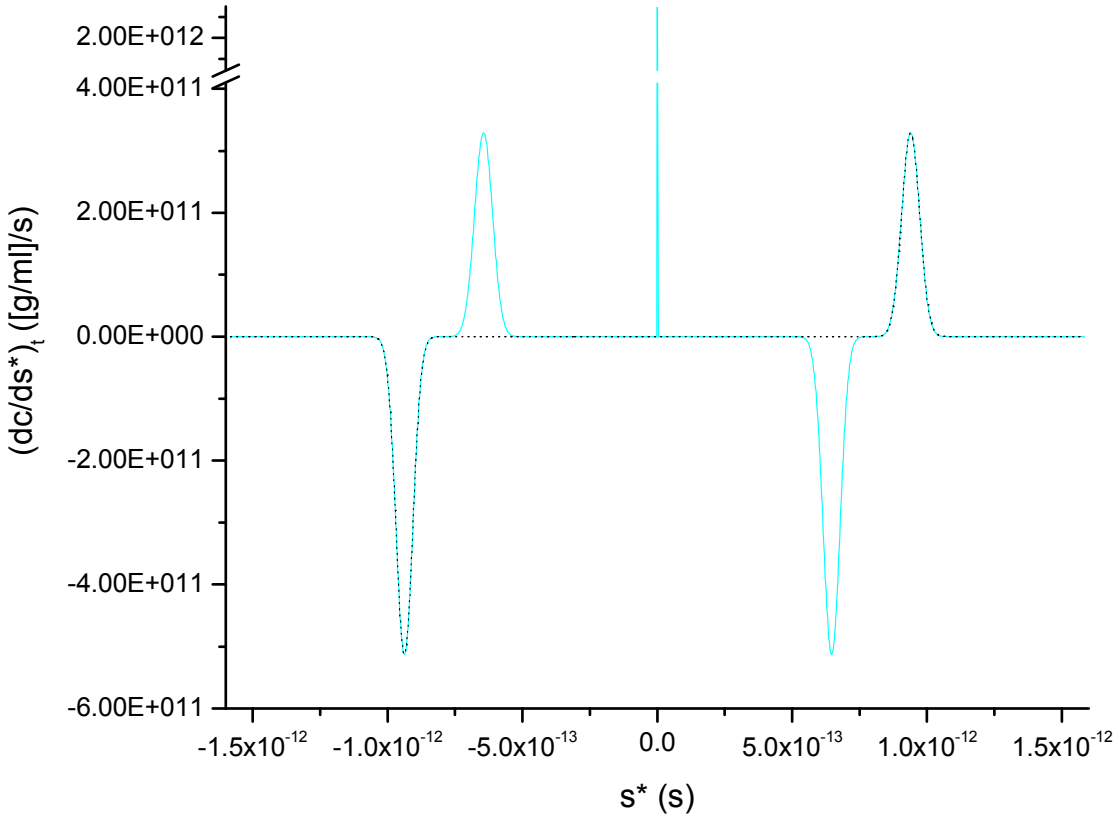

Figure 4. A plot of $\left(\frac{\partial c}{\partial s^*}\right)_t$ (——) versus s* at t = 2916 s. The results were obtained by direct differentiation of c with respect to s* at constant t, where the c versus s* data are those shown in Figure 3. Application of Equations 29 and 7 yielded q(s*,t) (·····). The spike about s* = 0 consists of just two points: $\left(\frac{\partial c}{\partial s^*}\right)_t$ = 3.462E12 [g/ml]/s at s* = -7.389E-16 s, $\left(\frac{\partial c}{\partial s^*}\right)_t$ = 3.461E12 [g/ml]/s at s* = 1.064E-15 s. Except for that spike, this figure is identical to Figure 6, where $\left(\frac{\partial c}{\partial s^*}\right)_t$ at t = 2916 s is obtained using Equation 3, and is practically identical to Figure 20, where

$\frac{\Delta c}{\Delta s^*}$ at t = 2916 s is the finite form of $\left(\frac{\partial c}{\partial s^*}\right)_t$ obtained using Equation 6.

$\left(\frac{\partial c}{\partial s^*}\right)_t$ *from* $\left(\frac{\partial c}{\partial r}\right)_t$

The product of $\left(\frac{\partial c}{\partial r}\right)_t$ and $\left(\frac{\partial r}{\partial s^*}\right)_t$ yields $\left(\frac{\partial c}{\partial s^*}\right)_t$ (Equation 3), where $\left(\frac{\partial r}{\partial s^*}\right)_t$ is equal to $r\omega^2 t$ (Equation 28). Figure 5 shows the results of differentiating c with respect to r at constant t, where the c versus r data are those shown in Figure 2, excluding the supernatant and pellet regions. (In the figures that follow, the derivative of c with respect to r at constant t is denoted as $\left(\frac{\partial c}{\partial r}\right)_t$, but estimated as $\frac{\Delta c}{\Delta r}$.)

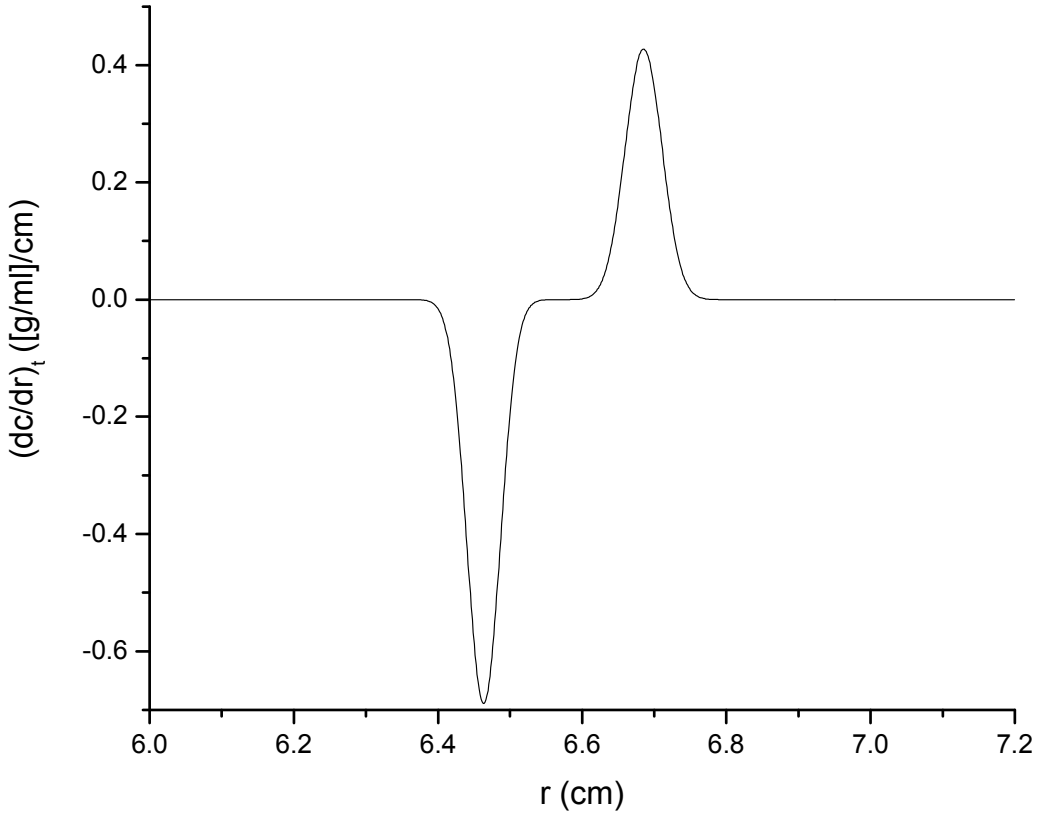

Figure 5. A plot of $\left(\frac{\partial c}{\partial r}\right)_t$ versus r at t = 2916 s. The results are from the direct differentiation of c with respect to r at constant t, where the c versus r data are those shown in Figure 2, minus the data from the supernatant and pellet regions.

Figure 6 shows $\left(\frac{\partial c}{\partial s^*}\right)_t$ calculated from $\left(\frac{\partial c}{\partial r}\right)_t$ using Equations 3 and 28, along with q(s*,t) (Equation 7), which differs from $\left(\frac{\partial c}{\partial s^*}\right)_t$ in being equal to zero wherever $Q_{s^*,t} < 0$ (Equation 29). As two values of s* are obtained for each value of r at time t, two values of $\left(\frac{\partial c}{\partial r}\right)_t$ are obtained for each value of r at time t. Because the supernatant and pellet regions were excluded from data used to generate Figure 5, Figure 6 does not exhibit spikes in $\left(\frac{\partial c}{\partial s*}\right)_t$ toward s* = s^*_{-x}, s* = 0 or s*

$= s^*_{+x}$.

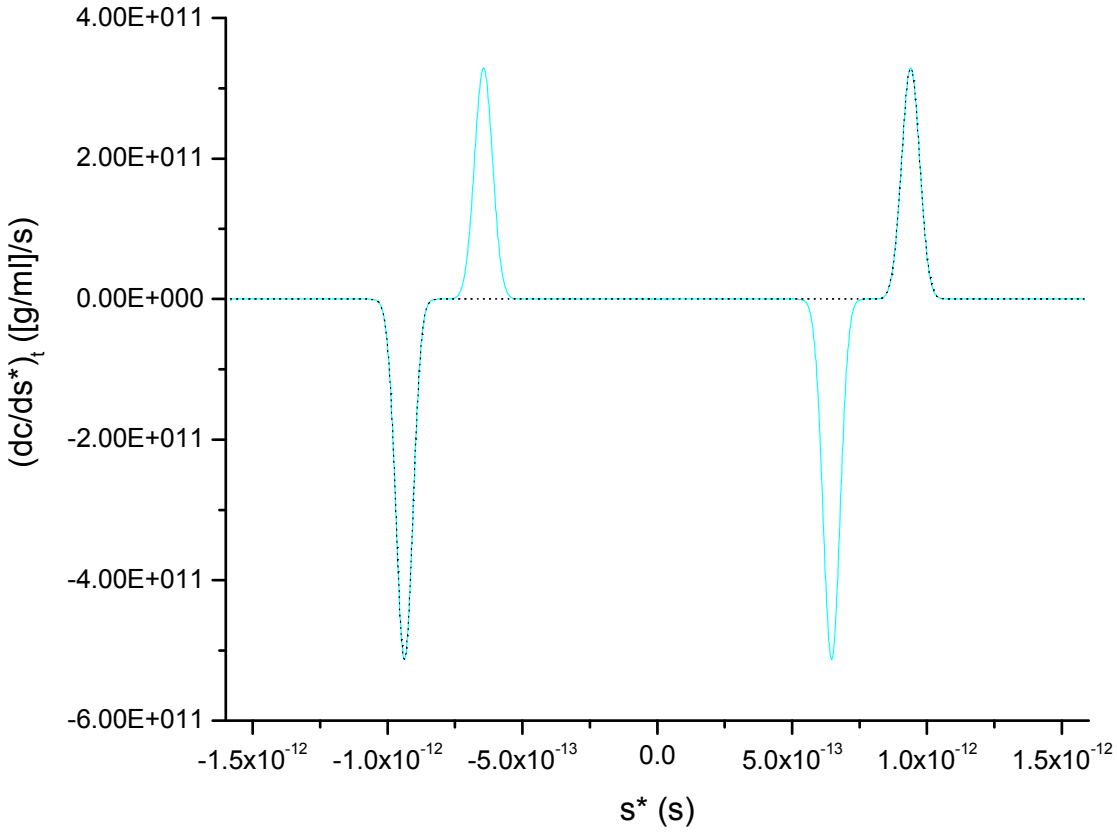

Figure 6. $\left(\frac{\partial c}{\partial s*}\right)_t$ (——) and q(s*,t) (·····) versus s* at t = 2916 s. The $\left(\frac{\partial c}{\partial r}\right)_t$ values plotted against r in Figure 5 were multiplied by $\left(\frac{\partial r}{\partial s*}\right)_t$ to obtain $\left(\frac{\partial c}{\partial s*}\right)_t$, the values of which were then plotted against s* in this figure. Application of Equations 7 and 29 to $\left(\frac{\partial c}{\partial s*}\right)_t$ yielded q(s*,t). Except at the two points about s* = 0, this figure is identical to Figure 4, where c at t = 2916 s is differentiated with respect to s*. Additionally, this figure is practically identical to Figure 20, where $\frac{\Delta c}{\Delta s^*}$ at t = 2916 s is the finite form of $\left(\frac{\partial c}{\partial s^*}\right)_t$ obtained using Equation 6.

$\left(\frac{\partial c}{\partial s^*}\right)_t$ *from* $\left(\frac{\partial c}{\partial t}\right)_r$ *and* $\left(\frac{\partial c}{\partial t}\right)_{s*}$ *via finite difference approximations - I*

According to Equation 6, the product of $\left[\left(\frac{\partial c}{\partial t}\right)_r - \left(\frac{\partial c}{\partial t}\right)_{s^*}\right]$ and $\left(\frac{\partial t}{\partial s^*}\right)_r$ yields $\left(\frac{\partial c}{\partial s^*}\right)_t$. Finite differences in c, t and s* can be used to approximate the values of $\left(\frac{\partial c}{\partial t}\right)_r$, $\left(\frac{\partial c}{\partial t}\right)_{s^*}$ and $\left(\frac{\partial t}{\partial s^*}\right)_r$, and if the finite differences in the independent variables, s* and t, are small enough, those approximate values can be used to evaluate $\left(\frac{\partial c}{\partial s^*}\right)_t$ with acceptable accuracy. Implicit in this approach is the fact that data are usually collected experimentally, or generated numerically, at discrete radial positions, r_h, and discrete times, t_ε, such that no data exist between one radial positions and the next (r_h and r_{h+1}) or one time and the next (t_ε and $t_{\varepsilon+1}$). The discontinuous nature of the data with respect to r renders the evaluation of the finite form of $\left(\frac{\partial c}{\partial s^*}\right)_t$ somewhat challenging.

Assuming that data are collected at the same radial positions at each time point, the advantage of a finite-difference application of Equation 6 is that, for the $\left(\frac{\partial c}{\partial t}\right)_r$ term at least, TI noise is eliminated. Furthermore, the finite approximations of $\left(\frac{\partial c}{\partial t}\right)_r$ and $\left(\frac{\partial c}{\partial t}\right)_{s^*}$ will include the same offset due to the RI noise of the two data sets used to evaluate them. Thus, any RI noise is eliminated when the finite form of $\left(\frac{\partial c}{\partial t}\right)_{s^*}$ is subtracted from the finite form of $\left(\frac{\partial c}{\partial t}\right)_r$. TI noise, however, is not eliminated in the course of evaluating the finite approximations of $\left(\frac{\partial c}{\partial t}\right)_{s^*}$. The elimination of RI and TI noise from $\left(\frac{\partial c}{\partial s^*}\right)_t$, determined from finite-difference forms of Equation 3 or Equation 6, is explored in a subsequent section (Equations 88 to 99; Table 1; Figures 40 to 50).

In what follows, the finite differences used in the time-derivative approach are defined, and their

distinguishing characteristics are first illustrated through an example involving an unsuitably large time difference. Results obtained with an appropriate time difference are presented thereafter.

Figure 7 shows c versus r at four times during the AUC simulation of the hypothetical system described in Figure 2.

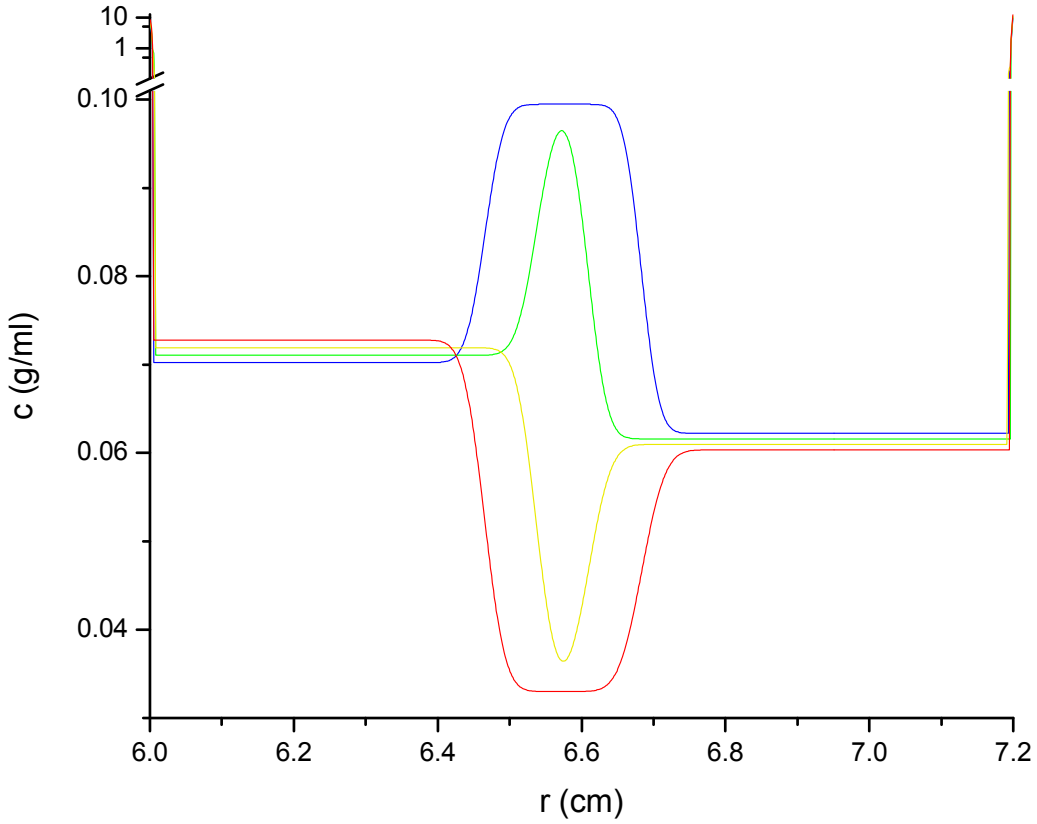

Figure 7. Plots of c versus r at t = 2010 s (——), t = 2310 s (——), t = 2610 s (——) and t = 2910 s (——), with the supernatant (toward r_m = 6 cm) and pellet (toward r_b = 7.2 cm) regions of c shown on a logarithmic scale above the break. (A few erratic points in the supernatant and pellet regions have been smoothed.) The data are from a simulation of a concentration-

independent, three-component system subjected to AUC at 60,000 RPM, and described in detail in Figure 2.

At a given radial position, r, the difference between c at two time points is denoted as Δc_r. Figure 8 shows Δc_r for the r-by-r difference between c at $t = t_2 = 2910$ s and c at $t = t_1 = 2010$ s. As the data were generated at the same radial positions at each time point, the calculation of Δc_r did not require interpolating the data at one time to match the r values of the data at the other time.

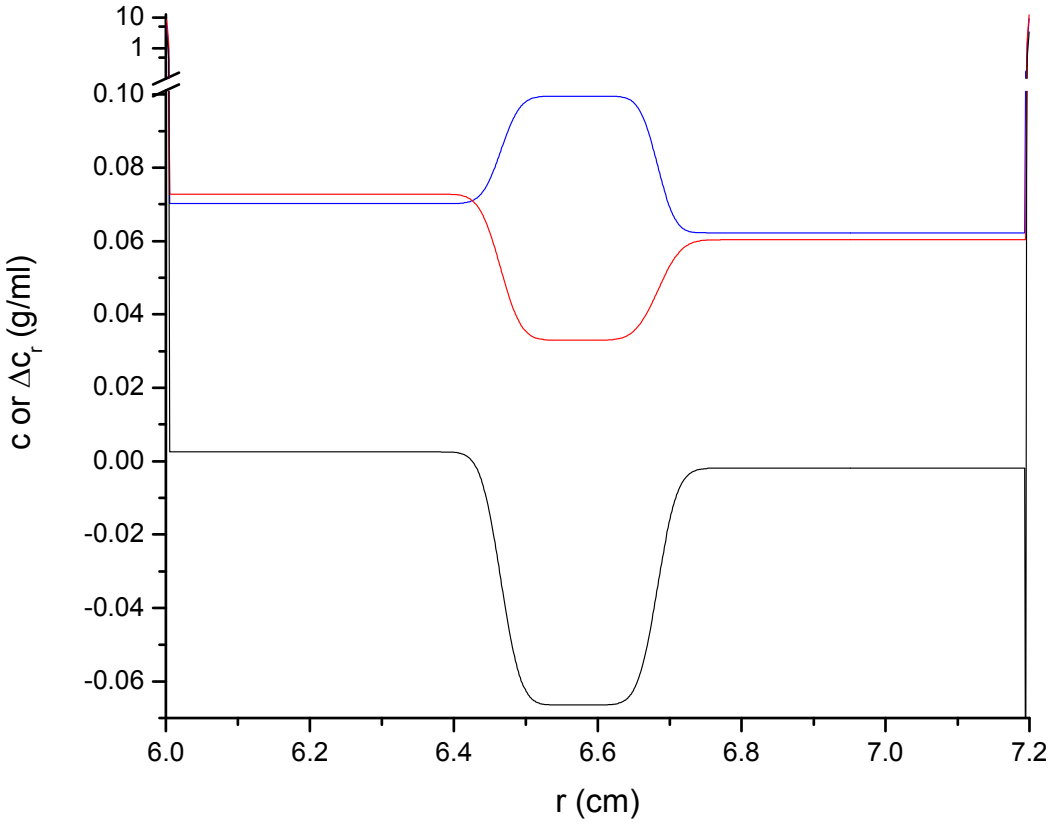

Figure 8. A plot of Δc_r versus r (——), where, at each point r, Δc_r is equal to c at $t_2 = 2910$ s (——) minus c at $t_1 = 2010$ s (——), which are two of the four curves shown in Figure 7. The supernatant (toward $r_m = 6$ cm) and pellet (toward $r_b = 7.2$ cm) regions of c are shown on a logarithmic scale above the break. In the course of calculating Δc_r, any TI noise is eliminated at

each radial position.

Figure 9 is a transformation of Figure 7 from c versus r to c versus s*.

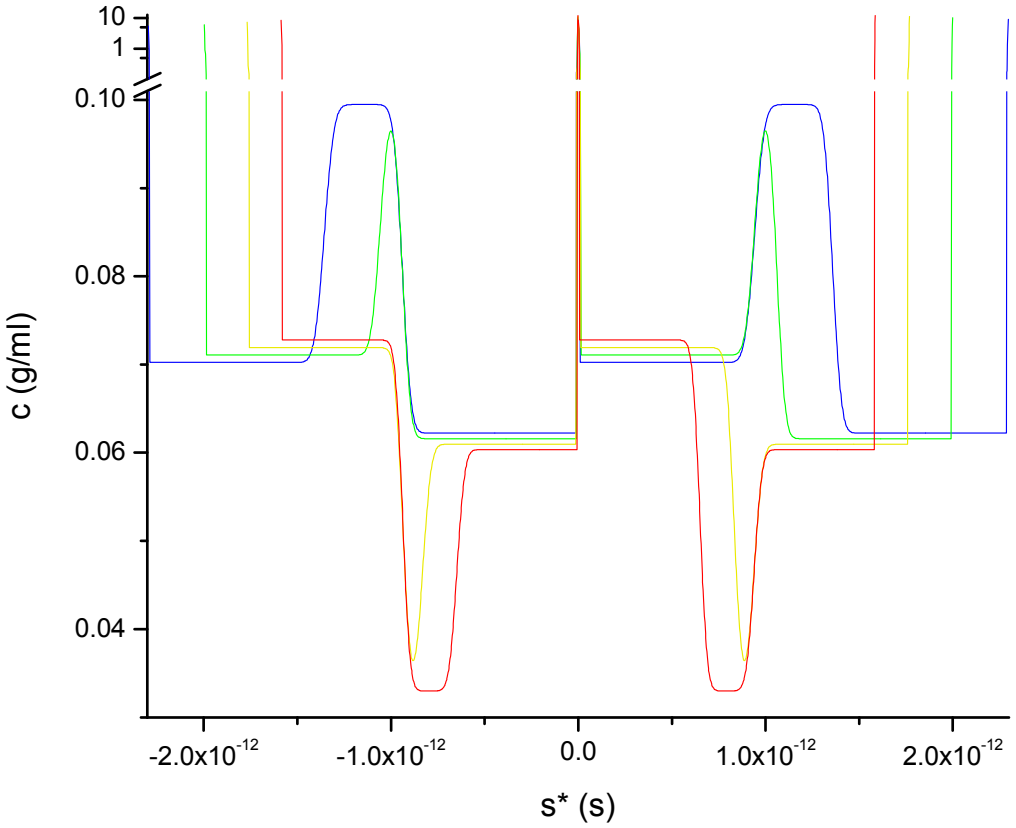

Figure 9. Plots of c versus s* at t = 2010 s (——), s* at t = 2310 s (——), s* at t = 2610 s (——) and s* at t = 2910 s (——), with the supernatant (toward the s* = s^*_{-x} and s* = 0) and pellet (toward s* = s^*_{+x} and s* = 0) regions of c shown on a logarithmic scale above the break. (A few erratic points in the supernatant and pellet regions have been smoothed.) The data are from a simulation of a concentration-independent, three-component system subjected to AUC at 60,000 RPM, and described in detail in Figure 2. These same data are plotted as c versus r in Figure 7. Here, c at each time has been plotted against its respective t-dependent values of s*, of which two

are calculated from each t-independent value of r. (See Figure 3 for a similar transformation.) As time increases, c maps to a decreasing range of s*. Thus, the extrema of s* approach zero symmetrically from above and below as t approaches infinity. (See Figure 1. Also see Figure 10, which plots r versus s* for the times that apply to this figure.)

Figure 9 shows how plots of c versus s* are affected by the time-dependence of the range of s*. A comparison of Figures 7 and 9 shows that the values of c at a given position r at two different times will not have either of their corresponding s* values in common, except where $\frac{r}{r_0}$ equals one, in which case the corresponding s* value equals zero (Equation 27). That the values of c at the same radial position but different times will not generally map to a common value of s* is simply due to r values being time-invariant, while, as Equations 27 describes, and as Figure 10 illustrates, s* is inversely proportional to t. (In contrast to Figure 1, r is treated as a function of s* in Figure 10, even though the functional relationship is the other way around. The apparent functionality is reversed in Figure 10 to provide a convenient comparison with Figure 9, where c is plotted as a function of s*.)

As r_0 can equal r_m or r_b, in Figure 10, r consists of two discontinuous lines at each time, t. Differentiating Equation 26 with respect to s* at constant t yields $\left(\frac{\partial r}{\partial s^*}\right)_t = \omega^2 t r_0 e^{s^*\omega^2 t} = r\omega^2 t$ (Equation 28), except where r is discontinuous or equal to one of its extrema. In general, where r is continuous and not equal to one of its extrema, the k^{th} derivative of r with respect to s* at constant t is $\left(\frac{\partial^k r}{\partial s^{*k}}\right)_t = (\omega^2 t)^k r_0 e^{s^*\omega^2 t} = r(\omega^2 t)^k$.

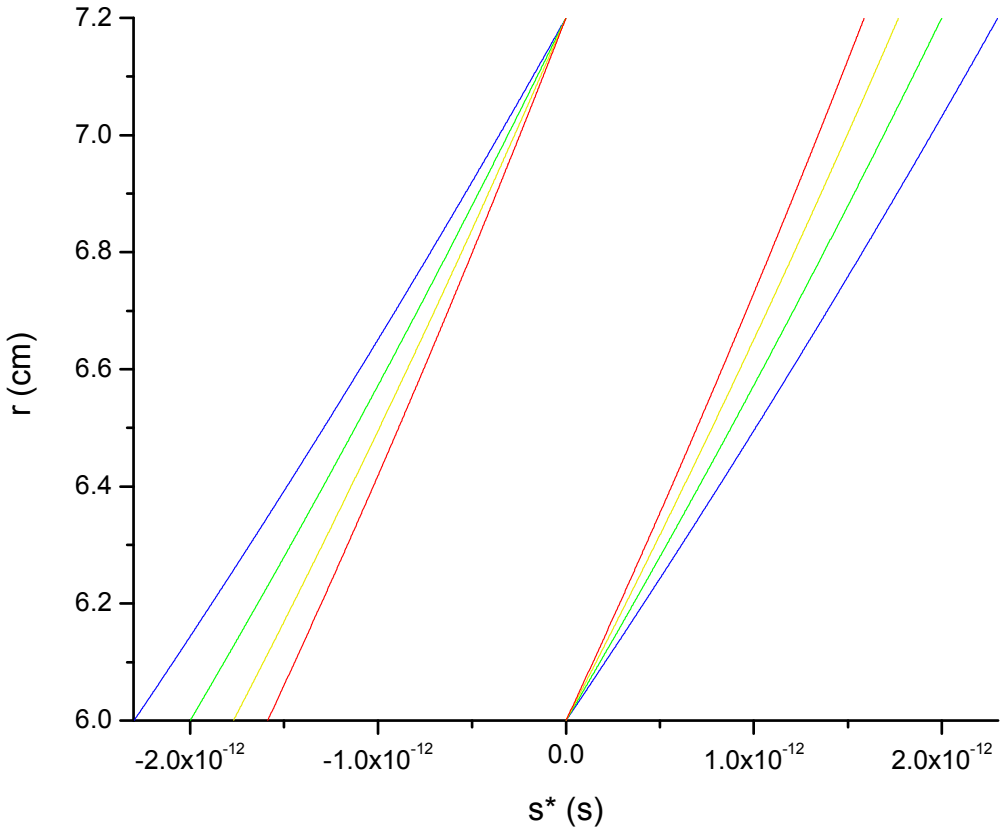

Figure 10. A plot of r versus s* at the times, t = 2010 s (——), t = 2310 s (——), t = 2610 s (——) and t = 2910 s (——), pertaining to data shown in Figures 7 to 9, for which r_m = 6 cm, r_b = 7.2 cm, and ω is that calculated for 60,000 RPM (Equation 11). Figure 1 also illustrates the relationship between t, r and s*, but with the r and s* axes exchanged.

At each apparent sedimentation coefficient, s*, the difference between c at two time points is denoted as Δc_{s^*}. Figure 11 shows Δc_{s^*} for the s*-by-s* difference between c at t_2 = 2910 s and c at t_1 = 2010 s. As the data were generated at the same radial positions but different time points, the calculation of Δc_s required interpolating the data at one time to match the s* values of the data at the other time. Given the time-dependence of s* values (Figures 9 and 10; Equation 27), matched s* values at two different times will generally correspond to mismatched r values (Equation 26).

For the subtraction shown in Figure 11, s* values at the earlier time were interpolated to match s* values at the later time. This pattern, whereby the result of subtraction is expressed in terms of s* values of the later time point, is repeated in all such interpolations that follow.

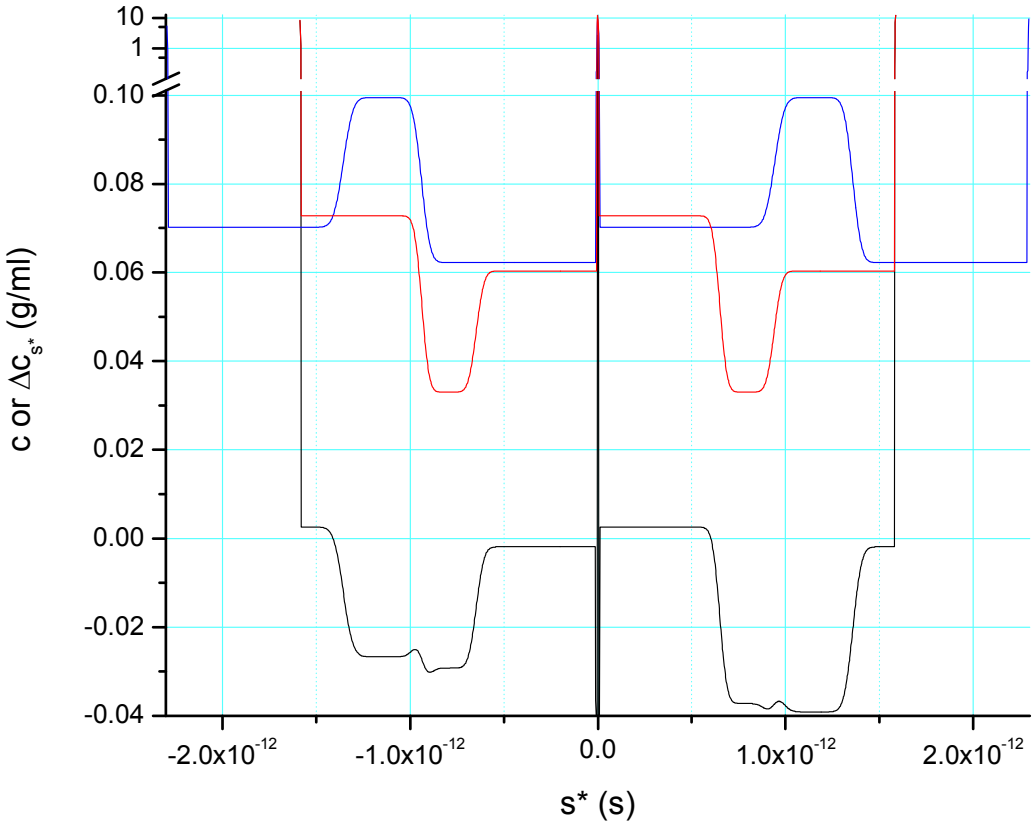

Figure 11. A plot of Δc_{s^*} versus s* at t = 2910 s (——), where, at each point s*, Δc_{s^*} is equal to c at t_2 = 2910 s (——) minus an interpolated value of c at t_1 = 2010 s (——). The supernatant (toward the s* = s^*_{-x} and s* = 0) and pellet (toward s* = s^*_{+x} and s* = 0) regions of c are shown on a logarithmic scale above the break. The concentration data at times t_2 and t_1 are two of the four sets of such data that are plotted against s* in Figure 9, and plotted against c in Figure 7. Compare this figure with Figure 8, which shows Δc_r versus r, where, at each point r, Δc_r is equal to c at t_2 minus c at t_1. TI noise is not eliminated in the course of calculating Δc_{s^*}, but in this case, the

data, which come from the simulation described in Figure 2, are nearly noise-free.

As noted with respect to Figures 7 and 9, values of c at the same radial position r but different times t will not generally map to a common value of s*. The values of s* at t_2 are given by

$$s_2^* = \frac{1}{\omega^2 t_2} ln\left(\frac{r_h}{r_0}\right),$$

(39)

where r_h is an actual radial position where a value of c is recorded at each time. The interpolated values of s* at t_1 are given by

$$s_{1*}^* = \frac{1}{\omega^2 t_1} ln\left(\frac{r_1}{r_0}\right)$$

(40)

where r_1 is an interpolated radial position with respect to the original c versus r data at t_2. As the set of all s_{1*}^* equals the set of all s_2^*, the right-hand sides of Equations 39 and 40 can be equated and solved for r_1 to obtain

$$r_1 = \left(r_h^{t_1} r_0^{t_2 - t_1}\right)^{\frac{1}{t_2}} = \left(r_h^{t_1} r_0^{\Delta t}\right)^{\frac{1}{t_2}},$$

(41)

where $\Delta t = t_2 - t_1$.

At each value of $s^* = s_2^* = s_{1*}^*$ (Equations 39 and 40), an interpolated value of the TI noise at $r_1 = r_0 e^{s_{1*}^* \omega^2 t_1}$ will be subtracted from the actual TI noise at $r_h = r_0 e^{s_2^* \omega^2 t_2}$. As can be seen from Equation 41, in the limit as t_1 approaches t_2, r_1 approaches r_h. Thus, the closer Δt is to zero, the more nearly it will be that TI noise is eliminated in the course of calculating Δc_{s*}. As will be shown (Figure 43), however, in the 60,000 RPM case, even for a Δt of just 6 s, a substantial amount of TI

noise can remain in Δc_{s*}.

The time difference that pertains to both Δc_r in Figure 8 and Δc_{s*} in Figure 11 is $\Delta t = t_2 - t_1 = 900$ s, where $t_2 = 2910$ s and $t_1 = 2010$ s. As will be shown, this Δt is too large, relative to the time scale of transport in the system examined, to yield acceptable approximations of $\left(\frac{\partial c}{\partial t}\right)_r$ and $\left(\frac{\partial c}{\partial t}\right)_{s^*}$ from $\frac{\Delta c_r}{\Delta t}$ and $\frac{\Delta c_{s*}}{\Delta t}$, respectively. For the purpose of illustrating the distinguishing features of $\left(\frac{\partial c}{\partial t}\right)_r$ and $\left(\frac{\partial c}{\partial t}\right)_{s^*}$, however, such an excessive Δt is ideal. Therefore, this example with $\Delta t = 900$ s will be used to obtain an admittedly poor approximation of $\left(\frac{\partial c}{\partial s^*}\right)_t$ before moving on to an example with an appropriately smaller Δt. Continuing, for the moment, with the current example, Figure 12 shows $\frac{\Delta c_r}{\Delta t}$, $\frac{\Delta c_{s*}}{\Delta t}$ and $\left(\frac{\Delta c_r}{\Delta t} - \frac{\Delta c_{s*}}{\Delta t}\right)$ versus s* at 2910 s, and $\Delta t = 900$ s.

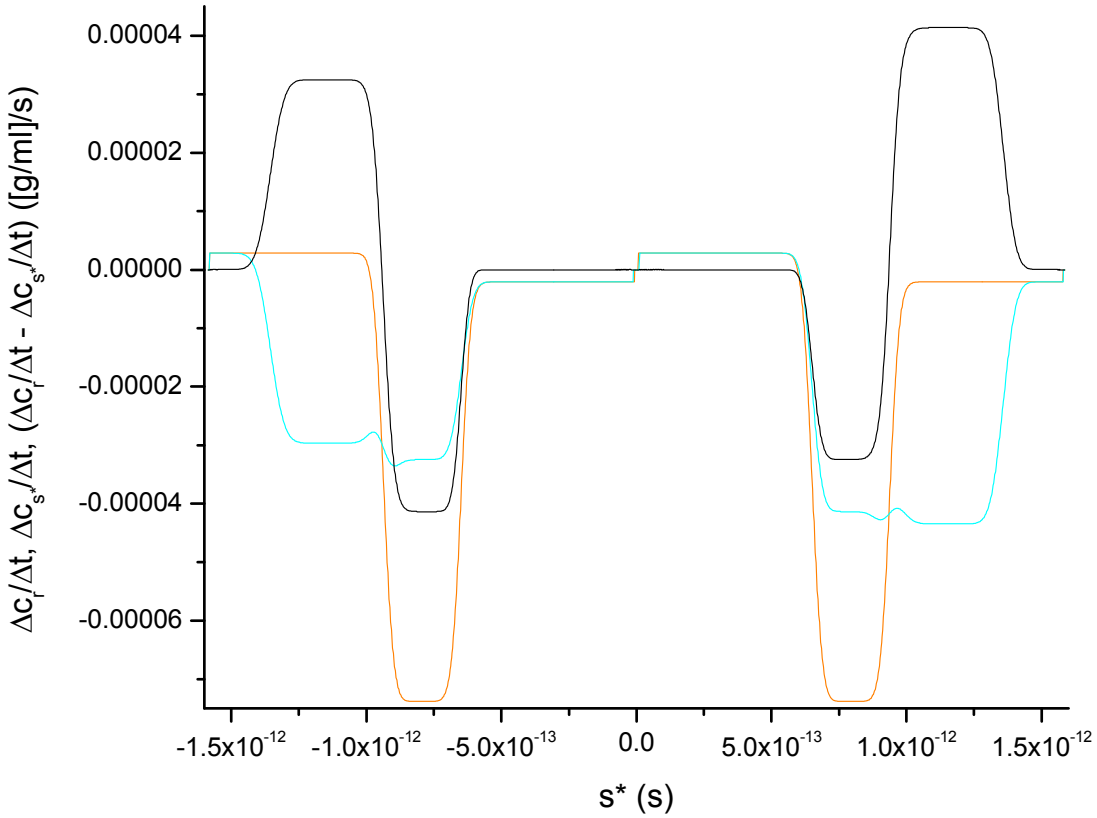

Figure 12. Plots of $\frac{\Delta c_r}{\Delta t}$ (——), $\frac{\Delta c_{s*}}{\Delta t}$ (——) and $\left(\frac{\Delta c_r}{\Delta t} - \frac{\Delta c_{s*}}{\Delta t}\right)$ (——) versus s* at $t_2 = 2910$ s. Where $\frac{\Delta c_{s*}}{\Delta t}$ and $\frac{\Delta c_r}{\Delta t}$ overlap, only $\frac{\Delta c_{s*}}{\Delta t}$ is seen. The concentration differences, Δc_r (Figure 8) and Δc_{s*} (Figure 11), were each divided by Δt to obtain $\frac{\Delta c_r}{\Delta t}$ and $\frac{\Delta c_{s*}}{\Delta t}$, respectively. The time increment, Δt, is equal to $t_2 - t_1$, where $t_1 = 2010$ s. Thus, $\Delta t = 900$ s. Due to the decrease in the range of s* as t increases (Figures 9 and 10), there are no data beyond the extrema in s* at the highest value of t, which is $t_2 = 2910$ s in this case. While Δc_{s*} in Figure 11 and $\frac{\Delta c_{s*}}{\Delta t}$ in this figure are both plotted against s* at t_2, Δc_r is plotted against r in Figure 8. The radial position, r, for each value of Δc_r in Figure 8 is the radial position used to calculate both corresponding values of s* at t_2 against which duplicate $\frac{\Delta c_r}{\Delta t}$ values have been plotted in this figure. (See Figures 3 and 9 for similar

transformations.) The $\frac{\Delta c_{s*}}{\Delta t}$ values (as a function of s* at t_2) were subtracted from the $\frac{\Delta c_r}{\Delta t}$ values (as a function of s* at t_2), s*-by-s*, to obtain $\left(\frac{\Delta c_r}{\Delta t} - \frac{\Delta c_{s*}}{\Delta t}\right)$ as a function of s* at t_2.

The approximation of $\left(\frac{\partial c}{\partial s^*}\right)_t$ is calculated as

$$\frac{\Delta c}{\Delta s^*} = \left(\frac{\Delta c_r}{\Delta t} - \frac{\Delta c_{s*}}{\Delta t}\right)\frac{\Delta t}{\Delta s_r^*},$$

(42)

where $\frac{\Delta t}{\Delta s_r^*}$ is an approximation of $\left(\frac{\partial t}{\partial s^*}\right)_r$ and, on the basis of Equation 27,

$$\Delta s_r^* = \frac{1}{\omega^2}\left[\frac{1}{t_2} - \frac{1}{t_1}\right] ln\left(\frac{r_h}{r_0}\right) = \left[\frac{-\Delta t}{\omega^2 t_1 t_2}\right] ln\left(\frac{r_h}{r_0}\right)$$

(43)

is the change in s* from time t_1 to time t_2 at radial position r. Each of the two possible values of r_0 is discussed with respect to Equation 27. As noted with respect to Equation 39, r_h is an actual radial position where a value of c is recorded at each time.

In general, $\Delta t = t_2 - t_1$. In this example, $t_1 = 2010$ s and $t_2 = 2910$ s. Equation 30 states that $\left(\frac{\partial t}{\partial s^*}\right)_r$ is equal to $-\frac{t}{s^*}$, and for $t_2 = t$,

$$\lim_{t_1 \to t} \frac{\Delta t}{\Delta s_r^*} = -\frac{t}{\frac{1}{\omega^2 t} ln\left(\frac{r}{r_0}\right)} = \left(\frac{\partial t}{\partial s^*}\right)_r .$$

(44)

As $\left(\frac{\Delta c_r}{\Delta t} - \frac{\Delta c_{s*}}{\Delta t}\right)$ is the finite form of $\left[\left(\frac{\partial c}{\partial t}\right)_r - \left(\frac{\partial c}{\partial t}\right)_{s^*}\right]$, positive values of $\left(\frac{\Delta c_r}{\Delta t} - \frac{\Delta c_{s*}}{\Delta t}\right)$ will give rise to

redundant values of $\frac{\Delta c}{\Delta s^*}$ (Equation 42), just as positive values of $\left[\left(\frac{\partial c}{\partial t}\right)_r - \left(\frac{\partial c}{\partial t}\right)_{s^*}\right]$ will give rise to redundant values of $\left(\frac{\partial c}{\partial s^*}\right)_t$. (See the discussion following Equation 30.) Redundant values of $\frac{\Delta c}{\Delta s^*}$ can be identified by substituting $\frac{\Delta c}{\Delta s^*}$ for $\left(\frac{\partial c}{\partial s^*}\right)_t$ in Equation 29, which defines $Q_{s^*,t}$. If $Q_{s^*,t} > 0$, $\frac{\Delta c}{\Delta s^*}$ is essential and e(s*,t) is equated to zero, but if $Q_{s^*,t} \leq 0$, e(s*,t) is equated to $\frac{\Delta c}{\Delta s^*}$. Substituting $\frac{\Delta c}{\Delta s^*}$ for $\left(\frac{\partial c}{\partial s^*}\right)_t$ in Equation 7 results in q(s*,t) being equal to $\frac{\Delta c}{\Delta s^*}$ if $\frac{\Delta c}{\Delta s^*}$ is essential, and zero otherwise.

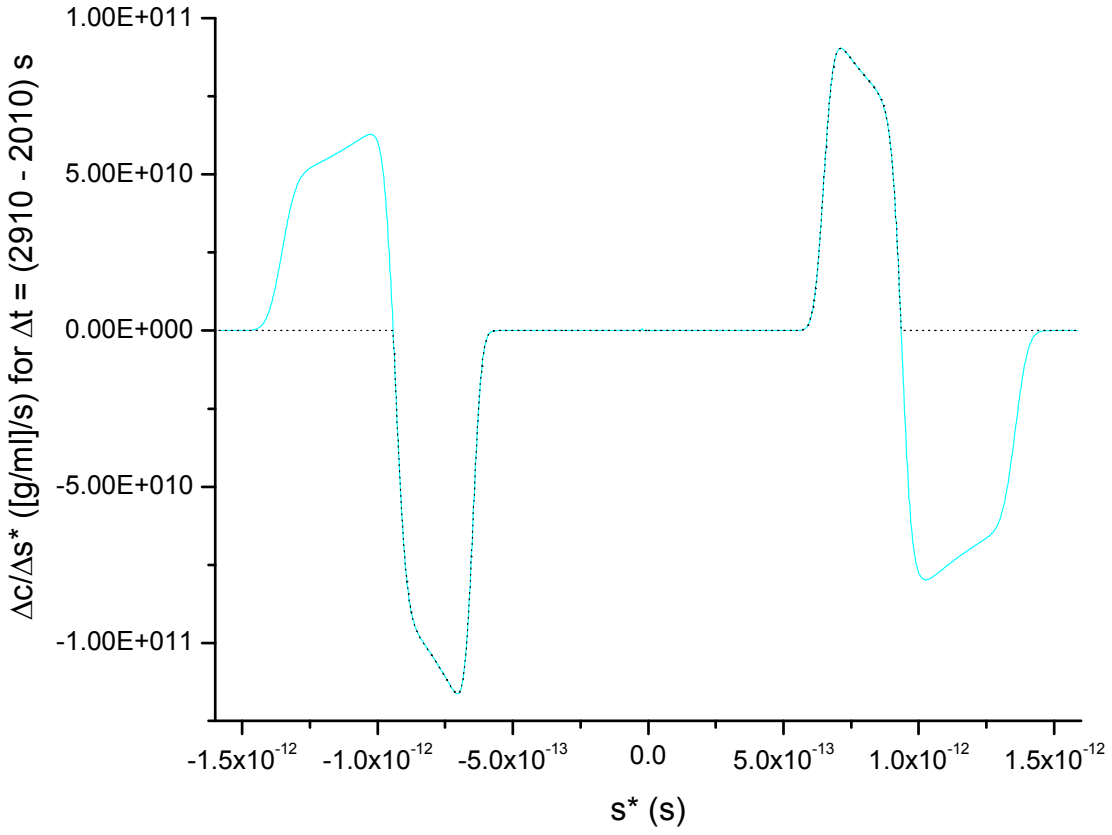

Figure 13. A plot of $\frac{\Delta c}{\Delta s^*}$ (——) versus s* at t = 2910 s. Equation 42 (the finite form of Equation 6) was used to obtain $\frac{\Delta c}{\Delta s^*}$ from $\left(\frac{\Delta c_r}{\Delta t} - \frac{\Delta c_{s*}}{\Delta t}\right)$, where Δt = (2910 - 2010) s = 900 s. Equation 43 was

used to calculate Δs_r^*, and $\frac{\Delta t}{\Delta s_r^*}$ was used to approximate $\left(\frac{\partial t}{\partial s^*}\right)_r$ in Equation 42. The essential values of $\frac{\Delta c}{\Delta s^*}$ yielded q(s*,t) (·····).

Figure 13 shows $\frac{\Delta c}{\Delta s^*}$ versus s* at t_2, where $\frac{\Delta c}{\Delta s^*}$ was evaluated by Equation 42 (the finite-difference approximation of Equation 6) in the case of $\Delta t = t_2 - t_1 = 900$ s. Figure 14 compares $\frac{\Delta c}{\Delta s^*}$ from Figure 13 with the corresponding results, $\left(\frac{\partial c}{\partial s^*}\right)_t$ versus s* at $t_1 = 2010$ s and $\left(\frac{\partial c}{\partial s^*}\right)_t$ versus s* at $t_2 = 2910$ s, obtained by the finite-difference approximation of Equation 3.

In Figure 14, within $s^* < 0$, the negative, and hence essential values of $\left(\frac{\partial c}{\partial s^*}\right)_t$ at $t_1 = 2010$ s and $\left(\frac{\partial c}{\partial s^*}\right)_t$ at $t_2 = 2910$ s are found in the same range of s* (-11E-13 s to -8E-13 s). Similarly, within $s^* > 0$, the positive, and hence essential values of $\left(\frac{\partial c}{\partial s^*}\right)_t$ at t_1 and $\left(\frac{\partial c}{\partial s^*}\right)_t$ at t_2 are also found in the same range of s* (8E-13 s to 11E-13 s). Below $s^* = 0$, the negative values of $\frac{\Delta c}{\Delta s^*}$ are skewed toward the positive values of $\left(\frac{\partial c}{\partial s^*}\right)_t$ at t_2, and the positive values of $\frac{\Delta c}{\Delta s^*}$ are skewed toward the positive values of $\left(\frac{\partial c}{\partial s^*}\right)_t$ at t_1. Above $s^* = 0$, the positive values of $\frac{\Delta c}{\Delta s^*}$ are skewed toward the negative values of $\left(\frac{\partial c}{\partial s^*}\right)_t$ at t_2, and the negative values of $\frac{\Delta c}{\Delta s^*}$ are skewed toward the negative values of $\left(\frac{\partial c}{\partial s^*}\right)_t$ at t_1. The results shown in this comparison suggest that $\frac{\Delta c}{\Delta s^*}$ will approximate $\left(\frac{\partial c}{\partial s^*}\right)_t$ poorly whenever $\Delta t = t_2 - t_1$ is sufficiently large that the redundant values of $\left(\frac{\partial c}{\partial s^*}\right)_t$ at t_1 and $\left(\frac{\partial c}{\partial s^*}\right)_t$ at t_2 occupy significantly different ranges of s*.

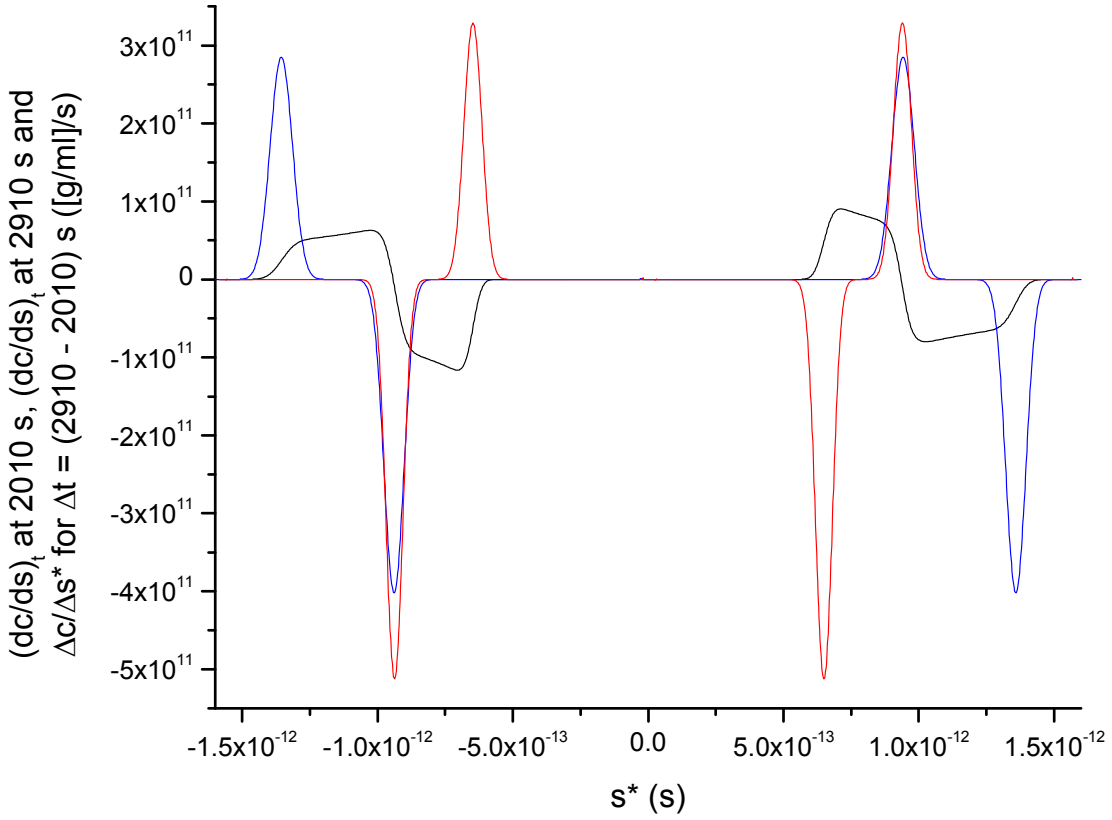

Figure 14. Plots of $\left(\frac{\partial c}{\partial s^*}\right)_t$ versus s* at $t_1 = 2010$ s (——),$\left(\frac{\partial c}{\partial s^*}\right)_t$ versus s* at $t_2 = 2910$ s (——) and $\frac{\Delta c}{\Delta s^*}$ versus s* at t_2 (——), which also appears in Figure 13. Equation 3 was used to determine $\left(\frac{\partial c}{\partial s^*}\right)_t$ at t_1 and t_2 from its respective $\left(\frac{\partial c}{\partial r}\right)_t$ at t_1 and t_2, where each $\left(\frac{\partial c}{\partial r}\right)_t$ was obtained by differentiating the corresponding data set shown in Figure 7.

As noted with respect to Equation 27, there is one radial position, $r = (r_m r_b)^{0.5}$, for which, at any given time, the positive s* equals the absolute value of the negative s*. For the example shown here, $(r_m r_b)^{0.5} = 6.573$ cm, which, at t = 2910 s, gives rise to s* = -7.935E-13 s and s* = 7.935E-13 s. Thus, at a given time, for any function such as c, $\left(\frac{\partial c}{\partial r}\right)_t$, $\left(\frac{\partial c}{\partial t}\right)_r$ or Δc_r that is s*-independent but is nevertheless plotted against s*, the same value of the function is guaranteed to be found at both

values of s* arising from $r = (r_m r_b)^{0.5}$. (Such is the case for c and $\frac{\Delta c_r}{\Delta t}$ in Figures 9 and 12, respectively, for example.) For any function that is s*-dependent, such as $\left(\frac{\partial c}{\partial t}\right)_{s^*}$, Δc_{s*}, $\left(\frac{\partial c}{\partial s^*}\right)_t$ or g(s*), different values of the function are as likely as not to be found at any pair of s* values arising from a single value of r, no matter what value of t is used to calculate s*. Fairly good illustrations of this characteristic can be seen in Figures 11 to 13.

$\left(\frac{\partial c}{\partial s^*}\right)_t$ *from* $\left(\frac{\partial c}{\partial t}\right)_r$ *and* $\left(\frac{\partial c}{\partial t}\right)_{s*}$ *via finite difference approximations - II*

In this section, the approximation of $\left(\frac{\partial c}{\partial s^*}\right)_t$ is repeated but Δt is reduced to $t_3 - t_2 = 6$ s, with $t_2 = 2910$ s and $t_3 = 2916$ s. Figure 15 shows c versus r at t_2 and t_3, while the result of subtracting the former from the latter at each point r and dividing by Δt is presented in Figure 16 as $\frac{\Delta c_r}{\Delta t}$ versus r. As the concentration data are arrayed against the same set of radial positions from one time to the next, any TI noise is eliminated in the course of calculating $\frac{\Delta c_r}{\Delta t}$.

In Figure 17, c at t_2 and c at t_3 are plotted against their respective s* values. The radial positions are the same for both data sets, but the s* values, being time-dependent (Equation 27; Figures 1 and 10), are not. Thus, to obtain Δc_{s*} versus s* at t_3, interpolated values of c at t_2 were subtracted from the actual values of c at t_3. (In the process, an interpolated value of the TI noise at $s^* = s_{2*}^* = \frac{1}{\omega^2 t_2} ln\left(\frac{r_2}{r_0}\right)$ was subtracted from the actual TI noise at $s^* = s_3^* = \frac{1}{\omega^2 t_3} ln\left(\frac{r_h}{r_0}\right)$, where r_h is an actual radial position at which a value of c is recorded at each time, r_2 is an interpolated radial position with respect to the original c versus r data at t_2, and the set of all s_{2*}^* is equal to the set of all s_3^*. By the same approach that yielded Equation 41, $r_2 = \left(r_h^{t_2} r_0^{t_3 - t_2}\right)^{\frac{1}{t_3}}$ is obtained.)

Division of these Δc_{s*} values by Δt then gave $\frac{\Delta c_{s*}}{\Delta t}$ as a function of s* at t_3. In Figure 18, these $\frac{\Delta c_{s*}}{\Delta t}$ values are plotted against the s* values calculated for $t = t_3$.

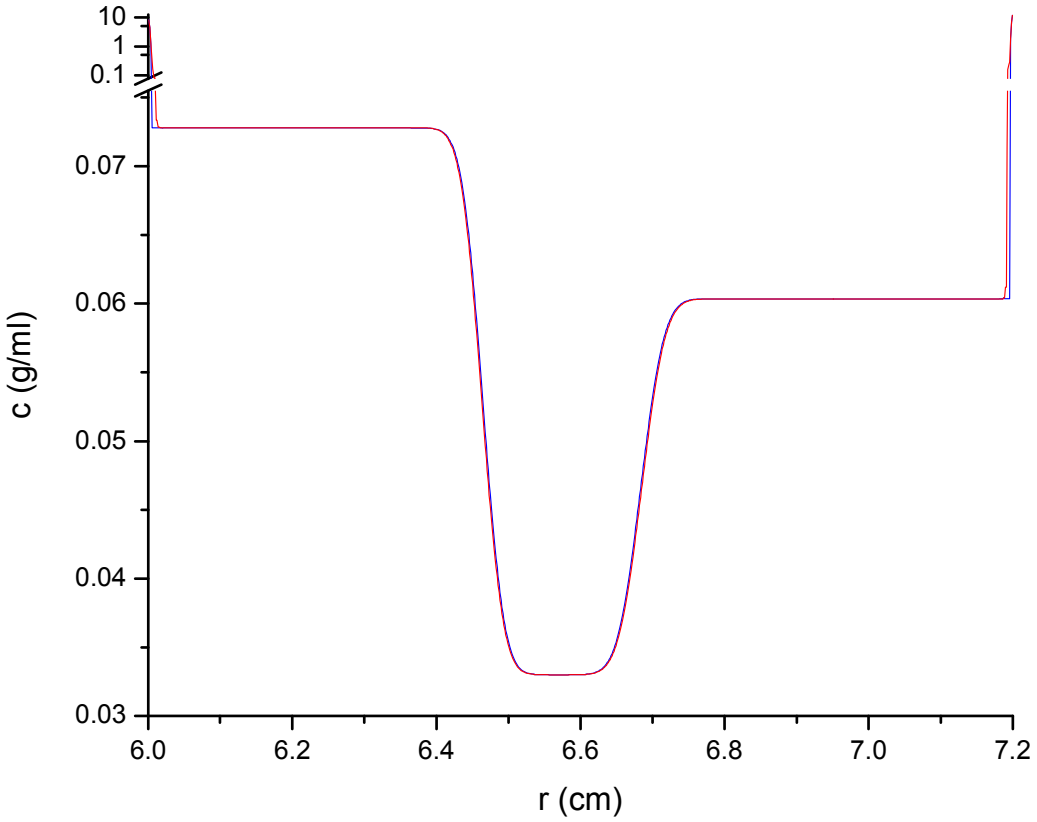

Figure 15. Plots of c versus r at $t_2 = 2910$ s (——) and $t_3 = 2916$ s (——), with the supernatant (toward $r_m = 6$ cm) and pellet (toward $r_b = 7.2$ cm) regions of c shown on a logarithmic scale above the break. (A few erratic points in the supernatant and pellet regions have been smoothed.) The data are from a simulation of a concentration-independent, three-component system subjected to AUC at 60,000 RPM, and described in detail in Figure 2.

Figure 15 illustrates how little c has changed from t_2 to t_3, compared to the change in c seen

between t_1 and t_2 (Figure 8).

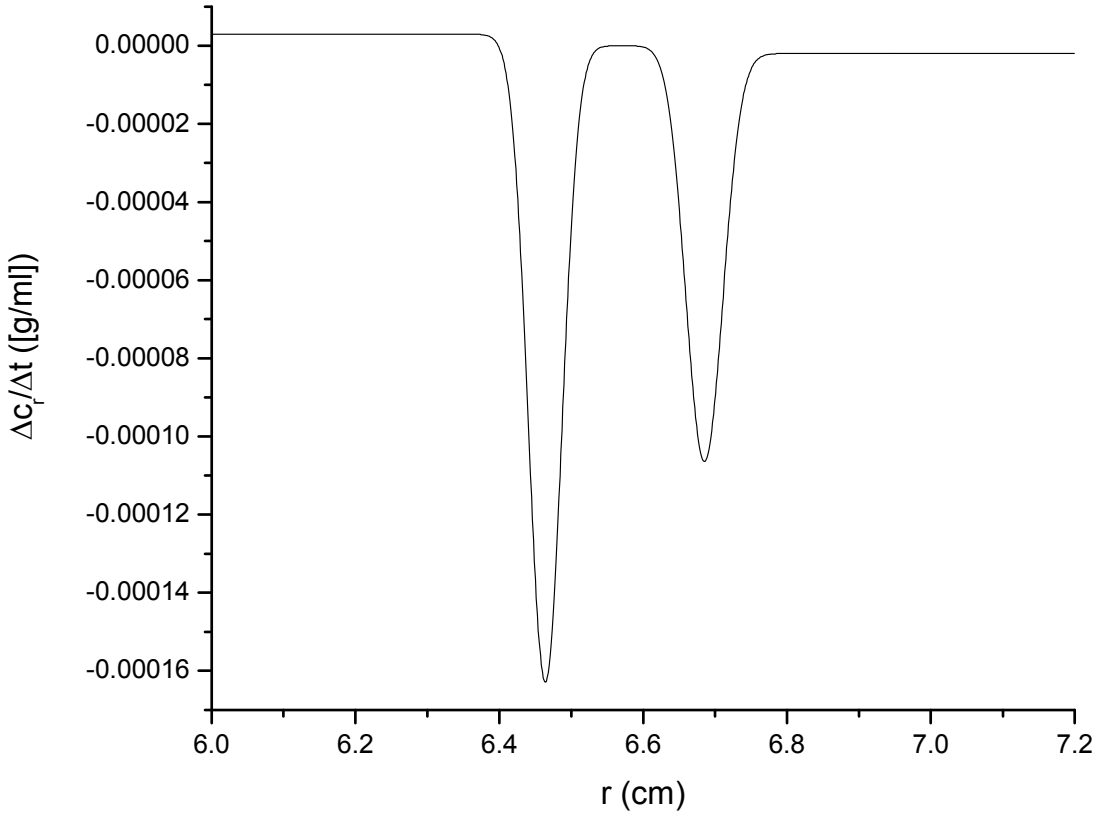

Figure 16. A plot of $\frac{\Delta c_r}{\Delta t}$ versus r (——), where, at each point r, Δc_r is equal to c at $t_3 = 2916$ s minus c at $t_2 = 2910$ s. The time increment is $\Delta t = t_3 - t_2 = 6$ s. Thus, $\frac{\Delta c_r}{\Delta t}$ is an approximation of $\left(\frac{\partial c}{\partial t}\right)_r$ within Δt. In the course of calculating Δc_r, any TI noise is eliminated at each radial position.

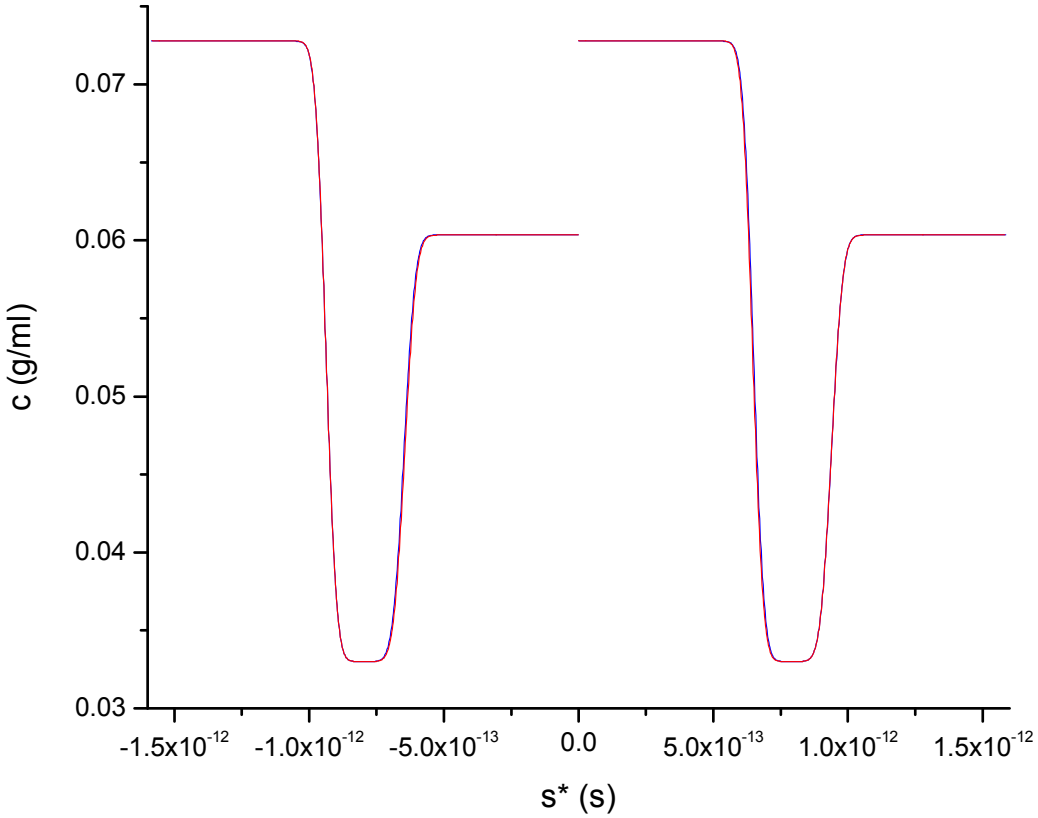

Figure 17. Plots of c versus s* at $t_2 = 2910$ s (——) and $t_3 = 2916$ s (——). These same data are plotted as c versus r in Figure 15. Here, c at each time has been plotted against its respective t-dependent values of s*, of which two are calculated from each t-independent value of r. (See Figures 3 and 9 for similar transformations.) In further contrast to Figure 15, the supernatant (between r = 6.01831 cm and $r_m = 6$ cm in Figure 15) and pellet (between r = 7.18593 cm and $r_b = 7.2$ cm in Figure 15) regions of c have been removed from the data used in this figure, and replaced with the adjacent plateau values of c. Although the range of s* decreases as t increases, the difference between t_3 and t_2 is small enough that the effect is not obvious in this case. (See Figure 9 for comparison.)

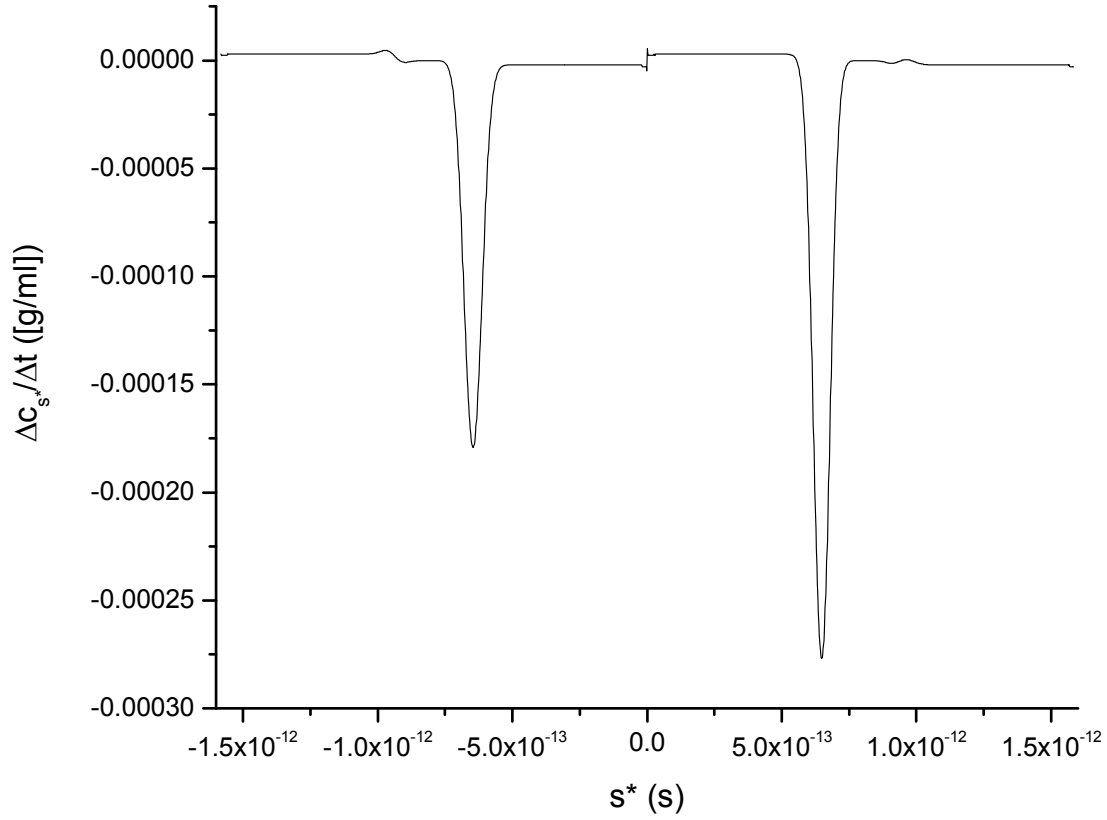

Figure 18. A plot of $\frac{\Delta c_{s*}}{\Delta t}$ versus s* at $t_3 = 2916$ s (——), where, at each point s*, Δc_{s*} is equal to c at t_3 minus an interpolated value of c at $t_2 = 2910$ s. The time increment is $\Delta t = t_3 - t_2 = 6$ s. Division of Δc_{s*} by Δt yields $\frac{\Delta c_{s*}}{\Delta t}$. As noted with respect to Figure 11 and Equation 41, TI noise is not eliminated in the course of calculating Δc_{s*}. In this case, however, the data, which come from the simulation described in Figure 2, are nearly noise-free.

In Figure 19, $\frac{\Delta c_r}{\Delta t}$, $\frac{\Delta c_{s*}}{\Delta t}$ and $\left(\frac{\Delta c_r}{\Delta t} - \frac{\Delta c_{s*}}{\Delta t}\right)$ are all plotted against s* at $t_3 = 2916$ s. (Figure 16 shows $\frac{\Delta c_r}{\Delta t}$ versus r at t_3, but in Figure 19, it is plotted against the pairs of s* values that, using Equation 27, are calculated, for $t = t_3$, from each r value. Figure 18 presents an isolated view of $\frac{\Delta c_{s*}}{\Delta t}$ versus s* at $t_3 = 2916$ s.) Subtracting $\frac{\Delta c_{s*}}{\Delta t}$ from $\frac{\Delta c_r}{\Delta t}$, s*-by-s*, yields $\left(\frac{\Delta c_r}{\Delta t} - \frac{\Delta c_{s*}}{\Delta t}\right)$.

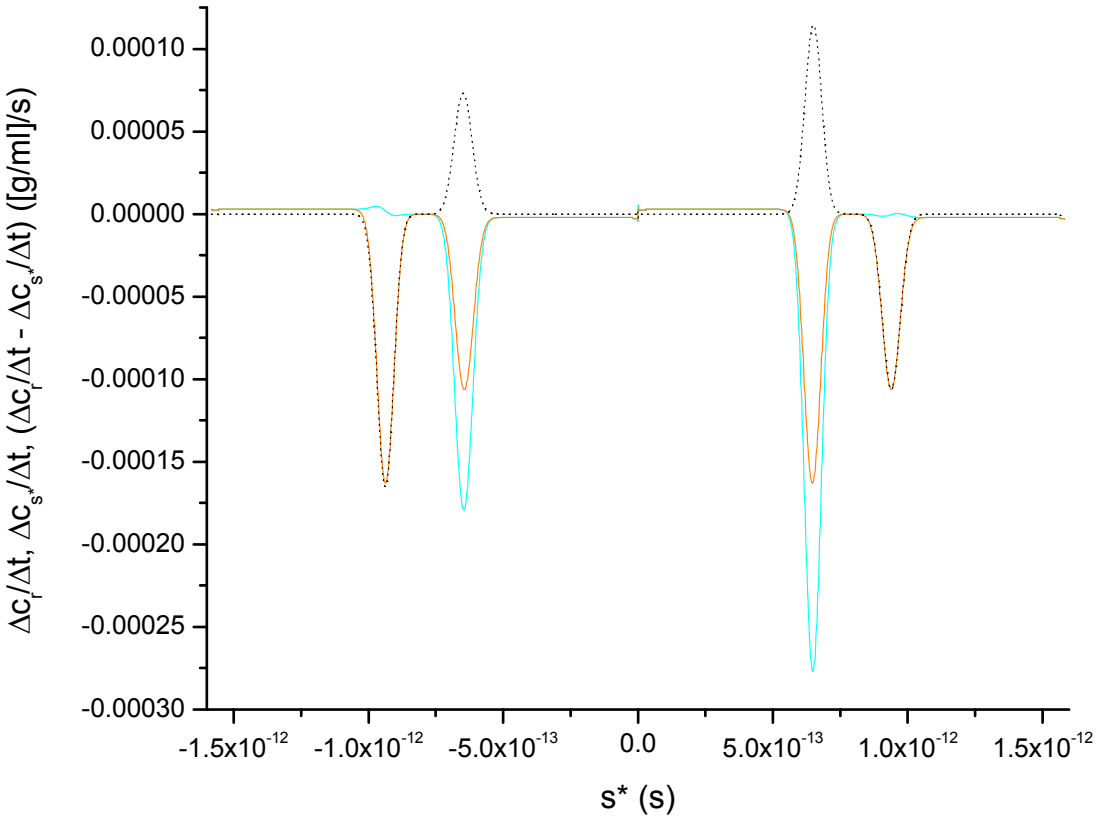

Figure 19. Plots of $\frac{\Delta c_r}{\Delta t}$ (——), $\frac{\Delta c_{s*}}{\Delta t}$ (——) and $\left(\frac{\Delta c_r}{\Delta t} - \frac{\Delta c_{s*}}{\Delta t}\right)$ (·····) versus s* at $t_3 = 2916$ s. Where $\frac{\Delta c_r}{\Delta t}$ and $\frac{\Delta c_{s*}}{\Delta t}$ overlap, only $\frac{\Delta c_r}{\Delta t}$ is seen. The time increment, Δt, is equal to $t_3 - t_2$, where $t_2 = 2910$ s. Thus, $\Delta t = 6$ s. The radial position, r, for each value of $\frac{\Delta c_r}{\Delta t}$ in Figure 16 is the radial position used to calculate both corresponding values of s* at t_3 against which duplicate $\frac{\Delta c_r}{\Delta t}$ values have been plotted in this figure. (See Figures 3, 9 and 12 for similar transformations.) The $\frac{\Delta c_{s*}}{\Delta t}$ values (as a function of s* at t_3) were subtracted from the $\frac{\Delta c_r}{\Delta t}$ values (as a function of s* at t_3), s*-by-s*, to obtain $\left(\frac{\Delta c_r}{\Delta t} - \frac{\Delta c_{s*}}{\Delta t}\right)$ as a function of s* at t_3.

As $\left(\frac{\Delta c_r}{\Delta t} - \frac{\Delta c_{s*}}{\Delta t}\right)$ is the finite form of $\left[\left(\frac{\partial c}{\partial t}\right)_r - \left(\frac{\partial c}{\partial t}\right)_{s^*}\right]$, positive values of $\left(\frac{\Delta c_r}{\Delta t} - \frac{\Delta c_{s*}}{\Delta t}\right)$ will give rise to redundant values of $\frac{\Delta c}{\Delta s^*}$ (Equation 42), just as positive values of $\left[\left(\frac{\partial c}{\partial t}\right)_r - \left(\frac{\partial c}{\partial t}\right)_{s^*}\right]$ will give rise to redundant values of $\left(\frac{\partial c}{\partial s^*}\right)_t$. (See the discussions following Equations 30 and 44.) The redundant values of $\frac{\Delta c}{\Delta s^*}$ are collected in e(s*,t) by substituting $\frac{\Delta c}{\Delta s^*}$ for $\left(\frac{\partial c}{\partial s^*}\right)_t$ in Equation 29, equating e(s*,t) to $\frac{\Delta c}{\Delta s^*}$ wherever $Q_{s^*,t} \leq 0$, and equating e(s*,t) to zero otherwise. Substituting $\frac{\Delta c}{\Delta s^*}$ for $\left(\frac{\partial c}{\partial s^*}\right)_t$ in Equation 7 results in q(s*,t), which differs from $\frac{\Delta c}{\Delta s^*}$ in being equal to zero wherever $Q_{s^*,t} < 0$ (Equation 29).

Figure 20 presents $\left(\frac{\partial c}{\partial s^*}\right)_t$ in the form of $\frac{\Delta c}{\Delta s^*}$ versus s* at $t_3 = 2916$ s and $\Delta t = 6$ s. Figure 20 also shows q(s*,t), as determined by the application of Equations 29 and 7 to the values of $\frac{\Delta c}{\Delta s^*}$ shown in the same figure. (Equation 42, which is the finite form of Equation 6, was used to obtain $\frac{\Delta c}{\Delta s^*}$ from $\left(\frac{\Delta c_r}{\Delta t} - \frac{\Delta c_{s*}}{\Delta t}\right)$. Equation 43 was used to calculate Δs_r^*, and $\frac{\Delta t}{\Delta s_r^*}$ was used to approximate $\left(\frac{\partial t}{\partial s^*}\right)_r$ in Equation 42.) The results shown in Figure 20 are practically identical to those shown in Figure 6 (where $\left(\frac{\partial c}{\partial s^*}\right)_t$ is calculated from $\left(\frac{\partial c}{\partial r}\right)_t$ using Equations 3 and 28) and, minus the spike around s* = 0, Figure 4 (where c at t = 2916 s is differentiated with respect to s*).

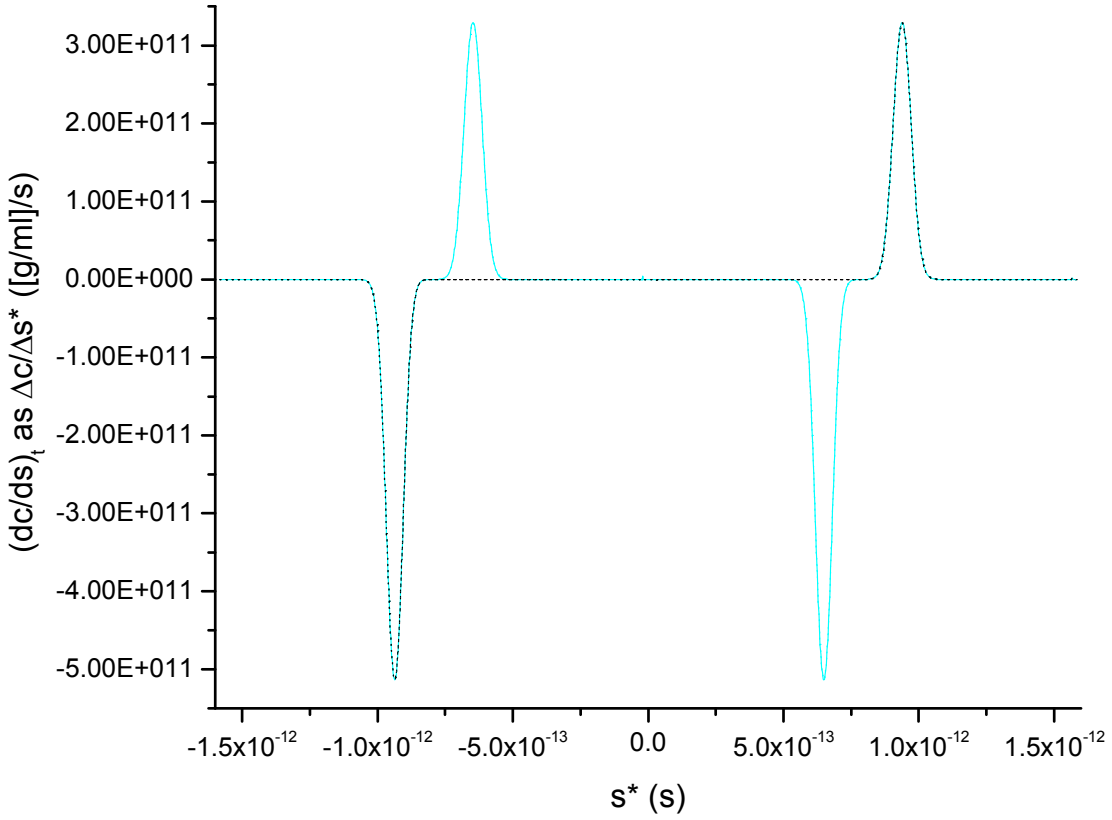

Figure 20. A plot of $\frac{\Delta c}{\Delta s^*}$ (——) versus s* at t = 2916 s. Equation 42 (the finite form of Equation 6) was used to obtain $\frac{\Delta c}{\Delta s^*}$ from $\left(\frac{\Delta c_r}{\Delta t} - \frac{\Delta c_{s*}}{\Delta t}\right)$, where Δt = (2916 - 2910) s = 6 s. (Equation 43 was used to calculate Δs_r^*, and $\frac{\Delta t}{\Delta s_r^*}$ was used to approximate $\left(\frac{\partial t}{\partial s^*}\right)_r$ in Equation 42.) The essential values of $\frac{\Delta c}{\Delta s^*}$ yielded q(s*,t) (·····). This figure is practically identical to Figure 6 and, minus the spike around s* = 0, Figure 4.

A comparison of Figures 19 and 20 shows that $\left(\frac{\partial c}{\partial t}\right)_{s^*}$ (or its finite approximation, $\frac{\Delta c_{s*}}{\Delta t}$) contributes little to the peaks and valleys of q(s*,t). The small magnitude and weak dependence of $\left(\frac{\partial c}{\partial t}\right)_{s^*}$ on time in the vicinity of essential peaks and valleys of $\left(\frac{\partial c}{\partial s^*}\right)_t$ is a result of the relatively

slow changes of those peaks and valleys with time, except when oppositely directed boundaries overlap. (See Figures 24 to 26.)

As Figures 19 and 20 illustrate, the importance of $\left(\frac{\partial c}{\partial t}\right)_{s^*}$ lies partly in its contribution to e(s*,t), for if $\left(\frac{\partial c}{\partial t}\right)_{s^*}$ were not subtracted from $\left(\frac{\partial c}{\partial t}\right)_{r}$ (or its finite approximation, $\frac{\Delta c_r}{\Delta t}$), all of the peaks and valleys of $\left(\frac{\partial c}{\partial t}\right)_{r}$ would be deemed essential, but only half of them would truly be essential. The subtraction of $\frac{\Delta c_{s*}}{\Delta t}$ from $\frac{\Delta c_r}{\Delta t}$ (the approximation of $\left(\frac{\partial c}{\partial t}\right)_{r} - \left(\frac{\partial c}{\partial t}\right)_{s^*}$ in the finite time increment, Δt) is also needed to correct for any radial dilution/concentration that Δc_{s*} and Δc_r accumulate during Δt. As noted with respect to Equation 41 and Figure 17, however, TI noise is not eliminated in the course of calculating Δc_{s*}. (See Equations 88 to 99; Table 1; Figures 40 to 50.) Thus, $\frac{\Delta c}{\Delta s^*}$ will ultimately include $-\frac{\Delta t}{\Delta s_r^*}$ times whatever TI noise is present in $\frac{\Delta c_{s*}}{\Delta t}$. (See Equations 42 to 44.)

Calculating g(s) from q(s*,t), and G(s*) from g(s*)*

Equation 32 was applied to q(s*,t) from Figure 20, in which $t = t_3 = 2916$ s, and the result, g(s*), is plotted against s* at t_3 in Figure 21.

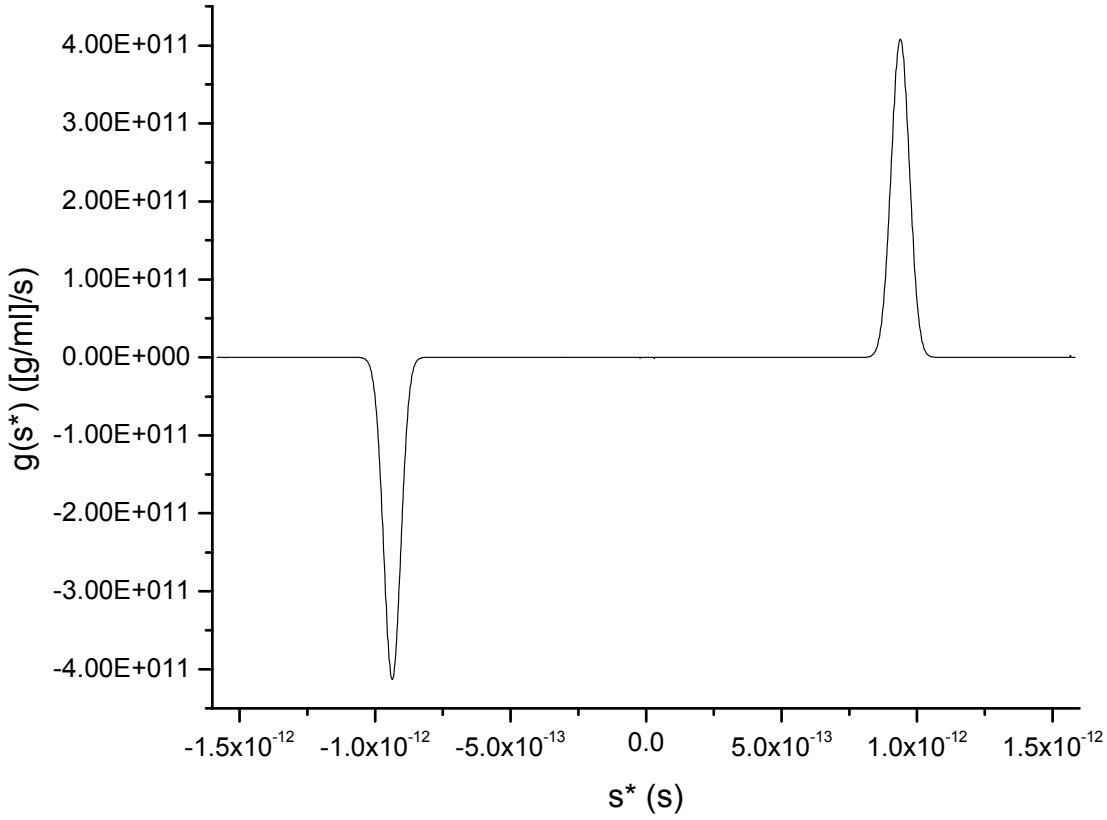

Figure 21. The sedimentation coefficient distribution function, g(s*) $= q(s^*, t)e^{2s^*\omega^2 t}$ (Equation 32), versus s* at $t_3 = 2916$ s (——). The results shown in this figure are practically indistinguishable from those obtained when Equation 32 is applied to q(s*,t) determined either (as in Figure 4, minus the spike around s* = 0) from $\left(\frac{\partial c}{\partial s^*}\right)_t$ obtained by direct differentiation of c with respect to s at constant t, or (as in Figure 6) from $\left(\frac{\partial c}{\partial s^*}\right)_t$ obtained by the application of Equations 3 and 28 to $\left(\frac{\partial c}{\partial r}\right)_t$.

Figure 22 shows the cumulative distribution function (Equation 38), G(s*), at $t = t_3$. This function integrates |g(s*)| from s^*_{-x} to any given value of s*, and thus yields the total concentration of all solutes characterised by an apparent sedimentation coefficient less than or equal to s* at any

given time.

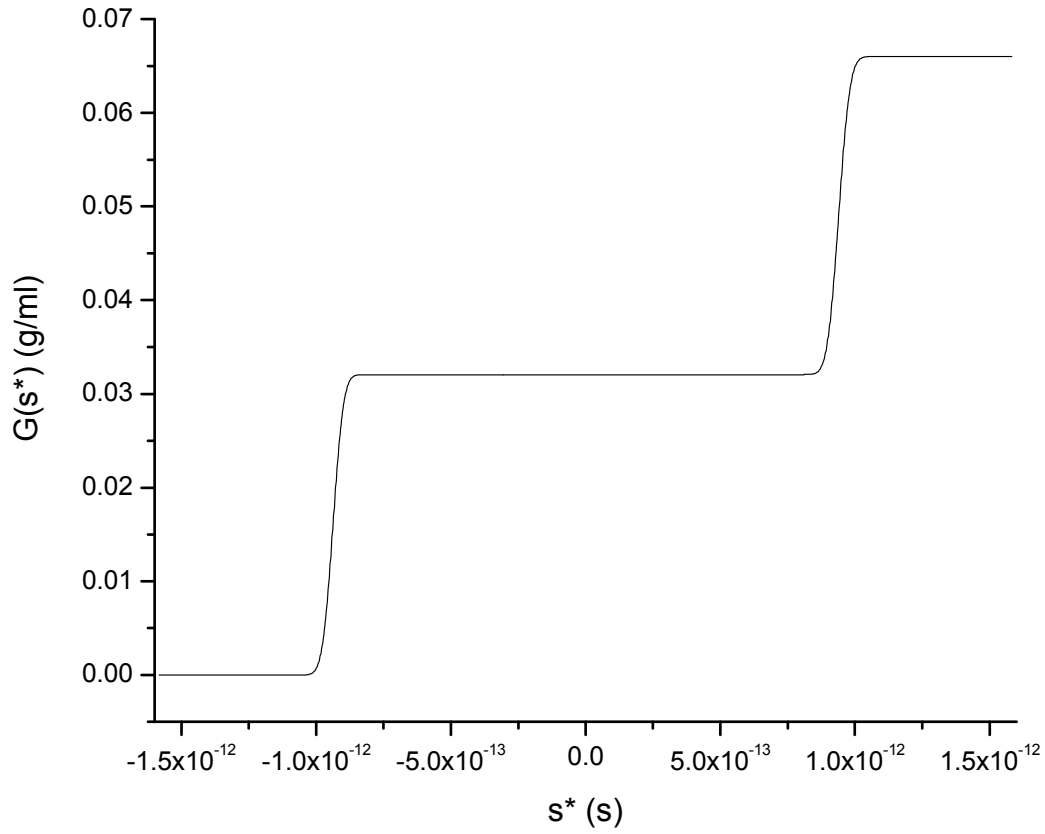

Figure 22. The cumulative distribution function (Equation 38), G(s*), versus s*, for t = t_3 = 2916 s (——). To obtain G(s*) at all s* within $s^*_{-x} \leq s^* \leq s^*_{+x}$, the absolute value of g(s*) at t_3 (Figure 21) was integrated from s^*_{-x} to each value of s*.

Time-dependence of g(s) and G(s*) in the model, concentration-independent system*

The simulation described in Figure 2 involves two oppositely directed solutes, plus one neutrally buoyant solute. That simulation is the source of the data shown in Figure 23. Those data encompass the time during which the boundaries of the two oppositely directed solutes cross paths. At t = 2010 s, well before they cross, and at 2910 s, well after they cross, the two

oppositely directed boundaries are completely distinct and separate. Thus, the g(s*) (Figure 26) and G(s*) (Figure 27) results for t = 2010 s and t = 2910 s are accurate, in that all the information that this analytical method could possibly reveal is present. For a period of time between 2010 s and 2910 s, however, the two boundaries pass through each other. At t = 2310 s, the plateau that had previously existed between the two boundaries has disappeared. At 2460 s, the two boundaries have overlapped to such an extent that there appears to be just one small boundary, with the solute having the higher plateau concentration determining the apparent direction of transport, which is toward the meniscus in this example. At 2610 s, the two boundaries have not yet separated to reveal the concentration of the neutrally buoyant solute.

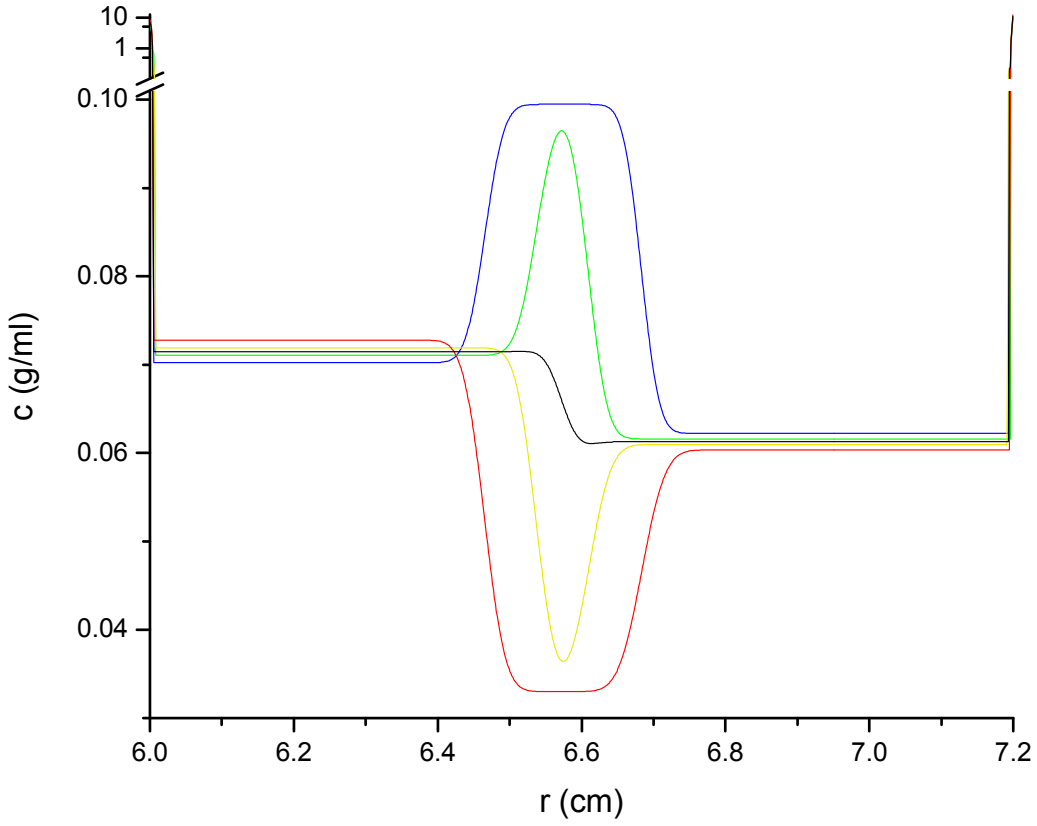

Figure 23. Plots of c versus r at t = 2010 s (——), t = 2310 s (——), t = 2460 s (——), t = 2610 s (——) and t = 2910 s (——), with the supernatant (toward r_m = 6 cm) and pellet (toward r_b =

7.2 cm) regions of c shown on a logarithmic scale above the break. (A few erratic points in the supernatant and pellet regions have been smoothed.) All but the data at t = 2460 s are also shown in Figure 7. The data are from a simulation of a concentration-independent, three-component system subjected to AUC at 60,000 RPM, and described in detail in Figure 2.

As noted in Figure 2, at t_0, at all r, c_1 = 3.389E-02 g/ml, c_3 = 3.211E-02 g/ml and c_2 = 3.300E-02 g/ml. In Figure 23, at t = 2910 s, in the region of lowest concentration (between r = 6.55 cm and r = 6.61 cm, approximately), c = c_2, which, due to s_2 being equal to zero throughout the system at all times, is unchanged from its value at t_0.

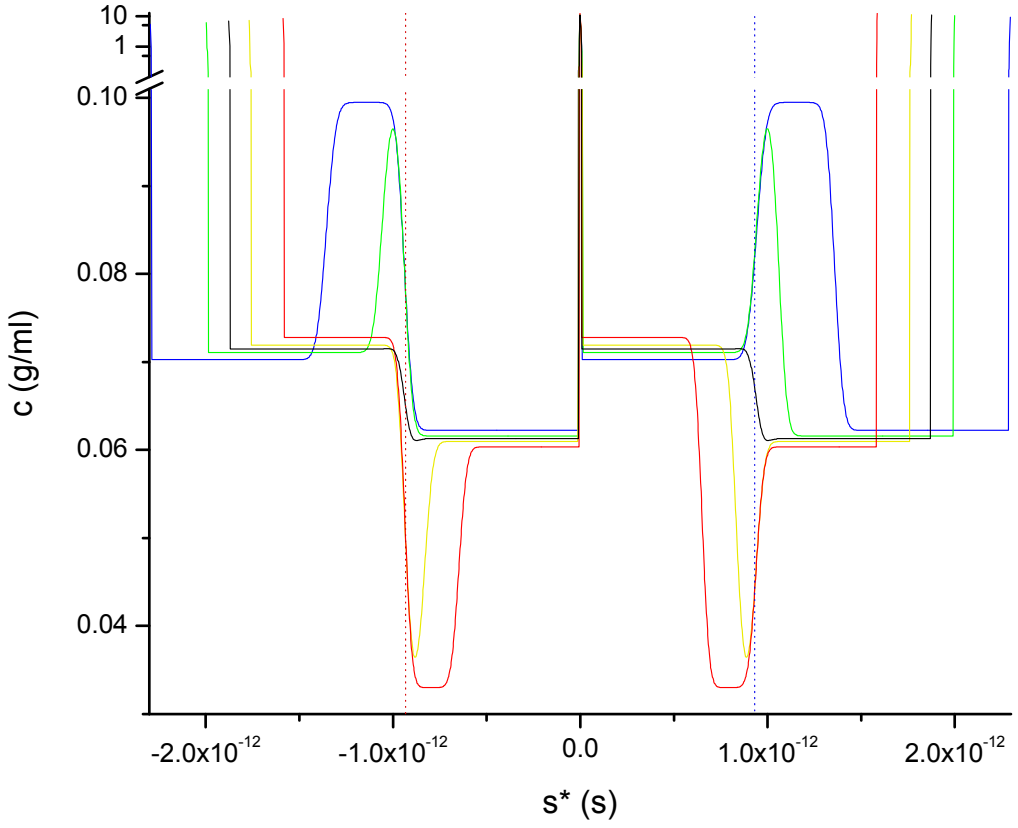

Figure 24. Plots of c versus s* at t = 2010 s (——), t = 2310 s (——), t = 2460 s (——), t = 2610

s (——) and t = 2910 s (——), with the supernatant (toward the s* = s^*_{-x} and s* = 0) and pellet (toward s* = s^*_{+x} and s* = 0) regions of c shown on a logarithmic scale above the break. (A few erratic points in the supernatant and pellet regions have been smoothed.) These same data are plotted as c versus r in Figure 23. Figure 24 is identical to Figure 9, except for the addition of the data at t = 2460 s, and the inclusion of vertical lines to mark where s_1 (····· at 9.324E-13 s) and s_3 (····· at -9.324E-13 s) lie on the s* scale. Figure 2 describes the system. Figure 10 illustrates the decreasing range of s* with time.

A comparison of c versus s data at different times (Figure 24) leads to the expectation that, except when oppositely directed boundaries overlap, as they do at t = 2460 s, $\left(\frac{\partial c}{\partial s^*}\right)_t$ will be least dependent on time where s* approaches the sedimentation coefficient of a positively or negatively-buoyant solute. Results consistent with this expectation, and its exception, are shown in Figure 25, which presents $\left(\frac{\partial c}{\partial s^*}\right)_t$ versus s* at the same times for which data are shown in Figures 23 and 24.

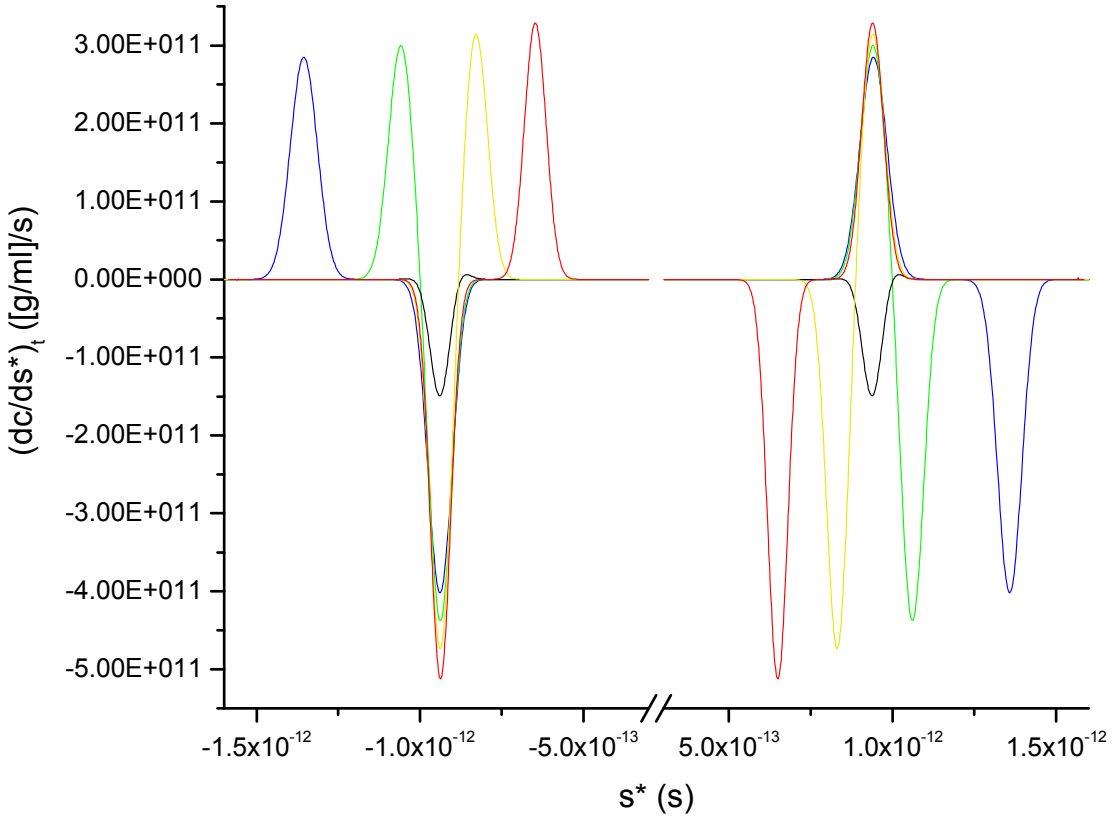

Figure 25a. Plots of $\left(\frac{\partial c}{\partial s^*}\right)_t$ versus s* at t = 2010 s (——), t = 2310 s (——), t = 2460 s (——), t = 2610 s (——) and t = 2910 s (——). Equation 3 was used to determine $\left(\frac{\partial c}{\partial s^*}\right)_t$ from $\left(\frac{\partial c}{\partial r}\right)_t$ at each time, and $\left(\frac{\partial c}{\partial r}\right)_t$ was obtained by differentiating the corresponding data set shown in Figure 23. To better illustrate the most instructive changes in $\left(\frac{\partial c}{\partial s^*}\right)_t$ with time, the narrow regions where spikes occur in $\left(\frac{\partial c}{\partial s^*}\right)_t$ (towards the extrema of s* and about s* = 0), and broader regions where $\left(\frac{\partial c}{\partial s^*}\right)_t = 0$, are not shown. The full-scale version is shown in Figure 25b.

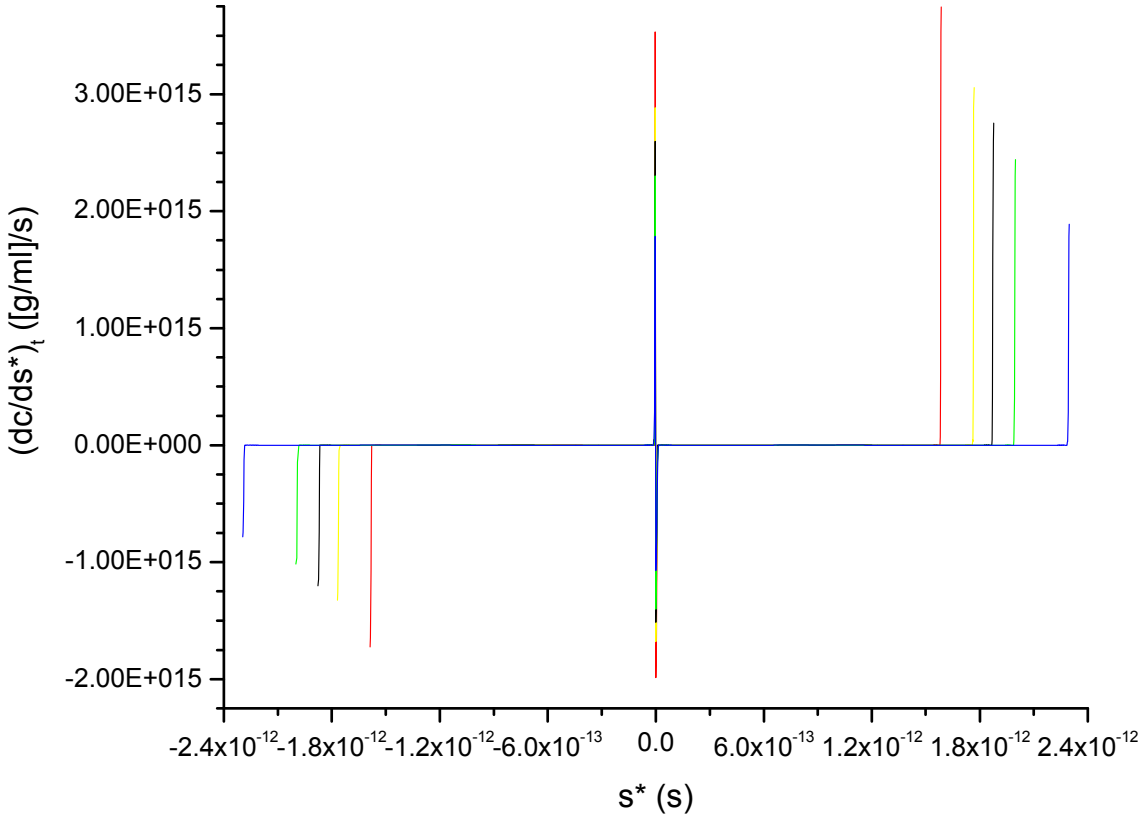

Figure 25b. Plots of $\left(\frac{\partial c}{\partial s^*}\right)_t$ versus s* at t = 2010 s (——), t = 2310 s (——), t = 2460 s (——), t = 2610 s (——) and t = 2910 s (——). This figure is the full-scale version of Figure 25a.

The redundant $\left(\frac{\partial c}{\partial s^*}\right)_t$ values are those for which $\left(\frac{\partial c}{\partial s^*}\right)_t > 0$ where $s^* < 0$, or $\left(\frac{\partial c}{\partial s^*}\right)_t < 0$ where $s^* > 0$. The essential values are those for which the signs of $\left(\frac{\partial c}{\partial s^*}\right)_t$ and s* are the same. Figure 25 shows that the location of the redundant values of $\left(\frac{\partial c}{\partial s^*}\right)_t$ is highly time-dependent, even in a concentration-independent system such as that simulated for this example. In contrast, the essential values of $\left(\frac{\partial c}{\partial s^*}\right)_t$ are weakly time-dependent in such a system.

As the location of redundant values is highly time-dependent, while the location of essential values is relatively constant with time, there is a period when the redundant values overlap the essential values to a greater or lesser extent. In this example, that period starts shortly before t = 2310 s, and ends shortly after t = 2610 s. The data at 2460 s approximately coincide with the middle of that period. As a result, at t = 2310 s and t = 2610 s, small regions of overlap are seen in what would otherwise be low-magnitude regions of the redundant and essential peaks and valleys of $\left(\frac{\partial c}{\partial s^*}\right)_t$. A t = 2460 s, however, the overlap is almost total, and as the concentration-difference across the boundary of the positively-buoyant solute is greater than that of the negatively-buoyant solute (as can be inferred from the plateau concentration being higher toward the meniscus than it is toward the base in Figure 23), there are almost no positive values of $\left(\frac{\partial c}{\partial s^*}\right)_t$ seen anywhere at that time.

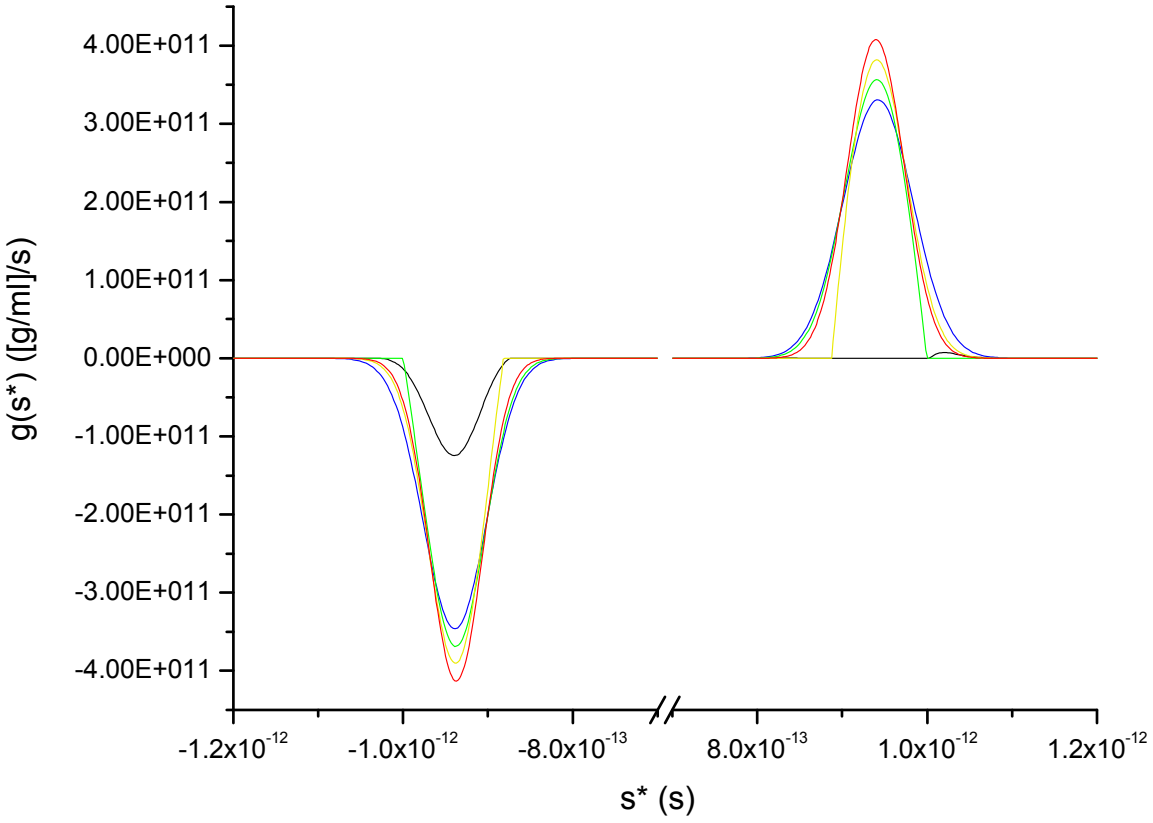

Figure 26a. Plots of g(s*) versus s* at t = 2010 s (——), t = 2310 s (——), t = 2460 s (——), t = 2610 s (——) and t = 2910 s (——). To better illustrate the most instructive changes in g(s*) with time, the narrow regions where spikes occur in g(s*) (towards the extrema of s*), and broader regions where g(s*) = 0, are not shown. Equation 29 was used to determine q(s*,t) (Equation 7) from $\left(\frac{\partial c}{\partial s^*}\right)_t$ (Figure 25) at each time, and Equation 32 was used to obtain g(s*) from q(s*,t) at each time. The s* values encompassed by a peak or valley in g(s*) at time t can be viewed as characterising a boundary region in a plot of c versus r at time t. (The plots of c versus r shown in Figure 23 are those from which the g(s*) plots in this figure are derived.) A full-s*-scale version of |g(s*)| versus s*, with the extreme values of |g(s*)| plotted on a logarithmic scale, is shown in Figure 26b.

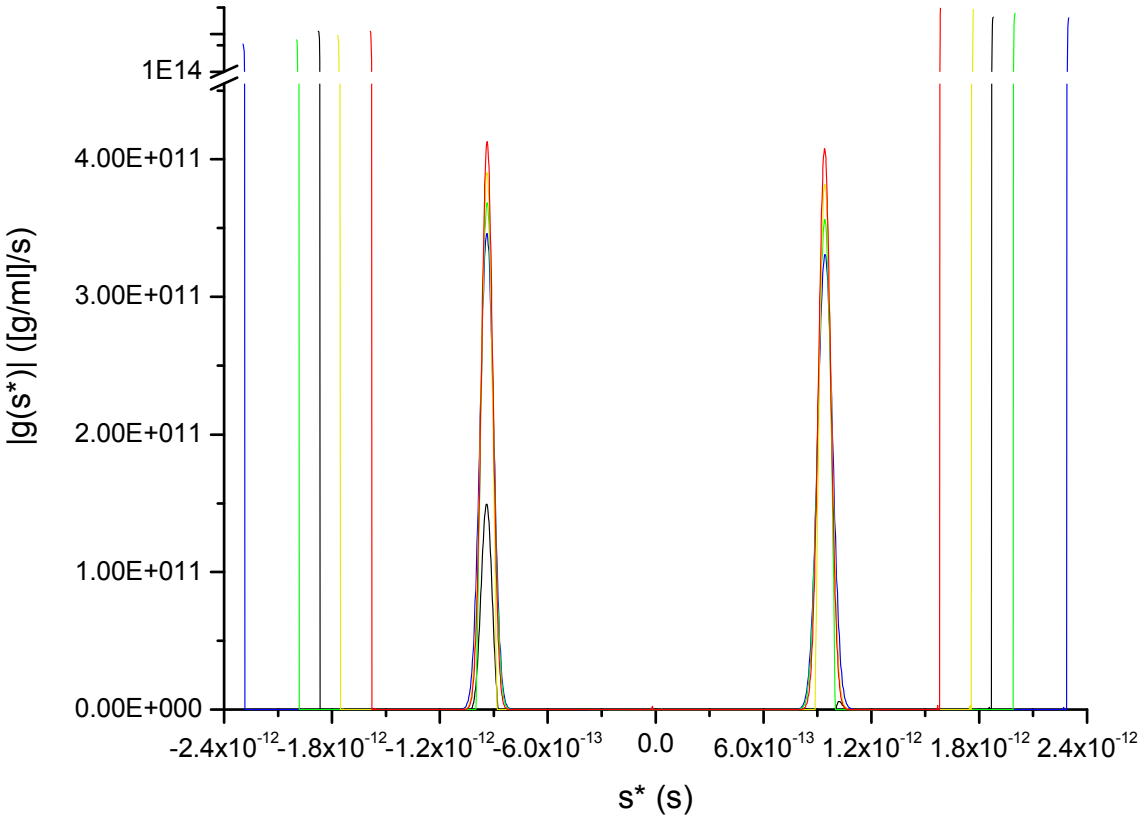

Figure 26b. Plots of |g(s*)| versus s* at t = 2010 s (——), t = 2310 s (——), t = 2460 s (——), t = 2610 s (——) and t = 2910 s (——). This figure is the full-s*-scale version of the data shown in Figure 26a. The absolute value of g(s*) is presented to get the most use possible from a single |g(s*)|-axis break, above which, data are shown on a logarithmic scale. All g(s*) values are negative below s* = 0, and all g(s*) values are positive above s* = 0. The region about s* = 0 is devoid of |g(s*)| values greater than zero because all the $\left(\frac{\partial c}{\partial s^*}\right)_t$ values in that region (Figure 25b) are redundant.

As noted in Figure 2, at all t and all r, s_1 = 9.324E-13 s, $s_3 = -s_1$, $s_2 = 0$, D_1 = 9.126E-08 cm²/s, D_3

$= D_1$ and $D_2 = 7.243\text{E-}08$ cm^2/s. Thus, all of the transport coefficients were independent of concentration throughout the system at all times in this example. Given this, and given that there was no overlap in the oppositely directed boundaries at t = 2010 s and 2910 s (Figure 23), the differences in g(s*) at those times (Figure 26) are attributable to the range of s* (Equation 27; Figures 1 and 10) decreasing in proportion to $\frac{1}{t}$, while, due to diffusion, the range of r occupied by a boundary region increases in proportion to $\frac{1}{\sqrt{t}}$ (van Holde, 1985). Thus, as a comparison at these two time points shows (Figure 26a), the g(s*) peaks and valleys sharpen with time. That is, g(s*) peaks grow higher with time, g(s*) valleys grow deeper with time, and with respect to s*, the breadth of those peaks and valleys narrows with time. In the simplest case, which applies to the results at t = 2010 s and t = 2910 s, the area of those peaks and valleys, of which G(s*) is a cumulative measure (Figure 27), is time-independent.

The overlap of the boundaries of the two oppositely directed solutes (Figures 23 and 24) results in the overlap of redundant and essential values of $\left(\frac{\partial c}{\partial s^*}\right)_t$ in Figure 25. At t = 2310 s and t = 2610 s, the overlaps are slight (Figure 23). Due to these slight overlaps, at t = 2310 s, g(s*) is clipped toward the extrema in s*, while at t = 2610 s, g(s*) is clipped toward s* = 0 (Figure 26). At t = 2460 s, the almost total overlap of the boundaries (Figure 23) results in a broadly reduced magnitude of g(s*) for the solute of higher plateau concentration, while the overlap of redundant and essential values of $\left(\frac{\partial c}{\partial s^*}\right)_t$ (Figure 25) leads to a near absence of |g(s*)| values greater than zero for the solute of lower plateau concentration (Figure 26). In Figure 27, the times affected by overlaps show variously reduced G(s*) magnitudes, compared to those at 2010 s and 2910 s.

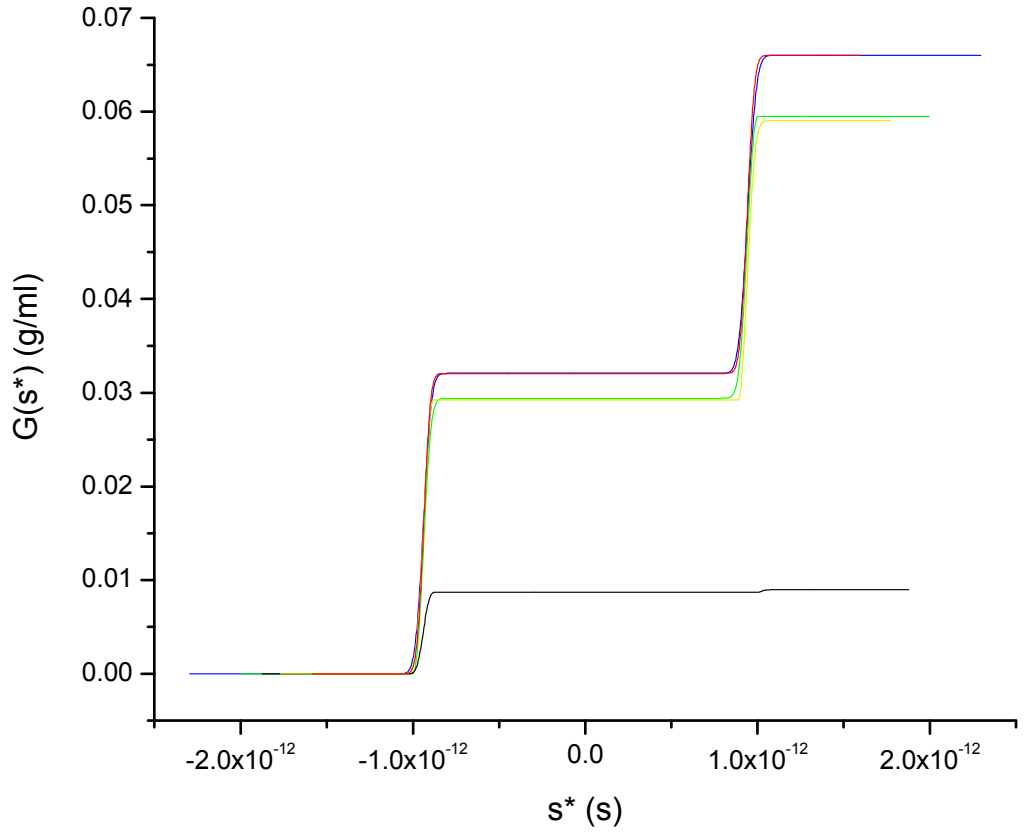

Figure 27. Plots of G(s*) versus s* at t = 2010 s (——), t = 2310 s (——), t = 2460 s (——), t = 2610 s (——) and t = 2910 s (——). Equation 38 was used to determine G(s*) from g(s*) (Figure 26) at each time. Only the peaks and valleys in g(s*) actually shown in Figure 26a were included in the calculation of G(s*) in this figure. (In Equation 38, for each time, the lower limit of integration was set sufficiently above s^*_{-x}, and the upper limit of integration was kept sufficiently below s^*_{+x}, to exclude the spikes in g(s*) at the extrema in s*.)

The G(s*) results (Figure 27) at t = 2010 s and t = 2910 s are consistent with the expectation that the area of each peak or valley in g(s*) (Figure 26) is independent of time, provided that: overlapping boundaries do not affect g(s*); the boundaries that give rise to g(s*) at each time are within the extrema of s* at all times; and the solute concentrations do not change with time due

to chemical reactions.

The slight overlap of boundaries at t = 2310 s and t = 2610 s (Figure 23) results in clipping of g(s*) at those times (Figure 26), which accounts for the slightly lower plateau values of G(s*) at those times, as compared with the corresponding values of G(s*) at t = 2010 s and t = 2910 s. The near complete overlap of boundaries at t = 2460 s (Figure 23) greatly reduces g(s*) values at that time (Figure 26), especially in the $s^* > 0$ range. As a result, at t = 2460 s, the maximum value of G($s^* < 0$) is just 27% of that at t = 2010 s or t = 2910 s. The effect of the near total overlap on g($s^* > 0$) is such that, at t = 2460 s, the maximum value of G($s^* > 0$) is little greater than the maximum value of G($s^* < 0$).

The G(s*) results from Figure 27 are re-plotted against a truncated range of s* in Figure 29. Thus, in the latter figure, it is easier to see, by comparing the results at t = 2910 s with those at t = 2010 s, that as time passes, changes in G(s*) occur over a smaller range of s*. This effect is due to the sharpening of g(s*) peaks and valleys with time (Figure 26).

*Weight-average s**

The equation for the weight-average apparent sedimentation coefficient within $s^*_{low} \leq s^* \leq s^*_{high}$ can be written as

$$s^*_w\left(s^*_{low}, s^*_{high}\right) = \frac{\int_{s^*_{low}}^{s^*_{high}} s^* \, |g(s^*)| ds^*}{G\left(s^*_{high}\right) - G\left(s^*_{low}\right)}.$$

(45)

At t = 2910 s, $s^*_w(s^*_{-x}, 0)$ = -9.376E-13 s and $s^*_w(0, s^*_{+x})$ = 9.398E-13 s. The corresponding input

values, s_3 and s_1, were -9.324E-13 and 9.324E-13, respectively.

A comparison of |g(s)| and ls-g(s*): c-independent transport*

Using least-squares boundary modeling as implemented in SEDFIT (Schuck & Rossmanith, 2000), the apparent sedimentation coefficient distribution functions, in the form of ls-g(s*), were obtained for data within 6 s of those shown in Figure 23. The Svedberg, which is equal to 10^{-13} seconds, is the dimension of the apparent sedimentation coefficient returned by SEDFIT. Thus, the dimensions of ls-g(s*) are those of the signal (optical density, fringe displacement, etc.) per Svedberg. For the concentration-independent simulation results shown here, the signal had dimensions of g/ml.

To calculate G(s*) from ls-g(s*), g ls-g(s*) was used in place of |g(s*)| in Equation 38, and the limits of integration were expressed in Svedberg. A comparison of |g(s*)| and ls-g(s*) analyses is presented in Figure 28. Figure 29 shows G(s*) from |g(s*)|, mainly, and Figure 31 shows G(s*) from ls-g(s*) exclusively.

Each ls-g(s*) analysis shown in Figure 28 was applied to three data sets, each consisting of c versus r data at a central time point (Figure 23), or at a time 6 s before or 6 s after. Thus, the ls-g(s*) analyses of Figure 28 are comparable to the g(s*) analyses just discussed (Figure 26). (Figure 2 describes the details of the simulation from which the data were obtained.) Within the ls-g(s*)-analysis software, the positions of the radial extrema of the system were set to the known positions of the meniscus ($r_m = 6$ cm) and the base ($r_b = 7.2$ cm). The lower and upper radial limits of analysis were set at $r_m + 0.02$ cm and $r_b - 0.02$ cm, respectively, and were chosen

to include as much of any upwardly or downwardly translating boundaries as possible, while excluding regions where back-diffusion or computational artefacts near the meniscus or base were evident. A range of -12 Svedberg to 12 Svedberg, with a resolution of 240 points, was used in each ls-g(s*) analysis. In all analyses, neither the TI noise nor the meniscus position was fit, and as the confidence level was set to 0, no regularisation was applied to the results of the analysis. In half the analyses, the RI noise was fit, and in half, it was not.

For |g(s*)|, the maximum range of s* is given by the extrema, s^*_{-x} (Equation 35) and s^*_{+x} (Equation 36), and the maximum resolution is equal to twice the number of radial positions at which concentration data were recorded. For all the results of simulations shown here, the number of such radial positions was 900 (Moody, 2012).

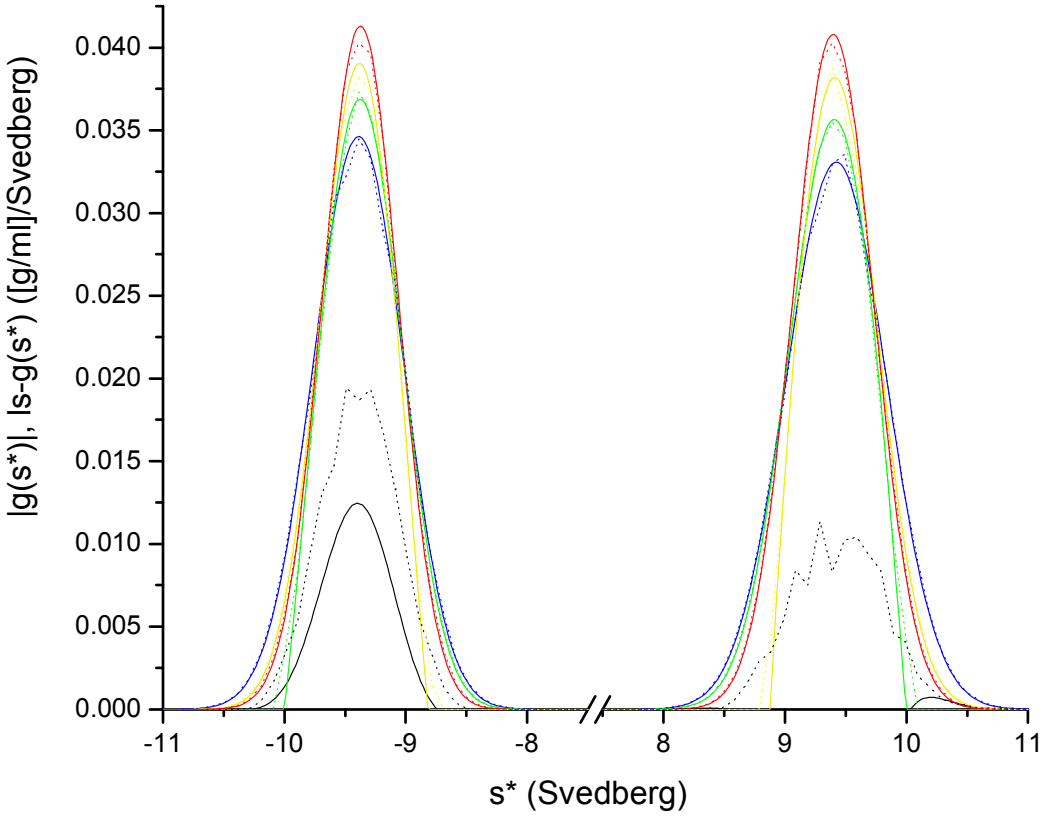

Figure 28. Plots of $|g(s^*)|\left(\frac{10^{-13}\ s}{Svedberg}\right)$ versus $\left(\frac{1\ Svedberg}{10^{-13}\ s}\right)s^*$ at t = 2010 s (——), t = 2310 s (——), t = 2460 s (——), t = 2610 s (——) and t = 2910 s (——), together with plots of ls-g(s*) versus $\left(\frac{1\ Svedberg}{10^{-13}\ s}\right)s^*$ at t = 2010 s ± 6 s (·····), t = 2310 s ± 6 s (·····), t = 2460 s ± 6 s (·····), t = 2610 s ± 6 s (·····) and t = 2910 s ± 6 s (·····). This graph is similar to that of Figure 26, which shows the same g(s*) data used to obtain the $|g(s^*)|\left(\frac{10^{-13}\ s}{Svedberg}\right)$ data shown here. Each ls-g(s*) analysis was applied to three data sets spaced closely in time, with an intervals of 6 s separating the central time point from the time before or after. In the analysis used to obtain the ls-g(s*) results shown here, the RI noise was fit.

Figure 28 shows that, normalised to the Svedberg scale, |g(s*)| is identical to ls-g(s*) at all but one of the times compared. At t = 2460 s, when the boundaries of the two oppositely directed solutes almost totally overlap (Figure 23), the ls-g(s*) results are less reduced in magnitude than the |g(s*)| results. Thus, as Figure 29 shows, at t = 2460 s, G(s*) from ls-g(s*) attains higher values than G(s*) from |g(s*)|, though both fall well short of the most accurate G(s*) results, which are those pertaining to t = 2010 s and t = 2910 s.

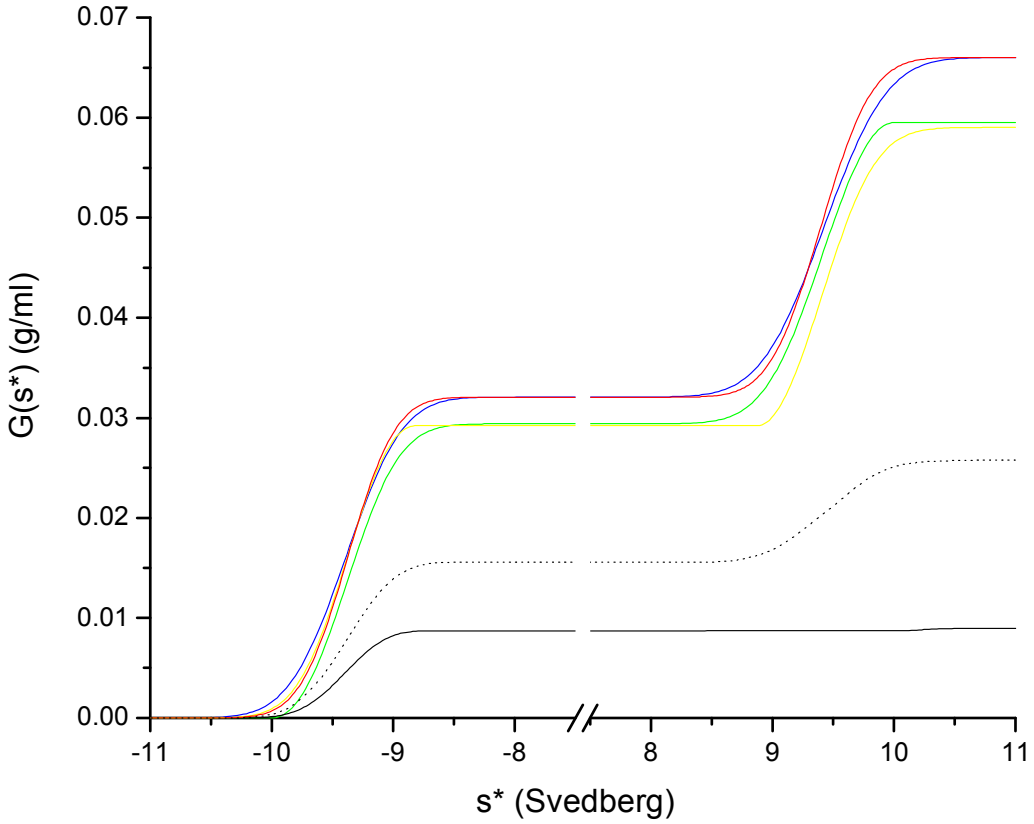

Figure 29. Plots of G(s*) versus s*, including the results obtained by the application of Equation 38 to g(s*) (Figures 26 and 28) at t = 2010 s (——), t = 2310 s (——), t = 2460 s (——), t = 2610 s (——) and t = 2910 s (——), along with the results obtained by the application of Equation 38 to ls-g(s*) (Figure 28) at t = 2460 s ± 6 s (·····). (The results from g(s*) are also shown in Figure 27, but on a different scale.)

Figures 26 to 29 show that misleading results, such as those at or about t = 2460 s, can be obtained when g(s*) or ls-g(s*) analysis is applied to data that span a short time range. As a comparison of Figures 48 and 50 will show, the likelihood of obtaining misleading results from ls-g(s*) analysis is low, except when too few data sets from too short a short time period are included in the analysis. As the aim here was to compare ls-g(s*) results with g(s*) results

pertaining to discrete times, however, the ls-g(s*) analysis was intentionally applied to unusually short periods in this case.

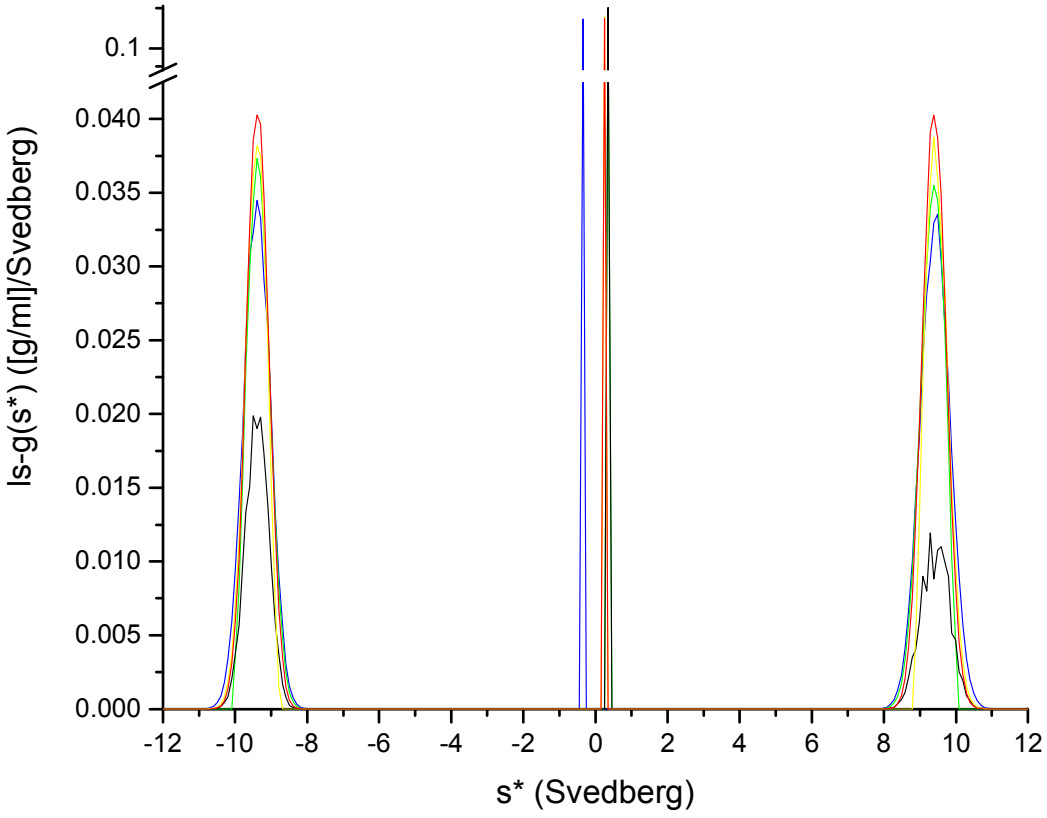

Figure 30. Plots of ls-g(s*) versus $\left(\frac{1\ Svedberg}{10^{-13}\ s}\right)$s* at t = 2010 s ± 6 s (——), t = 2310 s ± 6 s (——), t = 2460 s ± 6 s (——), t = 2610 s ± 6 s (——) and t = 2910 s ± 6 s (——). The only difference between these results and the ls-g(s*) results shown in Figure 28 is that, in this case, the RI noise was not fit in the ls-g(s*) analysis. The data are shown on a logarithmic scale above the break.

Figure 30 shows the ls-g(s*) results obtained when the RI noise is not fit. (If these ls-g(s*) results were set to zero between -1 Svedberg and 1 Svedberg, they would not significantly differ from

the ls-g(s*) results obtained when the RI noise is fit.) With the lower and upper limits of integration of Equation 34 equal to -1 Svedberg and 1 Svedberg, respectively, the data of Figure 30 yield $\Delta c = 0.0328$ g/ml $= 0.9942c_2$ at t = 2010 s $\pm$ 6 s, $\Delta c = 0.0361$ g/ml $= 1.0949c_2$ at t = 2310 s $\pm$ 6 s, $\Delta c = 0.0522$ g/ml $= 1.5818c_2$ at t = 2460 s $\pm$ 6 s, $\Delta c = 0.0364$ g/ml $= 1.1033c_2$ at t = 2610 s $\pm$ 6 s and $\Delta c = 0.0332$ g/ml $= 1.0058c_2$ at t = 2910 s $\pm$ 6 s, where $c_2 = 0.0330$ g/ml is the concentration of the neutrally buoyant solute (Figure 2).

It appears, then, that ls-g(s*) analysis can yield informative estimates of the amount of neutrally buoyant material present in a system, provided that an accurate result can be obtained without fitting either the RI or TI noise. (With respect to the data in this example, fitting the TI noise, but not the RI noise, results in a severe loss of information regarding the solutes that are not neutrally buoyant. Fitting the RI noise, or fitting both types of noise, results in a severe loss of information regarding the solutes that are neutrally buoyant.) The Δc results suggest, however, that as the overlap of the two oppositely directed solutes becomes significant, the amount of neutrally buoyant material present in the system is increasingly overestimated.

Figure 31 shows the G(s*) results obtained from ls-g(s*) when the RI noise was not fit (Figure 30). At those times when there is an absence of overlaps in the boundaries of the two oppositely directed solutes (Figure 23), G(s*) attains a maximum values of approximately 99.8% (at t ≃ 2010 s) and 100.2% (at t ≃ 2910 s) of the total solute concentration of 0.099 g/ml (Figure 2). At those times when there is a slight overlap in the boundaries of the two oppositely directed solutes (Figure 23), G(s*) attains maximum values of approximately 97.2% (at t ≃ 2310 s) and 96.8% (at t ≃ 2610 s) of the total solute concentration of 0.099 g/ml. When (at t ≃ 2460 s) there is an almost total overlap of the boundaries of the two oppositely directed solutes (Figure 23),

G(s*) attains a value maximum value of approximately 80.7% of the total solute concentration of 0.099 g/ml.

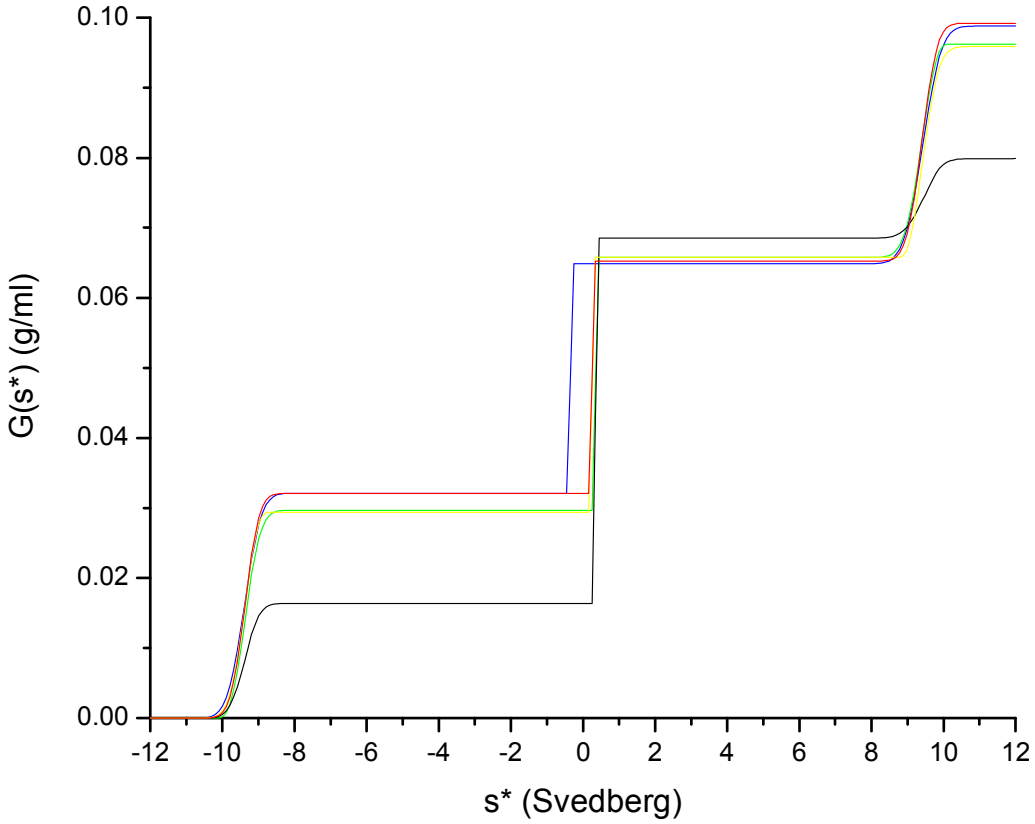

Figure 31. Plots of G(s*) versus $\left(\frac{1\ Svedberg}{10^{-13}\ s}\right)$s* for the results obtained by the application of Equation 38 to ls-g(s*) (Figure 30) at t = 2010 s ± 6 s (——), t = 2310 s ± 6 s (——), t = 2460 s ± 6 s (——), t = 2610 s ± 6 s (——) and t = 2910 s ± 6 s (——),where the RI noise was not fit in the ls-g(s*) analysis.

A comparison of |g(s)| and ls-g(s*): c-dependent transport*

Both g(s*), as determined from the derivative of c with respect to s* at constant t, and ls-g(s*), as

determined from SEDFIT (Schuck & Rossmanith, 2000), were obtained using data from a previously described (Moody, 2012) simulation of transport in a concentration-dependent system subjected to AUC at 60,000 RPM system. (See Moody, 2012: Figures 1 and 2, $K_a = 30.325$ ml/g.)

The concentration-dependent system includes 12 positively-buoyant solutes and 12 negatively-buoyant solutes (Moody, 2012: Table 1), each having a total mass concentration of [0.001 g/ml]/24, and each having concentration-dependent transport coefficients (Moody, 2012: Equations 5 to 18). The arbitrary unit (AU) of the signal of each low-concentration solute is numerically equivalent to the mg/ml concentration scale. (The signal-per-mass-concentration factor is 1000 AU/[g/ml].)

The concentration-dependent system also includes 3 high-concentration solutes, of which, the most neutrally-buoyant is the hetero-dimeric product of a mass-action association of the other two high-concentration solutes (forward rate constant of $k_{for} = 30{,}000$ [ml/g]/s, equilibrium constant of $K_a = 30.325$ ml/g). The transport coefficients of each high-concentration solute are also concentration-dependent (Moody, 2012: Equations 5 to 18). The partial specific volume, $\bar{\nu}_k$, of the hetero-dimeric solute is equal to $\frac{1}{\rho_0}$, where ρ_0 is the solvent density, which is equal to 1.08225 g/ml. The high-concentration solutes are measured on the g/ml concentration scale.

The solute concentrations, the basic transport parameters (Moody, 2012: Table 1) and the parameters that mediate concentration dependence (Moody, 2012: Equations 14 to 18) are such that each of the low-concentration solutes exhibits Johnston-Ogston effects. In the limit as c approaches zero, the characteristics of high-concentration solutes 1, 14 and 27 of the

concentration-dependent system (Moody, 2012: Table 1) approach the characteristics of solutes 1, 2 and 3, respectively, of the concentration-independent system (Figure 2). The initial concentrations of solutes 1, 27 and 14 were $c_1 = 3.389\text{E-}02$ g/ml, $c_{27} = 3.211\text{E-}02$ g/ml, $c_{14} = 3.300\text{E-}02$ g/ml, which, respectively but not coincidentally, are the same as c_1, c_3 and c_2 of the system described in Figure 2.

One set of signal versus r data was used in each g(s*) analysis (Figures 36 and 37). The data analysed were from three times (Figures 32 and 33): 21 min, 51 min or 81 min. For each of those times, two sets of data were examined, with one set consisting of the combined signal from all 24 low-concentration solutes (Moody, 2012: Figure 1, $K_a = 30.325$ ml/g), and the other set consisting of the combined concentration of all 3 high-concentration solutes (Moody, 2012: Figure 2, $K_a = 30.325$ ml/g). The most direct approach, in which $\left(\frac{\partial c}{\partial s^*}\right)_t$ is obtained from c versus s* data, was used to obtain g(s*) in each case.

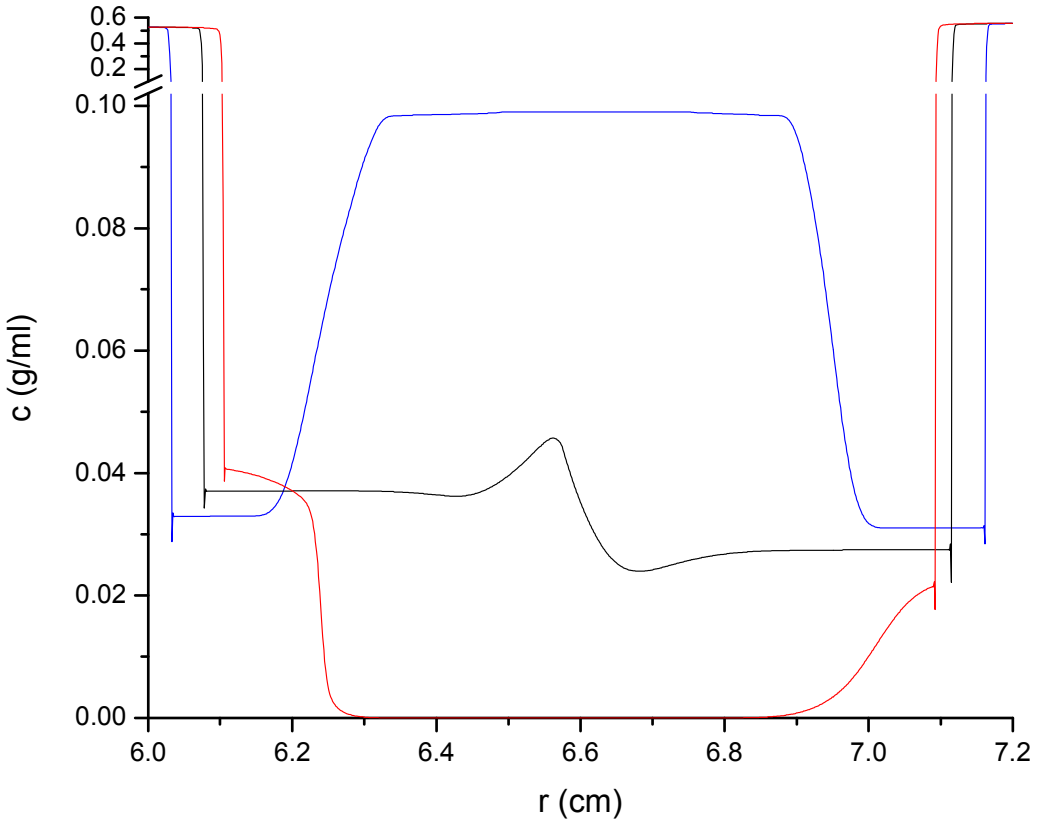

Figure 32. The sum of the concentration of all high-concentration solutes versus r in the concentration-dependent system at t = 21 min (——), t = 51 min (——) and t = 81 min (——). High concentration data in the pellet and supernatant are shown on a compressed scale above the break in the c-axis.

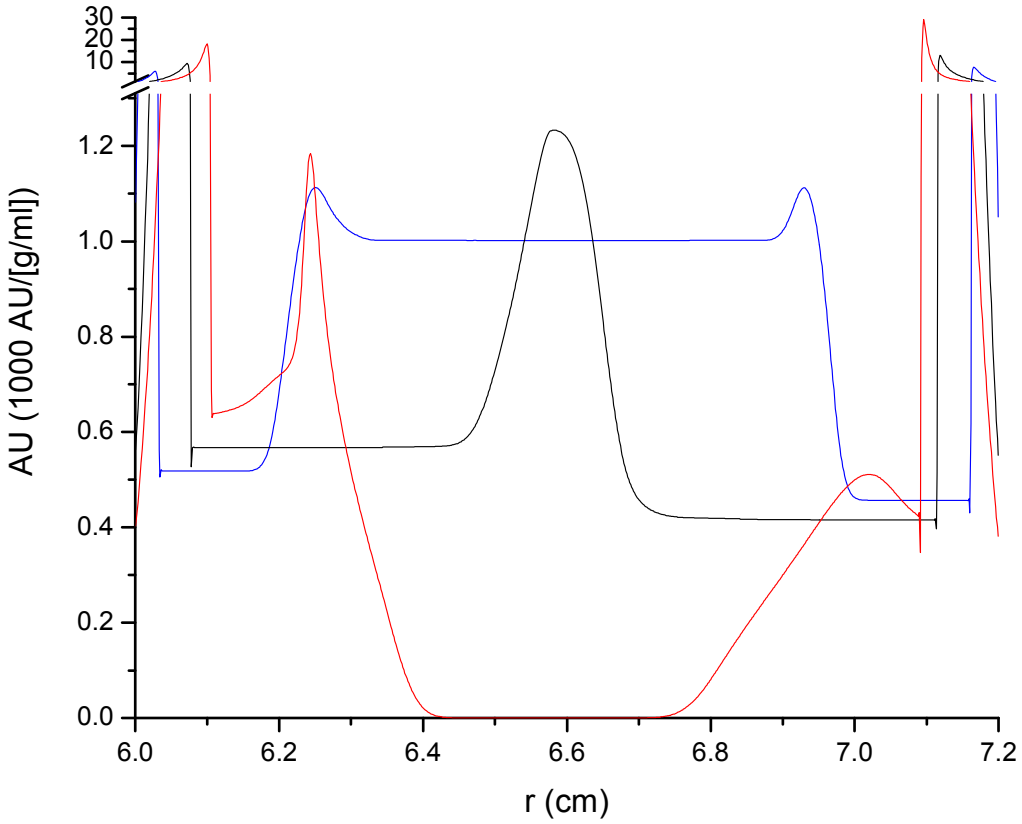

Figure 33. The sum of the signal from all low-concentration solutes versus r in the concentration-dependent system at t = 21 min (——), t = 51 min (——) and t = 81 min (——). High concentration data in the pellet and supernatant are shown on a compressed scale above the break in the AU-axis.

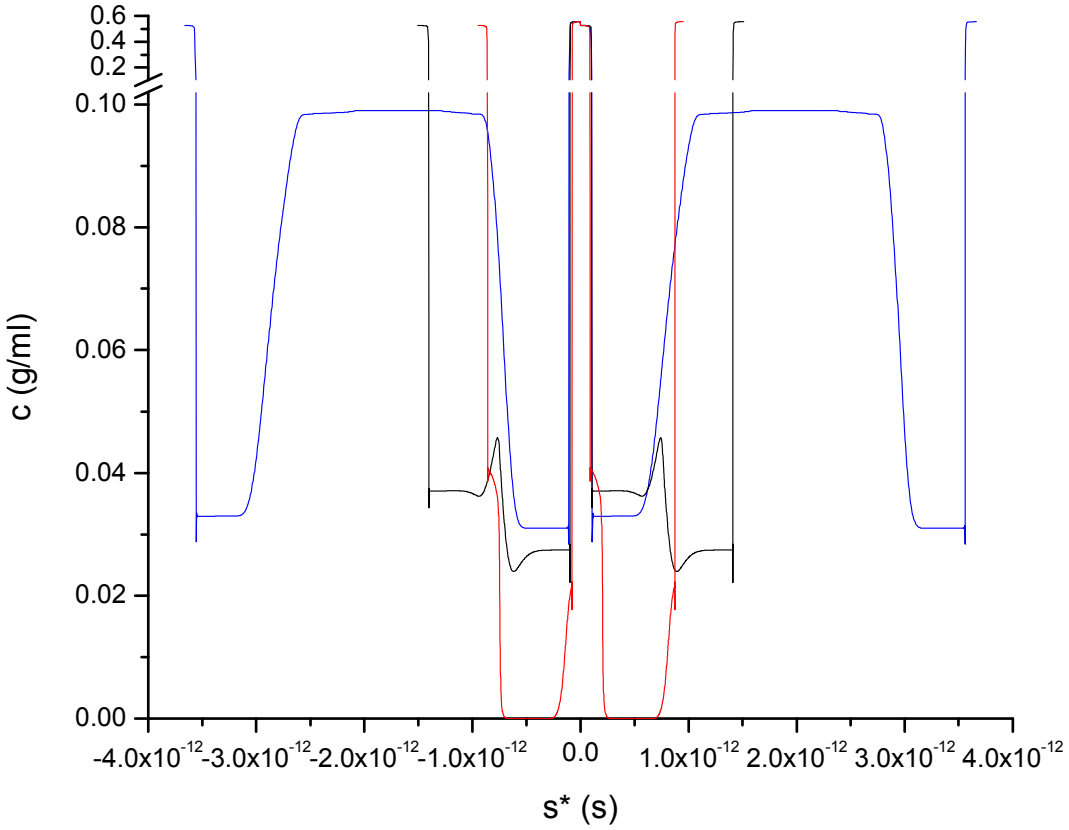

Figure 34. The sum of the concentration of all high-concentration solutes versus s* in the concentration-dependent system at t = 21 min (——), t = 51 min (——) and t = 81 min (——). High concentration data in the pellet and supernatant are shown on a compressed scale above the break in the c-axis.

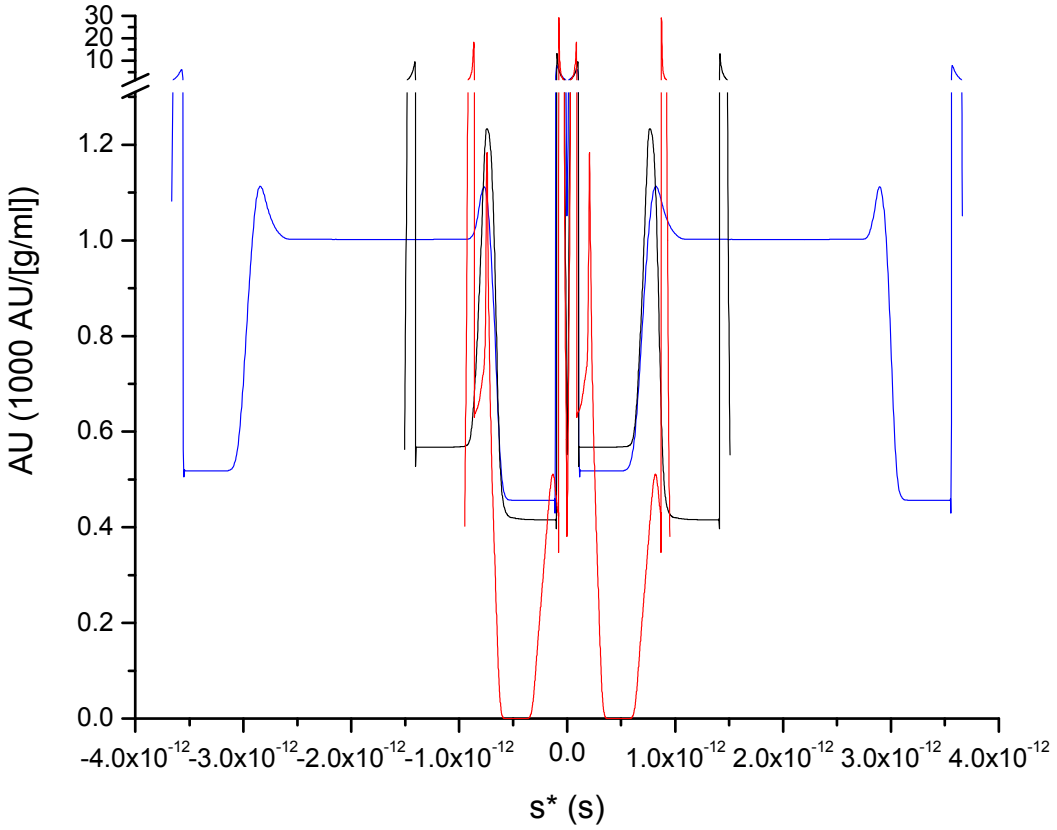

Figure 35. The sum of the signal from all low-concentration solutes versus s* in the concentration-dependent system at t = 21 min (——), t = 51 min (——) and t = 81 min (——). High concentration data in the pellet and supernatant are shown on a compressed scale above the break in the AU-axis.

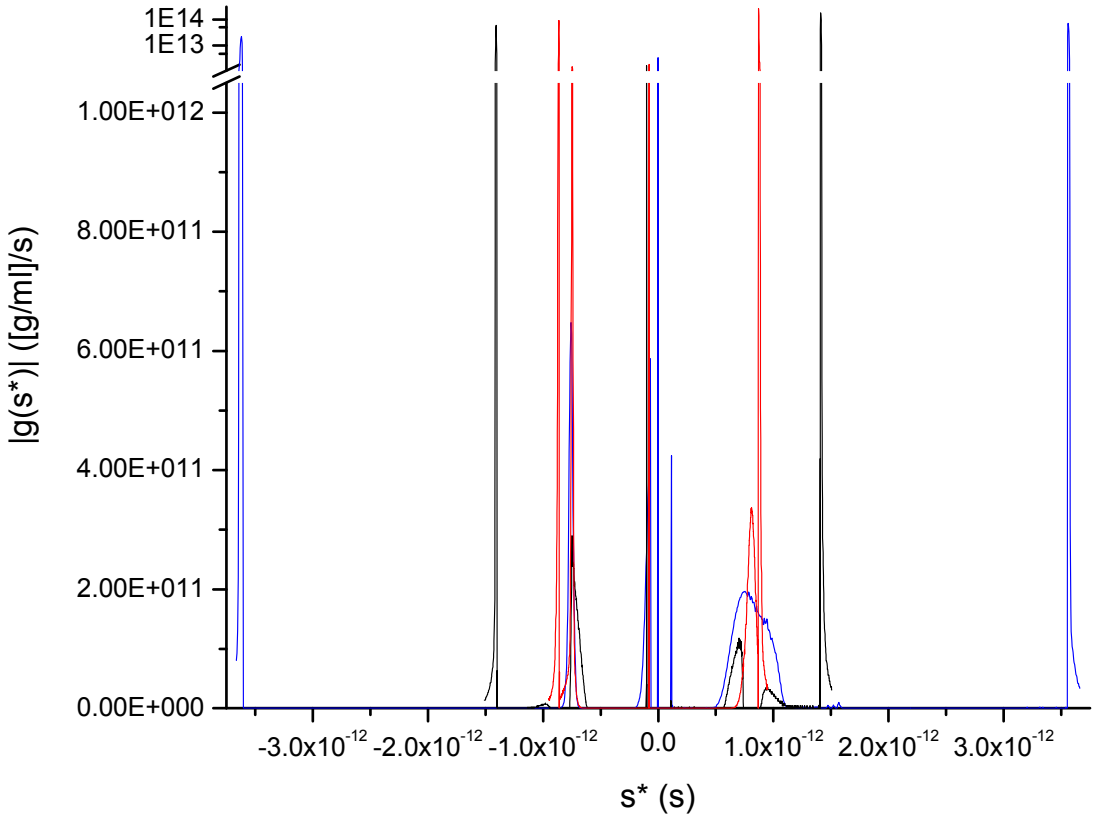

Figure 36a. Full s* range: |g(s*)| versus s* for the high-concentration data (Figures 32 and 34) of the concentration-dependent system at t = 21 min (——), t = 51 min (——) and t = 81 min (——). Data are shown on a logarithmic scale above the break in the |g(s*)|-axis.

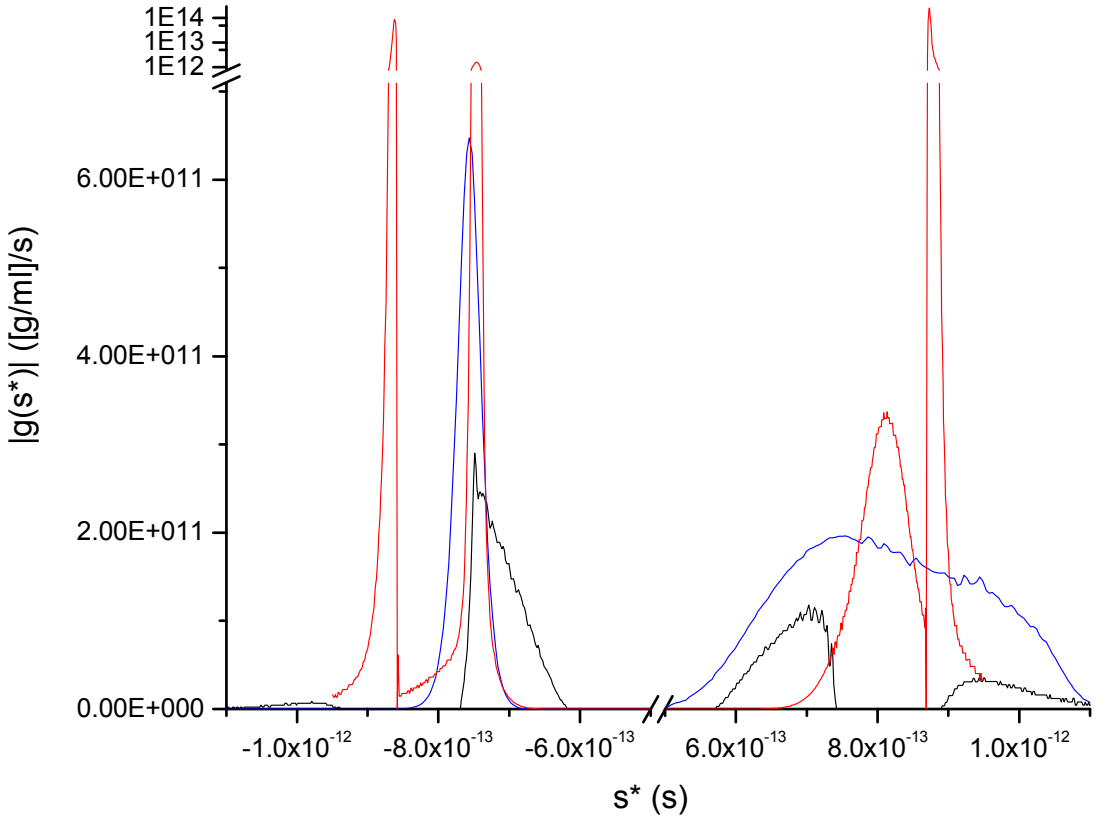

Figure 36b. Edited s* range: |g(s*)| versus s* for the high-concentration data (Figures 32 and 34) of the concentration-dependent system at t = 21 min (——), t = 51 min (——) and t = 81 min (——). Data are shown on a logarithmic scale above the break in the |g(s*)|-axis.

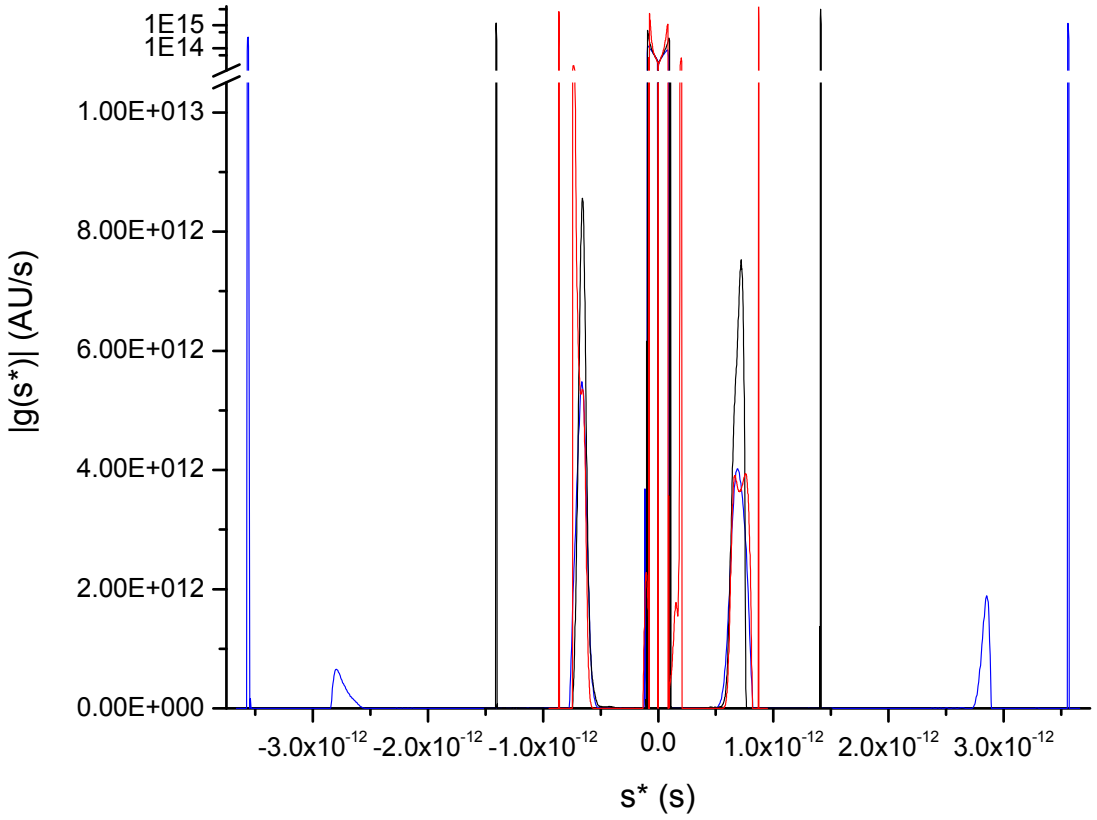

Figure 37a. Full s* range: |g(s*)| versus s* for the low-concentration data (Figures 33 and 35) of the concentration-dependent system at t = 21 min (——), t = 51 min (——) and t = 81 min (——). Data are shown on a logarithmic scale above the break in the |g(s*)|-axis.

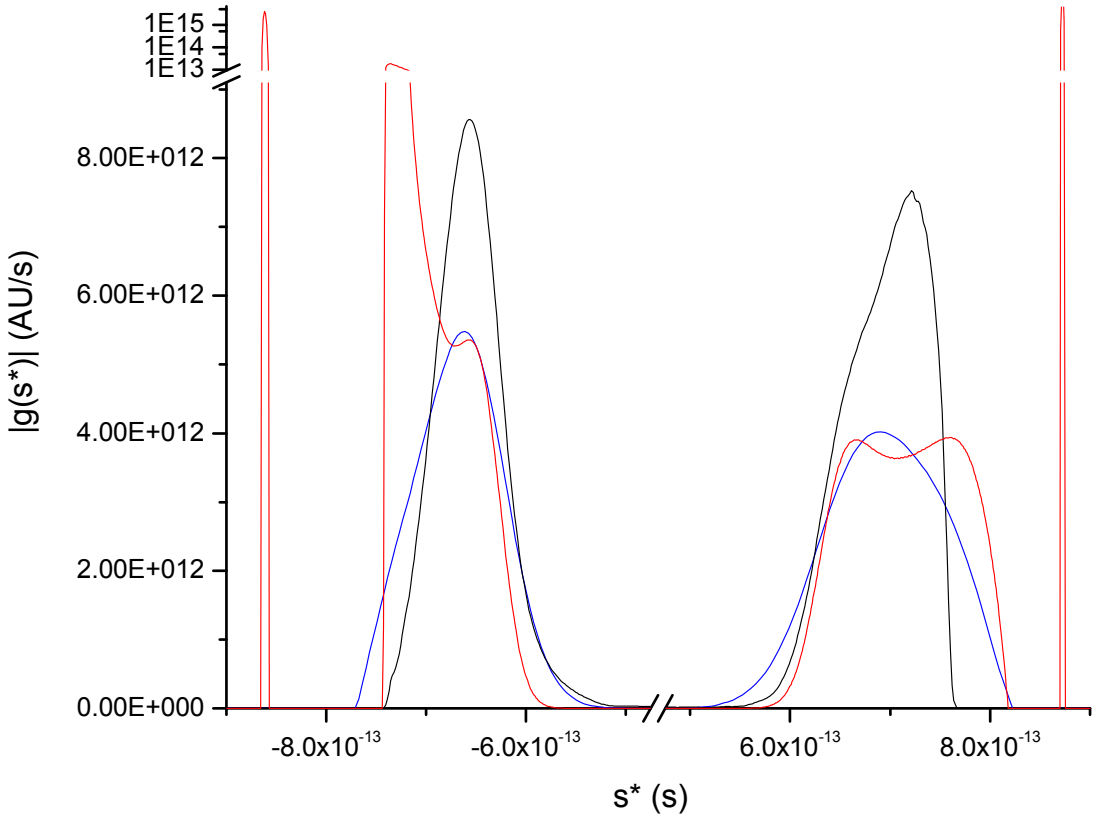

Figure 37b. Edited s* range: |g(s*)| versus s* for the low-concentration data (Figures 33 and 35) of the concentration-dependent system at t = 21 min (——), t = 51 min (——) and t = 81 min (——). Data are shown on a logarithmic scale above the break in the |g(s*)|-axis.

Three sets of signal versus r data were used in each ls-g(s*) analysis (Figures 38 and 39). The data analysed were from three time periods: 21 min ± 6 s, 51 min ± 6 s or 81 min ± 6 s. The data at the central time points of the ls-g(s*) analyses and the data shown in Figures 32 and 33 are the same. Within the analysis software, the positions of the radial extrema of the system were set to the known positions of the meniscus (r_m = 6 cm) and the base (r_b = 7.2 cm). In the truncated-range case, the lower and upper radial limits of analysis were set at r_m + 0.1124 cm and r_b – 0.1165 cm, respectively, and were chosen to include as much of any upwardly or downwardly

translating boundaries as possible, while excluding regions where back-diffusion near the meniscus or base was evident. In the full-range case, the lower and upper radial limits of analysis were set at $r_m + 0.01$ cm and $r_b - 0.01$ cm, respectively, and were chosen to include as much of the system as possible. The s* range and resolution used in the ls-g(s*) analyses depended on time: at t = 21 min, s* ranged from -42 Svedberg to 42 Svedberg, with a resolution of 840 points; at t = 51 min, s* ranged from -18 Svedberg to 18 Svedberg, with a resolution of 360 points; at t = 81 min, s* ranged from -12 Svedberg to 12 Svedberg, with a resolution of 240 points. In all analyses, neither the noise (whether TI or RI) nor the meniscus position was fit, and as the confidence level was set to 0, no regularisation was applied to the results of the analysis. To render the dimensionality of Figures 38 and 39 equivalent to that of Figures 36 and 37, the s* values returned by SEDFIT were multiplied by (10^{-13} s/Svedberg), and the ls-g(s*) values were multiplied by (1 Svedberg/10^{-13} s).

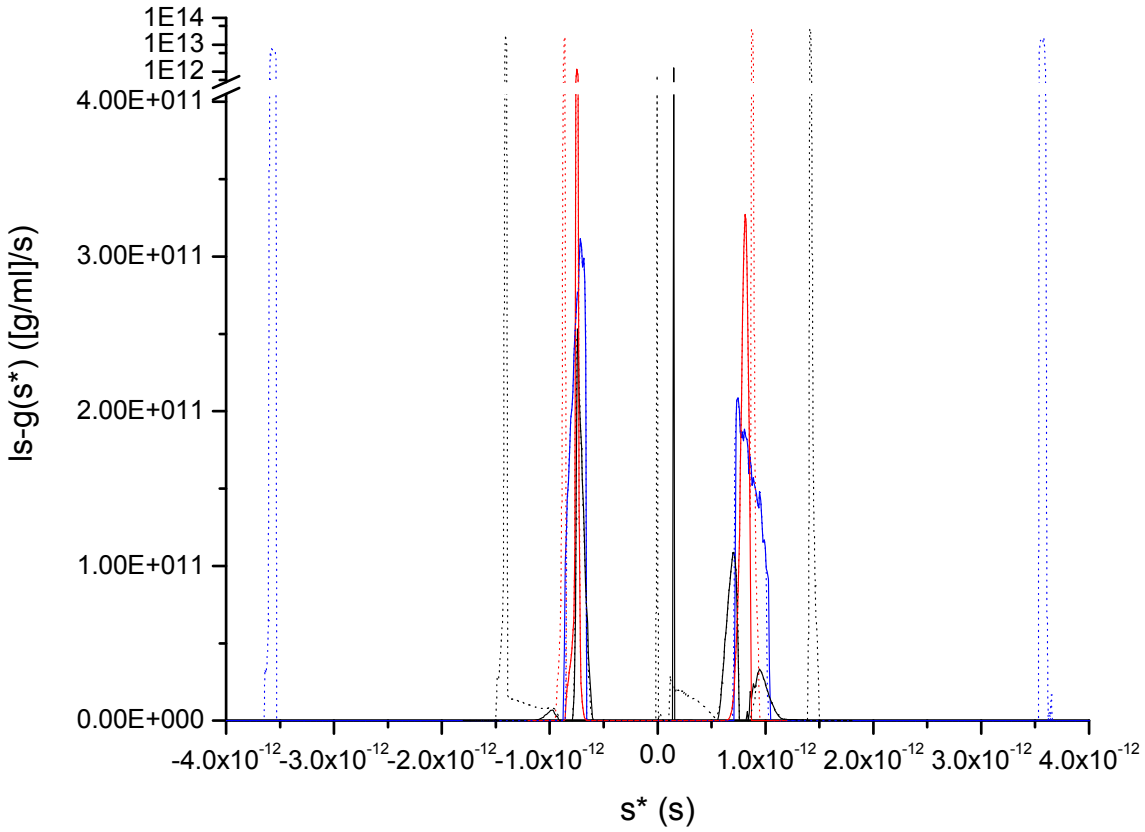

Figure 38a. Full s* range: ls-g(s*) versus s* for the high-concentration data (Figures 32 and 34) of the concentration-dependent system, fit with the lower and upper radial limits of analysis equal to r_m + 0.01 cm and r_b – 0.01 cm, respectively, at t = 21 min (·····), t = 51 min (·····) and t = 81 min (·····); and fit with the lower and upper radial limits of analysis equal to r_m + 0.1124 cm and r_b – 0.1165 cm, respectively, at t = 21 min (——), t = 51 min (——) and t = 81 min (——). Data are shown on a logarithmic scale above the break in the ls-g(s*)-axis.

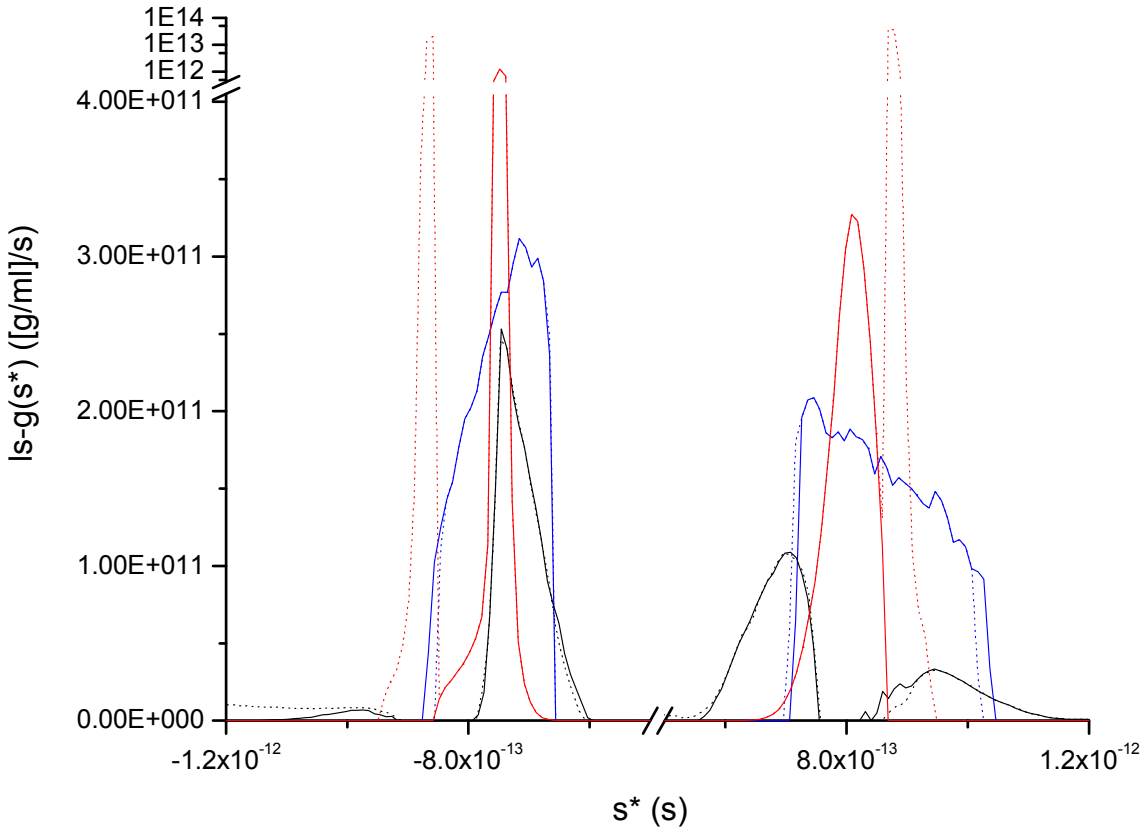

Figure 38b. Edited s* range: ls-g(s*) versus s* for the high-concentration data (Figures 32 and 34) of the concentration-dependent system, fit with the lower and upper radial limits of analysis equal to r_m + 0.01 cm and r_b – 0.01 cm, respectively, at t = 21 min (·····), t = 51 min (·····) and t = 81 min (·····); and fit with the lower and upper radial limits of analysis equal to r_m + 0.1124 cm and r_b – 0.1165 cm, respectively, at t = 21 min (——), t = 51 min (——) and t = 81 min (——). Data are shown on a logarithmic scale above the break in the ls-g(s*)-axis.

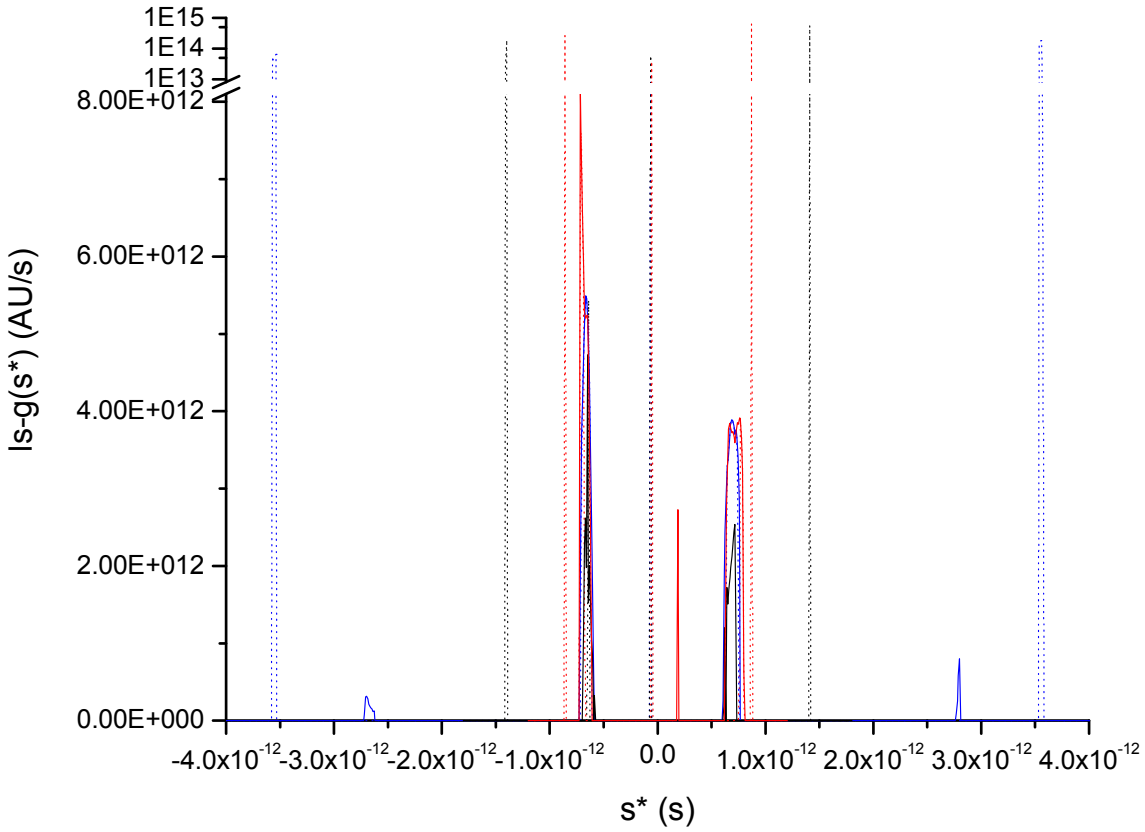

Figure 39a. Full s* range: ls-g(s*) versus s* for the low-concentration data (Figures 33 and 35) of the concentration-dependent system, fit with the lower and upper radial limits of analysis equal to r_m + 0.01 cm and r_b – 0.01 cm, respectively, at t = 21 min (·····), t = 51 min (·····) and t = 81 min (·····); and fit with the lower and upper radial limits of analysis equal to r_m + 0.1124 cm and r_b – 0.1165 cm, respectively, at t = 21 min (——), t = 51 min (——) and t = 81 min (——). Data are shown on a logarithmic scale above the break in the ls-g(s*)-axis.

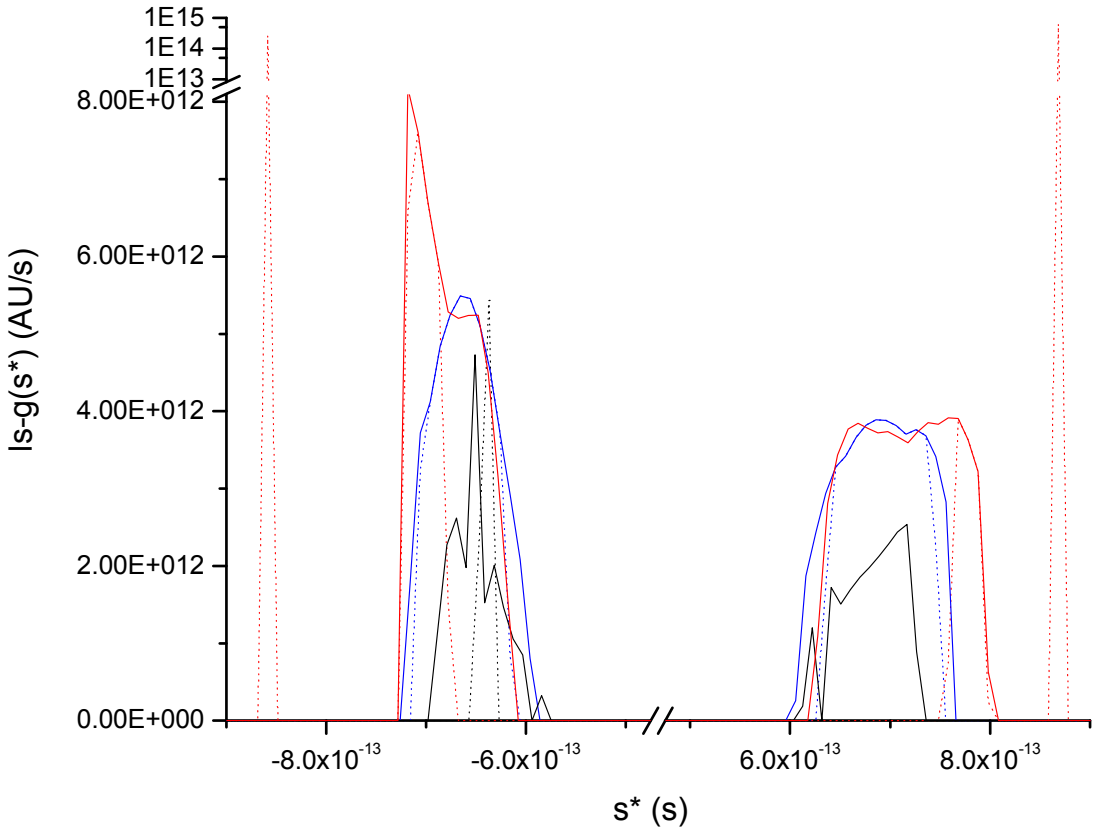

Figure 39b. Edited s* range: ls-g(s*) versus s* for the low-concentration data (Figures 33 and 35) of the concentration-dependent system, fit with the lower and upper radial limits of analysis equal to r_m + 0.01 cm and r_b – 0.01 cm, respectively, at t = 21 min (·····), t = 51 min (·····) and t = 81 min (·····); and fit with the lower and upper radial limits of analysis equal to r_m + 0.1124 cm and r_b – 0.1165 cm, respectively, at t = 21 min (——), t = 51 min (——) and t = 81 min (——). Data are shown on a logarithmic scale above the break in the ls-g(s*)-axis.

Figures 36 to 39 illustrate the time-dependence of |g(s*)| and ls-g(s*) results for a concentration-dependent system. Compared to the results for the concentration-independent example (Figures 28 and 30), the shape and position of the |g(s*)| and ls-g(s*) peaks are more variable in the concentration-dependent case. Nevertheless, the |g(s*)| and ls-g(s*) peaks of the high-

concentration solutes (Figures 36 and 38) appear to sharpen with time, as would be expected in the absence of any concentration dependence.

For the low-concentration results (Figures 37 and 39), the peaks in the vicinity of s* = -6.5E-13 s and s* = 6.5E-13 s show signs of splitting, but the newly developing pairs of peaks at t = 81 min occupy a similar range of s* as the corresponding peaks at t = 21 min. (From t = 21 min to t = 81 min, the range of s* occupied by these peaks grows more narrow as judged by the |g(s*)| results. Over the same time period, the negative-s* peak grows more narrow and the positive-s* peak broadens as judged by the ls-g(s*) results fit with the truncated range of s*.)

At each time point, ls-g(s*) fit with the truncated range of s* lacks the peaks in |g(s*)| that result from concentration gradients in the supernatant and pellet regions toward r_m = 6 cm and r_b = 7.2 cm, respectively (Figures 32 and 33). A comparison of Figures 36 and 38, which pertain to the high-concentration solutes, shows that |g(s*)| most resembles ls-g(s*) obtained with the broadest radial limits of analysis. A comparison of Figures 37 and 39, which pertain to the low-concentration solutes, shows that, within -8E-13 s < s* < 8E-13 s, |g(s*)| most resembles ls-g(s*) obtained with the most narrow radial limits of analysis, while, as might be expected, for s* < -8E-13 s and s* > 8E-13 s, |g(s*)| only resembles ls-g(s*) obtained with the broadest radial limits of analysis.

The greatest differences between |g(s*)| and ls-g(s*) are seen with the low-concentration data (Figures 37 and 39) at time t = 51 min, for which the ls-g(s*) results appear to be noisy and weakly responsive in the vicinity of s* = -6.5E-13 s and s* = 6.5E-13 s. That weak response is likely due to the substantial overlap of oppositely directed boundaries at that time. Although

ls-g(s*) appears to be less sensitive than g(s*) in this instance, the sensitivity of ls-g(s*) was greater than that of g(s*) in the case of the overlapping boundaries in the concentration-independent example discussed previously (t = 2460 s, Figure 28). With either approach, in general, analysis at multiple time points should reduce the extent to which instances of overlapping boundaries lead to erroneous conclusions.

The step function that describes c_{s^*}

As previously discussed, at any given time, the sum of an infinite number of step functions can be used to describe the total solute concentration at all radial positions. (Regions of supernatant and pellet accumulation can be included in such an approach, even though such regions are often excluded in any g(s*) analysis.) At a given time, t, at a given radial position, r, c_{s^*} (Equation 24), which is the concentration of a hypothetical solute characterised by s*, can be expressed as

$$c_{s^*} = \begin{Bmatrix} c_{p,s^*}[1 - H(r - r_{s^*})] \; for \; s^* \leq 0 \\ c_{p,s^*} H(r - r_{s^*}) \; for \; s^* \geq 0 \end{Bmatrix},$$

(46)

where

$$H(r - r_{s^*}) = \begin{Bmatrix} 1 \; for \; r - r_{s^*} \geq 0 \\ 0 \; for \; r - r_{s^*} < 0 \end{Bmatrix}$$

(47)

is the Heaviside step function as it applies to r – r_{s^*}. At time t, r_{s^*} is the boundary position of a hypothetical solute characterised by s* in the zero diffusion limit, and that boundary position is characterised by a hyper-sharp change in the solute concentration, c_{s^*}, from 0 to its plateau value, c_{p,s^*}. As r_{s^*} (Equation 23) and c_{p,s^*} (Equation 16) are time-dependent, c_{s^*} is time-dependent.

The sum of all c_{s^*} at a given radial position and time is equal to c at that position and time. As s* is continuous within $s^*_{-x} \leq s^* \leq s^*_{+x}$ (Equations 35 and 36), there is an infinite number of c_{s^*} values at a given position and time. There are also two oppositely buoyant hypothetical solutes that would each exhibit the same boundary position, r_{s^*}, at time t. At a given time, t, such solutes are related through

$$r_{s^*} = \begin{Bmatrix} r_{s^*_-} = r_b e^{s^*_- \omega^2 t} \\ r_{s^*_+} = r_m e^{s^*_+ \omega^2 t} \end{Bmatrix},$$

(48)

where the hypothetical solute of positive buoyancy is characterised by

$$s^*_- = \frac{1}{\omega^2 t} ln\left(\frac{r_{s^*_-}}{r_b}\right) < 0,$$

(49)

the hypothetical solute of negative buoyancy is characterised by

$$s^*_+ = \frac{1}{\omega^2 t} ln\left(\frac{r_{s^*_+}}{r_m}\right) > 0,$$

(50)

and the difference between the two s* values for which $r_{s^*_+} = r_{s^*_-} = r_{s^*}$ is

$$\Delta s^*_\pm = s^*_+ - s^*_- = \frac{1}{\omega^2 t} ln\left(\frac{r_b}{r_m}\frac{r_{s^*_+}}{r_{s^*_-}}\right) = \frac{1}{\omega^2 t} ln\left(\frac{r_b}{r_m}\right).$$

(51)

(The equation describing $\Delta s^*_\pm$ can also be obtained by equating the two expressions for r_{s^*} in Equation 48, and solving for $s^*_+ - s^*_-$.)

As $ln\left(\frac{r_{s^*_-}}{r_b}\right)$ and $ln\left(\frac{r_{s^*_+}}{r_m}\right)$ are proportional to t, s^*_- and s^*_+ are time-independent. As $ln\left(\frac{r_b}{r_m}\right)$ is a

constant, $\Delta s_{\pm}^{*}$ is inversely proportional to t. At any given time, then, $\left(\frac{\partial s_{-}^{*}}{\partial t}\right)_r = 0$ and $\left(\frac{\partial s_{+}^{*}}{\partial t}\right)_r = 0$, but $\left(\frac{\partial \Delta s_{\pm}^{*}}{\partial t}\right)_r = -\frac{\Delta s_{\pm}^{*}}{t}$. Any derivatives of s_{+}^{*}, s_{-}^{*} or $\Delta s_{\pm}^{*}$ at constant t are equal to zero.

Given Equations 49 and 50, which describe the two oppositely signed s* values, s_{-}^{*} and s_{+}^{*}, that characterise the two hypothetical solutes with oppositely directed boundaries at $r_{s_{+}^{*}} = r_{s_{-}^{*}} = r_{s^*}$ at time t, Equation 46 can be rewritten as

$$c_{s^*} = \begin{Bmatrix} c_{s_{-}^{*}} \\ c_{s_{+}^{*}} \end{Bmatrix} = \begin{Bmatrix} c_{p,s_{-}^{*}}\left[1 - H\left(r - r_{s_{-}^{*}}\right)\right] \\ c_{p,s_{+}^{*}} H\left(r - r_{s_{+}^{*}}\right) \end{Bmatrix} = \begin{Bmatrix} c_{p,s_{-}^{*}}\left[1 - H\left(r - r_b e^{s_{-}^{*}\omega^2 t}\right)\right] \\ c_{p,s_{+}^{*}} H\left(r - r_m e^{s_{+}^{*}\omega^2 t}\right) \end{Bmatrix},$$

(52)

where, at any given time, $c_{s_{-}^{*}}$ is the r-dependent concentration and $c_{p,s_{-}^{*}}$ is the r-independent plateau concentration of the hypothetical solute characterised by s_{-}^{*}, while $c_{s_{+}^{*}}$ is the r-dependent concentration and $c_{p,s_{+}^{*}}$ is the r-independent plateau concentration of the hypothetical solute characterised by s_{+}^{*}. In general, $c_{s_{-}^{*}}$, $c_{p,s_{-}^{*}}$, $c_{s_{+}^{*}}$ and $c_{p,s_{+}^{*}}$ are t-dependent.

At a given radial position, r, at a given time, t, the sum of all c_{s^*} as described by Equation 52 is equal to

$$c = \int_{c_{s_{-}^{*}=s_{-x}^{*}}}^{c_{s_{-}^{*}=0}} dc_{s_{-}^{*}} + \int_{c_{s_{+}^{*}=0}}^{c_{s_{+}^{*}=s_{+x}^{*}}} dc_{s_{+}^{*}}$$

$$= \int_{c_{s_{-}^{*}=s_{-x}^{*}}}^{c_{s_{-}^{*}=0}} \left[1 - H\left(r - r_b e^{s_{-}^{*}\omega^2 t}\right)\right] dc_{p,s_{-}^{*}} + \int_{c_{s_{+}^{*}=0}}^{c_{s_{+}^{*}=s_{+x}^{*}}} H\left(r - r_m e^{s_{+}^{*}\omega^2 t}\right) dc_{p,s_{+}^{*}}$$

(53a)

in the continuous case, and

$$c = \sum_{s_-^*=s_{-x}^*}^{0} c_{s_-^*} + \sum_{s_+^*=0}^{s_{+x}^*} c_{s_+^*} = \sum_{s_-^*=s_{-x}^*}^{0} c_{p,s_-^*}\left[1 - H\left(r - r_b e^{s_-^* \omega^2 t}\right)\right] + \sum_{s_+^*=0}^{s_{+x}^*} c_{p,s_+^*} H\left(r - r_m e^{s_+^* \omega^2 t}\right)$$

(53b)

in the discrete case.

If Equation 53 were used to differentiate c with respect to s* at constant t, or if Equation 3 were applied to Equation 53, only the essential values of $\left(\frac{\partial c}{\partial s^*}\right)_t$ would be obtained. To obtain the redundant values of $\left(\frac{\partial c}{\partial s^*}\right)_t$ from c described as a function of r and t, the step functions in Equation 52 must be written in terms of the s* values at which $\left(\frac{\partial c}{\partial s^*}\right)_t$ would be redundant. Doing so results in

$$c_{s^*} = \begin{Bmatrix} c_{s_-^*} \\ c_{s_+^*} \end{Bmatrix} = \begin{Bmatrix} c_{p,s_-^*}\left[1 - H\left(r - r_{s_-^*}\right)\right] \\ c_{p,s_+^*} H\left(r - r_{s_+^*}\right) \end{Bmatrix} = \begin{Bmatrix} c_{p,s_-^*}\left[1 - H\left(r - r_m e^{\{s_-^* + \Delta s_\pm^*\}\omega^2 t}\right)\right] \\ c_{p,s_+^*} H\left(r - r_b e^{\{s_+^* - \Delta s_\pm^*\}\omega^2 t}\right) \end{Bmatrix}.$$

(54)

At a given radial position, r, at a given time, t, the sum of all c_{s^*} as described by Equation 54 is

$$c = \int_{c_{s_-^*=s_{-x}^*}}^{c_{s_-^*=0}} dc_{s_-^*} + \int_{c_{s_+^*=0}}^{c_{s_+^*=s_{+x}^*}} dc_{s_+^*}$$

$$= \int_{c_{s_-^*=s_{-x}^*}}^{c_{s_-^*=0}} \left[1 - H\left(r - r_m e^{\{s_-^* + \Delta s_\pm^*\}\omega^2 t}\right)\right] dc_{p,s_-^*} + \int_{c_{s_+^*=0}}^{c_{s_+^*=s_{+x}^*}} H\left(r - r_b e^{\{s_+^* - \Delta s_\pm^*\}\omega^2 t}\right) dc_{p,s_+^*}$$

(55a)

in the continuous case, and

$$c = \sum_{s_-^*=s_{-x}^*}^{0} c_{s_-^*} + \sum_{s_+^*=0}^{s_{+x}^*} c_{s_+^*}$$

$$= \sum_{s_-^*=s_{-x}^*}^{0} c_{p,s_-^*}\left[1 - H\left(r - r_m e^{\left\{s_-^* + \Delta s_\pm^*\right\}\omega^2 t}\right)\right] + \sum_{s_+^*=0}^{s_{+x}^*} c_{p,s_+^*} H\left(r - r_b e^{\left\{s_+^* - \Delta s_\pm^*\right\}\omega^2 t}\right)$$

(55b)

in the discrete case.

Equations 53 and 55 both describe c as a function of r and t, and either can be used to determine $\left(\frac{\partial c}{\partial r}\right)_t$, but both are needed to determine $\left(\frac{\partial c}{\partial s^*}\right)_t$. The two expressions for $\left(\frac{\partial c}{\partial r}\right)_t$ will be obtained first, and to obtain $\left(\frac{\partial c}{\partial s^*}\right)_t$, Equation 3 will then be applied to both expressions for $\left(\frac{\partial c}{\partial r}\right)_t$.

As with c_{p,s^*} (Equation 16), c_{p,s_+^*} and c_{p,s_-^*} are dependent on t, but independent of r, so that, at any given time, $\left(\frac{\partial c_{p,s_+^*}}{\partial r}\right)_t = 0$ and $\left(\frac{\partial c_{p,s_-^*}}{\partial r}\right)_t = 0$. Thus, differentiating c with respect to r at constant t yields, using the discrete form of Equation 53 to express c,

$$\left(\frac{\partial c}{\partial r}\right)_t = \sum_{s_-^*=s_{-x}^*}^{0} \left(\frac{\partial c_{s_-^*}}{\partial r}\right)_t + \sum_{s_+^*=0}^{s_{+x}^*} \left(\frac{\partial c_{s_+^*}}{\partial r}\right)_t = \left(\frac{\partial c_{s^*}}{\partial r}\right)_t = \left\{\begin{matrix}\left(\frac{\partial c_{s_-^*}}{\partial r}\right)_t \\ \left(\frac{\partial c_{s_+^*}}{\partial r}\right)_t\end{matrix}\right\} = \left\{\begin{matrix}-c_{p,s_-^*}\delta\left(r - r_{s_-^*}\right) \\ c_{p,s_+^*}\delta\left(r - r_{s_+^*}\right)\end{matrix}\right\}$$

$$= \left\{\begin{matrix}-c_{p,s_-^*}\delta\left(r - r_b e^{s_-^*\omega^2 t}\right) \\ c_{p,s_+^*}\delta\left(r - r_m e^{s_+^*\omega^2 t}\right)\end{matrix}\right\},$$

(56a)

or, using the discrete form of Equation 55 to express c,

$$\left(\frac{\partial c}{\partial r}\right)_t = \sum_{s_-^*=s_{-x}^*}^{0}\left(\frac{\partial c_{s_-^*}}{\partial r}\right)_t + \sum_{s_+^*=0}^{s_{+x}^*}\left(\frac{\partial c_{s_+^*}}{\partial r}\right)_t = \left(\frac{\partial c_{s^*}}{\partial r}\right)_t = \begin{Bmatrix}\left(\frac{\partial c_{s_-^*}}{\partial r}\right)_t \\ \left(\frac{\partial c_{s_+^*}}{\partial r}\right)_t\end{Bmatrix} = \begin{Bmatrix}-c_{p,s_-^*}\delta\left(r - r_{s_-^*}\right) \\ c_{p,s_+^*}\delta\left(r - r_{s_+^*}\right)\end{Bmatrix}$$

$$= \begin{Bmatrix}-c_{p,s_-^*}\delta\left(r - r_m e^{\{s_-^* + \Delta s_\pm^*\}\omega^2 t}\right) \\ c_{p,s_+^*}\delta\left(r - r_b e^{\{s_+^* - \Delta s_\pm^*\}\omega^2 t}\right)\end{Bmatrix},$$

(56b)

where, in either case, for $r_{s^*} = r_{s_+^*}$ or $r_{s^*} = r_{s_-^*}$,

$$\delta(r - r_{s^*}) = \left(\frac{\partial H(r - r_{s^*})}{\partial r}\right)_t = \begin{Bmatrix}\infty\ for\ r - r_{s^*} = 0 \\ 0\ for\ r - r_{s^*} \neq 0\end{Bmatrix}$$

(57)

is the Dirac delta function as it applies to $r - r_{s^*}$. The sum of all $\left(\frac{\partial c_{s^*}}{\partial r}\right)_t$ at a given radial position and time is equal to $\left(\frac{\partial c}{\partial r}\right)_t$ at that position and time, and as with c_{s^*}, there is an infinite number of $\left(\frac{\partial c_{s^*}}{\partial r}\right)_t$ values at a given radial position and time. However, as $\delta(r - r_{s^*}) = 0$ except where $r = r_{s^*}$, at any time t, and at any position r, $\left(\frac{\partial c}{\partial r}\right)_t$ is equal to just the two nonzero values of $\left(\frac{\partial c_{s^*}}{\partial r}\right)_t$ for which $r = r_{s^*}$, those being $\left(\frac{\partial c_{s_-^*}}{\partial r}\right)_t$ and $\left(\frac{\partial c_{s_+^*}}{\partial r}\right)_t$. Hence, starting with either form of Equations 53 or 55, $\left(\frac{\partial c}{\partial r}\right)_t$ yields neither a summation nor an integral.

Calculating $\left(\frac{\partial c}{\partial s^*}\right)_t$ *from* $\left(\frac{\partial c}{\partial r}\right)_t$

Applying Equation 3 to the sum of both results given by Equation 56 yields

$$\left(\frac{\partial c}{\partial s^*}\right)_t = \left(\frac{\partial c}{\partial r}\right)_t \left(\frac{\partial r}{\partial s^*}\right)_t = \left(\frac{\partial c_{s^*}}{\partial r}\right)_t r\omega^2 t = \begin{Bmatrix} \left(\frac{\partial c_{s_-^*}}{\partial r}\right)_t r\omega^2 t \\ \left(\frac{\partial c_{s_+^*}}{\partial r}\right)_t r\omega^2 t \end{Bmatrix} = \begin{Bmatrix} -c_{p,s_-^*}\delta\left(r - r_{s_-^*}\right) r\omega^2 t \\ c_{p,s_+^*}\delta\left(r - r_{s_+^*}\right) r\omega^2 t \end{Bmatrix}$$

$$= \begin{Bmatrix} -c_{p,s_-^*}\left[\delta\left(r - r_b e^{s_-^*\omega^2 t}\right) + \delta\left(r - r_m e^{\{s_-^* + \Delta s_\pm^*\}\omega^2 t}\right)\right] r\omega^2 t \\ c_{p,s_+^*}\left[\delta\left(r - r_m e^{s_+^*\omega^2 t}\right) + \delta\left(r - r_b e^{\{s_+^* - \Delta s_\pm^*\}\omega^2 t}\right)\right] r\omega^2 t \end{Bmatrix}$$

$$= \begin{Bmatrix} -c_{p,s_-^*}\delta\left(r - r_b e^{s_-^*\omega^2 t}\right)\omega^2 t r_b e^{s_-^*\omega^2 t} - c_{p,s_-^*}\delta\left(r - r_m e^{\{s_-^* + \Delta s_\pm^*\}\omega^2 t}\right)\omega^2 t r_m e^{\{s_-^* + \Delta s_\pm^*\}\omega^2 t} \\ c_{p,s_+^*}\delta\left(r - r_m e^{s_+^*\omega^2 t}\right)\omega^2 t r_m e^{s_+^*\omega^2 t} + c_{p,s_+^*}\delta\left(r - r_b e^{\{s_+^* - \Delta s_\pm^*\}\omega^2 t}\right)\omega^2 t r_b e^{\{s_+^* - \Delta s_\pm^*\}\omega^2 t} \end{Bmatrix},$$

(58)

where $r_{s_+^*} = r_{s_-^*} = r_{s^*}$, and where the various forms of $\delta(r - r_{s^*})r\omega^2 t$ were equated to the corresponding forms of $\delta(r - r_{s^*})r_{s^*}\omega^2 t$ on the basis of $\delta(r - r_{s^*})$ being equal to zero for all $r \neq r_{s^*}$.

The properties of the Dirac delta function are such that

$$\delta(s^* - \varsigma^*) = \left(\frac{\partial H(s^* - \varsigma^*)}{\partial s^*}\right)_t = \left(\frac{\partial H(r - r_{s^*})}{\partial r}\right)_t \left(\frac{\partial r}{\partial s^*}\right)_t = \delta(r - r_{s^*})r\omega^2 t = \delta(r - r_{s^*})r_{s^*}\omega^2 t,$$

(59)

where $\delta(r - r_{s^*})r\omega^2 t$ can be equated to $\delta(r - r_{s^*})r_{s^*}\omega^2 t$ on the basis of $\delta(r - r_{s^*})$ being equal to zero for all $r \neq r_{s^*}$. As applied to c and $\left(\frac{\partial c}{\partial s^*}\right)_t$, in both the Heaviside step function, $H(s^* - \varsigma^*)$, and its Dirac delta function, $\delta(s^* - \varsigma^*)$, ς^* will be shown (Equations 64 and 67) to be one of the two values, s_+^* and s_-^*, that characterise the two hypothetical solutes with oppositely directed boundaries at $r_{s_+^*} = r_{s_-^*} = r_{s^*}$ at time t (Equation 48). Thus, in Equation 58,

$$-c_{p,s_-^*}\delta\left(r - r_b e^{s_-^*\omega^2 t}\right)\omega^2 t r_b e^{s_-^*\omega^2 t} = -c_{p,s_-^*}\delta(s^* - s_-^*) = q(s_-^*, t)\,,$$

(60)

$$c_{p,s_+^*}\delta\left(r - r_m e^{s_+^*\omega^2 t}\right)\omega^2 t r_m e^{s_+^*\omega^2 t} = c_{p,s_+^*}\delta(s^* - s_+^*) = q(s_+^*, t)\,,$$

(61)

$$-c_{p,s_-^*}\delta\left(r - r_m e^{\left\{s_-^* + \Delta s_\pm^*\right\}\omega^2 t}\right)\omega^2 t r_m e^{\left\{s_-^* + \Delta s_\pm^*\right\}\omega^2 t} = -c_{p,s_-^*}\delta\left(s^* - \left\{s_-^* + \Delta s_\pm^*\right\}\right) = e(s_-^*, t)$$

(62)

and

$$c_{p,s_+^*}\delta\left(r - r_b e^{\left\{s_+^* - \Delta s_\pm^*\right\}\omega^2 t}\right)\omega^2 t r_b e^{\left\{s_+^* - \Delta s_\pm^*\right\}\omega^2 t} = c_{p,s_+^*}\delta\left(s^* - \left\{s_+^* - \Delta s_\pm^*\right\}\right) = e(s_+^*, t)\,.$$

(63)

In Equation 62, $\left\{s_-^* + \Delta s_\pm^*\right\}$ is equal to the value of s_+^* that shares r_{s^*} in common with s_-^*, such that $r_{s^*} = r_m e^{\left\{s_-^* + \Delta s_\pm^*\right\}\omega^2 t} = r_b e^{s_-^*\omega^2 t}$. In Equation 63, $\left\{s_+^* - \Delta s_\pm^*\right\}$ is equal to the value of s_-^* that shares r_{s^*} in common with s_+^*, such that $r_{s^*} = r_b e^{\left\{s_+^* - \Delta s_\pm^*\right\}\omega^2 t} = r_m e^{s_+^*\omega^2 t}$.

The step-function form of c as a function of s and t*

For c expressed as a function of s* and t, c_{s^*} is the concentration of a hypothetical solute characterised by s*. In transforming the independent variables from r and t to s* and t, c at each radial position r becomes equal to c at the two corresponding values of s* given by Equation 27. At any given time, for c expressed as a function of s* and t, $c_{s_-^*}$ is the s*-dependent concentration and c_{p,s_-^*} is the plateau concentration of the hypothetical solute characterised by s_-^*, while $c_{s_+^*}$ is the s*-dependent concentration and c_{p,s_+^*} is the plateau concentration of the hypothetical solute characterised by s_+^*. In general, for c expressed as a function of s* and t, $c_{s_-^*}$, c_{p,s_-^*}, $c_{s_+^*}$ and c_{p,s_+^*} are t-dependent.

At a given apparent sedimentation coefficient, s*, at a given time, t, the sum of all c_{s^*} is equal to

$$c = \int_{c_{s_-^*=s_{-x}^*}}^{c_{s_-^*=0}} dc_{s_-^*} + \int_{c_{s_+^*=0}}^{c_{s_+^*=s_{+x}^*}} dc_{s_+^*}$$

$$= \int_{c_{s_-^*=s_{-x}^*}}^{c_{s_-^*=0}} \left\{[1 - H(s^* - s_-^*)] + \left[1 - H\left(s^* - \left\{s_-^* + \Delta s_\pm^*\right\}\right)\right]\right\} dc_{p,s_-^*}$$

$$+ \int_{c_{s_+^*=0}}^{c_{s_+^*=s_{+x}^*}} \left\{H(s^* - s_+^*) + H\left(s^* - \left\{s_+^* - \Delta s_\pm^*\right\}\right)\right\} dc_{p,s_+^*},$$

(64a)

in the continuous case, and

$$c = \sum_{s_-^*=s_{-x}^*}^{0} c_{s_-^*} + \sum_{s_+^*=0}^{s_{+x}^*} c_{s_+^*}$$

$$= \sum_{s_-^*=s_{-x}^*}^{0} c_{p,s_-^*}\left\{[1 - H(s^* - s_-^*)] + \left[1 - H\left(s^* - \left\{s_-^* + \Delta s_\pm^*\right\}\right)\right]\right\}$$

$$+ \sum_{s_+^*=0}^{s_{+x}^*} c_{p,s_+^*}\left\{H(s^* - s_+^*) + H\left(s^* - \left\{s_+^* - \Delta s_\pm^*\right\}\right)\right\},$$

(64b)

in the discrete case. The value of s_+^* that shares r_{s^*} in common with s_-^* has been expressed as $\left\{s_-^* + \Delta s_\pm^*\right\}$ in the integral with respect to $c_{s_-^*}$ or the sum over all s_-^*. The value of s_-^* that shares r_{s^*} in common with s_+^* has been expressed as $\left\{s_+^* - \Delta s_\pm^*\right\}$ in the integral with respect to $c_{s_+^*}$ or the sum over all s_+^*. The integrals or sums in which [1 – H(s* – $\{s_-^* + \Delta s_\pm^*\}$)] and H(s* – $\{s_+^* - \Delta s_\pm^*\}$) appear will give rise to the redundant values of $\left(\frac{\partial c}{\partial s^*}\right)_t$, while the integrals or sums in which [1 – H(s* – s_-^*)] and H(s* – s_+^*) appear will give rise to the essential values of $\left(\frac{\partial c}{\partial s^*}\right)_t$.

The Heaviside step functions in Equation 64 are described by

$$H(s^* - \varsigma^*) = \begin{Bmatrix} 1\ for\ s^* - \varsigma^* \geq 0 \\ 0\ for s^* - \varsigma^* < 0 \end{Bmatrix},$$

(65)

where ς* may equal s_-^*, $\{s_-^* + \Delta s_\pm^*\}$, s_+^* or $\{s_+^* - \Delta s_\pm^*\}$. The corresponding Dirac delta function is given by

$$\left(\frac{\partial H(s^* - \varsigma^*)}{\partial s^*}\right)_t \left(\frac{\partial (s^* - \varsigma^*)}{\partial s^*}\right)_t = \left(\frac{\partial H(s^* - \varsigma^*)}{\partial s^*}\right)_t \left[\left(\frac{\partial s^*}{\partial s^*}\right)_t - \left(\frac{\partial \varsigma^*}{\partial s^*}\right)_t\right] = \left(\frac{\partial H(s^* - \varsigma^*)}{\partial s^*}\right)_t$$

$$= \delta(s^* - \varsigma^*) = \begin{Bmatrix} \infty\ for\ s^* - \varsigma^* = 0 \\ 0\ for s^* - \varsigma^* \neq 0 \end{Bmatrix},$$

(66)

where $\left(\frac{\partial s^*}{\partial s^*}\right)_t = 1$ and, for ς* equal to s_-^*, $\{s_-^* + \Delta s_\pm^*\}$, s_+^* or $\{s_-^* - \Delta s_\pm^*\}$, $\left(\frac{\partial \varsigma^*}{\partial s^*}\right)_t = 0$. The relationship of δ(s* - ς*) to δ(r - r_{s^*}), is described by Equation 59.

Applying Equation 3 to $\left(\frac{\partial c_{p,s_-^*}}{\partial r}\right)_t = 0$ and $\left(\frac{\partial c_{p,s_+^*}}{\partial r}\right)_t = 0$ yields $\left(\frac{\partial c_{p,s_-^*}}{\partial s^*}\right)_t = \left(\frac{\partial c_{p,s_-^*}}{\partial r}\right)_t \left(\frac{\partial r}{\partial s^*}\right)_t = 0$ and $\left(\frac{\partial c_{p,s_+^*}}{\partial s^*}\right)_t = \left(\frac{\partial c_{p,s_+^*}}{\partial r}\right)_t \left(\frac{\partial r}{\partial s^*}\right)_t = 0$, respectively. Thus, using the discrete form of Equation 64 to express c,

$$\left(\frac{\partial c}{\partial s^*}\right)_t = \sum_{s_-^* = s_{-x}^*}^{0} \left(\frac{\partial c_{s_-^*}}{\partial s^*}\right)_t + \sum_{s_+^* = 0}^{s_{+x}^*} \left(\frac{\partial c_{s_+^*}}{\partial s^*}\right)_t = \left(\frac{\partial c_{s^*}}{\partial s^*}\right)_t = \begin{Bmatrix} \left(\frac{\partial c_{s_-^*}}{\partial s^*}\right)_t \\ \left(\frac{\partial c_{s_+^*}}{\partial s^*}\right)_t \end{Bmatrix}$$

$$= \begin{Bmatrix} -c_{p,s_-^*}\left[\delta(s^* - s_-^*) + \delta\left(s^* - \{s_-^* + \Delta s_\pm^*\}\right)\right] \\ c_{p,s_+^*}\left[\delta(s^* - s_+^*) + \delta\left(s^* - \{s_+^* - \Delta s_\pm^*\}\right)\right] \end{Bmatrix}$$

$$= \begin{Bmatrix} -c_{p,s_-^*}\delta(s^* - s_-^*) - c_{p,s_-^*}\delta\left(s^* - \{s_-^* + \Delta s_\pm^*\}\right) \\ c_{p,s_+^*}\delta(s^* - s_+^*) + c_{p,s_+^*}\delta\left(s^* - \{s_+^* - \Delta s_\pm^*\}\right) \end{Bmatrix} = \begin{Bmatrix} q(s_-^*, t) + e(s_-^*, t) \\ q(s_+^*, t) + e(s_+^*, t) \end{Bmatrix}$$

$$= q(s^*, t) + e(s^*, t),$$

(67)

where $q(s_-^*, t) = = -c_{p,s_-^*}\delta(s^* - s_-^*)$, $q(s_+^*, t) = c_{p,s_+^*}\delta(s^* - s_+^*)$, $e(s_-^*, t) = -c_{p,s_-^*}\delta\left(s^* - \left\{s_-^* + \Delta s_\pm^*\right\}\right)$ and $e(s_+^*, t) = c_{p,s_+^*}\delta\left(s^* - \left\{s_+^* - \Delta s_\pm^*\right\}\right)$. Equations 37 and 64 both describe c as a function of s* and t. Equation 67 describes the integrand of Equation 37.

Back-calculating $\left(\frac{\partial c}{\partial r}\right)_t$ *from* $\left(\frac{\partial c}{\partial s^*}\right)_t$

Applying Equations 3 and 28 to Equation 67, and using Equations 27, 49, 50 and 51 to express s*, s_-^*, s_+^* and $\Delta s_\pm^*$, respectively, in terms of ω, t, r, r_b and r_m, yields

$$\left(\frac{\partial c}{\partial s^*}\right)_t = \left(\frac{\partial c}{\partial s^*}\right)_t \left(\frac{\partial s^*}{\partial r}\right)_t = \left(\frac{\partial c_{s^*}}{\partial s^*}\right)_t \frac{1}{r\omega^2 t} = \begin{Bmatrix} \left(\frac{\partial c_{s_+^*}}{\partial s^*}\right)_t \frac{1}{r\omega^2 t} \\ \left(\frac{\partial c_{s_-^*}}{\partial s^*}\right)_t \frac{1}{r\omega^2 t} \end{Bmatrix}$$

$$= \begin{Bmatrix} -\frac{c_{p,s_-^*}}{r\omega^2 t}\left[\delta(s^* - s_-^*) + \delta\left(s^* - \left\{s_-^* + \Delta s_\pm^*\right\}\right)\right] \\ \frac{c_{p,s_+^*}}{r\omega^2 t}\left[\delta(s^* - s_+^*) + \delta\left(s^* - \left\{s_+^* - \Delta s_\pm^*\right\}\right)\right] \end{Bmatrix}$$

$$= \begin{Bmatrix} -\frac{c_{p,s_-^*}}{r_{s_-^*}\omega^2 t}\left[\delta\left(\frac{ln\left(\frac{r}{r_b}\right) - ln\left(\frac{r_{s_-^*}}{r_b}\right)}{\omega^2 t}\right) + \delta\left(\frac{ln\left(\frac{r}{r_m}\right) - \left\{ln\left(\frac{r_{s_-^*}}{r_b}\right) + ln\left(\frac{r_b}{r_m}\right)\right\}}{\omega^2 t}\right)\right] \\ \frac{c_{p,s_+^*}}{r_{s_+^*}\omega^2 t}\left[\delta\left(\frac{ln\left(\frac{r}{r_m}\right) - ln\left(\frac{r_{s_+^*}}{r_m}\right)}{\omega^2 t}\right) + \delta\left(\frac{ln\left(\frac{r}{r_b}\right) - \left\{ln\left(\frac{r_{s_+^*}}{r_m}\right) - ln\left(\frac{r_b}{r_m}\right)\right\}}{\omega^2 t}\right)\right] \end{Bmatrix}$$

$$= \begin{Bmatrix} -\frac{c_{p,s_-^*}}{r_{s_-^*}\omega^2 t}\left[\delta\left(\frac{ln\left(\frac{r}{r_b}\right) - ln\left(\frac{r_{s_-^*}}{r_b}\right)}{\omega^2 t}\right) + \delta\left(\frac{ln\left(\frac{r}{r_m}\right) - ln\left(\frac{r_{s_-^*}}{r_m}\right)}{\omega^2 t}\right)\right] \\ \frac{c_{p,s_+^*}}{r_{s_+^*}\omega^2 t}\left[\delta\left(\frac{ln\left(\frac{r}{r_m}\right) - ln\left(\frac{r_{s_+^*}}{r_m}\right)}{\omega^2 t}\right) + \delta\left(\frac{ln\left(\frac{r}{r_b}\right) - ln\left(\frac{r_{s_+^*}}{r_b}\right)}{\omega^2 t}\right)\right] \end{Bmatrix}$$

$$= \begin{Bmatrix} -\frac{c_{p,s_-^*}}{r_{s_-^*}\omega^2 t}\left[\delta\left(\frac{ln\left(\frac{r}{r_{s_-^*}}\right)}{\omega^2 t}\right) + \delta\left(\frac{ln\left(\frac{r}{r_{s_-^*}}\right)}{\omega^2 t}\right)\right] \\ \frac{c_{p,s_+^*}}{r_{s_+^*}\omega^2 t}\left[\delta\left(\frac{ln\left(\frac{r}{r_{s_+^*}}\right)}{\omega^2 t}\right) + \delta\left(\frac{ln\left(\frac{r}{r_{s_+^*}}\right)}{\omega^2 t}\right)\right] \end{Bmatrix} = \begin{Bmatrix} \frac{q(s_-^*,t)}{r_{s_-^*}\omega^2 t} + \frac{e(s_-^*,t)}{r_{s_-^*}\omega^2 t} \\ \frac{q(s_+^*,t)}{r_{s_+^*}\omega^2 t} + \frac{e(s_+^*,t)}{r_{s_+^*}\omega^2 t} \end{Bmatrix},$$

(68)

where the r in $r\omega^2 t$ is equated to the only value of r at which the Dirac delta function it divides is not equal to zero. Similarly, when expressing s* in terms of ω, t, r and r_0, r_0 is equated to the only one if its two possible values, r_m or r_b, that can yield a nonzero result for the Dirac delta function in which it appears. The entire exercise is somewhat futile, however, as once s*, s_-^*, s_+^* and $\Delta s_\pm^*$

are expressed in terms of ω, t, r, r_b and r_m, information by which $q(s_-^*,t)$ can be distinguished from $e(s_-^*,t)$, or $q(s_+^*,t)$ can be distinguished from $e(s_+^*,t)$, is lost upon simplification.

Expressing $\left(\frac{\partial c}{\partial t}\right)_{s^*}$ *and* $\left(\frac{\partial c}{\partial t}\right)_r$ *in terms of step functions*

Differentiating c with respect to t at constant r yields, using the discrete form of Equation 64 to express c,

$$\left(\frac{\partial c}{\partial t}\right)_r = \sum_{s_-^*=s_{-x}^*}^{0}\left(\frac{\partial c_{s_-^*}}{\partial t}\right)_r + \sum_{s_+^*=0}^{s_{+x}^*}\left(\frac{\partial c_{s_+^*}}{\partial t}\right)_r$$

$$= \sum_{s_-^*=s_{-x}^*}^{0}\left(\begin{array}{c}\left(\frac{\partial c_{p,s_-^*}}{\partial t}\right)_r\left\{[1-H(s^*-s_-^*)]+\left[1-H\left(s^*-\left\{s_-^*+\Delta s_\pm^*\right\}\right)\right]\right\}+\\ c_{p,s_-^*}\left(\frac{\partial\left\{[1-H(s^*-s_-^*)]+\left[1-H\left(s^*-\left\{s_-^*+\Delta s_\pm^*\right\}\right)\right]\right\}}{\partial t}\right)_r\end{array}\right)$$

$$+\sum_{s_+^*=0}^{s_{+x}^*}\left(\begin{array}{c}\left(\frac{\partial c_{p,s_+^*}}{\partial t}\right)_r\left\{H(s^*-s_+^*)+H\left(s^*-\left\{s_+^*-\Delta s_\pm^*\right\}\right)\right\}+\\ c_{p,s_+^*}\left(\frac{\partial\left\{H(s^*-s_+^*)+H\left(s^*-\left\{s_+^*-\Delta s_\pm^*\right\}\right)\right\}}{\partial t}\right)_r\end{array}\right)$$

$$= \left\{\begin{array}{c}\left(\begin{array}{c}c_{p,s_-^*}\frac{s_-^*}{t}\left[\delta(s^*-s_-^*)+\delta\left(s^*-\left\{s_-^*+\Delta s_\pm^*\right\}\right)\right]-\\ 2\omega^2\sum_{s_-^*=s_{-x}^*}^{0}s_-^*c_{p,s_-^*}\left\{[1-H(s^*-s_-^*)]+\left[1-H\left(s^*-\left\{s_-^*+\Delta s_\pm^*\right\}\right)\right]\right\}\end{array}\right)\\ \left(\begin{array}{c}-c_{p,s_+^*}\frac{s_+^*}{t}\left[\delta(s^*-s_+^*)+\delta\left(s^*-\left\{s_+^*-\Delta s_\pm^*\right\}\right)\right]-\\ 2\omega^2\sum_{s_+^*=0}^{s_{+x}^*}s_+^*c_{p,s_+^*}\left\{H(s^*-s_+^*)+H\left(s^*-\left\{s_+^*-\Delta s_\pm^*\right\}\right)\right\}\end{array}\right)\end{array}\right\}.$$

(69)

Equations 70 to 75, which follow, describe all the individual terms used to determine $\left(\frac{\partial c}{\partial t}\right)_r$.

At constant r, the time-derivatives of the Heaviside step functions of Equation 64 are given by

$$\left(\frac{\partial H(s^*-\varsigma^*)}{\partial t}\right)_r = \left(\frac{\partial H(s^*-\varsigma^*)}{\partial s^*}\right)_r \left(\frac{\partial (s^*-\varsigma^*)}{\partial t}\right)_r = \delta(s^*-\varsigma^*)\left[\left(\frac{\partial s^*}{\partial t}\right)_r - \left(\frac{\partial \varsigma^*}{\partial t}\right)_r\right]$$

$$= \delta(s^*-\varsigma^*)\left[\left(-\frac{s^*}{t}\right) - \left(\frac{\partial \varsigma^*}{\partial t}\right)_r\right] = -\delta(s^*-\varsigma^*)\left[\frac{s^*}{t} + \left(\frac{\partial \varsigma^*}{\partial t}\right)_r\right]$$

$$= -\delta(s^*-\varsigma^*)\left[\frac{\varsigma^*}{t} + \left(\frac{\partial \varsigma^*}{\partial t}\right)_r\right]$$

(70)

where $\left(\frac{\partial s^*}{\partial t}\right)_r$ is equal to the inverse of Equation 30, and where δ(s* – ς*)s* can be equated to δ(s* - ς*)ς* on the basis of δ(s* – ς*) being equal to zero for all s* ≠ ς*. As in Equation 65, ς* may equal s_-^*, $\{s_-^* + \Delta s_\pm^*\}$, s_+^* or $\{s_+^* - \Delta s_\pm^*\}$.

As s_-^* (Equation 49) and s_+^* (Equation 50) are time-independent, where ς* equals s_-^* or s_+^*, $\left(\frac{\partial \varsigma^*}{\partial t}\right)_r = 0$. As $\Delta s_\pm^*$ (Equation 51) is equal to a constant divided by t, however,

$$\left(\frac{\partial \Delta s_\pm^*}{\partial t}\right)_r = -\frac{\Delta s_\pm^*}{t}.$$

(71)

Thus, where ς* equals $\{s_-^* + \Delta s_\pm^*\}$,

$$-\delta(s^*-\varsigma^*)\left[\frac{\varsigma^*}{t} + \left(\frac{\partial \varsigma^*}{\partial t}\right)_r\right] = -\delta\left(s^* - \{s_-^* + \Delta s_\pm^*\}\right)\left[\frac{s_-^* + \Delta s_\pm^*}{t} + \left(\frac{\partial \Delta s_\pm^*}{\partial t}\right)_r\right]$$

$$= -\delta\left(s^* - \{s_-^* + \Delta s_\pm^*\}\right)\left[\frac{s_-^* + \Delta s_\pm^*}{t} - \frac{\Delta s_\pm^*}{t}\right] = -\delta\left(s^* - \{s_-^* + \Delta s_\pm^*\}\right)\frac{s_-^*}{t}.$$

(72)

Similarly, where ς* equals $\{s_+^* - \Delta s_\pm^*\}$,

$$-\delta(s^* - \varsigma^*)\left[\frac{\varsigma^*}{t} + \left(\frac{\partial \varsigma^*}{\partial t}\right)_r\right] = -\delta\left(s^* - \left\{s_+^* - \Delta s_\pm^*\right\}\right)\left[\frac{s_+^* - \Delta s_\pm^*}{t} - \left(\frac{\partial \Delta s_\pm^*}{\partial t}\right)_r\right]$$
$$= -\delta\left(s^* - \left\{s_+^* - \Delta s_\pm^*\right\}\right)\left[\frac{s_+^* - \Delta s_\pm^*}{t} + \frac{\Delta s_\pm^*}{t}\right] = -\delta\left(s^* - \left\{s_+^* - \Delta s_\pm^*\right\}\right)\frac{s_+^*}{t}.$$

(73)

By Equation 16, $c_{p,s_-^*} = c_{0,s_-^*} e^{-2s_-^*\omega^2 t}$ and $c_{p,s_+^*} = c_{0,s_+^*} e^{-2s_+^*\omega^2 t}$. Thus, the derivatives of c_{p,s_-^*} and c_{p,s_+^*} in Equation 69 can be written as

$$\left(\frac{\partial c_{p,s_-^*}}{\partial t}\right)_r = (-2s_-^*\omega^2) c_{0,s_-^*} e^{-2s_-^*\omega^2 t} = -2s_-^*\omega^2 c_{p,s_-^*}$$

(74)

and

$$\left(\frac{\partial c_{p,s_+^*}}{\partial t}\right)_r = (-2s_+^*\omega^2) c_{0,s_+^*} e^{-2s_+^*\omega^2 t} = -2s_+^*\omega^2 c_{p,s_+^*},$$

(75)

respectively.

Indirect determination of $\left(\frac{\partial c}{\partial t}\right)_{s^*}$

Incorporating the expressions for $\left(\frac{\partial c}{\partial s^*}\right)_t$ (Equation 67), $\left(\frac{\partial c}{\partial t}\right)_r$ (Equation 69) and $\left(\frac{\partial s^*}{\partial t}\right)_r$ (the inverse of Equation 30) in Equation 6, and solving for $\left(\frac{\partial c}{\partial t}\right)_{s^*}$, results in

$$\left(\frac{\partial c}{\partial t}\right)_{s^*} = \left(\frac{\partial c}{\partial t}\right)_r - \left(\frac{\partial c}{\partial s^*}\right)_t \left(\frac{\partial s^*}{\partial t}\right)_r$$

$$= \begin{Bmatrix} \left(\begin{matrix} c_{p,s_-^*} \frac{s_-^*}{t}\left[\delta(s^* - s_-^*) + \delta\left(s^* - \left\{s_-^* + \Delta s_\pm^*\right\}\right)\right] - \\ 2\omega^2 \sum_{s_-^* = s_{-x}^*}^{0} s_-^* c_{p,s_-^*}\left\{\left[1 - H(s^* - s_-^*)\right] + \left[1 - H\left(s^* - \left\{s_-^* + \Delta s_\pm^*\right\}\right)\right]\right\} \end{matrix} \right) \\ \left(\begin{matrix} -c_{p,s_+^*} \frac{s_+^*}{t}\left[\delta(s^* - s_+^*) + \delta\left(s^* - \left\{s_+^* - \Delta s_\pm^*\right\}\right)\right] - \\ 2\omega^2 \sum_{s_+^* = 0}^{s_{+x}^*} s_+^* c_{p,s_+^*}\left\{H(s^* - s_+^*) + H\left(s^* - \left\{s_+^* - \Delta s_\pm^*\right\}\right)\right\} \end{matrix} \right) \end{Bmatrix}$$

$$- \begin{Bmatrix} c_{p,s_-^*} \frac{s_-^*}{t}\left[\delta(s^* - s_-^*) + \delta\left(s^* - \left\{s_-^* + \Delta s_\pm^*\right\}\right)\left(1 + \frac{\Delta s_\pm^*}{s_-^*}\right)\right] \\ -c_{p,s_+^*} \frac{s_+^*}{t}\left[\delta(s^* - s_+^*) + \delta\left(s^* - \left\{s_+^* - \Delta s_\pm^*\right\}\right)\left(1 - \frac{\Delta s_\pm^*}{s_+^*}\right)\right] \end{Bmatrix}$$

$$= \begin{Bmatrix} \left(\begin{matrix} -c_{p,s_-^*} \frac{\Delta s_\pm^*}{t}\delta\left(s^* - \left\{s_-^* + \Delta s_\pm^*\right\}\right) - \\ 2\omega^2 \sum_{s_-^* = s_{-x}^*}^{0} s_-^* c_{p,s_-^*}\left\{\left[1 - H(s^* - s_-^*)\right] + \left[1 - H\left(s^* - \left\{s_-^* + \Delta s_\pm^*\right\}\right)\right]\right\} \end{matrix} \right) \\ \left(\begin{matrix} -c_{p,s_+^*} \frac{\Delta s_\pm^*}{t}\delta\left(s^* - \left\{s_+^* - \Delta s_\pm^*\right\}\right) - \\ 2\omega^2 \sum_{s_+^* = 0}^{s_{+x}^*} s_+^* c_{p,s_+^*}\left\{H(s^* - s_+^*) + H\left(s^* - \left\{s_+^* - \Delta s_\pm^*\right\}\right)\right\} \end{matrix} \right) \end{Bmatrix},$$

(76)

where

$$\left(\frac{\partial c}{\partial s^*}\right)_t\left(\frac{\partial s^*}{\partial t}\right)_r = \left\{\begin{matrix}\left(\frac{\partial c_{s_-^*}}{\partial s^*}\right)_t\left(\frac{\partial s^*}{\partial t}\right)_r \\ \left(\frac{\partial c_{s_+^*}}{\partial s^*}\right)_t\left(\frac{\partial s^*}{\partial t}\right)_r\end{matrix}\right\} = \left\{\begin{matrix}-c_{p,s_-^*}\left[\delta(s^*-s_-^*)\left(\frac{\partial s^*}{\partial t}\right)_r + \delta\left(s^*-\left\{s_-^*+\Delta s_\pm^*\right\}\right)\left(\frac{\partial s^*}{\partial t}\right)_r\right] \\ c_{p,s_+^*}\left[\delta(s^*-s_+^*)\left(\frac{\partial s^*}{\partial t}\right)_r + \delta\left(s^*-\left\{s_+^*-\Delta s_\pm^*\right\}\right)\left(\frac{\partial s^*}{\partial t}\right)_r\right]\end{matrix}\right\}$$

$$= \left\{\begin{matrix}-c_{p,s_-^*}\left[\delta(s^*-s_-^*)\left(-\frac{s^*}{t}\right) + \delta\left(s^*-\left\{s_-^*+\Delta s_\pm^*\right\}\right)\left(-\frac{s^*}{t}\right)\right] \\ c_{p,s_+^*}\left[\delta(s^*-s_+^*)\left(-\frac{s^*}{t}\right) + \delta\left(s^*-\left\{s_+^*-\Delta s_\pm^*\right\}\right)\left(-\frac{s^*}{t}\right)\right]\end{matrix}\right\}$$

$$= \left\{\begin{matrix}c_{p,s_-^*}\frac{1}{t}\left[\delta(s^*-s_-^*)s^* + \delta\left(s^*-\left\{s_-^*+\Delta s_\pm^*\right\}\right)s^*\right] \\ -c_{p,s_+^*}\frac{1}{t}\left[\delta(s^*-s_+^*)s^* + \delta\left(s^*-\left\{s_+^*-\Delta s_\pm^*\right\}\right)s^*\right]\end{matrix}\right\}$$

$$= \left\{\begin{matrix}c_{p,s_-^*}\frac{1}{t}\left[\delta(s^*-s_-^*)s_-^* + \delta\left(s^*-\left\{s_-^*+\Delta s_\pm^*\right\}\right)\left\{s_-^*+\Delta s_\pm^*\right\}\right] \\ -c_{p,s_+^*}\frac{1}{t}\left[\delta(s^*-s_+^*)s_+^* + \delta\left(s^*-\left\{s_+^*-\Delta s_\pm^*\right\}\right)\left\{s_+^*-\Delta s_\pm^*\right\}\right]\end{matrix}\right\}$$

$$= \left\{\begin{matrix}c_{p,s_-^*}\frac{s_-^*}{t}\left[\delta(s^*-s_-^*) + \delta\left(s^*-\left\{s_-^*+\Delta s_\pm^*\right\}\right)\left(1+\frac{\Delta s_\pm^*}{s_-^*}\right)\right] \\ -c_{p,s_+^*}\frac{s_+^*}{t}\left[\delta(s^*-s_+^*) + \delta\left(s^*-\left\{s_+^*-\Delta s_\pm^*\right\}\right)\left(1-\frac{\Delta s_\pm^*}{s_+^*}\right)\right]\end{matrix}\right\}.$$

(77)

In Equation 77, the value of s* obtained from $\left(\frac{\partial s^*}{\partial t}\right)_r$ is equated to the only value of s* at which the Dirac delta function it multiplies is not equal to zero.

Direct determination of $\left(\frac{\partial c}{\partial t}\right)_{s^*}$

At constant s*, the time-derivatives of the Heaviside step functions of Equation 64 are given by

$$\left(\frac{\partial H(s^*-\varsigma^*)}{\partial t}\right)_{s^*} = \left(\frac{\partial H(s^*-\varsigma^*)}{\partial s^*}\right)_{s^*}\left(\frac{\partial (s^*-\varsigma^*)}{\partial t}\right)_{s^*} = \delta(s^*-\varsigma^*)\left[\left(\frac{\partial s^*}{\partial t}\right)_{s^*} - \left(\frac{\partial \varsigma^*}{\partial t}\right)_{s^*}\right]$$

$$= \delta(s^*-\varsigma^*)\left[0-\left(\frac{\partial \varsigma^*}{\partial t}\right)_{s^*}\right] = -\delta(s^*-\varsigma^*)\left(\frac{\partial \varsigma^*}{\partial t}\right)_{s^*}.$$

(78)

As in Equations 65 and 70, ς* may equal s_-^*, $\{s_-^* + \Delta s_\pm^*\}$, s_+^* or $\{s_+^* - \Delta s_\pm^*\}$.

Again, as s_-^* (Equation 49) and s_+^* (Equation 50) are time-independent, where ς* equals s_-^* or s_+^*, $\left(\frac{\partial \varsigma^*}{\partial t}\right)_{s^*} = 0$. And again, as $\Delta s_\pm^*$ (Equation 51) is equal to a constant divided by t,

$$\left(\frac{\partial \Delta s_\pm^*}{\partial t}\right)_{s^*} = -\frac{\Delta s_\pm^*}{t} = \left(\frac{\partial \Delta s_\pm^*}{\partial t}\right)_r .$$

(79)

Thus, where ς* equals $\{s_-^* + \Delta s_\pm^*\}$,

$$= -\delta(s^* - \varsigma^*)\left(\frac{\partial \varsigma^*}{\partial t}\right)_{s^*} = -\delta\left(s^* - \{s_-^* + \Delta s_\pm^*\}\right)\left(\frac{\partial \Delta s_\pm^*}{\partial t}\right)_{s^*} = -\delta\left(s^* - \{s_-^* + \Delta s_\pm^*\}\right)\left[-\frac{\Delta s_\pm^*}{t}\right]$$
$$= \delta\left(s^* - \{s_-^* + \Delta s_\pm^*\}\right)\frac{\Delta s_\pm^*}{t}.$$

(80)

Similarly, where ς* equals $\{s_+^* - \Delta s_\pm^*\}$,

$$-\delta(s^* - \varsigma^*)\left(\frac{\partial \varsigma^*}{\partial t}\right)_{s^*} = -\delta\left(s^* - \{s_+^* - \Delta s_\pm^*\}\right)\left[-\left(\frac{\partial \Delta s_\pm^*}{\partial t}\right)_{s^*}\right] = -\delta\left(s^* - \{s_+^* - \Delta s_\pm^*\}\right)\left[\frac{\Delta s_\pm^*}{t}\right]$$
$$= -\delta\left(s^* - \{s_+^* - \Delta s_\pm^*\}\right)\frac{\Delta s_\pm^*}{t}.$$

(81)

The derivatives of c_{p,s_-^*} and c_{p,s_+^*} with respect to t at constant s* are

$$\left(\frac{\partial c_{p,s_-^*}}{\partial t}\right)_{s^*} = (-2s_-^*\omega^2)c_{0,s_-^*}e^{-2s_-^*\omega^2 t} = -2s_-^*\omega^2 c_{p,s_-^*} = \left(\frac{\partial c_{p,s_-^*}}{\partial t}\right)_r$$

(82)

and

$$\left(\frac{\partial c_{p,s_+^*}}{\partial t}\right)_{s^*} = (-2s_+^*\omega^2)c_{0,s_+^*}e^{-2s_+^*\omega^2 t} = -2s_+^*\omega^2 c_{p,s_+^*} = \left(\frac{\partial c_{p,s_+^*}}{\partial t}\right)_r ,$$

(83)

respectively.

Using Equation 64 to express c, and applying Equations 78 to 83, yields the same result for $\left(\frac{\partial c}{\partial t}\right)_{s^*}$ as that obtained in Equation 76. A comparison of Equations 69 and 76 shows that $\left(\frac{\partial c}{\partial t}\right)_r$ differs from $\left(\frac{\partial c}{\partial t}\right)_{s^*}$ solely with respect to the Dirac delta functions. In $\left(\frac{\partial c}{\partial t}\right)_r$ (Equation 69), the Dirac delta functions that contribute to the peaks and valleys of q(s*,t) and e(s*,t) are multiplied by either s_+^* or s_-^*. In $\left(\frac{\partial c}{\partial t}\right)_{s^*}$ (Equation 76), there is no Dirac delta function that would contribute to the peaks and valleys of q(s*,t), but the Dirac delta functions that contribute to the peaks and valleys of e(s*,t) are multiplied by $\Delta s_\pm^*$. As $\Delta s_\pm^* = s_+^* - s_-^*$ (Equation 51), $\left(\frac{\partial c}{\partial t}\right)_{s^*}$ makes a higher magnitude contribution to the peaks and valleys of e(s*,t) than $\left(\frac{\partial c}{\partial t}\right)_r$ does.

Calculating g(s) in terms of step functions*

Subtracting e(s*,t) (Equations 62 and 63) from Equation 58 yields

$$q(s^*,t) = \left(\frac{\partial c_{s^*}}{\partial s^*}\right)_t - e(s^*,t) = \begin{Bmatrix} \left(\frac{\partial c_{s_-^*}}{\partial s^*}\right)_t - e(s_-^*,t) \\ \left(\frac{\partial c_{s_+^*}}{\partial s^*}\right)_t - e(s_+^*,t) \end{Bmatrix}$$

$$= \begin{Bmatrix} -c_{0,s_-^*} e^{-2s_-^*\omega^2 t}\delta\left(r - r_b e^{s_-^*\omega^2 t}\right)\omega^2 t r_b e^{s_-^*\omega^2 t} \\ c_{0,s_+^*} e^{-2s_+^*\omega^2 t}\delta\left(r - r_m e^{s_+^*\omega^2 t}\right)\omega^2 t r_m e^{s_+^*\omega^2 t} \end{Bmatrix} = \begin{Bmatrix} q(s_-^*,t) \\ q(s_+^*,t) \end{Bmatrix}.$$

(84)

Subtracting e(s*,t) from Equation 67 yields

$$q(s^*,t)=\left(\frac{\partial c_{s^*}}{\partial s^*}\right)_t-e(s^*,t)=\begin{Bmatrix}\left(\frac{\partial c_{s_-^*}}{\partial s^*}\right)_t-e(s_-^*,t)\\ \left(\frac{\partial c_{s_+^*}}{\partial s^*}\right)_t-e(s_+^*,t)\end{Bmatrix}=\begin{Bmatrix}-c_{0,s_-^*}e^{-2s_-^*\omega^2t}\delta(s^*-s_-^*)\\ c_{0,s_+^*}e^{-2s_+^*\omega^2t}\delta(s^*-s_+^*)\end{Bmatrix}=\begin{Bmatrix}q(s_-^*,t)\\ q(s_+^*,t)\end{Bmatrix}.$$

(85)

Multiplying q(s*,t) (Equations 60 and 61) by $e^{2s^*\omega^2t}$, which, in Equations 84 or 85, involves multiplying the expressions for q(s_-^*,t) and q(s_+^*,t) by $e^{2s_-^*\omega^2t}$ and $e^{2s_+^*\omega^2t}$, respectively, normalises for the radial dilution/concentration effect, and thus yields

$$g(s^*)=q(s^*,t)e^{2s_\pm^*\omega^2t}=\begin{Bmatrix}q(s_-^*,t)\,e^{2s_-^*\omega^2t}\\ q(s_+^*,t)e^{2s_+^*\omega^2t}\end{Bmatrix}=\begin{Bmatrix}-c_{0,s_-^*}\delta\left(r-r_be^{s_-^*\omega^2t}\right)\omega^2tr_be^{s_-^*\omega^2t}\\ c_{0,s_+^*}\delta\left(r-r_me^{s_+^*\omega^2t}\right)\omega^2tr_me^{s_+^*\omega^2t}\end{Bmatrix}$$

$$=\begin{Bmatrix}-c_{0,s_-^*}\\ c_{0,s_+^*}\end{Bmatrix}\delta(r-r_{s^*})\omega^2tr_{s^*},$$

(86)

from Equation 84, and

$$g(s^*)=q(s^*,t)e^{2s_\pm^*\omega^2t}=\begin{Bmatrix}q(s_-^*,t)\,e^{2s_-^*\omega^2t}\\ q(s_+^*,t)e^{2s_+^*\omega^2t}\end{Bmatrix}=\begin{Bmatrix}-c_{0,s_-^*}\delta(s^*-s_-^*)\\ c_{0,s_+^*}\delta(s^*-s_+^*)\end{Bmatrix},$$

(87)

from Equation 85.

Applying finite-difference approximations of $\left(\frac{\partial c}{\partial t}\right)_{s^*}$ *and* $\left(\frac{\partial c}{\partial t}\right)_r$ *to experimental data*

Equations 69 and 76 can be applied to experimental data by using the finite-difference approximations, $\frac{\Delta c_r}{\Delta t}$ and $\frac{\Delta c_{s*}}{\Delta t}$, in place of $\left(\frac{\partial c}{\partial t}\right)_r$ and $\left(\frac{\partial c}{\partial t}\right)_{s^*}$, respectively, as was done in Figures 18 to 20. Subtracting $\frac{\Delta c_{s*}}{\Delta t}$ from $\frac{\Delta c_r}{\Delta t}$, and multiplying by $\frac{\Delta t}{\Delta s_r^*}$ (where Δs_r^* is given by Equation 43), yields

$\frac{\Delta c}{\Delta s^*}$ (Equation 42), which is the finite form of $\left(\frac{\partial c}{\partial s^*}\right)_t$. The time difference, Δt = t - [t - Δt], is that between the later and the earlier data sets employed.

As noted with respect to Figures 19 and 20, $\frac{\Delta c_{s*}}{\Delta t}$ contributes little to the peaks and valleys of q(s*,t), but is critical to identifying the redundant peaks and valleys that must be assigned to e(s*,t). Furthermore, away from the regions of $\frac{\Delta c_{s*}}{\Delta t}$ and $\frac{\Delta c_r}{\Delta t}$ that contribute to the peaks and valleys of e(s*,t) and q(s*,t), the subtraction of $\frac{\Delta c_{s*}}{\Delta t}$ from $\frac{\Delta c_r}{\Delta t}$ cancels any effects of radial dilution/concentration that Δc_{s*} and Δc_r accumulate during Δt. (The expectations arising from a comparison of Equations 69 and 76 are consistent with the results shown in Figures 19 to 20.)

The difference between the RI noise at times [t - Δt] and t should be the same for Δc_r and Δc_{s*}. Thus, any RI noise should be eliminated when $\frac{\Delta c_{s*}}{\Delta t}$ is subtracted from $\frac{\Delta c_r}{\Delta t}$ in the course of calculating $\frac{\Delta c}{\Delta s^*}$ (Equation 42). (Provided that transport is slow relative to Δt, $\langle \Delta c_r \rangle$ and $\langle \Delta c_{s*} \rangle$, which are the mean values of Δc_r and Δc_{s*}, respectively, can be fairly good approximations of the RI-noise difference within a given Δt.)

Time-independent (TI) noise is eliminated in the course of calculating Δc_r. As noted with respect to Equation 41 and Figure 20, however, TI noise is not eliminated in the course of calculating Δc_{s*}. Thus, $\frac{\Delta c}{\Delta s^*}$ will ultimately include $-\frac{\Delta t}{\Delta s_r^*}$ times whatever TI noise is present in $\frac{\Delta c_{s*}}{\Delta t}$. (See Equations 42 to 44.)

The iterative approach of Stafford (1992) calculates TI-noise-free approximations of $\frac{\Delta c_{s*}}{\Delta t}$ from $\frac{\Delta c_r}{\Delta t}$.

That iterative approach will not generate the $\frac{\Delta c_{s*}}{\Delta t}$ values needed to identify redundant peaks, however, and thus will not work for analytical systems in which s* ranges above and below zero.

In ls-g(s*) analysis, TI noise can be fit (Schuck & Rossmanith, 2000), but as discussed with respect to Figure 30, information regarding solutes that are not neutrally buoyant may be lost as a result. Fitting both the RI and TI noise results in a loss of information regarding neutrally buoyant solutes only, which is not such a high price to pay, as it is known that the vicinity of s* = 0 is where that information would be. As will be shown (Figures 48 and 50), however, misleading results can be obtained if too few data sets from too short a short time period are included in ls-g(s*) analysis. Thus, if g(s*) results are sought for an extremely narrow time range, alternative methods of eliminating TI noise are needed. One such method, which requires that there be data consisting of just TI noise plus an offset in the signal, is presented next.

Using data from early time-points to estimate the TI noise in $\frac{\Delta c_{s*}}{\Delta t}$*: Background*

The TI noise in any given set of $\frac{\Delta c_{s*}}{\Delta t}$ data can be determined from data obtained before any significant concentration gradients have developed, or, if the supernatant and pellet regions are on no interest, from data obtained after the solute concentration has been almost totally depleted between those regions. For data collected from a given system over time, subtracting the earliest data set from all subsequent data sets should eliminate the TI noise from the later data, at a cost of introducing an offset in the signal. As such an offset is a form of RI noise, it will be eliminated in the course of calculating $\frac{\Delta c}{\Delta s^*}$.

Although c, or the signal that corresponds to c, is a continuous function of r and t, data are only collected at discrete time-points and radial positions. Let c_a represent the signal as a function of r at the earliest time, t_a, that data were collected. Let c_m represent the signal as a function of r at time t_m, where t_m is much greater than t_a. Let c_n represent the signal as a function of r at time t_n, where t_n is also much greater than t_a, but only slightly greater than t_m. It is assumed that data are collected at the same radial positions at each time. (Any time-dependence in the alignment of the detection system with the chemical system, such as that due to rotor deformation with changing angular velocity, in ignored.) It is further assumed that the meniscus and base lie within $r_1 \leq r_h \leq r_N$, where h is the index of the N radial positions at which data are collected at each time. (Assuming that the index increases with increasing radial position, $r_1 < r_m$ and $r_b < r_N$.)

To evaluate $\frac{\Delta c_r}{\Delta t}$, the c-versus-r (or signal-versus-r) data at two time-points are used without prior transformation or interpolation. At each common r_h value, the concentration at the earlier time is subtracted from the concentration at the later time to obtain Δc_r. Dividing Δc_r by Δt yields $\frac{\Delta c_r}{\Delta t}$, where Δt is the time-difference between the two data sets.

To evaluate $\frac{\Delta c_{s*}}{\Delta t}$, the c-versus-r (or signal-versus-r) data at two time-points must first be transformed to c-versus-s* (or signal-versus-s*) data. Next, at least one of the transformed data sets must be interpolated, so that both transformed data sets share common values of s*. Following the transformations and interpolations, at each common s* value, the concentration at the earlier time is subtracted from the concentration at the later time to obtain Δc_{s*}. Dividing Δc_{s*} by Δt yields $\frac{\Delta c_{s*}}{\Delta t}$, where Δt is the time-difference between the two data sets.

In the example presented here, the time-difference, $\Delta t = \Delta t_{nm} = t_n - t_m$, is that which pertains to the two data sets, c_n versus r and c_m versus r. The corresponding concentration difference at constant r, $\Delta c_r = \Delta[c_{nm}]_r = c_n - c_m$, is that at each value of r_h, which the two data sets share in common by default. The corresponding concentration difference at constant s*, $\Delta c_{s^*} = \Delta[c_{nm}]_{s*}$, is that at each common s* value, and may equal $c_n - c_{m^*}$, $c_{n^*} - c_{m^*}$ or $c_{n^*} - c_m$, where c_{n^*} and c_{m^*} are interpolated values of c_n and c_m, respectively. Division of each $\Delta[c_{nm}]_r$ by Δt_{nm} yields $\frac{\Delta[c_{nm}]_r}{\Delta t_{nm}} = \frac{\Delta c_r}{\Delta t}$ as a function of the common values of r_h. Division of each $\Delta[c_{nm}]_{s*}$ by Δt_{nm} yields $\frac{\Delta[c_{nm}]_{s*}}{\Delta t_{nm}} = \frac{\Delta c_{s*}}{\Delta t}$ as a function of the common values of s*.

Let s_m^* represent s* at t_m, and let s_n^* represent s* at t_n, where both s_m^* and s_n^* are only calculated at $r = r_h$. By Equation 27,

$$s_m^* = \frac{1}{\omega^2 t_m} ln\left(\frac{r_h}{r_0}\right)$$

(88)

and

$$s_n^* = \frac{1}{\omega^2 t_n} ln\left(\frac{r_h}{r_0}\right).$$

(89)

As $t_n > t_m$, at a given value of r_h and a given value of r_0, $|s_n^*| < |s_m^*|$, and as the c-versus-r data are far from continuous, there are unlikely to be values of s_n^* and s_m^* in common. Thus, at a given value of s_n^* (where data exists for c_n), there will usually be no data for c_m. Likewise, at a given value of s_m^* (where data exists for c_m), there will usually be no data for c_n. To calculate $\Delta[c_{nm}]_{s*}$, which requires that the concentrations at two different times have s* values in common, at least one of the transformed data sets, c_m versus s_m^* or c_n versus s_n^*, must be interpolated.

Using the convention employed for the preceding examples (Figures 8 to 20), the earlier transformed data set, c_m versus s_m^*, is interpolated, and the later transformed data set, c_n versus s_n^*, is used as is. The interpolated values of c_m are denoted as c_{m*}. As a function of s*, the c_{m*} values are found at the corresponding, interpolated values of s_m^*, which are denoted as s_{m*}^*. As a function of r, the c_{m*} values are found at the corresponding, interpolated values of r_h, which are denoted as r_{m*}. By Equation 27,

$$s_{m*}^* = \frac{1}{\omega^2 t_m} ln\left(\frac{r_{m*}}{r_0}\right),$$

(90)

and as the s_{m*}^* values must equal the existing values of s_n^* , the right-hand sides of Equations 89 and 90 can be equated, and solved for r_{m*} to obtain

$$r_{m*} = \left(r_h^{t_m} r_0^{\Delta t_{nm}}\right)^{\frac{1}{t_n}}.$$

(91)

(For $r_{m*} = r_1$, $r_h = r_2$, $t_m = t_n$ and $\Delta t_{nm} = t_2 - t_1$, Equations 91 and 41 are identical.) In combination, Equations 27, 88, 90 and 91 yield

$$s_{m*}^* = s_m^* \frac{ln\left(\frac{r_{m*}}{r_0}\right)}{ln\left(\frac{r_h}{r_0}\right)} = \frac{1}{\omega^2 t_m} ln\left(\frac{r_{m*}}{r_0}\right) = \begin{Bmatrix} \frac{1}{\omega^2 t_m} ln\left(\left[\frac{r_h}{r_b}\right]^{\frac{t_m}{t_n}}\right) \le 0 \\ \frac{1}{\omega^2 t_m} ln\left(\left[\frac{r_h}{r_m}\right]^{\frac{t_m}{t_n}}\right) \ge 0 \end{Bmatrix}.$$

(92)

The concentration difference as a function of s_{m*}^* is $\Delta[c_{nm}]_{s*} = c_n - c_{m*}$, where c_n is that at s_n^*, c_{m*} is that at s_{m*}^*, and $s_{m*}^* = s_n^*$. Division of each $\Delta[c_{nm}]_{s*}$ by Δt_{nm} yields $\frac{\Delta[c_{nm}]_{s*}}{\Delta t_{nm}}$ as a function of either

s_n^* or s_{m*}^*. Although any function of s_n^* could also be considered a function of s_{m*}^*, s_n^* is regarded as the independent variable here, in part to be consistent with the convention adopted previously (Figures 11 to 13, and Figures 18 to 22), and in part because s_n^* is a less ambiguous function of a time than s_{m*}^* is. (As defined in Equation 89, s_n^* is a function of t_n, r_h, r_0 and ω. As defined in Equation 92, s_{m*}^* is a function of t_m, t_n, r_h, r_0 and ω. Thus, s_n^* depends on just one time, while s_{m*}^* depends on two times.)

At any given time, the RI noise at all values of r_h, and at all s* values derived from those values of r_h (Equations 88 and 89), must be equal. Furthermore, at any given time, the RI noise at all interpolated radial positions (Equation 91), and at all interpolated s* values (Equation 92) derived from those interpolated radial positions, must be equal to the RI noise at all values of r_h from which the interpolated radial positions arise. The RI noise at times t_a, t_m and t_n is denoted as RI_a, RI_m and RI_n, respectively. The contribution of RI noise to either $\Delta[c_{nm}]_r$ or $\Delta[c_{nm}]_{s*}$ is thus

$$\Delta RI_{nm} = RI_n - RI_m,$$

(93)

where ΔRI_{nm} is a function of t_m and t_n.

At any given radial position, the TI noise at times t_a, t_m and t_n must be equal. Let TI_h denote the TI noise at a given value of r_h, and let TI_{m*} denote the interpolated TI noise at a given value of r_{m*}. The contribution of TI noise to $\Delta[c_{nm}]_{s*}$ is thus

$$\Delta TI_{hm*} = TI_h - TI_{m*},$$

(94)

where ΔTI_{hm*} is a function of r_h and r_{m*}, which, in turn (Equation 91), is a function of t_m, t_n and r_h. (With respect to its usage, however, ΔTI_{hm*} is treated as a function of s_n^* (Equation 89).) The

contribution of TI noise to $\Delta[c_{nm}]_r$ is

$$\Delta TI_{hh} = TI_h - TI_h = 0.$$

(95)

In the limit as t_m approaches t_n, the set of all r_{m*} approaches the set of all r_h, at which point, ΔTI_{hm*} approaches ΔTI_{hh}.

According to Equations 93 and 94, the net contribution of the RI and TI noise to $\Delta[c_{nm}]_{s*}$ is $\Delta RI_{nm} + \Delta TI_{hm*}$. Substituting the c_a versus r data for both the c_m versus r and c_n versus r data in Equations 93 and 94, but keeping t_m and t_n as their respective time-points, results in $\Delta[c_{nm\rightarrow aa}]_{s*} = \Delta TI_{hm*} + \Delta RI_{nm\rightarrow aa}$, where the subscript, $nm \rightarrow aa$, indicates that c_a values have replaced both the c_n values and the c_m values used to calculate $\Delta[c_{nm}]_{s*}$.

With respect to s_n^*, $\Delta[c_{nm\rightarrow aa}]_{s*} = c_a - c_{a*}$, where c_a is that at s_n^*, c_{a*} is that at s_{m*}^*, and $s_{m*}^* = s_n^*$. With respect to radial position, $\Delta[c_{nm\rightarrow aa}]_{s*} = c_a - c_{a*}$, where c_a is that at r_h, c_{a*} is that at r_{m*}, and by Equation 91, $r_{m*} = \left(r_h^{t_m} r_0^{\Delta t_{nm}}\right)^{\frac{1}{t_n}}$. The c_{a*} values must be interpolated. The c_a values are used as is.

As the contribution of RI noise to $\Delta[c_{nm\rightarrow aa}]_{s*}$ is

$$\Delta RI_{nm\rightarrow aa} = RI_a - RI_a = 0,$$

(96)

$\Delta[c_{nm\rightarrow aa}]_{s*} = \Delta TI_{hm*}$. Thus, the difference, $\Delta[c_{nm}]_{s*} - \Delta[c_{nm\rightarrow aa}]_{s*}$, should be free of TI noise, but should have the same RI noise as $\Delta[c_{nm}]_{s*}$, which, in turn, has the same RI noise as $\Delta[c_{nm}]_r$. (With respect to either $\Delta[c_{nm}]_{s*}$ or $\Delta[c_{nm}]_r$, the contribution of RI noise is ΔRI_{nm} (Equation 93).)

Incorporating $\Delta[c_{nm\to aa}]_{s*}$ (a special case of Equation 94) into Equation 42 corrects $\frac{\Delta c}{\Delta s^*}$ for TI-noise. So-corrected, Equation 42 becomes

$$\frac{\Delta c}{\Delta s^*} = \left(\frac{\Delta[c_{nm}]_r}{\Delta t_{nm}} - \frac{\Delta[c_{nm}]_{s*} - \Delta[c_{nm\to aa}]_{s*}}{\Delta t_{nm}}\right)\frac{\Delta t_{nm}}{\Delta s_r^*},$$

(97)

where $\frac{\Delta t_{nm}}{\Delta s_r^*}$ is an approximation of $\left(\frac{\partial t}{\partial s^*}\right)_r$ and, on the basis of Equation 27 in general, and Equations 89 and 90 in particular,

$$\Delta s_r^* = s_n^* - s_{m*}^* = \frac{1}{\omega^2}\left[\frac{1}{t_n} - \frac{1}{t_m}\right] ln\left(\frac{r_h}{r_0}\right) = \left[\frac{-\Delta t_{nm}}{\omega^2 t_m t_n}\right] ln\left(\frac{r_h}{r_0}\right)$$

(98)

is the change in s* from time t_m to time t_n at radial position r_h. Each of the two possible values of r_0 is discussed with respect to Equation 27. (Substituting t_1 for t_m and t_2 for t_n in Equation 98 yields Equation 43.)

signal difference	$\Delta[c_{nm}]_r$	$\Delta[c_{nm}]_{s*}$	$\Delta[c_{nm\to aa}]_{s*}$
RI noise difference	$\Delta RI_{nm} = RI_n - RI_m$	$\Delta RI_{nm} = RI_n - RI_m$	$\Delta RI_{nm\to aa} = RI_a - RI_a = 0$
TI noise difference	$\Delta TI_{hh} = TI_h - TI_h = 0$	$\Delta TI_{hm*} = TI_h - TI_{m*}$	$\Delta TI_{hm*} = TI_h - TI_{m*}$

Table 1. The contribution of the RI and TI noise to $\Delta[c_{nm}]_r$, $\Delta[c_{nm}]_{s*}$ and $\Delta[c_{nm\to aa}]_{s*}$. (See Equations 93 to 96.)

The net contribution of the RI and TI noise (Table 1) to the difference, $\Delta[c_{nm}]_r - (\Delta[c_{nm}]_{s*} - \Delta[c_{nm\to aa}]_{s*})$, is zero. Thus, $\frac{\Delta c}{\Delta s^*}$ should be free of either RI or TI noise. Contributions from random noise will remain present in $\frac{\Delta c}{\Delta s^*}$, no matter how it is evaluated, however.

Using data from early time-points to estimate the TI noise in $\frac{\Delta c_{s*}}{\Delta t}$*: Illustrative example*

The figures that follow apply the method described in the preceding section to data that, but for the addition of RI and TI noise, and the retention of data in the supernatant and pellet regions, are identical to the data shown in Figure 15.

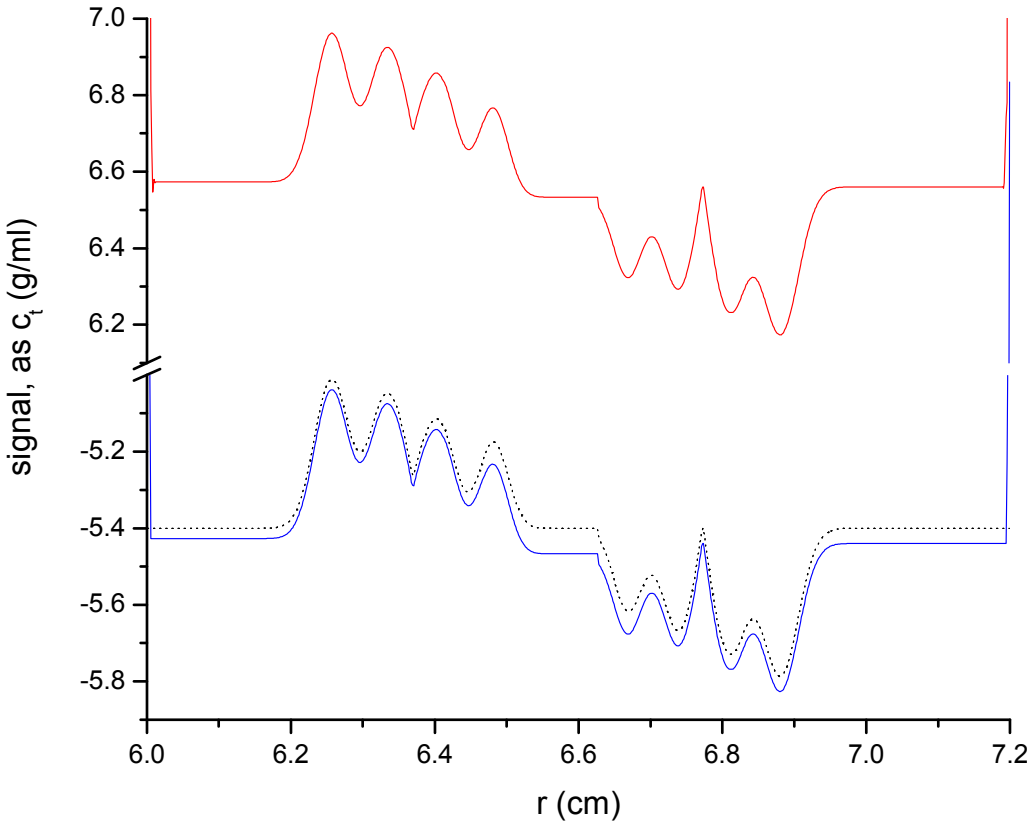

Figure 40. Plots of c_m versus $r = r_h$ at $t_m = 2910$ s (——), and c_n versus $r = r_h$ at $t_n = 2916$ s (——). With the RI and TI noise subtracted, and the supernatant and pellet regions excluded, these same data would be identical to the data shown in Figure 15. Also shown is c_a versus $r = r_h$ at $t_a = 0$ s (·····), which is an ideal initial time-point at which data are available from simulations, but is an admittedly inaccessible time-point with respect to experimental data. The

RI noise at $t_a = 0$ s, $t_m = 2910$ s and $t_n = 2916$ s, respectively, is $RI_a = -5.4$ g/ml, $RI_m = -5.5$ g/ml and $RI_n = 6.5$ g/ml. The TI noise is equal to $c_a - RI_a$.

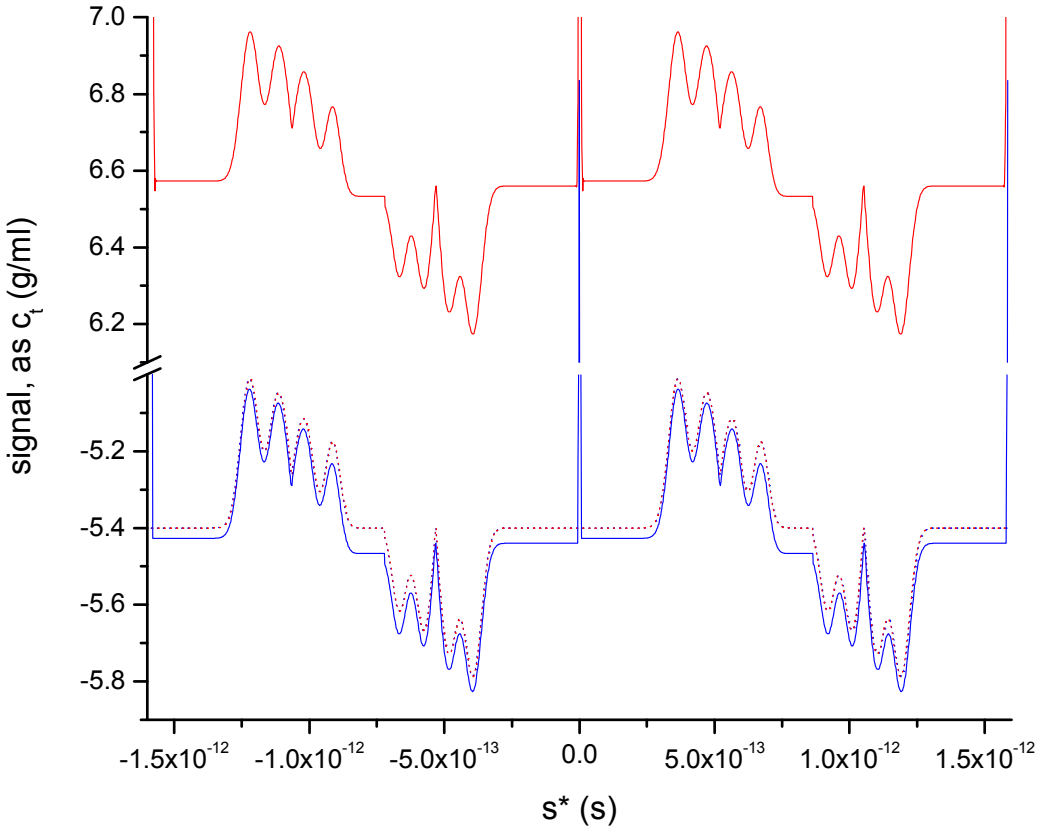

Figure 41. Plots of c_m versus $s^* = s_m^*$ at $t_m = 2910$ s (——), and c_n versus $s^* = s_n^*$ at $t_n = 2916$ s (——). With the RI and TI noise subtracted, and the supernatant and pellet regions excluded, these same data would be identical to the data shown in Figure 17. Also shown are c_a versus $s^* = s_m^*$ at $t_m = 2910$ s (·····) and c_a versus $s^* = s_n^*$ at $t_n = 2916$ s (·····), which do not quite overlap. The RI noise at $t_a = 0$ s, $t_m = 2910$ s and $t_n = 2916$ s, respectively, is $RI_a = -5.4$ g/ml, $RI_m = -5.5$ g/ml and $RI_n = 6.5$ g/ml.

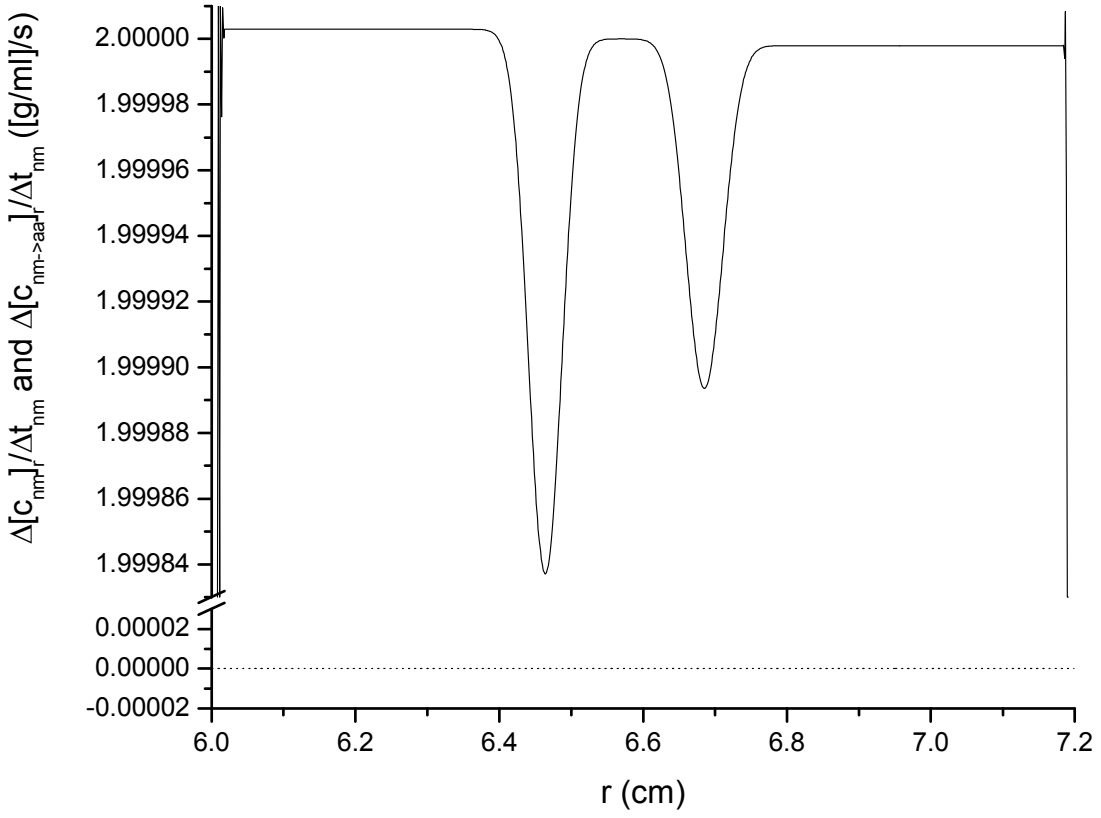

Figure 42. Plots of $\frac{\Delta[c_{nm}]_r}{\Delta t_{nm}}$ versus r = r_h (——) and $\frac{\Delta[c_{nm\rightarrow aa}]_r}{\Delta t_{nm}}$ versus r = r_h (·····), where Δt_{nm} = 2916 s – 2910 s. Except for an offset of $\frac{\Delta RI_{nm}}{\Delta t_{nm}} = \frac{12\ g/ml}{6\ s}$, and excluding the supernatant and pellet regions, $\frac{\Delta[c_{nm}]_r}{\Delta t_{nm}}$ would be identical to $\frac{\Delta c_r}{\Delta t}$, which is shown in Figure 16 as a function of r = r_h, and in Figure 19 as a function of s* = s_n^*. The RI noise at t_m = 2910 s and t_n = 2916 s, respectively, is RI_m = -5.5 g/ml and RI_n = 6.5 g/ml. Thus, $\Delta RI_{nm} = RI_n - RI_m$ = 12.0 g/ml, and $\frac{\Delta RI_{nm}}{\Delta t_{nm}}$ = 2.0 g/ml.

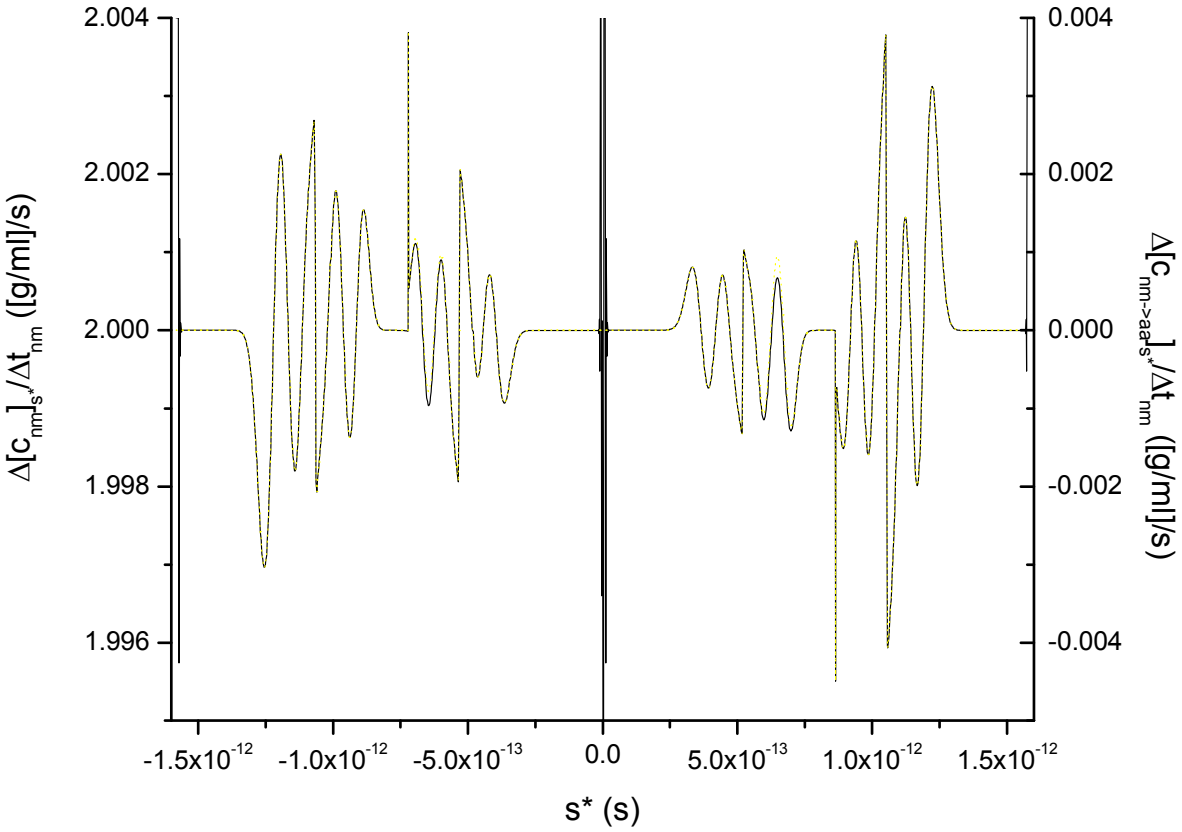

Figure 43. Plots of $\frac{\Delta[c_{nm}]_{s*}}{\Delta t_{nm}}$ versus s* = s_n^* (——) and $\frac{\Delta[c_{nm\rightarrow aa}]_{s*}}{\Delta t_{nm}}$ versus s* = s_n^* (·····), where Δt_{nm} = 2916 s – 2910 s. Compare these data, which show the consequences of RI noise (resulting in an offset of $\frac{\Delta RI_{nm}}{\Delta t_{nm}} = \frac{12\ g/ml}{6\ s}$) and TI noise (resulting in a fairly complicated oscillatory pattern), to $\frac{\Delta c_{s*}}{\Delta t}$ in Figure 18. The RI noise at t_m = 2910 s and t_n = 2916 s, respectively, is RI_m = -5.5 g/ml and RI_n = 6.5 g/ml. Thus, $\Delta RI_{nm} = RI_n - RI_m$ = 12.0 g/ml, and $\frac{\Delta RI_{nm}}{\Delta t_{nm}}$ = 2.0 [g/ml]/s. As $\Delta RI_{nm\rightarrow aa} = RI_a - RI_a$ = 0, $\frac{\Delta RI_{nm\rightarrow aa}}{\Delta t_{nm}}$ = 0 [g/ml]/s.

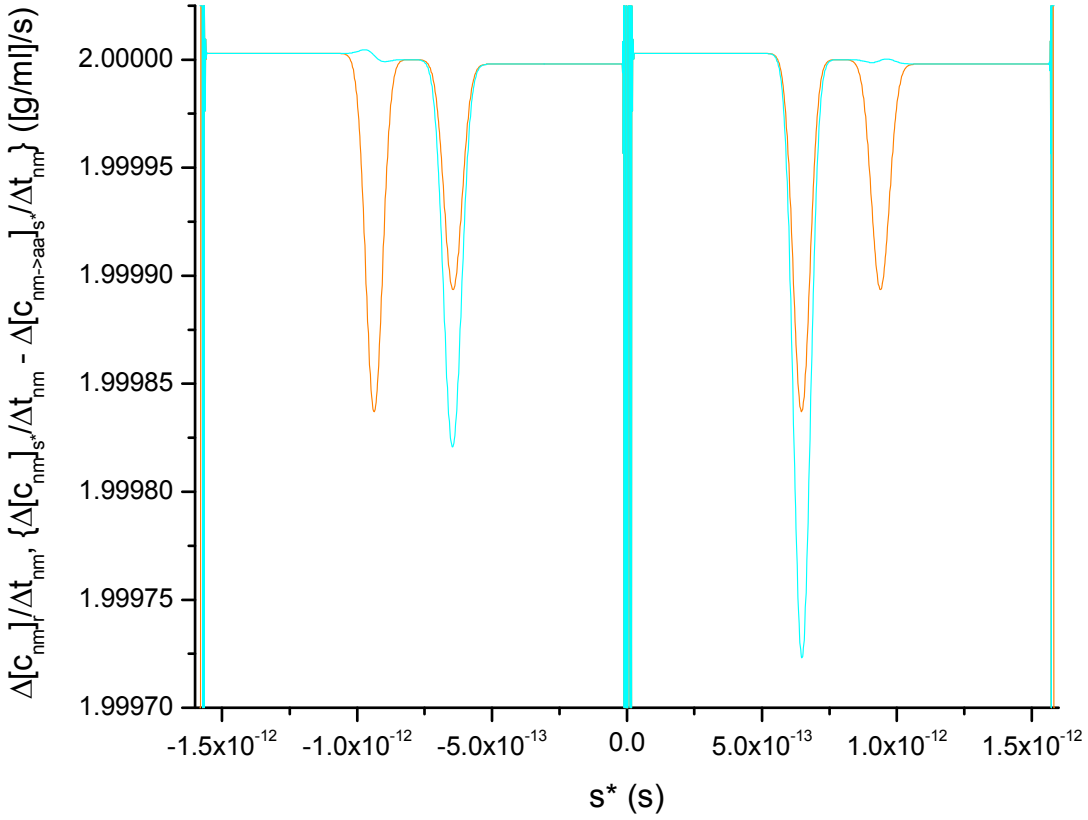

Figure 44. Plots of $\frac{\Delta[c_{nm}]_r}{\Delta t_{nm}}$ versus s* = s_n^* (——) and $\frac{\Delta[c_{nm}]_{s*}-\Delta[c_{nm\rightarrow aa}]_{s*}}{\Delta t_{nm}}$ versus s* = s_n^* (——), where Δt_{nm} = 2916 s – 2910 s. Compare these data, which show the consequences of RI noise (resulting in an offset of $\frac{\Delta RI_{nm}}{\Delta t_{nm}} = \frac{12\ g/ml}{6\ s}$), to $\frac{\Delta c_r}{\Delta t}$ and $\frac{\Delta c_{s*}}{\Delta t}$ in Figure 19.

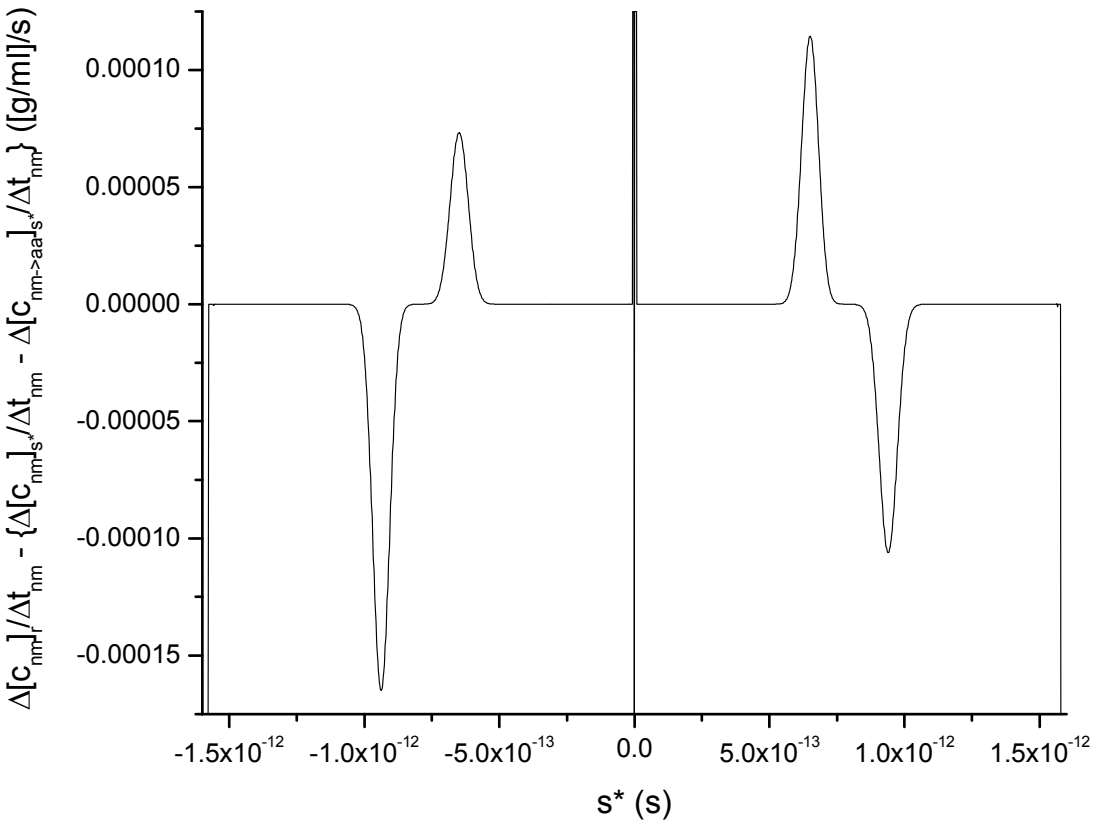

Figure 45. Plot of $\frac{\Delta[c_{nm}]_r}{\Delta t_{nm}} - \frac{\Delta[c_{nm}]_{s*} - \Delta[c_{nm\rightarrow aa}]_{s*}}{\Delta t_{nm}}$ versus s* = s_n^* (——), where Δt_{nm} = 2916 s – 2910 s. Except for points near s* = 0 and the extrema in s*, these data are identical to $\frac{\Delta c_r}{\Delta t} - \frac{\Delta c_{s*}}{\Delta t}$ in Figure 19. Table 1 shows the contribution of the RI and TI noise to $\Delta[c_{nm}]_r$, $\Delta[c_{nm}]_{s*}$ and $\Delta[c_{nm\rightarrow aa}]_{s*}$. The net contribution of the RI and TI noise to the difference, $\frac{\Delta[c_{nm}]_r}{\Delta t_{nm}} - \frac{\Delta[c_{nm}]_{s*} - \Delta[c_{nm\rightarrow aa}]_{s*}}{\Delta t_{nm}}$, is zero.

Applying Equations 97 and 98 to $\frac{\Delta[c_{nm}]_r}{\Delta t_{nm}} - \frac{\Delta[c_{nm}]_{s*} - \Delta[c_{nm\rightarrow aa}]_{s*}}{\Delta t_{nm}}$ (Figure 45) yields $\frac{\Delta c}{\Delta s^*}$, which, away from s* = 0 and the extrema in s*, is identical to $\frac{\Delta c}{\Delta s^*}$ in Figure 20, and elsewhere closely resembles $\left(\frac{\partial c}{\partial s^*}\right)_t$ at t = 2910 s (Figure 25). Applying Equations 29 and 7 to determine q(s*,t) from $\frac{\Delta c}{\Delta s^*}$, and

applying Equation 32 to normalise q(s*,t) for the effects of radial dilution/concentration, yields g(s*), which, away from s* = 0 and the extrema in s*, is identical to g(s*) in Figure 21, and elsewhere closely resembles g(s*) at t = 2910 s (Figure 26).

Calculating g(s) from the TI-noise corrected application of Equation 3*

Figure 46 presents |g(s*)| from $\frac{\Delta[c_{nm}]_r}{\Delta t_{nm}} - \frac{\Delta[c_{nm}]_{s*} - \Delta[c_{nm\to aa}]_{s*}}{\Delta t_{nm}}$ (Figure 45), along with |g(s*)| calculated from a TI-noise corrected application of Equation 3,

$$\left(\frac{\partial c}{\partial s^*}\right)_t = \left(\frac{\partial [c_n - c_a]}{\partial r}\right)_t \left(\frac{\partial r}{\partial s^*}\right)_t,$$

(99)

where, in $\left(\frac{\partial r}{\partial s^*}\right)_t = r\omega^2 t$ (Equation 28), $t = t_n = 2916$ s. The subtraction, $c_n - c_a$, yields a TI-noise corrected concentration, and the RI-noise that remains in $c_n - c_a$ is eliminated when the derivative, $\left(\frac{\partial [c_n - c_a]}{\partial r}\right)_t$, is taken. (Figure 40 shows c_n versus r and c_a versus r.) Figure 46 also includes the previously shown (Figure 26) results for |g(s*)| obtained by the application of Equation 3 to noise-free data (Figure 23) for which $t = t_m = 2910$ s. The results in all three cases are practically indistinguishable.

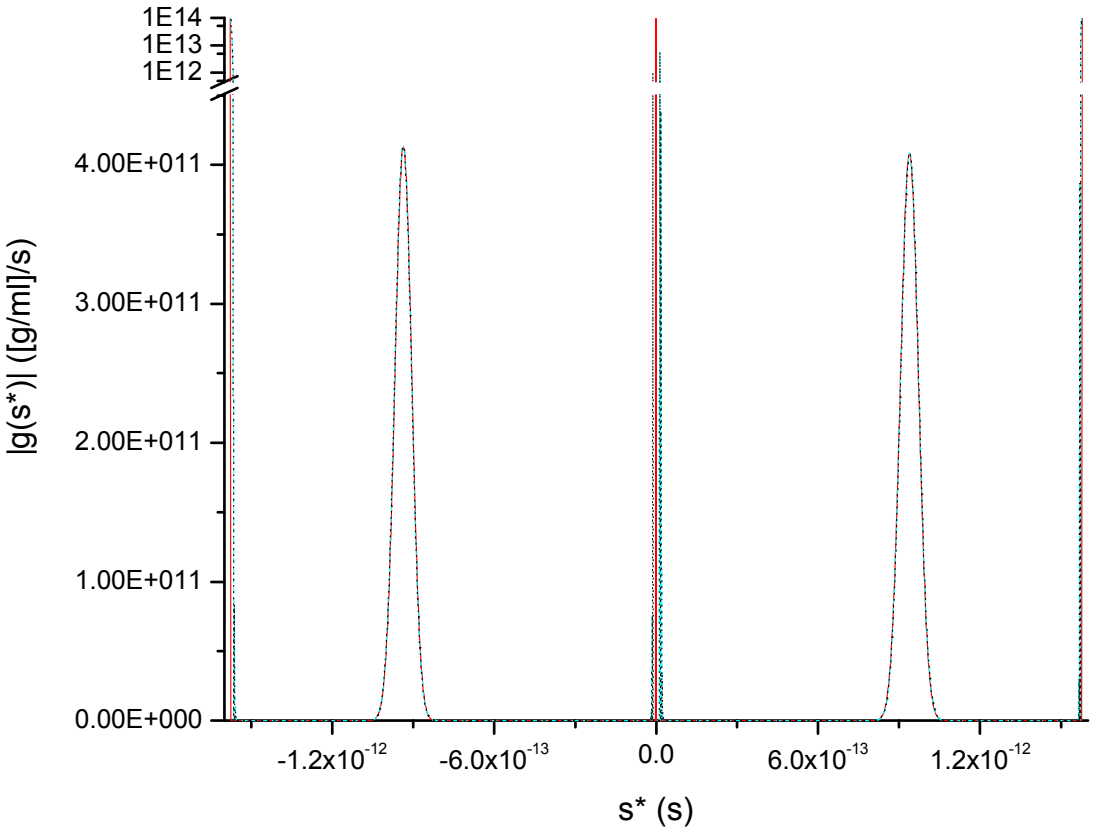

Figure 46. Plots of |g(s*)| versus s* at t = 2910 s (——) from Figure 26b, |g(s*)| versus s* at t = 2916 s (- - - - -) from $\frac{\Delta[c_{nm}]_r}{\Delta t_{nm}} - \frac{\Delta[c_{nm}]_{s*} - \Delta[c_{nm\rightarrow aa}]_{s*}}{\Delta t_{nm}}$ (Figure 45), and |g(s*)| versus s* at t = 2916 s (·····) from $\left(\frac{\partial c}{\partial s^*}\right)_t = \left(\frac{\partial [c_n - c_a]}{\partial r}\right)_t \left(\frac{\partial r}{\partial s^*}\right)_t$ (Equation 99), which is a TI-noise corrected application of Equation 3. Data are shown on a logarithmic scale above the |g(s*)|-axis break.

|g(s)| and ls-g(s*) results for data that include RI and TI noise*

In this section, the results of |g(s*)| and ls-g(s*) analysis of data that include noise are compared with the results of such analysis with noise-free data. With respect to the ls-g(s*) analysis, the effect of the number and time span of the data sets is also examined. In the first set of

comparisons, the ls-g(s*) analysis is applied to just three sets of data from an extremely short (12 s) period, while in the second set of comparisons, the ls-g(s*) analysis is applied to five sets of data from a substantially longer (900 s) period.

Each ls-g(s*) analysis shown in Figure 48 was applied to three data sets, each consisting of signal versus r or c versus r data at times $t = 2904$ s, $t = t_m = 2910$ s, or $t = t_n = 2916$ s. The data that included RI and TI noise are shown in Figure 47. The corresponding noise-free data are those at $t = 2910 \text{ s} \pm 6$ s, for which the results of previous ls-g(s*) analyses are shown in Figures 28 and 30.

For the ls-g(s*) analyses presented in Figure 48, the positions of the radial extrema of the system were set to the known positions of the meniscus ($r_m = 6$ cm) and the base ($r_b = 7.2$ cm); the lower and upper radial limits of analysis were set at $r_m + 0.02$ cm and $r_b - 0.02$ cm, respectively; a range of -12 Svedberg to 12 Svedberg, with a resolution of 240 points, was used; the meniscus position was not fit; and the confidence level was set to 0. Both the RI and TI noise were fit, except in one of the analyses of the noise-free data, in which neither were fit. (The ls-g(s*) analyses shown in Figures 28 and 30 did not include TI noise in any fit, but were otherwise identical to the analyses shown in Figure 48.)

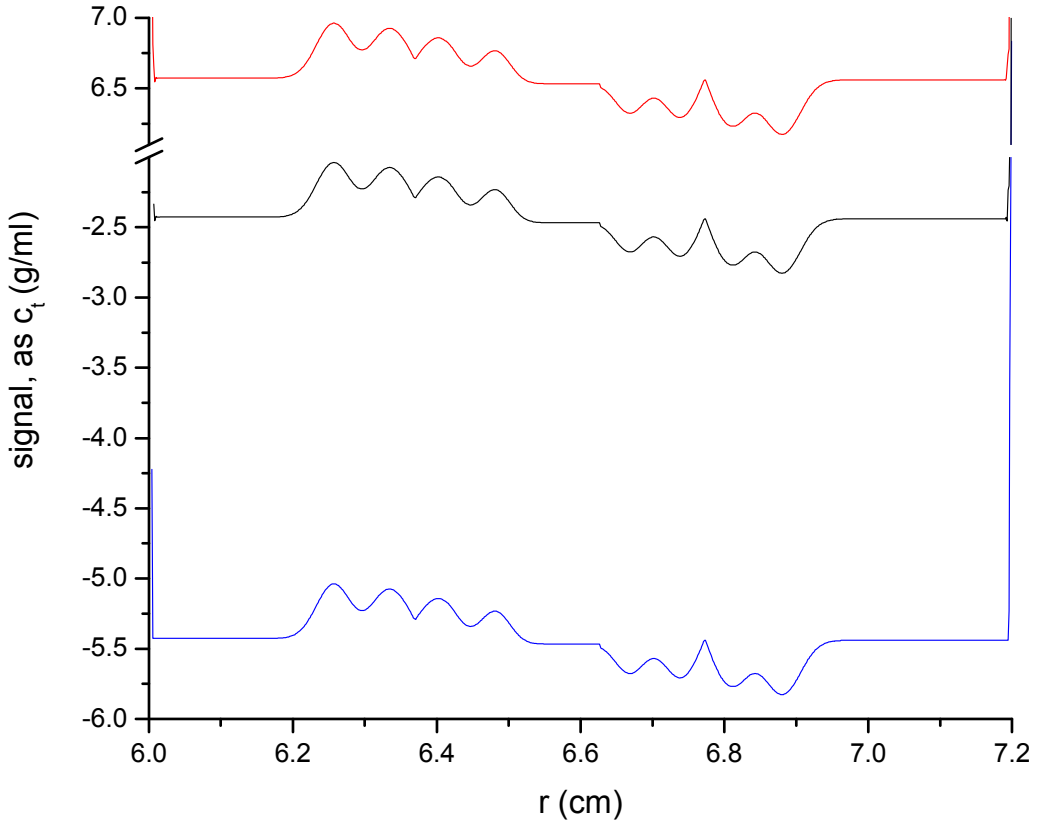

Figure 47. The previously shown (Figure 40) plots of c_m versus $r = r_h$ at $t_m = 2910$ s (——), and c_n versus $r = r_h$ at $t_n = 2916$ s (——). Also shown is c_l versus $r = r_h$ at $t_l = 2904$ s (——). The RI noise at $t_l = 2904$ s, $t_m = 2910$ s and $t_n = 2916$ s, respectively, is $RI_l = -2.5$ g/ml, $RI_m = -5.5$ g/ml and $RI_n = 6.5$ g/ml. As in Figure 40, the TI noise is equal to $c_a - RI_a$.

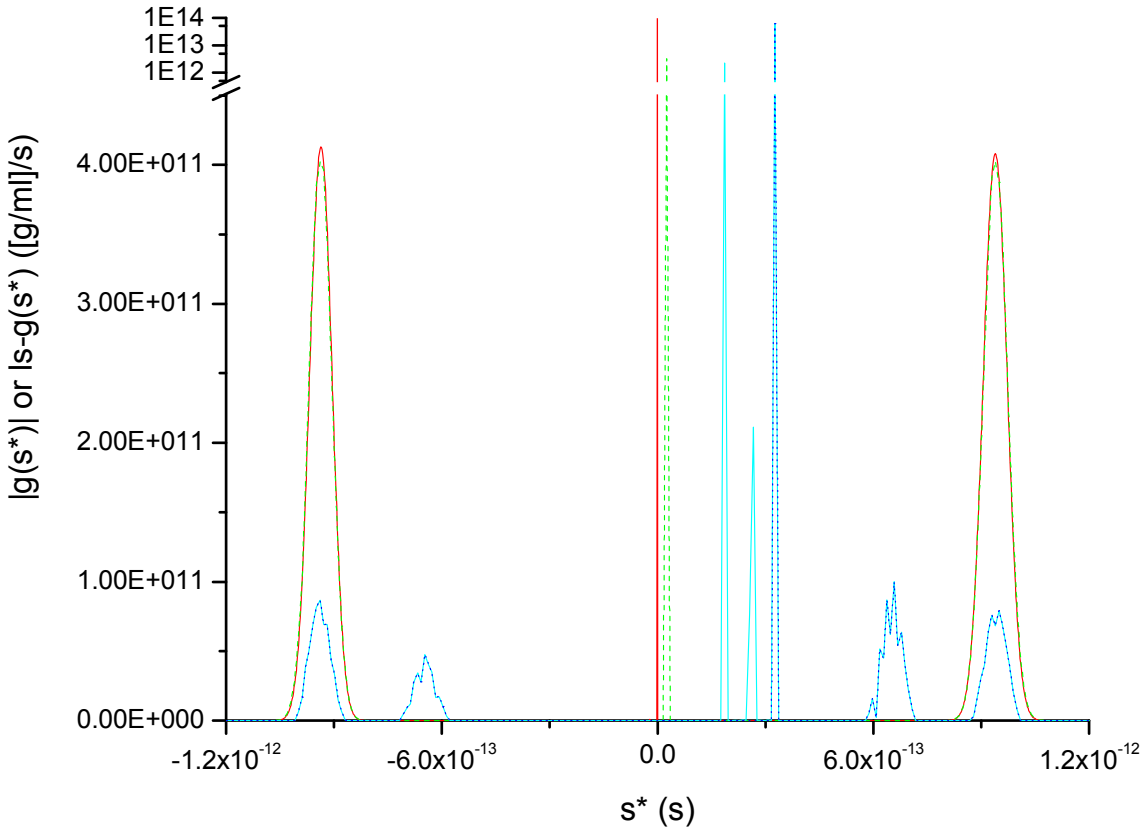

Figure 48. A plots of the previously shown (Figure 46) |g(s*)| versus s* results at t = 2916 s (——) from $\frac{\Delta[c_{nm}]_r}{\Delta t_{nm}} - \frac{\Delta[c_{nm}]_{s*} - \Delta[c_{nm \to aa}]_{s*}}{\Delta t_{nm}}$ (Figure 45). Also shown are the ls-g(s*) versus s* results, obtained with the RI and TI noise fit, for the three data sets (t = 2910 s ± 6 s) of Figure 47 (——). Additionally, the ls-g(s*) versus s* results, obtained with (·····) and without (- - - - -) the RI and TI noise fit, are shown for the equivalent noise-free data. (The noise-free data at the central time-point of t = 2910 s are found in Figure 23.) Data are shown on a logarithmic scale above the |g(s*)|-axis break. To put ls-g(s*) versus s* and |g(s*)| versus s* on the same scale, the s* values returned by SEDFIT were multiplied by (10^{-13} s/Svedberg), and the ls-g(s*) values were multiplied by (1 Svedberg/10^{-13} s).

In Figure 48, the ls-g(s*) results obtained with the noise-free data, and without fitting the RI or TI noise, closely resemble the corresponding |g(s*)| results. There is a substantial difference between any of the other corresponding ls-g(s*) and |g(s*)| results in Figure 48, however. The divergent results seem due to the shortness of the period (12 s) spanned by the three data sets used in the ls-g(s*) analyses. When that time-span is extended to 900 s, using five sets of either the noise-free data shown in Figure 23, or the corresponding data that include RI and TI noise (Figure 49), the ls-g(s*) results become much less distinguishable from one of the corresponding |g(s*)| results (Figure 50). Thus, the likelihood of obtaining misleading results from ls-g(s*) analysis seems to be low, except when too few data sets from too short a short time period are included in the analysis.

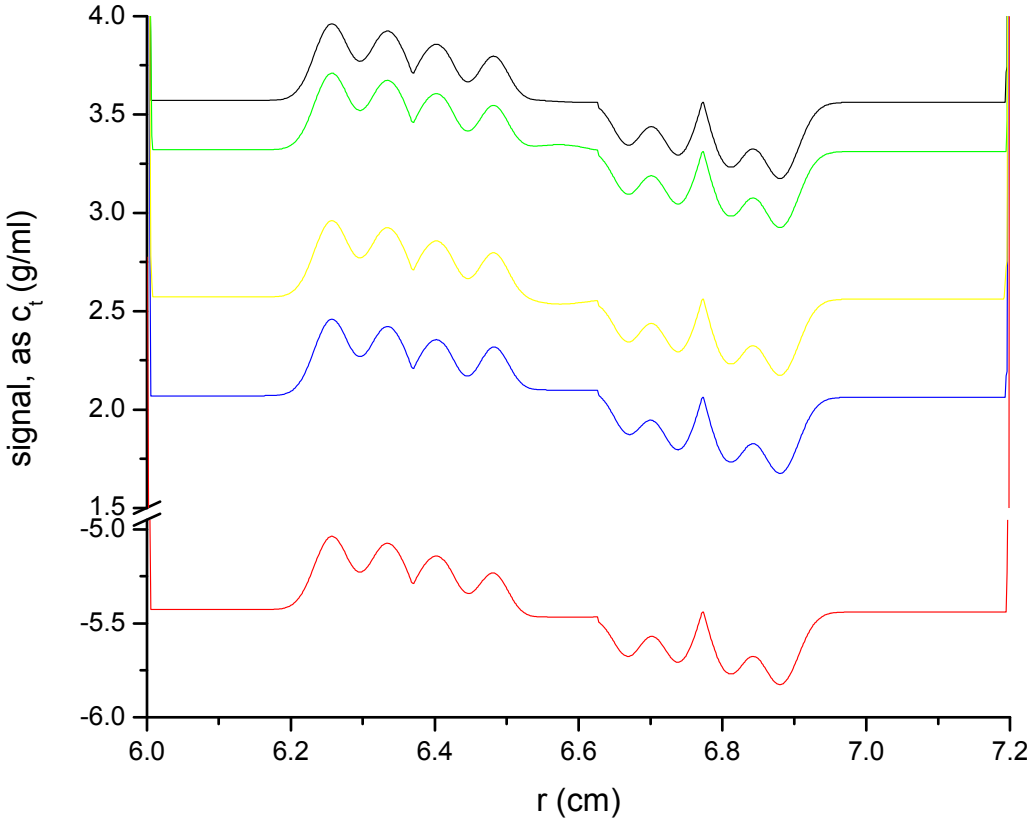

Figure 49. Plots of signal versus $r = r_h$ at $t = t_\theta = 2010$ s (——), $t = t_\iota = 2310$ s (——), $t = t_\kappa =$

2460 s (——) and t = t_λ = 2610 s (——), plus the previously shown (Figures 40 and 47) plot of c_m versus r = r_h at t = t_m = 2910 s (——). The RI noise at t_θ = 2010 s, t_ι = 2310 s, t_κ = 2460 s, t_λ = 2610 s and t_m = 2910 s, respectively, is RI_θ = 2.00 g/ml, RI_ι = 3.25 g/ml, RI_κ = 3.50 g/ml, RI_λ = 2.50 g/ml and RI_m = -5.50 g/ml. As in Figures 40 and 47, the TI noise is equal to c_a - RI_a.

Each of the two ls-g(s*) analyses shown in Figure 50 was applied to five data sets. In one analysis, the data were those shown in Figure 49, and included RI and TI noise. The corresponding noise-free data are those shown in Figure 23. The ls-g(s*) analyses presented in Figure 50 were conducted largely as described for those of Figure 48. Briefly, the positions of the radial extrema of the system were set to the known positions of the meniscus (r_m = 6 cm) and the base (r_b = 7.2 cm); the lower and upper radial limits of analysis were set at r_m + 0.02 cm and r_b – 0.02 cm, respectively; a range of -12 Svedberg to 12 Svedberg, with a resolution of 240 points, was used; the meniscus position was not fit; the confidence level was set to 0; and both the RI and TI noise were fit.

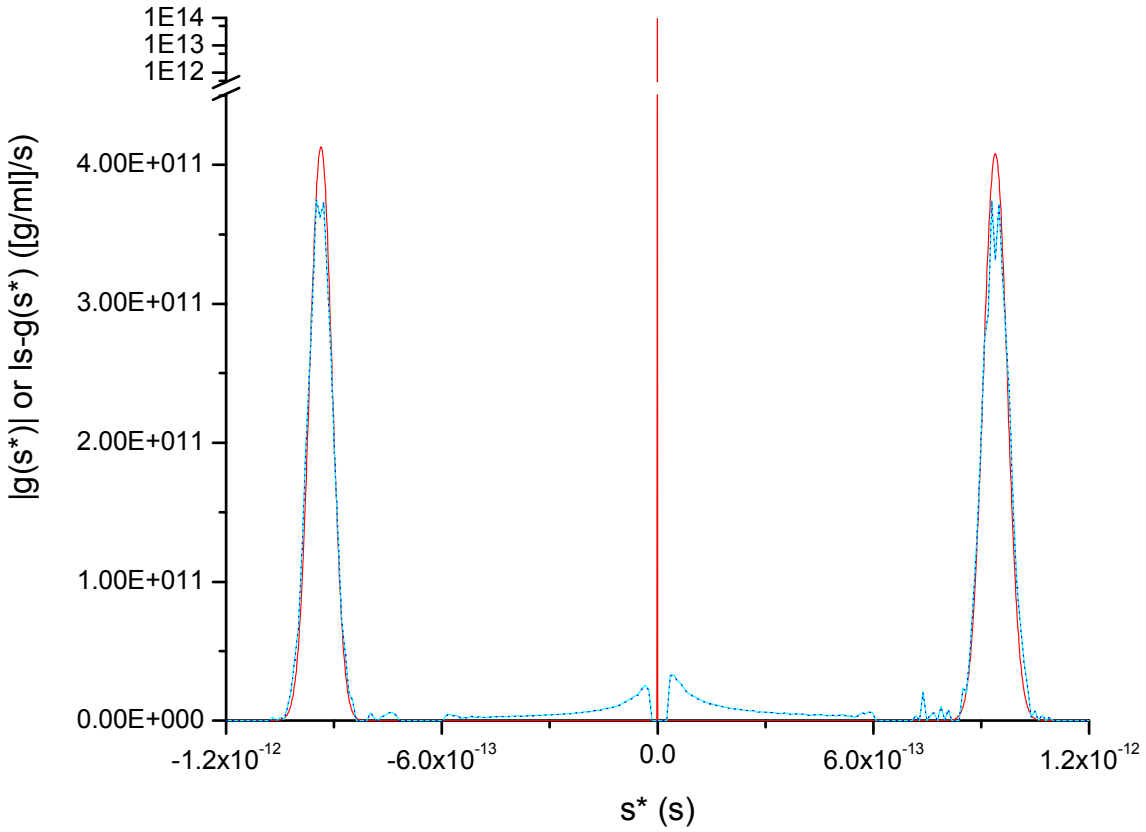

Figure 50. A plot of the previously shown (Figure 46) |g(s*)| versus s* results at t = 2916 s (——) from $\frac{\Delta[c_{nm}]_r}{\Delta t_{nm}} - \frac{\Delta[c_{nm}]_{s*} - \Delta[c_{nm \to aa}]_{s*}}{\Delta t_{nm}}$ (Figure 45). Also shown are the ls-g(s*) versus s* results, obtained with the RI and TI noise fit, for the five data sets (t = 2010 s to t = 2910 s) of Figure 49 (·····). Additionally, the ls-g(s*) versus s* results, obtained with the RI and TI noise fit, are shown for the equivalent noise-free data (——) of Figure 23. Data are shown on a logarithmic scale above the |g(s*)|-axis break. To put ls-g(s*) versus s* and |g(s*)| versus s* on the same scale, the s* values returned by SEDFIT were multiplied by (10^{-13} s/Svedberg), and the ls-g(s*) values were multiplied by (1 Svedberg/10^{-13} s).

g(v) analysis of data obtained by membrane-confined electrophoresis*

Membrane-confined electrophoresis (MCE) is similar enough to AUC that the data from both methods can be analysed in a similar fashion. The data collected during MCE include the values of a dependent variable related to the total mass concentration, c, of all solutes, and the corresponding independent variables of time, t, and spatial position, ξ. Data regarding electrical, temperature and other parameters that are likely to affect $\left(\frac{\partial c}{\partial \xi}\right)_t$ and $\left(\frac{\partial c}{\partial t}\right)_\xi$ are also recorded. The proportionality between an experimentally measured signal and a specific solute concentration may vary from one solute to another. For example, it is often the case that some solutes, such as buffer salts, are completely undetectable, or nearly so.

MCE differs from AUC with respect to the geometry and boundary characteristics of the system. In MCE, the sample occupies an open system with rectangular geometry. An electrical current, i, flows through semipermeable membranes that are in contact with dialysate at the top and the base of the system. Sufficiently large molecules, including macro-ions, remain between the membranes. Thus, MCE is an electrical analogue of AUC. Details regarding MCE can be found elsewhere (Laue et al., 1989), including the reference (Moody, 2011b) relied upon here.

Characteristics of v and g(v*)*

The apparent product of the electric field, E, and the electrophoretic mobility coefficient, u, is defined as the apparent electrophoretic velocity coefficient, v*. The distribution function of the electrophoretic velocity coefficient is g(v*). (Due to the concentration-dependent characteristics of both E and u, it is only practical to work with their product when defining the apparent

parameter that is analogous to s* in AUC. As will be discussed, after analysis, v* can be divided by an estimate of E, and g(v*) can be multiplied by the same estimate of E, in an effort to normalise the results for electric field strength.)

Each value of v* is a combined transformation of a value of ξ, a value of t, and a reference position. By definition, v* is equal to the electrophoretic velocity coefficient of a thermodynamically ideal solute that, in the limit of zero diffusion, would exhibit a hyper-sharp boundary in its concentration at a specific spatial position and a specific time. There are two possible orientations of that hyper-sharp boundary, one of which would arise from a negatively-directed solute for which v* is less than zero, the other of which would arise from a positively-directed solute for which v* is greater than zero. Thus, each value of v* describes the behaviour of a step function that can represent a hypothetical solute concentration in an all-or-none fashion.

Henceforth, a hypothetical solute is defined as an imaginary, thermodynamically ideal, non-diffusing solute characterised by a v* value and a constant of concentration. Of the two oppositely signed v* values that correspond to a transition in a hypothetical solute concentration at spatial position ξ and time t, the one having $v^* < 0$ corresponds to the transition for which the hypothetical solute concentration at time t is zero at all spatial positions greater than ξ, and the one having $v^* > 0$ corresponds to the transition for which the hypothetical solute concentration at time t is zero at all spatial positions less than ξ.

A hypothetical solute can be said to exhibit a zone of depletion where its concentration is zero, and a plateau region within which its concentration is greater than zero and independent of spatial position. The concentration of a hypothetical solute in its plateau region is, by virtue of

being independent of spatial position, called its plateau concentration. In MCE, the plateau concentration of a hypothetical solute is equal to a value that, due to the rectangular geometry of the system, is independent of time.

To within some approximation, g(v*) analysis reveals the relationship between v* values and the initial concentrations of the corresponding, hypothetical solutes. With the possible exceptions of the extreme time points, the number of v* values is infinite at any given time. Thus, within a g(v*) distribution, for any given hypothetical solute characterised by a randomly chosen v* value, the apparent initial concentration is most likely zero, or of a magnitude attributable to noise.

Given a function to convert between ξ and v* at any given time (Equation 117), the independent variables of MCE data can be transformed from t and ξ to t and v*. It is then possible to plot c versus v* at time t, but in doing so, the value of c at any single spatial position at that time will map to the two values of v* that are calculated for that spatial position and time. Likewise, following such a transformation, it is straightforward to obtain the derivative, $\left(\frac{\partial c}{\partial v^*}\right)_t$, which is single-valued when viewed as a function of v*, but is double-valued when viewed as a function of ξ.

At any given time, where $\left|\left(\frac{\partial c}{\partial \xi}\right)_t\right|$ is greater than zero at some value of ξ, $\left|\left(\frac{\partial c}{\partial v^*}\right)_t\right|$ will be greater than zero at the two values of v* calculated from that value of ξ, but the sign of $\left(\frac{\partial c}{\partial v^*}\right)_t$ will match the sign of just one of those v* values. The v* value where the signs of $\left(\frac{\partial c}{\partial v^*}\right)_t$ and v* match will be the v* value that matches the orientation of $\left(\frac{\partial c}{\partial \xi}\right)_t$ at the corresponding ξ value. Each $\left(\frac{\partial c}{\partial v^*}\right)_t$ that

matches the sign of v* is deemed essential with respect to calculating g(v*). Each $\left(\frac{\partial c}{\partial v^*}\right)_t$ that is opposite in sign to v* is deemed redundant, and a value of zero is used in its place when calculating g(v*). At any given time, half of the nonzero $\left(\frac{\partial c}{\partial v^*}\right)_t$ values will be deemed essential, and half will be deemed redundant.

Nullifying the redundant nonzero values of $\left(\frac{\partial c}{\partial v^*}\right)_t$ yields g(v*). The integral of |g(v*)| with respect to v* yields the cumulative distribution function, G(v*), which equates to a weakly time-dependent measure of the concentration of all solutes for which the apparent electrophoretic velocity coefficient is less than or equal to v*, but greater than or equal to the minimum possible value (Equation 124) of v* at some specific time.

Derivation of g(v)*

By an approach analogous to Bridgeman's (1942) derivation of g(s*), the derivation of g(v*) can start with the total differential of c with respect to ξ and t,

$$dc = \left(\frac{\partial c}{\partial \xi}\right)_t d\xi + \left(\frac{\partial c}{\partial t}\right)_\xi dt\,.$$

(100)

At constant t, this equation reduces to

$$dc_t = \left(\frac{\partial c}{\partial \xi}\right)_t d\xi.$$

(101)

Thus, where c is defined as a function of ξ and t, the partial derivative of c with respect to v* at constant t, obtained through division by an infinitesimally small change in v* at constant t, is

$$\left(\frac{\partial c}{\partial v^*}\right)_t = \left(\frac{\partial c}{\partial \xi}\right)_t \left(\frac{\partial \xi}{\partial v^*}\right)_t .$$

(102)

By an approach analogous to Stafford's (1992, 1994, 2000) derivation of g(s*), the derivation of g(v*) can also start with the total differential of c with respect to v* and t,

$$dc = \left(\frac{\partial c}{\partial v^*}\right)_t dv^* + \left(\frac{\partial c}{\partial t}\right)_{v^*} dt ,$$

(103)

from which, through division by an infinitesimally small change in t at constant ξ, the partial derivative of c with respect to t at constant ξ,

$$\left(\frac{\partial c}{\partial t}\right)_\xi = \left(\frac{\partial c}{\partial v^*}\right)_t \left(\frac{\partial v^*}{\partial t}\right)_\xi + \left(\frac{\partial c}{\partial t}\right)_{v^*},$$

(104)

is obtained. Solving Equation 104 for $\left(\frac{\partial c}{\partial v^*}\right)_t$ yields

$$\left(\frac{\partial c}{\partial v^*}\right)_t = \left[\left(\frac{\partial c}{\partial t}\right)_\xi - \left(\frac{\partial c}{\partial t}\right)_{v^*}\right]\left(\frac{\partial t}{\partial v^*}\right)_\xi .$$

(105)

Equation 105 can be applied using finite differences in c, t and v*. In the limit as the finite time-difference approaches zero, Equation 105 and Equation 102 yield identical results.

Of the four time-dependent effects described for AUC, one, the radial dilution/concentration effect, has no equivalent in MCE. The remaining three time-dependent effects exhibited by $\left(\frac{\partial c}{\partial s^*}\right)_t$ in AUC, however, do have equivalents that are exhibited by $\left(\frac{\partial c}{\partial v^*}\right)_t$ in MCE. The least subtle of these is the time dependence of the positions (in terms of v*) and magnitudes of redundant

nonzero values of $\left(\frac{\partial c}{\partial v^*}\right)_t$. As with g(s*) analysis, this is the one time dependence that can be unambiguously eliminated, which is accomplished simply by subtracting the redundant nonzero values from $\left(\frac{\partial c}{\partial v^*}\right)_t$. Doing so leaves, q(v*,t), which is the nonredundant derivative of c with respect to v* at constant t. As there is no spatial dilution/concentration effect with time in MCE,

$$g(v^*) = q(v^*, t) = \left(\frac{\partial c}{\partial v^*}\right)_t - e(v^*, t) \,,$$

(106)

where e(v*,t) is equal $\left(\frac{\partial c}{\partial v^*}\right)_t$ wherever and whenever $\left(\frac{\partial c}{\partial v^*}\right)_t$ is redundant, but is equal to zero at all other v* and t.

Just as redundant nonzero values of $\left(\frac{\partial c}{\partial s^*}\right)_t$ are found where s* reflects the location but not the sign of $\left(\frac{\partial c}{\partial r}\right)_t$, redundant nonzero values of $\left(\frac{\partial c}{\partial v^*}\right)_t$ are found where v* reflects the location but not the sign of $\left(\frac{\partial c}{\partial \xi}\right)_t$. Furthermore, given that $\left(\frac{\partial c}{\partial v^*}\right)_t = \left(\frac{\partial c}{\partial \xi}\right)_t \left(\frac{\partial \xi}{\partial v^*}\right)_t$ (Equation 102) and given that, as will be shown, $\left(\frac{\partial \xi}{\partial v^*}\right)_t$ cannot be less than zero (Equation 120), the signs of $\left(\frac{\partial c}{\partial \xi}\right)_t$ and $\left(\frac{\partial c}{\partial v^*}\right)_t$ must be the same, or $\left(\frac{\partial c}{\partial \xi}\right)_t$ and $\left(\frac{\partial c}{\partial v^*}\right)_t$ must both equal zero. Thus, $\left(\frac{\partial c}{\partial v^*}\right)_t$ is essential if the signs of v* and $\left(\frac{\partial c}{\partial v^*}\right)_t$ are the same, and $\left(\frac{\partial c}{\partial v^*}\right)_t$ is redundant if the signs of v* and $\left(\frac{\partial c}{\partial v}\right)_t$ are opposite. This distinction provides the basis for a test parameter,

$$Q_{v^*,t} = v^* \left(\frac{\partial c}{\partial v^*}\right)_t \,.$$

(107)

If $Q_{v^*,t} > 0$, $\left(\frac{\partial c}{\partial v^*}\right)_t$ is essential and e(v*,t) is equated to zero, but if $Q_{v^*,t} \leq 0$, e(v*,t) is equated to

$\left(\frac{\partial c}{\partial v^*}\right)_t$.

Nonzero diffusion coefficients and concentration-dependent transport affect g(v*) and g(s*) identically, and thus render g(v*) at least somewhat dependent on time.

Nonzero diffusion coefficients cause the peaks and valleys of $\left(\frac{\partial c}{\partial v^*}\right)_t$ and g(v*) to sharpen with time. As the range of v* occupied by a transition region of G(v*) coincides with the breadth of a corresponding peak or valley of g(v*), nonzero diffusion coefficients also cause transition regions of G(v*) to sharpen with time. The effect is due to the fact that the range of v* (Equations 124 and 125) narrows in proportion to $\frac{1}{t}$, while the range of ξ encompassed by a diffusing boundary region broadens in proportion to $\frac{1}{\sqrt{t}}$ in the simplest, concentration-independent case (van Holde, 1985). (In terms of c as a function of ξ and t, a boundary region can be defined as any region within ξ where $\left|\left(\frac{\partial c}{\partial \xi}\right)_t\right| \neq 0$ at time t.)

In the simplest case, compared to a concentration-independent system, concentration-dependent transport simply adds a time-dependence to the weight-average positions of the peaks and valleys of g(v*). Concentration-dependent transport may also skew the shape of a peak or valley, and a chemical reaction can render the area of a peak or valley time-dependent. Where concentration-dependent transport results in the MCE-equivalent of Johnston-Ogston effects, the number, position and magnitude of peaks and valleys in g(v*) can differ from that which would be seen otherwise. Any effect of concentration-dependent transport on g(v*) results in a corresponding effect on G(v*).

Equations of continuity and mass flow

The continuity equation for electrophoresis in a system with rectangular geometry can be written as

$$\left(\frac{\partial c}{\partial t}\right)_{\xi} = -\left(\frac{\partial I}{\partial \xi}\right)_{t},$$

(108)

where I is the total mass flow of all solutes.

In terms of D and u, the gradient-average diffusion and weight-average electrophoretic mobility coefficients, respectively, for all solute components,

$$I = uEc - D\left(\frac{\partial c}{\partial \xi}\right)_{t},$$

(109)

where the electric field, E, is a function of concentration gradients, electrical current, cross-sectional area and conductivity, which, in turn, is a function of the concentration, valence, electrophoretic mobility coefficient and diffusion coefficient of each solute (Equations H5 and H6 of Moody, 2011b). The diffusion coefficient (Equation A21, Moody, 2011b) of each solute and the electrophoretic mobility coefficient (Equation A22, Moody, 2011b) of each solute are dependent on the concentration of each solute, and the latter coefficient includes a term that is proportional to the solvent velocity (in the system frame of reference) divided by E.

The continuity equation in the limit as $\left(\frac{\partial c}{\partial \xi}\right)_{t}$ *approaches zero*

In regions of the system where $\left(\frac{\partial c}{\partial \xi}\right)_t = 0$, which condition can only persist if $\left(\frac{\partial uE}{\partial \xi}\right)_t = 0$ wherever $\left(\frac{\partial c}{\partial \xi}\right)_t = 0$, Equations 108 and 109 lead to

$$\lim_{\left(\frac{\partial c}{\partial \xi}\right)_t \to 0} \left(\frac{\partial c}{\partial t}\right)_\xi = \lim_{\left(\frac{\partial c}{\partial \xi}\right)_t \to 0} \left[-c\left(\frac{\partial uE}{\partial \xi}\right)_t - uE\left(\frac{\partial c}{\partial \xi}\right)_t\right] = 0.$$

(110)

To describe this condition in detail, let the lowest and highest spatial positions of a region where Equation 110 holds be denoted as ξ_{min} and ξ_{max}, respectively, where, in general, ξ_{min} and ξ_{max} are time-dependent. Within a time-dependent region where Equation 110 holds, which is to say, within $\xi_{min} \leq \xi \leq \xi_{max}$, $c = c_p$, where c_p is the time-independent plateau concentration. The plateau concentration is the total concentration of all solutes within $\xi_{min} \leq \xi \leq \xi_{max}$, and its time independence stems from the rectangular geometry of the system. For as long as the plateau region exists, $\left(\frac{\partial c_p}{\partial \xi}\right)_t = 0$, and wherever it exists, $\left(\frac{\partial c_p}{\partial t}\right)_\xi = 0$. As $c = c_p$ in a plateau region, it can be stated that, in general, $\left(\frac{\partial c}{\partial t}\right)_\xi = 0$ wherever $\left(\frac{\partial c}{\partial \xi}\right)_t = 0$.

In MCE, the initial time, t_0, can be equated to the time at which the electrical current starts to flow. For the systems considered here, the current is assumed to be constant from t_0 on, and t_0 is equated to 0. It is further assumed that, at t_0, at all ξ, $c = c_0$, where c_0 is the initial total concentration of all solutes. Thus, $c_p = c_0$ at t_0, at which time, $\xi_{min} = \xi_m$ and $\xi_{max} = \xi_b$, where $\xi_m = 0$ is the spatial position of the upper membrane (analogous to the meniscus position in AUC), and ξ_b is the spatial position of the lower membrane (analogous to the base of the system in AUC).

The equation of mass flow in the limit as $\left(\frac{\partial c}{\partial \xi}\right)_t$ *approaches zero*

In the limit as $\left(\frac{\partial c}{\partial \xi}\right)_t$ approaches 0, Equation 109 reduces to

$$\lim_{\left(\frac{\partial c}{\partial \xi}\right)_t \to 0} I = cuE \ .$$

(111)

The mass flow, I, is equal to cv, where, in the system frame of reference, v is the weight-average velocity of all solute components at t and ξ. Expressing v as $\frac{d\xi}{dt}$, and dividing Equation 111 by c, results in

$$\lim_{\left(\frac{\partial c}{\partial \xi}\right)_t \to 0} v = \frac{d\xi}{dt} = uE \ .$$

(112)

Wherever $\left(\frac{\partial c}{\partial \xi}\right)_t = 0$, $\left(\frac{\partial uE}{\partial \xi}\right)_t = 0$, in which case, if the functional form of the t-dependence of uE were known, Equation 112 might be solved by separation of variables and integration. Such a solution would take the form of

$$\int_{\xi_0}^{\xi_v} d\xi = \int_{t_0}^{t_v} uE dt \ ,$$

(113)

where ξ_0 would be the extreme radial position away from which a hypothetical solute with an electrophoretic velocity of uE would travel, and at time t_v, ξ_v would be the radial position of the transition in the concentration of that solute in the limit as its diffusion coefficient approached zero.

As $\left(\frac{\partial uE}{\partial \xi}\right)_t = 0$ wherever $\left(\frac{\partial c}{\partial \xi}\right)_t = 0$, and as $\left(\frac{\partial c}{\partial t}\right)_\xi = 0$ wherever $\left(\frac{\partial c}{\partial \xi}\right)_t = 0$, it follows that $\left(\frac{\partial uE}{\partial t}\right)_\xi = 0$ wherever $\left(\frac{\partial c}{\partial \xi}\right)_t = 0$. Given that Equation 113 applies to a plateau region, uE can be factored out of the integral on the right-hand side, and the equation can be evaluated. Outside of a plateau region, however, c will depend on time, and thus uE will usually depend on time. To find a solution that applies anywhere in the system, uE is redefined in such a way that the entire system can be described in terms of hypothetical solutes that exhibit neither diffusion nor a dependence on concentration.

As the relationship between uE and t is complicated, Equation 112 is solved using the same approach applied to the similar problems presented by Equations 13 and 20. The c-dependent parameter, uE, in Equation 112 is replaced with an infinite number of c-independent, and therefore t-independent, v* values, resulting in an infinite number of integrals, each of which applies to a hypothetical solute, and each of which is given by

$$\int_{\xi_0}^{\xi_{v^*}} d\xi = v^* \int_{t_0}^{t_{v^*}} dt,$$

(114)

where ξ_0 is the extreme radial position (ξ_m for $v^* > 0$, and ξ_b for $v^* < 0$) away from which a hypothetical solute of electrophoretic velocity coefficient v* travels, ξ_{v^*} is the spatial position of the transition in the concentration of that solute in the zero-diffusion limit, and t_{v^*} is the time that corresponds to the location of that transition at ξ_{v^*}.

For each such hypothetical solute, $\xi_0 = \xi_b$ if $v^* < 0$, and $\xi_0 = \xi_m$ if $v^* > 0$. At time t_{v^*}, at spatial

position ξ_{v^*}, each such solute exhibits a transition in concentration from 0 to c_{p,v^*}, where c_{p,v^*} is the time-independent plateau concentration of that solute. Thus, at any time, $c_{p,v^*} = c_{0,v^*}$, where c_{0,v^*} is the initial concentration of the hypothetical solute throughout the system. (In AUC, the plateau concentration of each hypothetical solute has a time-dependence described by Equation 74 or 75.) At any given time, the concentration of such a solute could be described by a step function equal to 0 from ξ_0 to ξ_{v^*}, and equal to c_{p,v^*} from ξ_{v^*} to the extremity at the opposite end of the system from ξ_0. (The extremity at the opposite end of the system from ξ_0 is ξ_m if $\xi_0 = \xi_b$, or at ξ_b if $\xi_0 = \xi_m$.)

The right-hand side of Equation 114 evaluates to $v^*t_{v^*}$, and the left-hand of Equation 114 evaluates to $\xi_{v^*} - \xi_0$. Solving for ξ_{v^*} yields

$$\xi_{v^*} = \xi_0 + v^* t_{v^*},$$

(115)

which describes the boundary position (the transition point of the corresponding step function) that would be observed for a purely hypothetical solute characterised by an electrophoretic velocity coefficient of v*, in the limit as D* (the solute's diffusion coefficient) approached zero.

If an analytic solution of Equations 113 existed, it would only apply to a plateau region. In contrast, Equation 115, which is the analytic solution of Equation 114, can be applied to the entire system. Thus, a description of the whole system is gained at the remarkably low cost of having to cast that description in terms of an infinite set of imaginary, nondiffusing, concentration-independent solutes.

Equation 110 shows that $c_{p,v^*} = c_{0,v^*}$ as long as the plateau region of which c_{p,v^*} is a part persists.

On that basis, and on the basis of Equation 115, the relationship between the plateau concentration and the boundary position of a hypothetical solute of electrophoretic velocity coefficient v*, in the limit as D* approaches zero, can be described by

$$c_{v^*} = \begin{cases} 0 \; at \begin{cases} \xi < \xi_{v^*} = \xi_m + v^* t_{v^*} \; for \; v^* > 0 \\ \xi > \xi_{v^*} = \xi_b + v^* t_{v^*} \; for \; v^* < 0 \end{cases} \\ c_{p,v^*} = c_{0,v^*} \; at \begin{cases} \xi \geq \xi_{v^*} = \xi_m + v^* t_{v^*} \; for \; v^* \geq 0 \\ \xi \leq \xi_{v^*} = \xi_b + v^* t_{v^*} \; for \; v^* \leq 0 \end{cases} \end{cases}.$$

(116)

Equation 116 describes c_{v^*} as a step function with a time-independent height of $c_{p,v^*} = c_{0,v^*}$, and a time-dependent transition at $\xi_0 + v^* t_{v^*}$ (Equation 115), where $\xi_0 = \xi_m$ for $v^* > 0$, and $\xi_0 = \xi_b$ for $v^* < 0$. Over time, for $v^* \neq 0$, the region in which $c_{v^*} = 0$ expands from ξ_0 to $\xi_0 + v^* t_{v^*}$. While c_{v^*} depends on ξ and t, c_{p,v^*} is time-independent and equal to c_{0,v^*} at all $\xi > \xi_0 + v^* t_{v^*}$ (Equation 115). Thus, in general, $\left(\frac{\partial c_{p,v^*}}{\partial \xi}\right)_t = 0$ and $\left(\frac{\partial c_{p,v^*}}{\partial t}\right)_\xi = 0$. As there is an infinite number of v* values, at any given time, there is an infinite number of step functions, each given by Equation 116. The sum of all such step functions at a given time yields c as a function of r at that time.

Transforming the independent variables from ξ and t to v and t*

Solving Equation 115 for v* yields

$$v^* = \frac{\xi_{v^*} - \xi_0}{t_{v^*}}.$$

(117)

For each time, t, the set of all spatial positions, ξ, is now equated to the set of boundary positions, ξ_{v^*}, needed to transform the independent variable ξ to the independent variable v*. Replacing ξ_{v^*}

and t_{v^*} of Equation 115 with ξ and t, respectively, results in

$$\xi = \xi_0 + v^* t \,,$$

(118)

which, solved for v*, yields

$$v^* = \frac{\xi - \xi_0}{t} = \begin{Bmatrix} \frac{\xi - \xi_b}{t} \leq 0 \\ \frac{\xi - \xi_m}{t} \geq 0 \end{Bmatrix}.$$

(119)

At $t > 0$, v* is a function of t, ξ and ξ_0, such that $v^* < 0$ for $\xi_0 > \xi$, $v^* = 0$ for $\xi_0 = \xi$, $v^* > 0$ for $\xi_0 < \xi$, and for a given value of $\xi - \xi_0$, $|v^*|$ decreases as t increases. As ξ_m and ξ_b are the two possible values of ξ_0, at a given $t > 0$, for each spatial position ξ within $\xi_m \leq \xi \leq \xi_b$, there are two values of v*. For each spatial position ξ within $\xi_m < \xi < \xi_b$, at a given $t > 0$, there is one negative and one positive value of v*. For $\xi = \xi_m$, one v* equals zero and the other is less than zero at any $t > 0$. For $\xi = \xi_b$, one v* equals zero and the other is greater than zero at any $t > 0$. At a given $t > 0$, the minimum value of v* occurs where $\xi = \xi_m$ and $\xi_0 = \xi_b$, while the maximum value of v* occurs where $\xi = \xi_b$ and $\xi_0 = \xi_m$. At t_0, v* is undefined for all ξ. As can be seen by equating $-\left(\frac{\xi - \xi_b}{t}\right)$ to $\frac{\xi - \xi_m}{t}$ and solving for ξ, there is one spatial position, $\xi = \frac{\xi_b + \xi_m}{2}$, for which, at any given time, the positive v* equals the absolute value of the negative v*.

Determining q(v,t) from* $\left(\frac{\partial c}{\partial v^*}\right)_t$*, and expressing g(v*) in terms of q(v*,t), ξ and t*

Differentiating Equation 118 with respect to v* at constant t yields

$$\left(\frac{\partial \xi}{\partial v^*}\right)_t = t.$$

(120)

As t cannot be less than zero, Equation 102, which states that $\left(\frac{\partial c}{\partial v^*}\right)_t = \left(\frac{\partial c}{\partial \xi}\right)_t \left(\frac{\partial \xi}{\partial v^*}\right)_t$, shows, in combination with Equation 120, that the signs of $\left(\frac{\partial c}{\partial v^*}\right)_t$ and $\left(\frac{\partial c}{\partial \xi}\right)_t$ must be the same at all $t > 0$.

The relationship between q(v*,t) and $\left[\left(\frac{\partial c}{\partial t}\right)_\xi - \left(\frac{\partial c}{\partial t}\right)_{v^*}\right]$ of Equation 105 becomes clear once $\left(\frac{\partial t}{\partial v^*}\right)_\xi$ has been expressed in terms of v* and t. Solving Equation 118 for t and differentiating with respect to v* at constant ξ yields

$$\left(\frac{\partial t}{\partial v^*}\right)_\xi = -\frac{\xi - \xi_0}{v^{*2}} = -\frac{t}{v^*}.$$

(121)

As t cannot be less than zero, Equation 121 shows that the signs of $\left(\frac{\partial t}{\partial v^*}\right)_\xi$ and v* are always opposite. Given this, and given the relationship (Equation 107) between v* and essential nonzero values of $\left(\frac{\partial c}{\partial v^*}\right)_t$, it follows that the sign of any essential nonzero value of $\left(\frac{\partial c}{\partial v^*}\right)_t$ and the sign of $\left(\frac{\partial t}{\partial v^*}\right)_\xi$ must be opposite at any time after t_0. Thus, in Equation 105, which states that $\left(\frac{\partial c}{\partial v^*}\right)_t = \left[\left(\frac{\partial c}{\partial t}\right)_\xi - \left(\frac{\partial c}{\partial t}\right)_{v^*}\right]\left(\frac{\partial t}{\partial v^*}\right)_\xi$, the difference, $\left[\left(\frac{\partial c}{\partial t}\right)_\xi - \left(\frac{\partial c}{\partial t}\right)_{v^*}\right]$, must be less than zero for all essential nonzero values of $\left(\frac{\partial c}{\partial v^*}\right)_t$, and must be greater than zero for all redundant nonzero values of $\left(\frac{\partial c}{\partial v^*}\right)_t$.

Concentration change across a transition point (ξ_{v^*}), and concentration within a v range*

A real boundary may encompass multiple species' boundaries, each of which is broadened by

diffusion and affected by the concentration of each species present. In g(v*) analysis, such a boundary is modeled as a set of hyper-sharp transitions in concentration, where each transition corresponds to a hypothetical solute characterised by a concentration-independent velocity coefficient of v*, an initial concentration of c_{0,v^*}, and a diffusion coefficient that approaches zero.

At a given time, t, the difference in the detectable concentration between two adjacent plateau regions separated by a boundary is Δc_e, where the subscript e indicates that e(v*,t), which are the redundant values of $\left(\frac{\partial c}{\partial v^*}\right)_t$, are included in the calculation of the quantity. In contrast to its AUC counterpart (Δc_t of Equation 33), Δc_e is a time-independent quantity, provided that it is calculated for a region in which $\left(\frac{\partial c}{\partial v^*}\right)_t$ is unaffected by overlapping boundaries of oppositely directed solutes. For a boundary located between $\xi_{v^*_{below}}$ and $\xi_{v^*_{above}}$,

$$\Delta c_e = \int_{v^*_{below}}^{v^*_{above}} \left(\frac{\partial c}{\partial v^*}\right)_t dv^*,$$

(122)

where v^*_{below} and v^*_{above} are calculated from $\xi_{v^*_{below}}$ and $\xi_{v^*_{above}}$, respectively, using Equation 119. In the plateau regions just below v^*_{below} and just above v^*_{above}, $\left(\frac{\partial c}{\partial v^*}\right)_t = 0$. If all v* are less than zero within $v^*_{below} \leq v^* \leq v^*_{above}$, as would be the case for $\xi_{v^*_{below}} = \xi_{max}$ of the plateau for which c is higher, Δc_e will be less than zero. If all v* are greater than zero within $v^*_{below} \leq v^* \leq v^*_{above}$, as would be the case for $\xi_{v^*_{above}} = \xi_{min}$ of the plateau for which c is higher, Δc_e will be greater than zero. (Respectively, ξ_{min} and ξ_{max} are the lowest and highest spatial positions of a region where Equation 110 holds.)

The cumulative concentration of detectable solutes that can be characterised by v* within v^*_{below}

$\leq v^* \leq v^*_{above}$ is

$$\Delta c = \int_{v^*_{below}}^{v^*_{above}} |g(v^*)| dv^*.$$

(123)

The result cannot be less than zero. If $v^*_{below} \leq v^* \leq v^*_{above}$ encompasses an entire peak or valley of g(v*), Δc should, in the absence of overlapping boundaries of oppositely directed and detectable solutes, be time-independent for concentration-independent systems, as well as for concentration-dependent systems in which the solute concentrations are not altered by chemical reactions.

The range of integration in Equation 123 can be extended to the extrema of v*. The extrema in v* are inversely proportional to t. At time t,

$$v^*_{-x} = \frac{\xi_m - \xi_b}{t}$$

(124)

is the minimum value of v*, and

$$v^*_{+x} = \frac{\xi_b - \xi_m}{t},$$

(125)

is the maximum value of v*. As noted with respect to Equation 119, each spatial position gives rise to two v* values. At $\xi = \xi_m$, $v^* = v^*_{-x}$ for $\xi_0 = \xi_b$ (Equation 124) and $v^* = 0$ for $\xi_0 = \xi_m$. Likewise, at $\xi = \xi_b$, $v^* = v^*_{+x}$ for $\xi_0 = \xi_m$ (Equation 125) and $v^* = 0$ for $\xi_0 = \xi_b$. With the integration limits of Equation 123 set to $v^*_{below} = v^*_{-x}$ and $v^*_{above} = v^*_{+x}$, Δc is equal to the apparent value of c_0, which is to say, the apparent initial concentration of all solutes that contribute to $\left(\frac{\partial c}{\partial v^*}\right)_t$, and thus contribute to g(v*).

The range of integration in Equation 122 can also be extended to the extrema of v*, and with the addition of an offset, can be used to reconstruct c as a function of v* and t. At any given time, t, the concentration at $v^* = v^*_{neg} < 0$ is given by

$$c = c_{-x} + \int_{v^*_{-x}}^{v^*_{neg}} \left(\frac{\partial c}{\partial v^*}\right)_t dv^*,$$

(126a)

and the concentration at $v^* = v^*_{pos} > 0$ is given by

$$c = c_{-x} + \int_{v^*_{-x}}^{0} \left(\frac{\partial c}{\partial v^*}\right)_t dv^* + \int_{0}^{v^*_{pos}} \left(\frac{\partial c}{\partial v^*}\right)_t dv^* = c_{0+} + \int_{0}^{v^*_{pos}} \left(\frac{\partial c}{\partial v^*}\right)_t dv^*,$$

(126b)

where, at time t, c_{-x} is equal to c corresponding to v*in the limit as v^*_{-x} is approached from above, and c_{0+} is equal to c corresponding to v*in the limit as 0 is approached from above. The offsets, c_{-x} and c_{0+}, should be equal.

Experimentally obtained data can be complicated by optical artefacts near ξ_m and ξ_b, as well as by inaccuracies wherever the solute concentration is outside the suitable range of the detection system, and over time, unsuitably high solute concentrations are likely to develop toward ξ_m or ξ_b. Outside of some well behaved simulations, then, when using Equation 126, the practical range of v* will not extend to either of the theoretical extrema, v^*_{-x} or v^*_{+x}. In general, to accommodate such limitations, the offset of Equation 126a will equal c corresponding to v*in the limit as its lowest practical negative value is approached from above, and the offset of Equation 126b will equal c corresponding to v*in the limit as its lowest practical positive value is approached from above.

The cumulative distribution function,

$$G(v^*) = \int_{v^*_{-x}}^{v^*} |g(\beta^*)| d\beta^*,$$

(127)

permits Equation 123 to be rewritten as $\Delta c = G(v^*_{above}) - G(v^*_{below})$. The cumulative distribution function is a measure of the concentration of all solutes for which the apparent electrophoretic velocity coefficient is less than or equal to v*, but greater than or equal to v^*_{-x} at some specific time. Nonzero diffusion coefficients and concentration-dependent transport render G(v*) at least somewhat dependent on time. Overlapping boundaries of oppositely directed solutes can render G(v*) highly dependent on time.

The step function that describes c_{v^*}

As previously discussed, at any given time, the sum of an infinite number of step functions can be used to describe the total solute concentration at all spatial positions. (Regions of supernatant and pellet accumulation can be included in such an approach, even though such regions are likely to be excluded in any g(v*) analysis.) At a given time, t, at a given spatial position, ξ, c_{v^*} (Equation 116), the concentration of a hypothetical solute characterised by v*, can be expressed as

$$c_{v^*} = \begin{Bmatrix} c_{p,v}[1 - H(\xi - \xi_{v^*})] \; for \; v^* \leq 0 \\ c_{p,v^*} H(\xi - \xi_{v^*}) \; for \; v^* \geq 0 \end{Bmatrix},$$

(128)

where

$$H(\xi - \xi_{v^*}) = \begin{Bmatrix} 1 \; for \; \xi - \xi_{v^*} \geq 0 \\ 0 \; for \; \xi - \xi_{v^*} < 0 \end{Bmatrix}$$

(129)

is the Heaviside step function as it applies to $\xi - \xi_{v^*}$. At time t, ξ_{v^*} is the boundary position of a hypothetical solute characterised by v* in the zero diffusion limit, and that boundary position is characterised by a hyper-sharp change in the solute concentration, c_{v^*}, from 0 to its plateau value, c_{p,v^*}. As c_{p,v^*} is time-independent (Equations 110 and 116), from t_0 on, $c_{p,v^*} = c_{0,v^*}$ at all ξ where c_{v^*} does not equal zero. Due to the time dependence of ξ_{v^*} (Equation 115), however, c_{v^*} (Equation 116) is time-dependent.

The sum of all c_{v^*} at a given spatial position and time is equal to c at that position and time. As v* is continuous within $v^*_{-x} \leq v^* \leq v^*_{+x}$ (Equations 124 and 125), there is an infinite number of c_{v^*} values at a given position and time. There are also two oppositely directed hypothetical solutes that would each exhibit the same boundary position, ξ_{v^*}, at time t. At a given time, t, such solutes are related through

$$\xi_{v^*} = \begin{Bmatrix} \xi_{v^*_-} = \xi_b + v^*_- t \\ \xi_{v^*_+} = \xi_m + v^*_+ t \end{Bmatrix},$$

(130)

where the negatively directed hypothetical solute is characterised by

$$v^*_- = \frac{\xi_{v^*_-} - \xi_b}{t} < 0,$$

(131)

the positively directed hypothetical solute is characterised by

$$v^*_+ = \frac{\xi_{v^*_+} - \xi_m}{t} > 0,$$

(132)

and the difference between the two v* values for which $\xi_{v^*_+} = \xi_{v^*_-} = \xi_{v^*}$ is

$$\Delta v_{\pm}^{*} = v_{+}^{*} - v_{-}^{*} = \frac{\left(\xi_{v_{+}^{*}} - \xi_{v_{-}^{*}}\right) + (\xi_b - \xi_m)}{t} = \frac{\xi_b - \xi_m}{t}.$$

(133)

(The equation describing $\Delta v_{\pm}^{*}$ can also be obtained by equating the two expressions for ξ_{v^*} in Equation 130, and solving for $v_{+}^{*} - v_{-}^{*}$.)

As $\left(\xi_{v_{-}^{*}} - \xi_b\right)$ and $\left(\xi_{v_{+}^{*}} - \xi_m\right)$ are proportional to t, v_{-}^{*} and v_{+}^{*} are time-independent. As $(\xi_b - \xi_m)$ is a constant, $\Delta v_{\pm}^{*}$ is inversely proportional to t. At any given time, then, $\left(\frac{\partial v_{-}^{*}}{\partial t}\right)_{\xi} = 0$ and $\left(\frac{\partial v_{+}^{*}}{\partial t}\right)_{\xi} = 0$, but $\left(\frac{\partial \Delta v_{\pm}^{*}}{\partial t}\right)_{\xi} = -\frac{\Delta v_{\pm}^{*}}{t}$. Any derivatives of v_{+}^{*}, v_{-}^{*} or $\Delta v_{\pm}^{*}$ at constant t are equal to zero.

Given Equations 131 and 132, which describe the two oppositely signed v* values, v_{-}^{*} and v_{+}^{*}, that characterise the two hypothetical solutes with oppositely directed boundaries at $\xi_{s_{+}^{*}} = \xi_{s_{-}^{*}} = \xi_{v^*}$ at time t, Equation 128 can be rewritten as

$$c_{v^*} = \begin{Bmatrix} c_{v_{-}^{*}} \\ c_{v_{+}^{*}} \end{Bmatrix} = \begin{Bmatrix} c_{p,v_{-}^{*}}\left[1 - H\left(\xi - \xi_{v_{-}^{*}}\right)\right] \\ c_{p,v_{+}^{*}} H\left(\xi - \xi_{v_{+}^{*}}\right) \end{Bmatrix} = \begin{Bmatrix} c_{p,v_{-}^{*}}[1 - H(\xi - [\xi_b + v_{-}^{*} t])] \\ c_{p,v_{+}^{*}} H(\xi - [\xi_m + v_{+}^{*} t]) \end{Bmatrix},$$

(134)

where, at any given time, $c_{v_{-}^{*}}$ is the ξ-dependent concentration and $c_{p,v_{-}^{*}}$ is the ξ-independent plateau concentration of the hypothetical solute characterised by v_{-}^{*}, while $c_{v_{+}^{*}}$ is the ξ-dependent concentration and $c_{p,v_{+}^{*}}$ is the ξ-independent plateau concentration of the hypothetical solute characterised by v_{+}^{*}. As $c_{p,v_{-}^{*}}$ and $c_{p,v_{+}^{*}}$ are t-independent, $c_{p,v_{-}^{*}} = c_{0,v_{-}^{*}}$ and $c_{p,v_{+}^{*}} = c_{0,v_{+}^{*}}$ at all times. Nevertheless, $c_{v_{-}^{*}}$ and $c_{v_{+}^{*}}$ are t-dependent by virtue of the t-dependence of $\xi_{v_{-}^{*}}$ and $\xi_{v_{+}^{*}}$, respectively.

At a given spatial position, ξ, at a given time, t, the sum of all c_{v^*} as described by Equation 134 is equal to

$$c = \int_{c_{v_-^*=v_{-x}^*}}^{c_{v_-^*=0}} dc_{v_-^*} + \int_{c_{v_+^*=0}}^{c_{v_+^*=v_{+x}^*}} dc_{v_+^*}$$

$$= \int_{c_{v_-^*=v_{-x}^*}}^{c_{v_-^*=0}} [1 - H(\xi - [\xi_b + v_-^* t])] dc_{p,v_-^*} + \int_{c_{v_+^*=0}}^{c_{v_+^*=v_{+x}^*}} H(\xi - [\xi_m + v_+^* t]) dc_{p,v_+^*}$$

(135a)

in the continuous case, and

$$c = \sum_{v_-^*=v_{-x}^*}^{0} c_{v_-^*} + \sum_{v_+^*=0}^{v_{+x}^*} c_{v_+^*} = \sum_{v_-^*=v_{-x}^*}^{0} c_{p,v_-^*}[1 - H(\xi - [\xi_b + v_-^* t])] + \sum_{v_+^*=0}^{v_{+x}^*} c_{p,v_+^*} H(\xi - [\xi_m + v_+^* t])$$

(135b)

in the discrete case.

If Equation 135 were used to differentiate c with respect to v* at constant t, or if Equation 102 were applied to Equation 135, only the essential values of $\left(\frac{\partial c}{\partial v^*}\right)_t$ would be obtained. To obtain the redundant values of $\left(\frac{\partial c}{\partial v^*}\right)_t$ from c described as a function of ξ and t, the step functions in Equation 134 must be written in terms of the v* values at which $\left(\frac{\partial c}{\partial v^*}\right)_t$ would be redundant. Doing so results in

$$c_{v^*} = \begin{Bmatrix} c_{v_-^*} \\ c_{v_+^*} \end{Bmatrix} = \begin{Bmatrix} c_{p,v_-^*}\left[1 - H\left(\xi - \xi_{v_-^*}\right)\right] \\ c_{p,v_+^*} H\left(\xi - \xi_{v_+^*}\right) \end{Bmatrix} = \begin{Bmatrix} c_{p,v_-^*}\left[1 - H\left(\xi - \left[\xi_m + \left\{v_-^* + \Delta v_\pm^*\right\} t\right]\right)\right] \\ c_{p,v_+^*} H\left(\xi - \left[\xi_b + \left\{v_+^* - \Delta v_\pm^*\right\} t\right]\right) \end{Bmatrix}.$$

(136)

At a given spatial position, ξ, at a given time, t, the sum of all c_{v^*} as described by Equation 136 is

$$c = \int_{c_{v_-^*=v_{-x}^*}}^{c_{v_-^*=0}} dc_{v_-^*} + \int_{c_{v_+^*=0}}^{c_{v_+^*=v_{+x}^*}} dc_{v_+^*}$$

$$= \int_{c_{v_-^*=v_{-x}^*}}^{c_{v_-^*=0}} \left[1 - H\left(\xi - \left[\xi_m + \left\{v_-^* + \Delta v_\pm^*\right\}t\right]\right)\right] dc_{p,v_-^*}$$

$$+ \int_{c_{v_+^*=0}}^{c_{v_+^*=v_{+x}^*}} H\left(\xi - \left[\xi_b + \left\{v_+^* - \Delta v_\pm^*\right\}t\right]\right) dc_{p,v_+^*}$$

(137a)

in the continuous case, and

$$c = \sum_{v_-^*=v_{-x}^*}^{0} c_{v_-^*} + \sum_{v_+^*=0}^{v_{+x}^*} c_{v_+^*}$$

$$= \sum_{v_-^*=v_{-x}^*}^{0} c_{p,v_-^*}\left[1 - H\left(\xi - \left[\xi_m + \left\{v_-^* + \Delta v_\pm^*\right\}t\right]\right)\right]$$

$$+ \sum_{v_+^*=0}^{v_{+x}^*} c_{p,v_+^*} H\left(\xi - \left[\xi_b + \left\{v_+^* - \Delta v_\pm^*\right\}t\right]\right)$$

(137b)

in the discrete case.

Equations 135 and 137 both describe c as a function of ξ and t, and either can be used to determine $\left(\frac{\partial c}{\partial \xi}\right)_t$, but both are needed to determine $\left(\frac{\partial c}{\partial v^*}\right)_t$. The two expressions for $\left(\frac{\partial c}{\partial \xi}\right)_t$ will be obtained first, and to obtain $\left(\frac{\partial c}{\partial v^*}\right)_t$, Equation 102 will then be applied to both expressions for $\left(\frac{\partial c}{\partial \xi}\right)_t$.

While c_{v^*} depends on ξ and t, c_{p,v^*} is time-independent and equal to c_{0,v^*} at all $\xi > \xi_0 + v^*t$ (Equation 118). Thus, in general, $\left(\frac{\partial c_{p,v^*}}{\partial \xi}\right)_t = 0$ and $\left(\frac{\partial c_{p,v^*}}{\partial t}\right)_\xi = 0$.

As $c_{p,v_-^*} = c_{0,v_-^*}$ at all ξ where $c_{v_-^*}$ does not equal zero, and $c_{p,v_+^*} = c_{0,v_+^*}$ at all ξ where $c_{v_+^*}$ does not equal zero, $\left(\frac{\partial c_{p,v_+^*}}{\partial \xi}\right)_t = 0$ and $\left(\frac{\partial c_{p,v_-^*}}{\partial \xi}\right)_t = 0$. Thus, differentiating c with respect to ξ at constant t yields, using the discrete form of Equation 135 to express c,

$$\left(\frac{\partial c}{\partial \xi}\right)_t = \sum_{v_-^* = v_{-x}^*}^{0} \left(\frac{\partial c_{v_-^*}}{\partial \xi}\right)_t + \sum_{v_+^* = 0}^{s_{+x}^*} \left(\frac{\partial c_{v_+^*}}{\partial \xi}\right)_t = \left(\frac{\partial c_{v^*}}{\partial \xi}\right)_t = \begin{Bmatrix} \left(\frac{\partial c_{v_-^*}}{\partial \xi}\right)_t \\ \left(\frac{\partial c_{v_+^*}}{\partial \xi}\right)_t \end{Bmatrix} = \begin{Bmatrix} -c_{p,v_-^*}\delta\left(\xi - \xi_{v_-^*}\right) \\ c_{p,v_+^*}\delta\left(\xi - \xi_{v_+^*}\right) \end{Bmatrix}$$

$$= \begin{Bmatrix} -c_{p,v_-^*}\delta(\xi - [\xi_b + v_-^* t]) \\ c_{p,v_+^*}\delta(\xi - [\xi_m + v_+^* t]) \end{Bmatrix},$$

(138a)

or, using the discrete form of Equation 137 to express c,

$$\left(\frac{\partial c}{\partial \xi}\right)_t = \sum_{v_-^* = v_{-x}^*}^{0} \left(\frac{\partial c_{v_-^*}}{\partial \xi}\right)_t + \sum_{v_+^* = 0}^{v_{+x}^*} \left(\frac{\partial c_{v_+^*}}{\partial \xi}\right)_t = \left(\frac{\partial c_{v^*}}{\partial \xi}\right)_t = \begin{Bmatrix} \left(\frac{\partial c_{v_-^*}}{\partial \xi}\right)_t \\ \left(\frac{\partial c_{v_+^*}}{\partial \xi}\right)_t \end{Bmatrix} = \begin{Bmatrix} -c_{p,v_-^*}\delta\left(\xi - \xi_{v_-^*}\right) \\ c_{p,v_+^*}\delta\left(\xi - \xi_{v_+^*}\right) \end{Bmatrix}$$

$$= \begin{Bmatrix} -c_{p,v_-^*}\delta\left(\xi - \left[\xi_m + \left\{v_-^* + \Delta v_\pm^*\right\}t\right]\right) \\ c_{p,v_+^*}\delta\left(\xi - \left[\xi_b + \left\{v_+^* - \Delta v_\pm^*\right\}t\right]\right) \end{Bmatrix},$$

(138b)

where, in either case, for $\xi_{v^*} = \xi_{v_+^*}$ or $\xi_{v^*} = \xi_{v_-^*}$,

$$\delta(\xi - \xi_{v^*}) = \left(\frac{\partial H(\xi - \xi_{v^*})}{\partial \xi}\right)_t = \begin{Bmatrix} \infty \; for \; \xi - \xi_{v^*} = 0 \\ 0 \; for \; \xi - \xi_{v^*} \neq 0 \end{Bmatrix}$$

(139)

is the Dirac delta function as it applies to $\xi - \xi_{v^*}$. The sum of all $\left(\frac{\partial c_{v^*}}{\partial \xi}\right)_t$ at a given spatial position and time is equal to $\left(\frac{\partial c}{\partial \xi}\right)_t$ at that position and time, and as with c_{v^*}, there is an infinite number of $\left(\frac{\partial c_{v^*}}{\partial \xi}\right)_t$ values at a given spatial position and time. However, as $\delta(\xi - \xi_{v^*}) = 0$ except where $\xi = \xi_{v^*}$,

at any time t, and at any position ξ, $\left(\frac{\partial c}{\partial \xi}\right)_t$ is equal to just the two nonzero values of $\left(\frac{\partial c_{v^*}}{\partial \xi}\right)_t$ for which $\xi = \xi_{v^*}$, those being $\left(\frac{\partial c_{v_-^*}}{\partial \xi}\right)_t$ and $\left(\frac{\partial c_{v_+^*}}{\partial \xi}\right)_t$. Hence, starting with either form of Equations 135 or 137, $\left(\frac{\partial c}{\partial \xi}\right)_t$ yields neither a summation nor an integral.

Calculating $\left(\frac{\partial c}{\partial v^*}\right)_t$ *from* $\left(\frac{\partial c}{\partial \xi}\right)_t$

Applying Equation 102 to the sum of both results given by Equation 138 yields

$$\left(\frac{\partial c}{\partial v^*}\right)_t = \left(\frac{\partial c}{\partial \xi}\right)_t \left(\frac{\partial \xi}{\partial v^*}\right)_t = \left(\frac{\partial c_{v^*}}{\partial \xi}\right)_t t = \begin{Bmatrix} \left(\frac{\partial c_{v_-^*}}{\partial \xi}\right)_t t \\ \left(\frac{\partial c_{v_+^*}}{\partial \xi}\right)_t t \end{Bmatrix} = \begin{Bmatrix} -c_{p,v_-^*}\delta\left(\xi - \xi_{v_-^*}\right)t \\ c_{p,v_+^*}\delta\left(\xi - \xi_{v_+^*}\right)t \end{Bmatrix}$$

$$= \begin{Bmatrix} -c_{p,v_-^*}\left[\delta(\xi - [\xi_b + v_-^* t]) + \delta\left(\xi - \left[\xi_m + \left\{v_-^* + \Delta v_\pm^*\right\}t\right]\right)\right]t \\ c_{p,v_+^*}\left[\delta(\xi - [\xi_m + v_+^* t]) + \delta\left(\xi - \left[\xi_b + \left\{v_+^* - \Delta v_\pm^*\right\}t\right]\right)\right]t \end{Bmatrix}$$

$$= \begin{Bmatrix} -c_{0,v_-^*}\delta(\xi - [\xi_b + v_-^* t])t - c_{0,v_-^*}\delta\left(\xi - \left[\xi_m + \left\{v_-^* + \Delta v_\pm^*\right\}t\right]\right)t \\ c_{0,v_+^*}\delta(\xi - [\xi_m + v_+^* t])t + c_{0,v_+^*}\delta\left(\xi - \left[\xi_b + \left\{v_+^* - \Delta v_\pm^*\right\}t\right]\right)t \end{Bmatrix},$$

(140)

where use has been made of the fact that $c_{p,v_-^*} = c_{0,v_-^*}$ and $c_{p,v_+^*} = c_{0,v_+^*}$.

The properties of the Dirac delta function are such that

$$\delta(v^* - \beta^*) = \left(\frac{\partial H(v^* - \beta^*)}{\partial v^*}\right)_t = \left(\frac{\partial H(\xi - \xi_v)}{\partial \xi}\right)_t \left(\frac{\partial \xi}{\partial v^*}\right)_t = \delta(\xi - \xi_v)t.$$

(141)

As applied to c and $\left(\frac{\partial c}{\partial v^*}\right)_t$, in both the Heaviside step function, H(v* – β*), and its Dirac delta function, δ(v* – β*), β* will be shown (Equations 146 and 149) to be one of the two values, v_+^*

and v_-^*, that characterise the two hypothetical solutes with oppositely directed boundaries at $\xi_{s_+^*}$ $= \xi_{s_-^*} = \xi_{v^*}$ at time t (Equation 130). Thus, in Equation 140,

$$-c_{0,v_-^*}\delta(\xi - [\xi_b + v_-^* t])t = -c_{0,v_-^*}\delta(v^* - v_-^*) = q(v_-^*, t)\,,$$

(142)

$$c_{0,v_+^*}\delta(\xi - [\xi_m + v_+^* t])t = c_{0,v_+^*}\delta(v^* - v_+^*) = q(v_+^*, t),$$

(143)

$$-c_{0,v_-^*}\delta\big(\xi - \big[\xi_m + \{v_-^* + \Delta v_\pm^*\}t\big]\big)t = -c_{0,v_-^*}\delta\big(v^* - \{v_-^* + \Delta v_\pm^*\}\big) = e(v_-^*, t)$$

(144)

and

$$c_{0,v_+^*}\delta\big(\xi - \big[\xi_b + \{v_+^* - \Delta v_\pm^*\}t\big]\big)t = c_{0,v_+^*}\delta\big(v^* - \{v_+^* - \Delta v_\pm^*\}\big) = e(v_+^*, t).$$

(145)

In Equation 144, $\{v_-^* + \Delta v_\pm^*\}$ is equal to the value of v_+^* that shares ξ_{v^*} in common with v_-^*, such that $\xi_{v^*} = \xi_m + \{v_-^* + \Delta v_\pm^*\}t = \xi_b + v_-^* t$. In Equation 145, $\{v_+^* - \Delta v_\pm^*\}$ is equal to the value of v_-^* that shares ξ_{v^*} in common with v_+^*, such that $\xi_{v^*} = \xi_b + \{v_+^* - \Delta v_\pm^*\}t = \xi_m + v_+^* t$.

The step-function form of c as a function of v and t*

For c expressed as a function of v* and t, c_{v^*} is the concentration of a hypothetical solute characterised by v*. In transforming the independent variables from ξ and t to v* and t, c at each spatial position ξ becomes equal to c at the two corresponding values of v* given by Equation 119. At any given time, for c expressed as a function of v* and t, $c_{v_-^*}$ is the v*-dependent concentration and c_{p,v_-^*} is the plateau concentration of the hypothetical solute characterised by v_-^*, while $c_{v_+^*}$ is the v*-dependent concentration and c_{p,v_+^*} is the plateau concentration of the

hypothetical solute characterised by v_+^*. As c_{p,v_-^*} and c_{p,v_+^*} are t-independent, $c_{p,v_-^*} = c_{0,v_-^*}$ and $c_{p,v_+^*} = c_{0,v_+^*}$ at all times. Nevertheless, $c_{v_-^*}$ and $c_{v_+^*}$, as they appear in the equation describing c as a function of v* and t (Equation 146), are t-dependent by virtue of the t-dependence of v* (Equation 119) and $\Delta v_\pm^*$ (Equation 133).

At a given apparent electrophoretic velocity coefficient, v*, at a given time, t, the sum of all c_{v^*} is equal to

$$c = \int_{c_{v_-^*=v_{-x}^*}}^{c_{v_-^*=0}} dc_{v_-^*} + \int_{c_{v_+^*=0}}^{c_{v_+^*=v_{+x}^*}} dc_{v_+^*}$$

$$= \int_{c_{v_-^*=v_{-x}^*}}^{c_{v_-^*=0}} \left\{[1 - H(v^* - v_-^*)] + \left[1 - H\left(v^* - \left\{v_-^* + \Delta v_\pm^*\right\}\right)\right]\right\} dc_{p,v_-^*}$$

$$+ \int_{c_{v_+^*=0}}^{c_{v_+^*=v_{+x}^*}} \left\{H(v^* - v_+^*) + H\left(v^* - \left\{v_+^* - \Delta v_\pm^*\right\}\right)\right\} dc_{p,v_+^*},$$

(146a)

in the continuous case, and

$$c = \sum_{v_-^*=v_{-x}^*}^{0} c_{v_-^*} + \sum_{v_+^*=0}^{v_{+x}^*} c_{v_+^*}$$

$$= \sum_{v_-^*=v_{-x}^*}^{0} c_{p,v_-^*}\left\{[1 - H(v^* - v_-^*)] + \left[1 - H\left(v^* - \left\{v_-^* + \Delta v_\pm^*\right\}\right)\right]\right\}$$

$$+ \sum_{v_+^*=0}^{v_{+x}^*} c_{p,v_+^*}\left\{H(v^* - v_+^*) + H\left(v^* - \left\{v_+^* - \Delta v_\pm^*\right\}\right)\right\}$$

$$= \sum_{v_-^*=v_{-x}^*}^{0} c_{0,v_-^*}[1 - H(v^* - v_-^*)] + \sum_{v_-^*=v_{-x}^*}^{0} c_{0,v_-^*}\left[1 - H\left(v^* - \left\{v_-^* + \Delta v_\pm^*\right\}\right)\right]$$

$$+ \sum_{v_+^*=0}^{v_{+x}^*} c_{0,v_+^*} H(v^* - v_+^*) + \sum_{v_+^*=0}^{v_{+x}^*} c_{0,v_+^*} H\left(v^* - \left\{v_+^* - \Delta v_\pm^*\right\}\right),$$

(146b)

in the discrete case. The value of v_+^* that shares ξ_{v^*} in common with v_-^* has been expressed as $\left\{v_-^* + \Delta v_\pm^*\right\}$ in the integral with respect to $c_{v_-^*}$ or the sum over all v_-^*. The value of v_-^* that shares ξ_{v^*} in common with v_+^* has been expressed as $\left\{v_+^* - \Delta v_\pm^*\right\}$ in the integral with respect to $c_{v_+^*}$ or the sum over all v_+^*. The integrals or sums in which [1 – H(v* – $\{v_-^* + \Delta v_\pm^*\}$)] and H(v* – $\{v_+^* - \Delta v_\pm^*\}$) appear will give rise to the redundant values of $\left(\frac{\partial c}{\partial v^*}\right)_t$, while the integrals or sums in which [1 – H(v* – v_-^*)] and H(v* – v_+^*) appear will give rise to the essential values of $\left(\frac{\partial c}{\partial v^*}\right)_t$.

The Heaviside step functions in Equation 146 are described by

$$H(v^* - \beta^*) = \begin{Bmatrix} 1\ for\ v^* - \beta^* \geq 0 \\ 0\ for v^* - \beta^* < 0 \end{Bmatrix},$$

(147)

where β* may equal v_-^*, $\left\{v_-^* + \Delta v_\pm^*\right\}$, v_+^* or $\left\{v_-^* - \Delta v_\pm^*\right\}$. The corresponding Dirac delta function is

given by

$$\left(\frac{\partial H(v^*-\beta^*)}{\partial v^*}\right)_t\left(\frac{\partial (v^*-\beta^*)}{\partial v^*}\right)_t=\left(\frac{\partial H(v^*-\beta^*)}{\partial v^*}\right)_t\left[\left(\frac{\partial v^*}{\partial v^*}\right)_t-\left(\frac{\partial \beta^*}{\partial v^*}\right)_t\right]=\left(\frac{\partial H(v^*-\beta^*)}{\partial v^*}\right)_t$$

$$=\delta(v^*-\beta^*)=\begin{Bmatrix}\infty\, for\, v^*-\beta^*=0\\ 0\, for v^*-\beta^*\neq 0\end{Bmatrix},$$

(148)

where $\left(\frac{\partial v^*}{\partial v^*}\right)_t=1$ and, for β* equal to v_-^*, $\{v_-^*+\Delta v_\pm^*\}$, v_+^* or $\{v_+^*-\Delta v_\pm^*\}$, $\left(\frac{\partial \beta^*}{\partial v^*}\right)_t=0$. The relationship of δ(v* - β*) to δ(ξ - ξ_{v^*}), is described by Equation 141.

Applying Equation 102 to $\left(\frac{\partial c_{p,v_-^*}}{\partial \xi}\right)_t=\left(\frac{\partial c_{0,v_-^*}}{\partial \xi}\right)_t=0$ and $\left(\frac{\partial c_{p,v_+^*}}{\partial \xi}\right)_t=\left(\frac{\partial c_{0,v_+^*}}{\partial \xi}\right)_t=0$ yields $\left(\frac{\partial c_{p,v_-^*}}{\partial v^*}\right)_t=\left(\frac{\partial c_{p,v_-^*}}{\partial \xi}\right)_t\left(\frac{\partial \xi}{\partial v^*}\right)_t=0$ and $\left(\frac{\partial c_{p,v_+^*}}{\partial v^*}\right)_t=\left(\frac{\partial c_{p,v_+^*}}{\partial \xi}\right)_t\left(\frac{\partial \xi}{\partial v^*}\right)_t=0$, respectively. Thus, using the discrete form of Equation 146 to express c,

$$\left(\frac{\partial c}{\partial v^*}\right)_t=\sum_{v_-^*=v_{-x}^*}^{0}\left(\frac{\partial c_{v_-^*}}{\partial v^*}\right)_t+\sum_{v_+^*=0}^{v_{+x}^*}\left(\frac{\partial c_{v_+^*}}{\partial v^*}\right)_t=\left(\frac{\partial c_{v^*}}{\partial v^*}\right)_t=\begin{Bmatrix}\left(\frac{\partial c_{v_-^*}}{\partial v^*}\right)_t\\ \left(\frac{\partial c_{v_+^*}}{\partial v^*}\right)_t\end{Bmatrix}$$

$$=\begin{Bmatrix}-c_{p,v_-^*}\left[\delta(v^*-v_-^*)+\delta\left(v^*-\{v_-^*+\Delta v_\pm^*\}\right)\right]\\ c_{p,v_+^*}\left[\delta(v^*-v_+^*)+\delta\left(v^*-\{v_+^*-\Delta v_\pm^*\}\right)\right]\end{Bmatrix}$$

$$=\begin{Bmatrix}-c_{0,v_-^*}\delta(v^*-v_-^*)-c_{0,v_-^*}\delta\left(v^*-\{v_-^*+\Delta v_\pm^*\}\right)\\ c_{0,v_+^*}\delta(v^*-v_+^*)+c_{0,v_+^*}\delta\left(v^*-\{v_+^*-\Delta v_\pm^*\}\right)\end{Bmatrix}=\begin{Bmatrix}q(v_-^*,t)+e(v_-^*,t)\\ q(v_+^*,t)+e(v_+^*,t)\end{Bmatrix}$$

$$=q(v^*,t)+e(v^*,t),$$

(149)

where $q(v_-^*,t)=-c_{0,v_-^*}\delta(v^*-v_-^*)$, $q(v_+^*,t)=c_{0,v_+^*}\delta(v^*-v_+^*)$, $e(v_-^*,t)=-c_{0,v_-^*}\delta\left(v^*-\{v_-^*+\Delta v_\pm^*\}\right)$ and $e(v_+^*,t)=c_{0,v_+^*}\delta\left(v^*-\{v_+^*-\Delta v_\pm^*\}\right)$. Equations 126 and 146 both describe c as a function of v* and t. Equation 149 describes the integrand of Equation 126.

Back-calculating $\left(\frac{\partial c}{\partial \xi}\right)_t$ *from* $\left(\frac{\partial c}{\partial v^*}\right)_t$

Applying Equations 102 and 120 to Equation 149, and using Equations 119, 131, 132 and 133 to express v*, v_-^*, v_+^* and $\Delta v_\pm^*$, respectively, in terms of t, ξ, ξ_b and ξ_m, yields

$$\left(\frac{\partial c}{\partial v^*}\right)_t = \left(\frac{\partial c}{\partial v^*}\right)_t \left(\frac{\partial v^*}{\partial \xi}\right)_t = \left(\frac{\partial c_{v^*}}{\partial v^*}\right)_t \frac{1}{t} = \begin{Bmatrix} \left(\frac{\partial c_{v_-^*}}{\partial v^*}\right)_t \frac{1}{t} \\ \left(\frac{\partial c_{v_+^*}}{\partial v^*}\right)_t \frac{1}{t} \end{Bmatrix}$$

$$= \begin{Bmatrix} -\frac{c_{0,v_-^*}}{t}\left[\delta(v^* - v_-^*) + \delta\left(v^* - \left\{v_-^* + \Delta v_\pm^*\right\}\right)\right] \\ \frac{c_{0,v_+^*}}{t}\left[\delta(v^* - v_+^*) + \delta\left(v^* - \left\{v_+^* - \Delta v_\pm^*\right\}\right)\right] \end{Bmatrix}$$

$$= \begin{Bmatrix} -\frac{c_{0,v_-^*}}{t}\left[\delta\left(\frac{\xi - \xi_b}{t} - \frac{\xi_{v_-^*} - \xi_b}{t}\right) + \delta\left(\frac{\xi - \xi_m}{t} - \left\{\frac{\xi_{v_-^*} - \xi_b}{t} + \frac{\xi_b - \xi_m}{t}\right\}\right)\right] \\ \frac{c_{0,v_+^*}}{t}\left[\delta\left(\frac{\xi - \xi_m}{t} - \frac{\xi_{v_+^*} - \xi_m}{t}\right) + \delta\left(\frac{\xi - \xi_b}{t} - \left\{\frac{\xi_{v_+^*} - \xi_m}{t} - \frac{\xi_b - \xi_m}{t}\right\}\right)\right] \end{Bmatrix}$$

$$= \begin{Bmatrix} -\frac{c_{0,v_-^*}}{t}\left[\delta\left(\frac{\xi - \xi_b}{t} - \frac{\xi_{v_-^*} - \xi_b}{t}\right) + \delta\left(\frac{\xi - \xi_m}{t} - \frac{\xi_{v_-^*} - \xi_m}{t}\right)\right] \\ \frac{c_{0,v_+^*}}{t}\left[\delta\left(\frac{\xi - \xi_m}{t} - \frac{\xi_{v_+^*} - \xi_m}{t}\right) + \delta\left(\frac{\xi - \xi_b}{t} - \frac{\xi_{v_+^*} - \xi_b}{t}\right)\right] \end{Bmatrix}$$

$$= \begin{Bmatrix} -\frac{c_{0,v_-^*}}{t}\left[\delta\left(\frac{\xi - \xi_{v_-^*}}{t}\right) + \delta\left(\frac{\xi - \xi_{v_-^*}}{t}\right)\right] \\ \frac{c_{0,v_+^*}}{t}\left[\delta\left(\frac{\xi - \xi_{v_+^*}}{t}\right) + \delta\left(\frac{\xi - \xi_{v_+^*}}{t}\right)\right] \end{Bmatrix} = \begin{Bmatrix} \frac{q(v_-^*, t)}{t} + \frac{e(v_-^*, t)}{t} \\ \frac{q(v_+^*, t)}{t} + \frac{e(v_+^*, t)}{t} \end{Bmatrix},$$

(150)

where, when expressing v* in terms of t, ξ and ξ_0, ξ_0 is equated to the only one if its two possible values, ξ_m or ξ_b, that can yield a nonzero result for the Dirac delta function in which it appears. The entire exercise is somewhat futile, however, as once v*, v_-^*, v_+^* and $\Delta v_\pm^*$ are expressed in

terms of t, ξ, ξ_b and ξ_m, information by which q(v_-^*,t) can be distinguished from e(v_-^*,t), or q(v_+^*,t) can be distinguished from e(v_+^*,t), is lost upon simplification.

Expressing $\left(\frac{\partial c}{\partial t}\right)_{v^*}$ *and* $\left(\frac{\partial c}{\partial t}\right)_{\xi}$ *in terms of step functions*

Differentiating c with respect to t at constant ξ yields, using the discrete form of Equation 146 to express c,

$$\left(\frac{\partial c}{\partial t}\right)_{\xi} = \sum_{v_-^*=v_{-x}^*}^{0} \left(\frac{\partial c_{v_-^*}}{\partial t}\right)_{\xi} + \sum_{v_+^*=0}^{v_{+x}^*} \left(\frac{\partial c_{v_+^*}}{\partial t}\right)_{\xi}$$

$$= \sum_{v_-^*=v_{-x}^*}^{0} \left(\begin{array}{l} \left(\frac{\partial c_{0,s_-^*}}{\partial t}\right)_{\xi} \left\{[1 - H(v^* - v_-^*)] + \left[1 - H\left(v^* - \left\{v_-^* + \Delta v_{\pm}^*\right\}\right)\right]\right\} + \\ c_{0,s_+^*} \left(\frac{\partial \left\{[1 - H(v^* - v_-^*)] + \left[1 - H\left(v^* - \left\{v_-^* + \Delta v_{\pm}^*\right\}\right)\right]\right\}}{\partial t}\right)_{\xi} \end{array} \right)$$

$$+ \sum_{v_+^*=0}^{v_{+x}^*} \left(\begin{array}{l} \left(\frac{\partial c_{0,s_+^*}}{\partial t}\right)_{\xi} \left\{H(v^* - v_+^*) + H\left(v^* - \left\{v_+^* - \Delta v_{\pm}^*\right\}\right)\right\} + \\ c_{0,s_+^*} \left(\frac{\partial \left\{H(v^* - v_+^*) + H\left(v^* - \left\{v_+^* - \Delta v_{\pm}^*\right\}\right)\right\}}{\partial t}\right)_{\xi} \end{array} \right)$$

$$= c_{0,s_-^*} \frac{v_-^*}{t} \left[\delta(v^* - v_-^*) + \delta\left(v^* - \left\{v_-^* + \Delta v_{\pm}^*\right\}\right)\right]$$

$$- c_{0,s_+^*} \frac{v_+^*}{t} \left[\delta(v^* - v_+^*) + \delta\left(v^* - \left\{v_+^* - \Delta v_{\pm}^*\right\}\right)\right].$$

(151)

Equations 152 to 157, which follow, describe all the individual terms used to determine $\left(\frac{\partial c}{\partial t}\right)_{\xi}$.

At constant ξ, the time-derivatives of the Heaviside step functions of Equation 146 are given by

$$\left(\frac{\partial H(v^*-\beta^*)}{\partial t}\right)_\xi = \left(\frac{\partial H(v^*-\beta^*)}{\partial v^*}\right)_\xi \left(\frac{\partial (v^*-\beta^*)}{\partial t}\right)_\xi = \delta(v^*-\beta^*)\left[\left(\frac{\partial v^*}{\partial t}\right)_\xi - \left(\frac{\partial \beta^*}{\partial t}\right)_\xi\right]$$

$$= \delta(v^*-\beta^*)\left[\left(-\frac{v^*}{t}\right) - \left(\frac{\partial \beta^*}{\partial t}\right)_\xi\right] = -\delta(v^*-\beta^*)\left[\frac{v^*}{t} + \left(\frac{\partial \beta^*}{\partial t}\right)_\xi\right]$$

$$= -\delta(v^*-\beta^*)\left[\frac{\beta^*}{t} + \left(\frac{\partial \beta^*}{\partial t}\right)_\xi\right]$$

(152)

where $\left(\frac{\partial v^*}{\partial t}\right)_\xi$ is equal to the inverse of Equation 121, and where δ(v* – β*)v* can be equated to δ(v* - β*)β* on the basis of δ(v* – β*) being equal to zero for all v* ≠ β*. As in Equation 147, β* may equal v_-^*, $\{v_-^* + \Delta v_\pm^*\}$, v_+^* or $\{v_+^* - \Delta v_\pm^*\}$.

As v_-^* (Equation 131) and v_+^* (Equation 132) are time-independent, where β* equals v_-^* or v_+^*, $\left(\frac{\partial v^*}{\partial t}\right)_\xi = 0$. As $\Delta v_\pm^*$ (Equation 133) is equal to a constant divided by t, however,

$$\left(\frac{\partial v^*}{\partial t}\right)_\xi = -\frac{\Delta v_\pm^*}{t}.$$

(153)

Thus, where β* equals $\{v_-^* + \Delta v_\pm^*\}$,

$$-\delta(v^*-\beta^*)\left[\frac{\beta^*}{t} + \left(\frac{\partial \beta^*}{\partial t}\right)_\xi\right] = -\delta\left(v^* - \{v_-^* + \Delta v_\pm^*\}\right)\left[\frac{v_-^* + \Delta v_\pm^*}{t} + \left(\frac{\partial \Delta v_\pm^*}{\partial t}\right)_\xi\right]$$
$$= -\delta\left(v^* - \{v_-^* + \Delta v_\pm^*\}\right)\left[\frac{v_-^* + \Delta v_\pm^*}{t} - \frac{\Delta v_\pm^*}{t}\right] = -\delta\left(v^* - \{v_-^* + \Delta v_\pm^*\}\right)\frac{v_-^*}{t}.$$

(154)

Similarly, where β* equals $\{v_+^* - \Delta v_\pm^*\}$,

$$-\delta(v^*-\beta^*)\left[\frac{\beta^*}{t} + \left(\frac{\partial \beta^*}{\partial t}\right)_\xi\right] = -\delta\left(v^* - \{v_+^* - \Delta v_\pm^*\}\right)\left[\frac{v_+^* - \Delta v_\pm^*}{t} - \left(\frac{\partial \Delta v_\pm^*}{\partial t}\right)_\xi\right]$$
$$= -\delta\left(v^* - \{v_+^* - \Delta v_\pm^*\}\right)\left[\frac{v_+^* - \Delta v_\pm^*}{t} + \frac{\Delta v_\pm^*}{t}\right] = -\delta\left(v^* - \{v_+^* - \Delta v_\pm^*\}\right)\frac{v_+^*}{t}.$$

(155)

As c_{0,v_-^*} and c_{0,v_+^*} are time-independent,

$$\left(\frac{\partial c_{0,v_-^*}}{\partial t}\right)_\xi = 0$$

(156)

and

$$\left(\frac{\partial c_{0,v_+^*}}{\partial t}\right)_\xi = 0.$$

(157)

Indirect determination of $\left(\frac{\partial c}{\partial t}\right)_{v^*}$

Incorporating the expressions for $\left(\frac{\partial c}{\partial v^*}\right)_t$ (Equation 149), $\left(\frac{\partial c}{\partial t}\right)_\xi$ (Equation 151) and $\left(\frac{\partial v^*}{\partial t}\right)_\xi$ (the inverse of Equation 121) in Equation 105, and solving for $\left(\frac{\partial c}{\partial t}\right)_{v^*}$, results in

$$\left(\frac{\partial c}{\partial t}\right)_{v^*} = \left(\frac{\partial c}{\partial t}\right)_\xi - \left(\frac{\partial c}{\partial v^*}\right)_t \left(\frac{\partial v^*}{\partial t}\right)_\xi$$

$$= \left\{ c_{0,s_-^*} \frac{v_-^*}{t}\left[\delta(v^* - v_-^*) + \delta\left(v^* - \left\{v_-^* + \Delta v_\pm^*\right\}\right)\right] \right.$$

$$\left. - c_{0,s_+^*} \frac{v_+^*}{t}\left[\delta(v^* - v_+^*) + \delta\left(v^* - \left\{v_+^* - \Delta v_\pm^*\right\}\right)\right] \right\}$$

$$- \begin{Bmatrix} c_{0,v_-^*} \frac{v_-^*}{t}\left[\delta(v^* - v_-^*) + \delta\left(v^* - \left\{v_-^* + \Delta v_\pm^*\right\}\right)\left(1 + \frac{\Delta v_\pm^*}{v_-^*}\right)\right] \\ -c_{0,v_+^*} \frac{v_+^*}{t}\left[\delta(v^* - v_+^*) + \delta\left(v^* - \left\{v_+^* - \Delta v_\pm^*\right\}\right)\left(1 - \frac{\Delta v_\pm^*}{v_+^*}\right)\right] \end{Bmatrix}$$

$$= \begin{Bmatrix} -c_{0,v_-^*} \frac{\Delta v_\pm^*}{t}\delta\left(v^* - \left\{v_-^* + \Delta v_\pm^*\right\}\right) \\ -c_{0,v_+^*} \frac{\Delta v_\pm^*}{t}\delta\left(v^* - \left\{v_+^* - \Delta v_\pm^*\right\}\right) \end{Bmatrix},$$

(158)

where

$$\left(\frac{\partial c}{\partial v^*}\right)_t \left(\frac{\partial v^*}{\partial t}\right)_\xi = \begin{Bmatrix} \left(\frac{\partial c_{v_-^*}}{\partial v^*}\right)_t \left(\frac{\partial v^*}{\partial t}\right)_\xi \\ \left(\frac{\partial c_{v_+^*}}{\partial v^*}\right)_t \left(\frac{\partial v^*}{\partial t}\right)_\xi \end{Bmatrix}$$

$$= \begin{Bmatrix} -c_{0,v_-^*}\left[\delta(v^* - v_-^*)\left(\frac{\partial v^*}{\partial t}\right)_\xi + \delta\left(v^* - \left\{v_-^* + \Delta v_\pm^*\right\}\right)\left(\frac{\partial v^*}{\partial t}\right)_\xi\right] \\ c_{0,v_+^*}\left[\delta(v^* - v_+^*)\left(\frac{\partial v^*}{\partial t}\right)_\xi + \delta\left(v^* - \left\{v_+^* - \Delta v_\pm^*\right\}\right)\left(\frac{\partial v^*}{\partial t}\right)_\xi\right] \end{Bmatrix}$$

$$= \begin{Bmatrix} -c_{0,v_-^*}\left[\delta(v^* - v_-^*)\left(-\frac{v^*}{t}\right) + \delta\left(v^* - \left\{v_-^* + \Delta v_\pm^*\right\}\right)\left(-\frac{v^*}{t}\right)\right] \\ c_{0,v_+^*}\left[\delta(v^* - v_+^*)\left(-\frac{v^*}{t}\right) + \delta\left(v^* - \left\{v_+^* - \Delta v_\pm^*\right\}\right)\left(-\frac{v^*}{t}\right)\right] \end{Bmatrix}$$

$$= \begin{Bmatrix} c_{0,v_-^*}\frac{1}{t}\left[\delta(v^* - v_-^*)v^* + \delta\left(v^* - \left\{v_-^* + \Delta v_\pm^*\right\}\right)v^*\right] \\ -c_{0,v_+^*}\frac{1}{t}\left[\delta(v^* - v_+^*)v^* + \delta\left(v^* - \left\{v_+^* - \Delta v_\pm^*\right\}\right)v^*\right] \end{Bmatrix}$$

$$= \begin{Bmatrix} c_{0,v_-^*}\frac{1}{t}\left[\delta(v^* - v_-^*)v_-^* + \delta\left(v^* - \left\{v_-^* + \Delta v_\pm^*\right\}\right)\left\{v_-^* + \Delta v_\pm^*\right\}\right] \\ -c_{0,v_+^*}\frac{1}{t}\left[\delta(v^* - v_+^*)v_+^* + \delta\left(v^* - \left\{v_+^* - \Delta v_\pm^*\right\}\right)\left\{v_+^* - \Delta v_\pm^*\right\}\right] \end{Bmatrix}$$

$$= \begin{Bmatrix} c_{0,v_-^*}\frac{v_-^*}{t}\left[\delta(v^* - v_-^*) + \delta\left(v^* - \left\{v_-^* + \Delta v_\pm^*\right\}\right)\left(1 + \frac{\Delta v_\pm^*}{v_-^*}\right)\right] \\ -c_{0,v_+^*}\frac{v_+^*}{t}\left[\delta(v^* - v_+^*) + \delta\left(v^* - \left\{v_+^* - \Delta v_\pm^*\right\}\right)\left(1 - \frac{\Delta v_\pm^*}{v_+^*}\right)\right] \end{Bmatrix}.$$

(159)

In Equation 159, the value of v* obtained from $\left(\frac{\partial v^*}{\partial t}\right)_\xi$ is equated to the only value of v* at which the Dirac delta function it multiplies is not equal to zero.

Direct determination of $\left(\frac{\partial c}{\partial t}\right)_{v^*}$

At constant v*, the time-derivatives of the Heaviside step functions of Equation 146 are given by

$$\left(\frac{\partial H(v^*-\beta^*)}{\partial t}\right)_{v^*} = \left(\frac{\partial H(v^*-\beta^*)}{\partial s^*}\right)_{v^*}\left(\frac{\partial (v^*-\beta^*)}{\partial t}\right)_{v^*} = \delta(s^*-\varsigma^*)\left[\left(\frac{\partial v^*}{\partial t}\right)_{v^*} - \left(\frac{\partial \beta^*}{\partial t}\right)_{v^*}\right]$$

$$= \delta(v^*-\beta^*)\left[0 - \left(\frac{\partial \beta^*}{\partial t}\right)_{v^*}\right] = -\delta(v^*-\beta^*)\left(\frac{\partial \beta^*}{\partial t}\right)_{v^*}.$$

(160)

As in Equations 147 and 152, β* may equal v_-^*, $\{v_-^* + \Delta v_\pm^*\}$, v_+^* or $\{v_+^* - \Delta v_\pm^*\}$.

Again, as v_-^* (Equation 131) and v_+^* (Equation 132) are time-independent, where β* equals v_-^* or v_+^*, $\left(\frac{\partial \beta^*}{\partial t}\right)_{v^*} = 0$. And again, as $\Delta v_\pm^*$ (Equation 133) is equal to a constant divided by t,

$$\left(\frac{\partial \Delta v_\pm^*}{\partial t}\right)_{v^*} = -\frac{\Delta v_\pm^*}{t} = \left(\frac{\partial \Delta v_\pm^*}{\partial t}\right)_{\xi}.$$

(161)

Thus, where β* equals $\{v_-^* + \Delta v_\pm^*\}$,

$$= -\delta(v^*-\beta^*)\left(\frac{\partial \beta^*}{\partial t}\right)_{v^*} = -\delta\left(v^* - \{v_-^* + \Delta v_\pm^*\}\right)\left(\frac{\partial \Delta v_\pm^*}{\partial t}\right)_{s^*} = -\delta\left(v^* - \{v_-^* + \Delta v_\pm^*\}\right)\left[-\frac{\Delta v_\pm^*}{t}\right]$$
$$= \delta\left(v^* - \{v_-^* + \Delta v_\pm^*\}\right)\frac{\Delta v_\pm^*}{t}.$$

(162)

Similarly, where β* equals $\{v_+^* - \Delta v_\pm^*\}$,

$$-\delta(v^*-\beta^*)\left(\frac{\partial \beta^*}{\partial t}\right)_{v^*} = -\delta\left(v^* - \{v_+^* - \Delta v_\pm^*\}\right)\left[-\left(\frac{\partial \Delta v_\pm^*}{\partial t}\right)_{s^*}\right] = -\delta\left(v^* - \{v_+^* - \Delta v_\pm^*\}\right)\left[\frac{\Delta v_\pm^*}{t}\right]$$
$$= -\delta\left(v^* - \{v_+^* - \Delta v_\pm^*\}\right)\frac{\Delta v_\pm^*}{t}.$$

(163)

As c_{0,v_-^*} and c_{0,v_+^*} are time-independent,

$$\left(\frac{\partial c_{0,v_-^*}}{\partial t}\right)_{v^*} = 0$$

(164)

and

$$\left(\frac{\partial c_{0,v_+^*}}{\partial t}\right)_{v^*} = 0\,.$$

(165)

Using Equation 146 to express c, and applying Equations 160 to 165, yields the same result for $\left(\frac{\partial c}{\partial t}\right)_{v^*}$ as that obtained in Equation 158. A comparison of Equations 151 and 158 shows that $\left(\frac{\partial c}{\partial t}\right)_{\xi}$ differs from $\left(\frac{\partial c}{\partial t}\right)_{v^*}$ solely with respect to the Dirac delta functions. In $\left(\frac{\partial c}{\partial t}\right)_{\xi}$ (Equation 151), the Dirac delta functions that contribute to the peaks and valleys of q(v*,t) and e(v*,t) are multiplied by either v_+^* or v_-^*. In $\left(\frac{\partial c}{\partial t}\right)_{v^*}$ (Equation 158), there is no Dirac delta function that would contribute to the peaks and valleys of q(v*,t), but the Dirac delta functions that contribute to the peaks and valleys of e(v*,t) are multiplied by $\Delta v_{\pm}^*$. As $\Delta v_{\pm}^* = v_+^* - v_-^*$ (Equation 133), $\left(\frac{\partial c}{\partial t}\right)_{v^*}$ makes a higher magnitude contribution to the peaks and valleys of e(v*,t) than $\left(\frac{\partial c}{\partial t}\right)_{\xi}$ does.

Calculating g(v) in terms of step functions*

Subtracting e(v*,t) (Equations 144 and 145) from Equation 140 yields

$$g(v^*) = q(v^*,t) = \left(\frac{\partial c_{v^*}}{\partial v^*}\right)_t - e(v^*,t) = \begin{Bmatrix} \left(\frac{\partial c_{v_-^*}}{\partial v^*}\right)_t - e(v_-^*,t) \\ \left(\frac{\partial c_{v_+^*}}{\partial v^*}\right)_t - e(v_+^*,t) \end{Bmatrix} = \begin{Bmatrix} -c_{0,v_-^*}\delta(\xi - [\xi_b + v_-^* t])t \\ c_{0,v_+^*}\delta(\xi - [\xi_m + v_+^* t])t \end{Bmatrix}$$

$$= \begin{Bmatrix} q(v_-^*,t) \\ q(v_+^*,t) \end{Bmatrix}.$$

(166)

Subtracting e(v*,t) from Equation 149 yields

$$g(v^*) = q(v^*,t) = \left(\frac{\partial c}{\partial v^*}\right)_t - e(v^*,t) = \begin{Bmatrix} \left(\frac{\partial c_{v_-^*}}{\partial v^*}\right)_t - e(v,t) \\ \left(\frac{\partial c_{v_+^*}}{\partial v^*}\right)_t - e(v_+^*,t) \end{Bmatrix} = \begin{Bmatrix} -c_{0,v_-^*}\delta(v^* - v_-^*) \\ c_{0,v_+^*}\delta(v^* - v_+^*) \end{Bmatrix}$$

$$= \begin{Bmatrix} q(v_-^*,t) \\ q(v_+^*,t) \end{Bmatrix}.$$

(167)

Normalising v and g(v*) for electric field strength*

Given an estimate of the electric field, E, the apparent electrophoretic mobility coefficient can be calculated as

$$u^* = \frac{v^*}{E},$$

(168)

which normalises v* for E, while the distribution function of the apparent electrophoretic mobility coefficient,

$$g(u^*) = g(v^*)E$$

(169)

normalises g(v*) for E. Estimating E is complicated by its dependence on many parameters, some of which can vary with spatial position and, prior to the system achieving steady state, are likely to vary with time. Nevertheless, given the current, i, the cross-sectional area of the system, A, and the conductivity of the solution κ, a first approximation of the electric field can be calculated as

$$E \simeq \frac{i}{\kappa A}.$$

(170)

Using Equations 168 to 170, g(u*) versus u* can be determined for data from a single system studied at multiple currents, where all conditions except current are the same during the collection of all data sets. Such a collection of data can be fit in a process that refines the estimated values of E at each current. Assuming, for example, that the peaks and valleys of g(u*) versus u* should superimpose, the value of E used to obtain g(u*) versus u* at each current can be adjusted until the best superimposition is achieved. The fact that E should approach zero as current approaches zero can be incorporated as a constraint imposed on the fit.

References

Moody, T. P. (2012). Johnston-Ogston effects in AUC simulations of two model systems based on polystyrene beads that are polydisperse with respect to specific gravity. http://moodybiophysicalconsulting.blogspot.com/.

Moody, T. P. (2011a). An irreversible thermodynamic description of analytical

ultracentrifugation (AUC) applied to a solution of the time- and gravitational-potential-space-dependent Lamm equation. http://moodybiophysicalconsulting.blogspot.com/.

Moody, T. P. (2011b). An irreversible thermodynamic description of membrane-confined electrophoresis (MCE) applied to a solution of the time- and electrical-potential-space-dependent continuity equation for MCE. http://moodybiophysicalconsulting.blogspot.com/.

Claverie, J.-M., Dreux, H., and Cohen, R. (1975). Sedimentation of generalized systems of interacting particles. I. Solution of systems of complete Lamm equations. *Biopolymers*. **14**, 1685-1700.

Bridgeman, W. B. (1942). Some physical chemical characteristics of glycogen. *J. Am. Chem. Soc.*, **64**, 2349-2356.

Stafford, W. F. (1992). Boundary analysis in sedimentation transport experiments: A procedure for obtaining sedimentation coefficient distributions using the time derivative of the concentration profile. *Anal. Biochem.*, **203**, 295-301.

Stafford, W. F. (1994). Boundary analysis in sedimentation velocity experiments. *Methods Enzymol.*, **240**, 478-501.

Stafford, W. F. (2000). Analysis of reversibly interacting macromolecular systems by time derivative sedimentation velocity. *Methods Enzymol.*, **323**, 302-325.

Schuck, P., & Rossmanith, P. (2000). Determination of the sedimentation coefficient distribution by least squares boundary modeling. *Biopolymers*, **54**, 328-341.

van Holde, K. E. Introduction to transport processes: Diffusion. In *Physical Biochemistry*, second edition. Prentice-Hall, Englewood Cliffs, NJ, 1985, pp. 93-109.

Laue, T. M., Hazard, A. L. , Ridgeway, T. M., and Yphantis, D. A. (1989). Direct determination of macromolecular charge by equilibrium electrophoresis, *Anal. Biochem.* **182** 377-382.